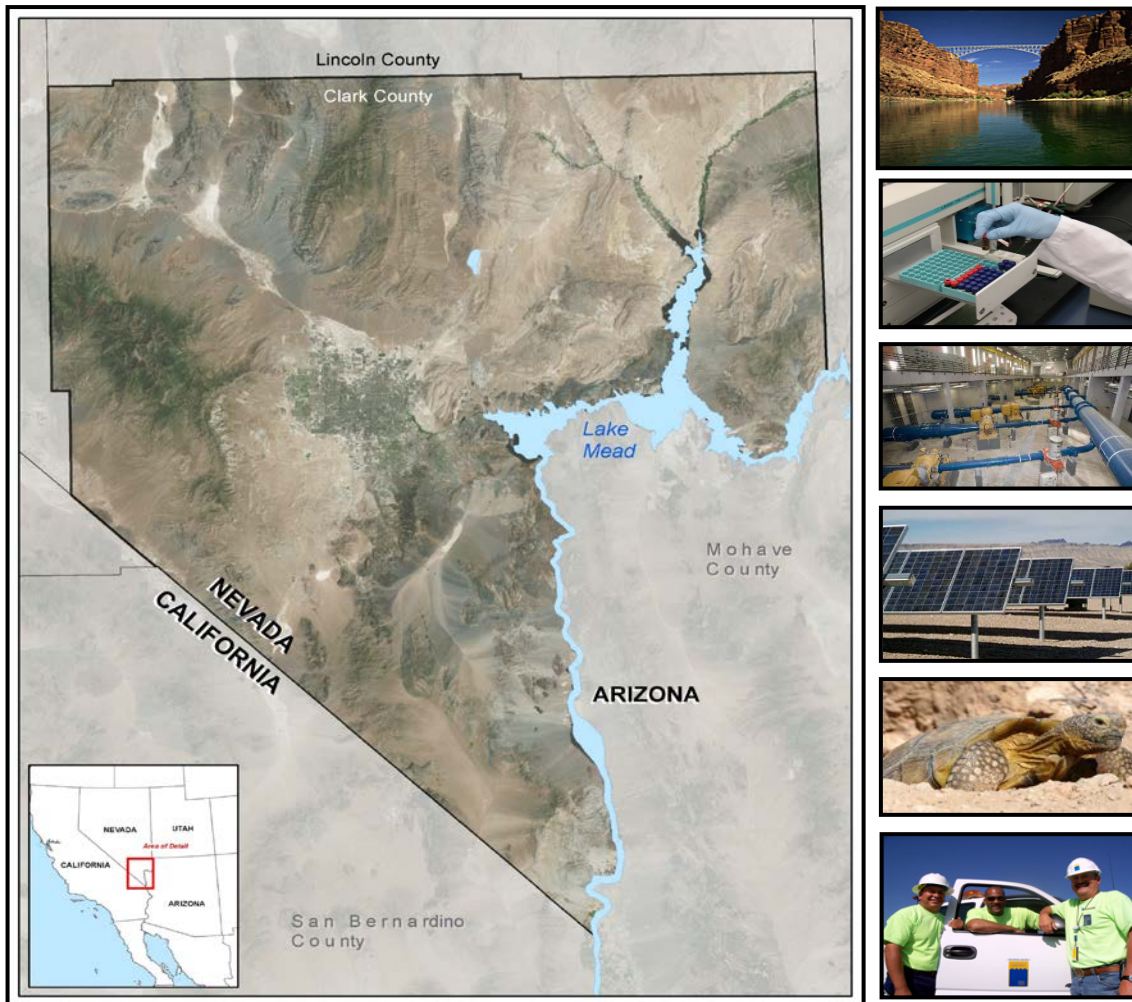# Climate Conditions in Clark County, NV

An Evaluation of Historic and Projected Future Climate using Global Climate Models
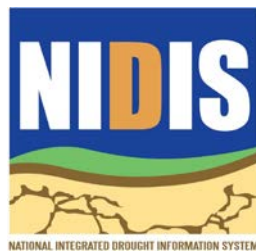
2018   Julie Kalansky, Amanda Sheffield, Daniel Cayan, David Pierce

Acknowledgements

Contents

Executive Summary

Extreme weather events can cause critical community services to fail. Municipalities use knowledge of past droughts, floods and heat waves to reduce the risk of service failure in the future. However, using the past to plan for future climate extremes may no longer be sufficient. Climate in the southwest has changed over the last century. The decade 2001‑2010 was the warmest and the fourth driest in the Southwest of all decades from 1901 to 2010 (Hoerling et al. 2013). In response, municipalities, including water purveyors, are using information from climate models to develop scenarios of what the climate, including extreme weather events, could be like in the future. While regional observations are valuable, advances in climate science have made it possible to project future climate scenarios at a more localized scale. The results from this study provide a range of locally specific future climate conditions that may be used to support future planning studies.

The Southern Nevada Water Authority (SNWA) contracted scientists with the California Nevada Applications Program (CNAP)[1] to evaluate and summarize climate data for their service area. This report examines and summarizes historical and projected future climate data specific to Clark County, Nevada. These analyses rely on local weather station information and data from a select suite of global climate models (GCMs) that best represent local, historical climate conditions.

The study is comprised of three main components:

1. Compilation and summary of historical, local climate data
2. Selection of representative GCMs, and
3. Evaluation and summary of future projections

Compilation and Summary of Historical, Local Climate Data

Historical temperature and precipitation records from six stations in Clark County, were examined for trends and changes in long-term variability. Warming temperatures in Clark County are consistent with warming trends observed nationally and globally. The magnitude and pace of local warming is largely driven by warmer nighttime temperatures (i.e. daily minimum temperatures "T_{min}"), although a weaker upward trend in daytime temperatures (i.e. daily maximum temperatures "T_{max}") is also present at some of the stations. The increase in T_{min} at McCarran Airport is the strongest of all stations and is likely strongly influenced by the urban heat island effect (Figure E-1). The shoulder seasons (spring and fall) have the largest year-to-year temperature variability, meaning they are less predictable using the thirty-year average (e.g. climatology) (Figure E-2).

---

[1] CNAP is a National Oceanic and Atmospheric Administration, Regional Integrated Sciences and Assessments (NOAA-RISA) team, at Scripps Institution of Oceanography at the University of California San Diego
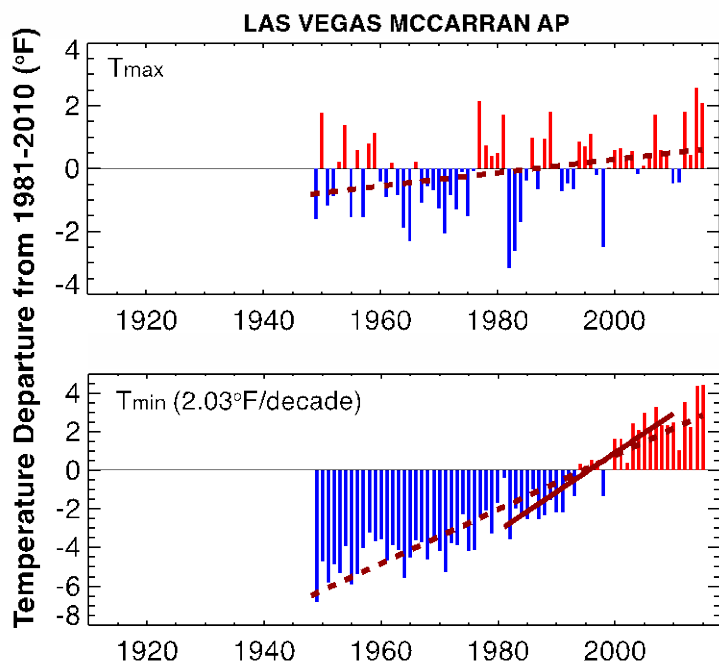
Figure E-1. Annual T_{max} and T_{min} departure from the 1981-2010 average climatology at Las Vegas McCarran Airport. The dashed trend lines are over the entire station record and the solid over the 1981-2010 time period. Only trends that are statistically significant using a Kendall-Mann test are shown. All anomalies are relative to the annual mean value between 1981 and 2010. Notice the greater rate of change in T_{min} than T_{max}.
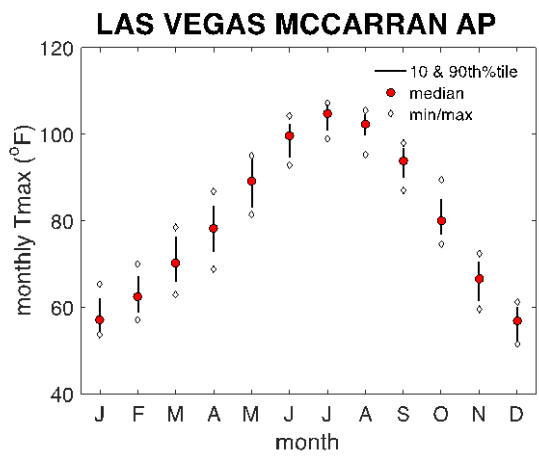
Figure E-2. For each month (January to December) from 1981-2010, the median monthly T_{max} (°F) is represented by the red circles; whereas the line illustrates the range of temperatures in the 10th to 90th percentiles. The diamonds represent the maximum and minimum monthly T_{max} values between 1981 and 2010. The shoulder seasons, Spring (March, April, May) and Fall (October, November) have a large range in values.

The small amount of precipitation that falls in southern Nevada arrives primarily during the winter or late summer. Low-pressure systems sitting over the region brings storms carrying

moisture from the Pacific to Clark County in the winter. Clark County is situated at the north-western extent of the North American Monsoon (Monsoon), which transports moisture from the Gulf of California in late summer to the region. Average precipitation at McCarran airport is 4.2 inches/year with 43% of the rainfall occurring in the winter months, and 22% during the Monsoon season from July through September. Clark County experiences large year-to-year variability in precipitation; years with increased frequency and intensity of the largest storms (5% of wettest days) typically result in wet years (Figure E-3). Historical observations indicate there are no trends in changing precipitation. Nor is there an indication in the last 30-50 years that the frequency or intensity of the most extreme precipitation events (99th percentile events) has increased.

Only a weak relationship is observed between El Niño-Southern Oscillation (ENSO) phase and climate in southern Nevada. La Niña events tend towards slightly warmer and drier conditions in Clark County, while there is a tendency towards cooler and wetter conditions during El Niño events. El Niño-Southern Oscillation (ENSO) explains 18% of the variability in winter precipitation and provides bounds on what to expect for winter (December-April) precipitation and temperatures for the region.

The final section of the historical analysis revealed that wet winter months and cold winter months often have signature atmospheric patterns, with low-pressure systems present over the region. In contrast, heatwaves are typically associated with high-pressure systems over the southwestern U.S.
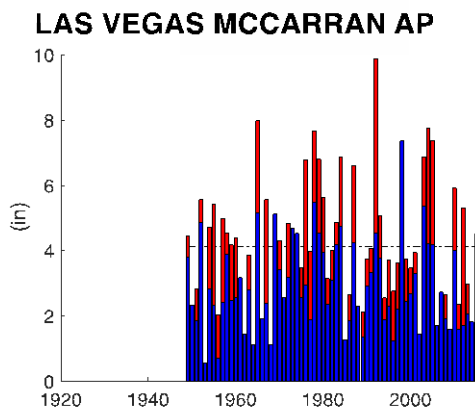
Figure E-3. Total annual rainfall (inches) at Las Vegas McCarran Airport. The dashed line is the average annual rainfall for the period-of-record (1948-2016). The height of the bar represents the total annual precipitation and the red portion is the contribution from events at or exceeding the 95th percentile.

Selection of Representative Global Climate Models

The global climate model (GCM) selection process was based on the work of Cayan and Tyree (2015) which compared the historical GCM runs against observations. From an original list of over 30 GCMs, models were eliminated based on global, regional and local evaluations, in that

order. The global and regional evaluations were determined by previous studies. Southern Nevada specific parameters were selected to reflect characteristics of local climate, including seasonal temperature variability, the number of wet days during winter and summer, and the atmospheric circulation patterns associated with cold months, wet months and heat waves. This process resulted in the selection of six GCMs considered to be representative of local climate conditions in Clark County, Nevada (Figure E-4). None of the models were ranked as "best" for all evaluation components, nor were any of the selected models in the bottom tier for any evaluation component.

Choosing Global Climate Models for Southern Nevada Water Authority

Criteria
- Scientists recommend using information from several Global Climate Models
- Using information from all available GCMs isn't practical
- Remove GCMs that fall short in representing historical climate and hydrologic processes important for Southern Nevada

Method

Global

Western U.S.

Southern Nevada

6 GCMs

Start with 31[1] GCMs

Global Climate Evaluation[2,3]
Evaluate how each GCM represents global historical
- Solar Radiation
- Air Temperature
- Atmospheric Pressure, Wind

Remove ~12 GCMs

Western U.S. Climate Evaluation[4]
Evaluate how each GCM represents Western US historical
- Air temperature & Precipitation
- Atmospheric Pressure Patterns
- El Nino Southern Oscillation Patterns

Remove ~4 GCMs

Southern Nevada Climate & Extremes Evaluation
Evaluate how each GCM represents Southern Nevada historical
- Air Temperature
- Precipitation
- Atmospheric Circulation Patterns

Remove 9 GCMs

GCM Recommendations for Southern Nevada
The remaining 6 GCMs are recommended for SNWA because they represent important components of historical climate at global, regional, and statewide scales.

References:
[1]Available GCMs at the start of the investigation period and similar to Cayan et al. (2015).
[2]Gleckler, P. J., K. E. Taylor, and C. Dourtriaux: Performance metrics for climate models, J. Geophys. Res.-Atmos (2008).
[3]IPCC, Climate Change 2013: The Physical Science Basis, Cambridge University Press, Cambridge, UK and New York (2013).
[4]Rupp, D. E., J. T. Abatzoglou, K. C. Hegewisch, P. W. Mote: Evaluation of CMIP5 20th century climate simulations for the Pacific Northwest USA, J. Geophys. Res.-Atmos (2013).

Figure E-4. Flowchart representing the global climate model (GCM) selection process. Note that the first two steps are described in more detail in Cayan and Tyree, 2015. The figure is modified from Cayan and Tyree, 2015.

Evaluation and Summary of Future Projections

A similar rate of warming is expected in the near term (prior to 2050) regardless of greenhouse gas (GHG) concentrations. Globally and locally, warming is a function of increasing concentrations of greenhouse gases in the atmosphere (IPCC 2013). To represent a range of possible Clark County future climate conditions, two different GHG emission concentrations were used. These include, Representative Concentration Pathway 4.5 (RCP 4.5), which represents a significant reduction in GHG emissions in the future, and RCP 8.5, which represents a business as usual scenario. It is only after the middle of the century that the benefits of mitigating GHG emissions today, would be gained. Strong mitigation now could reduce the amount of warming by the end of the century by approximately 3.6 °F.

Differences in warming prior to 2050 reflect model simulation differences. Based on the suite of six GCMs, warming could range between 3-5°F by 2030-2050 and 5-10°F by 2100 in southern Nevada (Figure E-5). The largest seasonal temperature changes in the future occur in the fall, closely followed by the summer and particularly for nighttime temperatures.

By mid-century, Clark County will likely experience approximately 40 – 50 more days above 100°F compared to today (Figure E-6). Temperatures rapidly rise through the end of the century under RCP8.5, where extreme heat days (>115-120°F) are projected to increase to over 50 days per year.

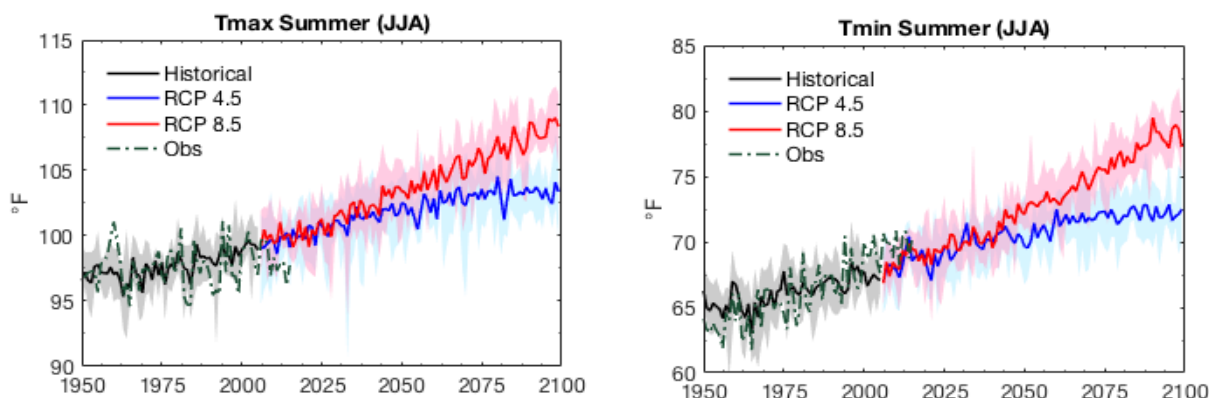*Figure E-5. Historical and future projections for Clark County summer T_{max} (left) and T_{min} (right), spatially averaged for Clark County and from the six selected GCMs. The shaded area represents the window, or range, of the six models, and the bold line is the ensemble mean, or average, of the six models. The black shows the historical model runs and the green dashed line shows the historical data.*
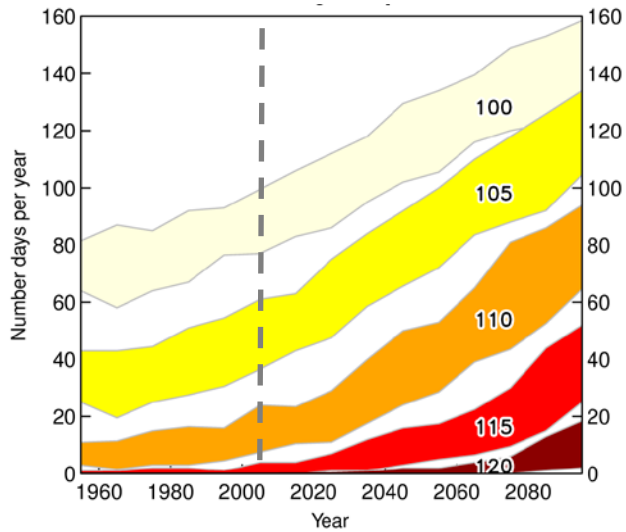
Figure E-6. Range of the six GCMs RCP8.5 projected average number of days in Clark County at or above the indicated temperature threshold (°F) in each decade from the 1950's to the 2090's. The dashed line illustrates the division between the historical model scenarios and future climate scenarios.

Projected changes in precipitation are small and highly uncertain, in part due to the large natural interannual and decadal variability of precipitation in the region, but also because rainfall is difficult to model given GCM resolution. Projections indicate increasing precipitation variability and more frequent extreme precipitation events in the future. Seasonally, spring may be drier by the end of the century, although the number of wet days will increase which means fewer large springtime precipitation events.

1. Introduction

Earth's climate is changing at a pace and in a pattern not explainable by natural influences. Global annual average temperature has increased by more than 1.2°F (0.7°C) for the period 1986–2016 relative to 1901–1960 (USGCRP, 2018, in review). Climate scientists, using global climate models (GCMs), project substantial warming through the 21st century in the desert southwest, though the magnitude of the warming varies by location (IPCC, 2013; USGCRP, 2014).

In 2016, Nevada's largest wholesale drinking water provider, the Southern Nevada Water Authority (SNWA), contracted the California Nevada Applications Program (CNAP) scientists, part of the National Oceanic and Atmospheric Administration Regional Integrated Sciences and Assessments (NOAA RISAs) program, to obtain future climate information specific to Clark County, NV. The study objective was to select a suite of GCMs that closely simulate historic conditions specific to Clark County, from over 30 GCMs, and summarize the range in climate variability and projected warming through the year 2100.

The CNAP research team is based at Scripps Institution of Oceanography and the University of California, San Diego. CNAP is one of 11 NOAA RISA teams that provide decision-makers and policy planners data and guidance on complex climate information to meet their planning needs.

This report is organized by the tasks conducted to accomplish the study:

- Chapter 2: Examines historical climatology of Clark County, including spatial and temporal variability, from weather stations throughout Clark County with greater than 30 years of data;
- Chapter 3: Following the methodology of Cayan et al., 2015, determines the climate models that best represent Clark County climate by comparing the climate models historical simulations to the actual historical data;
- Chapter 4: Evaluates and summarizes the range of simulated future climate conditions from the selected GCM datasets; and
- Chapter 5: Summarizes conclusions from the analyses and provides recommended next steps.

Each chapter represents a task from the study, plus a final chapter summarizing conclusions and next steps.

2. Historical Climate Variability

2.1 Introduction

Spatial variability in temperature and precipitation is strongly guided by topography in Clark County. Both the coolest and wettest parts of the county are in the Spring Mountains, followed by the Sheep Mountains (Figure 2-1 and Figure 2-2). Besides these two regions, the remainder of the county receives between 4-8 inches of rain annually, which makes the county one of the driest in the U.S.

Precipitation in the region has two main seasons. The primary precipitation season occurs during winter months, December, January and February, but there is a second peak in the summer months of July and August. Winter precipitation is generally associated with synoptic scale low pressure systems, which take various forms but include the inland penetration of atmospheric rivers (Rutz et al., 2014) and cutoff lows. Atmospheric rivers that affect the western U.S. are relatively narrow bands of highly concentrated water vapor originating over the North Pacific and usually occurring within and influenced by the dynamics of a winter storm system. Cutoff lows, which also affect southern Nevada weather, are cyclonic circulation features and can produce substantial precipitation, partly because they are slow moving and can remain over a region for more than one day. Regional summer precipitation is from the North American Monsoon (Monsoon) (Adams and Comrie, 1997). The Monsoon is a thermally driven circulation pattern involving summer warming of the North American land mass that transports, intermittently, a warm moist flow and convective rainfall into parts of Mexico and the Southwest U.S. Southern Nevada is at the northern extent of the Monsoon. The remainder of this section will use daily station weather data to examine the temporal and spatial variability that underpin the climatological maps.
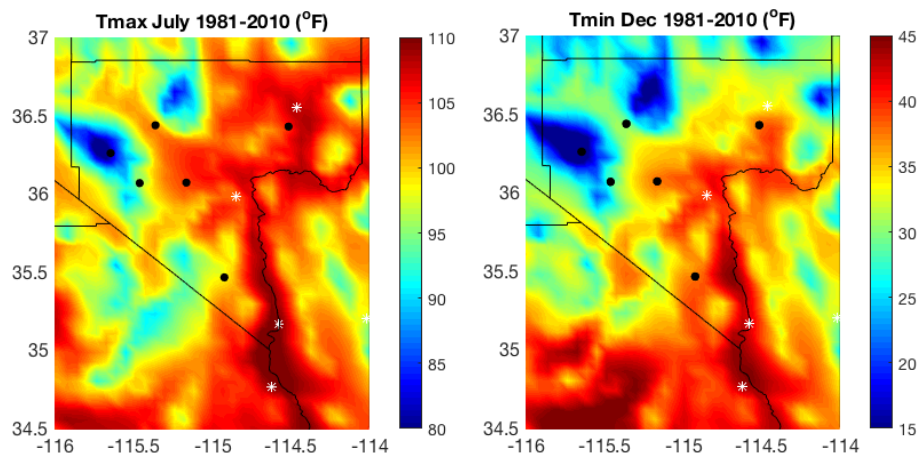

Figure 2-1. July T$_{max}$ and December T$_{min}$ averaged between 1981 and 2010 (^{o}F) are shown for Clark County and the surrounding area using data from Livneh et al. 2015. The Livneh et al. 2015 dataset is used instead of PRISM because the method focused on capturing orographic precipitation, and because it extends into Mexico improving the representativeness of the Monsoon. The black circles represent the six stations that were the focus of the historical climate analysis in this study, and the white asterisks represent the remaining stations that are included in the appendix.
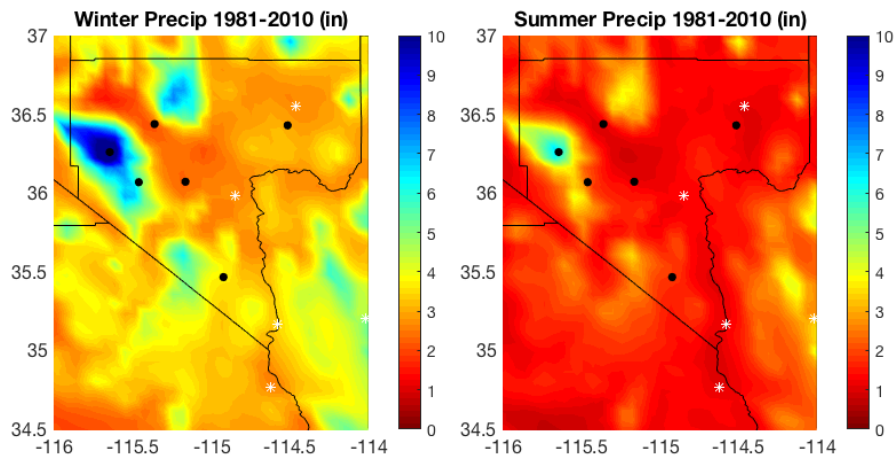
Figure 2-2. 1981-2010 average winter (December, January, February, March) and summer (June, July, August) seasonal precipitation totals (inches) shown for Clark County and surrounding area using data from Livneh et al. 2015.

2.2 Methodology

Eleven National Weather Service (NWS) Cooperative Observer Program (COOP) Network stations throughout Clark County and the surrounding region were initially reviewed for length of record, continuity of data, and spatial coverage (Table 2-1). COOP stations are daily weather observations of T_{max}, T_{min}, and precipitation. From these eleven stations, six stations were selected as "primary" stations because they had data that began in or prior to 1981, were still active at the time of this study, and are dispersed throughout Clark County such that they are representative of the different micro-climates within the study area. Information for the five stations that were not used in the analysis can be found in the appendix.

Valley of Fire State Park is located at the lowest elevation, 2000 ft, while Mt. Charleston is located at the highest elevation, 7460 ft (Figure 2-3). McCarran Airport (McCarran) has the most continuous data record with no missing data and a record beginning in 1948. Due to the continuity and length of record, this station is often used as a proxy for the region. Throughout the report, McCarran is used for comparison to other records or for highlighting a specific variable. One of the objectives of this section was to examine the spatial variability of the region and thus, McCarran data was used as a baseline to which other stations were compared.
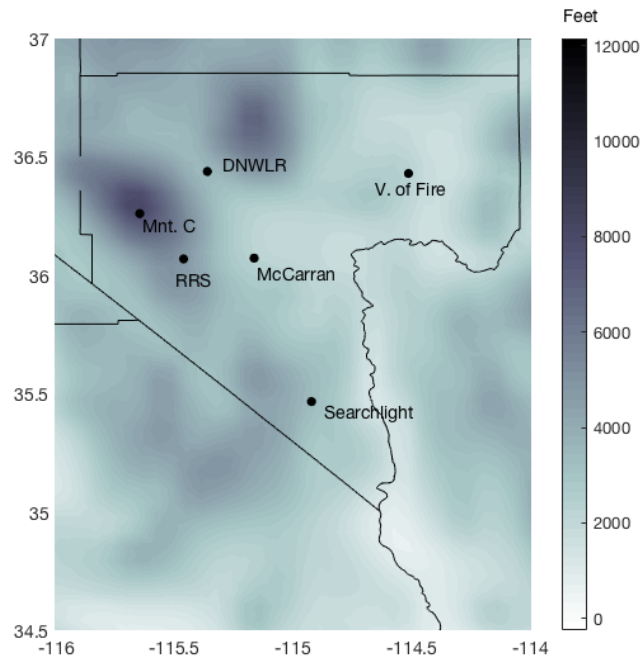
Figure 2-3. An elevation map with the six stations used in the report, and include Las Vegas McCarran Airport (McCarran), Mount Charleston (Mnt. C), Red Rock Spring Mountain (RRS), Desert National Wildlife Range (DNWLR), Valley of Fire (V. of Fire), and Searchlight. Clark County is outlined in black.

Statistically significant trends in T_{min}, T_{max}, or total precipitation were tested using the Mann-Kendall test. The Mann-Kendall test is frequently used to detect trends in climate variables that vary seasonally and tend not to be normally distributed. Ultimately the test statistically assesses if there is a monotonic upward or downward trend in the variable of interest over time. For all significance tests, a 95% confidence level was used. Figures of monthly averages use the 30-year climatological normal period of 1981-2010, unless noted, whereas time series figures use the entire period-of-record. Years with more than 10% of missing data were removed from the time series analysis and months with more than 15 missing days were removed from the monthly analyses (Table 2-1).

Table 2-1. Stations names, ID, location, elevation, period-of-record, number of valid observations and the percentage of missing values during the time of record. The stations in bold are the six that are analyzed in greater detail. *Indicates USHCN[2] station, otherwise GHCN[3] station.

Station Name	Station ID	Latitude Longitude	Elevation (feet)	Valid Date Range (MM-YYYY)	Data Points from Entire Record through 2015					
					Number of Observations			Percent of Missing Data		
					T_{max}	T_{min}	Precipitation	T_{max}	T_{min}	Precipitation
LAUGHLIN	USC00264480	35.17 ˚N -114.58˚E	605 ft (184.4 m)	10/1983 – Present	10106	9643	10200	4.41	8.79	3.52
NEEDLES*	USW00023179	34.77˚N -114.62˚E	890 ft (271.3 m)	03/1940 – Present	27428	27428	27511	1.12	1.12	0.83
OVERTON	USC00265846	36.55˚N -114.46˚E	1250 ft (381 m)	01/1992 – Present	8649	8555	7755	1.27	2.34	11.47
VALLEY OF FIRE SP	USC00268588	36.43˚N -114.5˚E	2000 ft (609.6 m)	11/1972 – Present	15004	14856	15655	6.76	7.68	2.71
LAS VEGAS MCCARRAN AP	USW00023169	36.07˚N -115.16˚E	2180 ft (664.5 m)	12/1948 – Present	24937	24937	24937	0	0	0
BOULDER CITY*	USC00261071	35.98˚N -114.85˚E	2500 ft (762.0 m)	08/1931 – 04/2006	24103	24303	24398	3.37	2.57	2.18
DESERT NATL WL RANGE	USC00262243	36.44˚N -115.36˚E	2914 ft (888.2 m)	04/1940 – Present	26454	26323	27209	5.57	6.04	2.88
KINGMAN*	024645 or 024639	35.20˚N -114.02˚E	3539 ft (1078.7 m)	09/1967 – 12/1989	8143	8143	8143	0	0	0
SEARCHLIGHT*	USC00267369	35.47˚N -114.92˚E	3540 ft (1079.0 m)	12/1913 – Present	35201	36113	36315	6.43	4.00	3.47
RED ROCK SPG MT RCF	USC00266691	36.07˚N -115.46˚E	3780 ft (1152.1 m)	05/1977 – Present	13304	13130	13775	8.12	9.32	4.87
MT. CHARLESTON	USC00265400	36.26˚N -115.64˚E	7460 ft (2273.8 m)	01/1980 – Present	13137	13074	13164	1.85	2.32	1.65

---

[2] The U.S. Historical Climatology Network (USHCN) data are used to quantify national- and regional-scale temperature changes in the contiguous United States (CONUS). The USHCN is a designated subset of the NOAA Cooperative Observer Program (COOP) Network with sites selected according to their spatial coverage, record length, data completeness, and historical stability.

[3] The Global Historical Climatology Network (GHCN) is an integrated database of climate summaries from land surface stations across the globe that have been subjected to a common suite of quality assurance reviews.
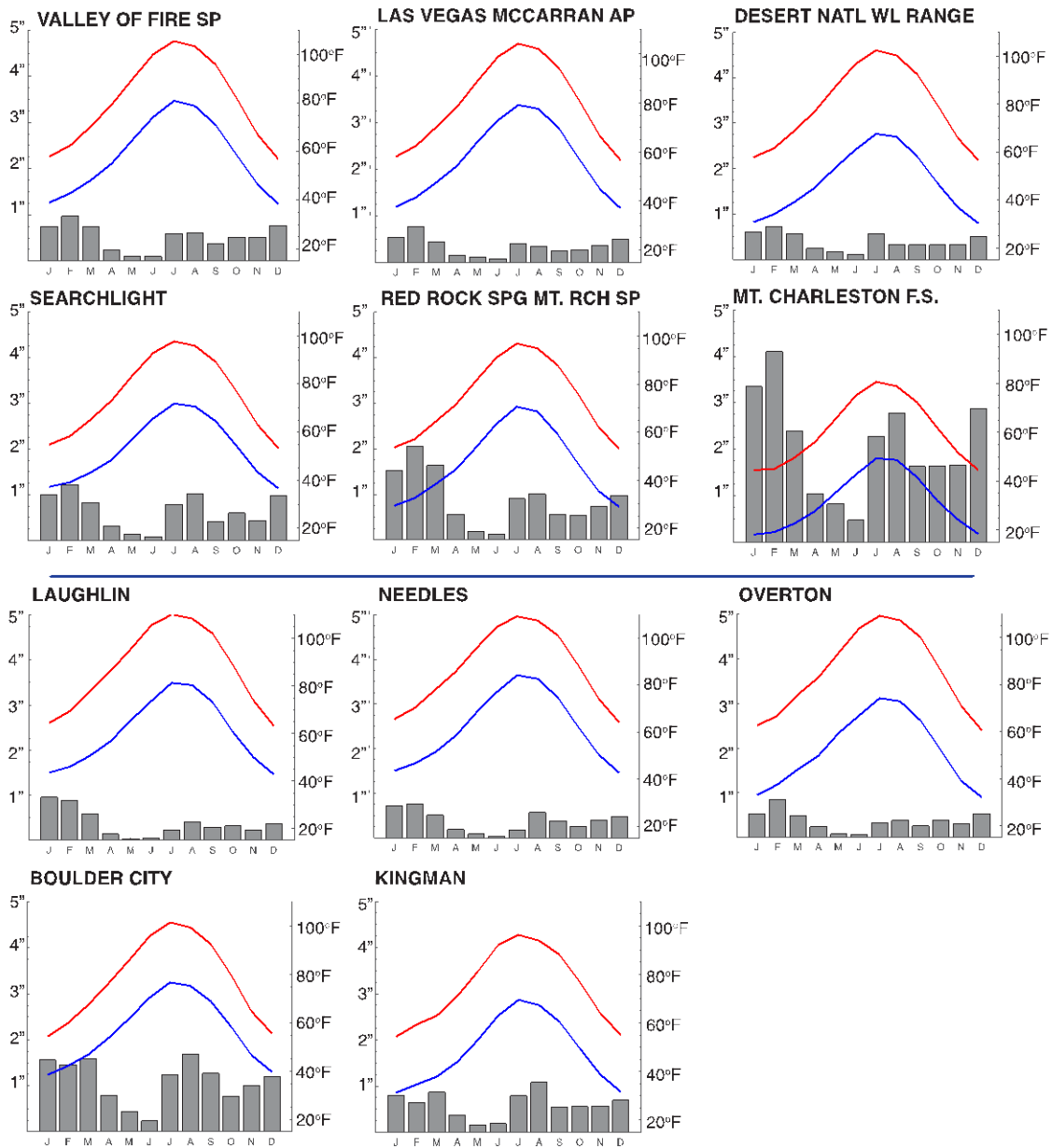
Figure 2-4. Colored lines show average monthly T_{max} (red) and T_{min} (blue) (^{o}F) while monthly precipitation totals (inches) are shown as grey bars. The stations in the top two rows are calculated for a record from 1981-2010 while the remaining figures use various time periods given the period of observations (Table 2-1). All stations show a peak in precipitation in January and February associated with winter storms and a second peak in July and August associated with the summer monsoon. Warmest temperatures are in July followed by August.

16

2.3 Results

2.3.1 Temperature

December and January are the coolest months for T_{max} and T_{min}, while July followed by August have the highest temperatures (Figure 2-4). For T_{max}, the only location that has a significant trend for the period between 1981-2010 is Valley of Fire State Park (0.59˚F per decade); McCarran Airport and Dessert National Wildlife Range have significant trends over their respective period-of-record, though the trends are weaker (~0.20˚F per decade) than Valley of Fire. Upward temperature trends are much stronger for T_{min} than for T_{max}, which has also been documented in California and globally (Figure 2-5 and Figure 2-6) (Gordero et al. 2011; Karl et al., 1993; Easterling et al., 1997). All stations show a significant warming trend in T_{min} for both the period-of-record and from 1981-2010 except for Red Rock Springs, which is likely the result of missing years due to missing data.

The T_{min} trend for McCarran is the highest, 2.0˚F per decade, which is more than double any other station. The much larger trend in T_{min} for McCarran is likely caused by a growing urban heat island effect. Several large cities have documented increased warming as a result of the urban heat island effect, which has been shown to have a greater impact on nighttime temperatures (Karl et al., 1993). The urban heat island effect is caused by the urbanized environment absorbing more solar radiation during the day and releasing the heat more slowly at night than the natural open land and vegetation it replaced (Rizwan et al., 2008). Nighttime temperatures are less able to cool down, resulting in a greater increase in T_{min} as compared to T_{max}. The difference in trends between T_{max} and T_{min} are also reflected in the 30-year moving averages of T_{max} and T_{min} (Table 2-2 and Table 2-3), with the largest change in the 30-year average for T_{max} of 0.4˚F at McCarran and the largest change in the 30-year average for T_{min} of 4.0˚F at McCarran. Seasonally, summer, (June-September), and fall (October-November) have the stronger trends in T_{max} and T_{min} relative to winter (December-March) and spring (April-May) (not shown).

Outside of Las Vegas in the more rural areas of Clark County, the urban heat island effect is less likely to influence T_{min}, suggesting other mechanisms may explain the difference between the T_{min} and T_{max} in these regions. Irrigation has also been shown to decrease T_{max} while not affecting T_{min} as significantly (Lobell and Bonfils, 2008). Whether irrigation is having a similar impact in Clark County as has been shown elsewhere in the West might be explored in follow-up studies. Aerosol particles, including their impacts on cloud development, are suggested to be a cooling counterpart to rising daily global temperatures (IPCC 2007; 2013). More specifically, aerosol particles and their interaction with solar energy may cool days and warm nights, thus acting to buffer T_{max} while amplifying nighttime T_{min}. Aerosols can also impact regional cloud cover; however, these impacts are specific to local atmospheric conditions (Albrecht, 1989; Twomey, 1977), and cloud cover is relatively low in southern Nevada so this effect may be minimal.
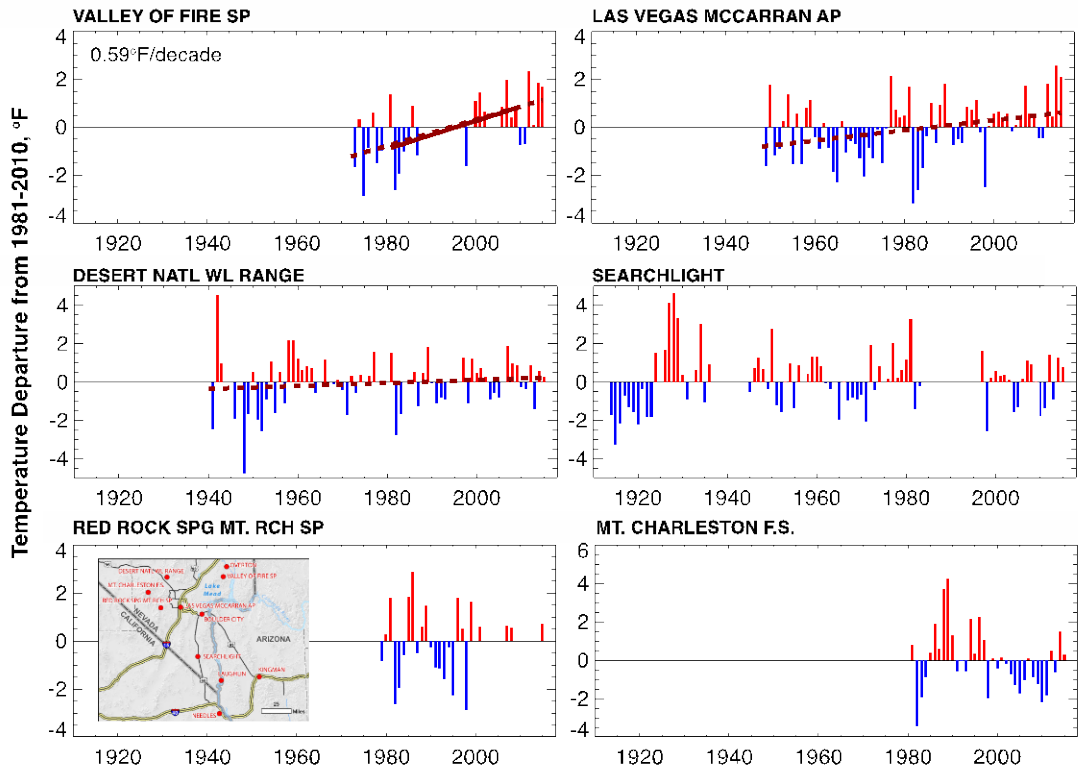
Figure 2-5. The annual T_{max} departure from the 1981-2010 average climatology. The dashed trend lines are for the entire station record and the solid between 1981 and 2010. Only trends that are statistically significant using a Kendall-Mann test are shown. All anomalies are relative to the annual mean value from 1981-2010. Note the different y-axis by station.

Table 2-2. The 30-year average of annual average T_{max} (˚F)

Annual Average T_{max} (˚F)				
	1951-1980	1961-1990	1971-2000	1981-2010
VALLEY OF FIRE SP	N/A	N/A	N/A	81.0
MCCARRAN AP	79.7	79.7	79.9	80.1
DESERT NATL WL RANGE	78.9	78.9	78.8	78.8
SEARCHLIGHT	75.3	75.3	76.7	75.3
RED ROCK SPG	N/A	N/A	N/A	74.3
MT. CHARLESTON	N/A	N/A	N/A	60.6
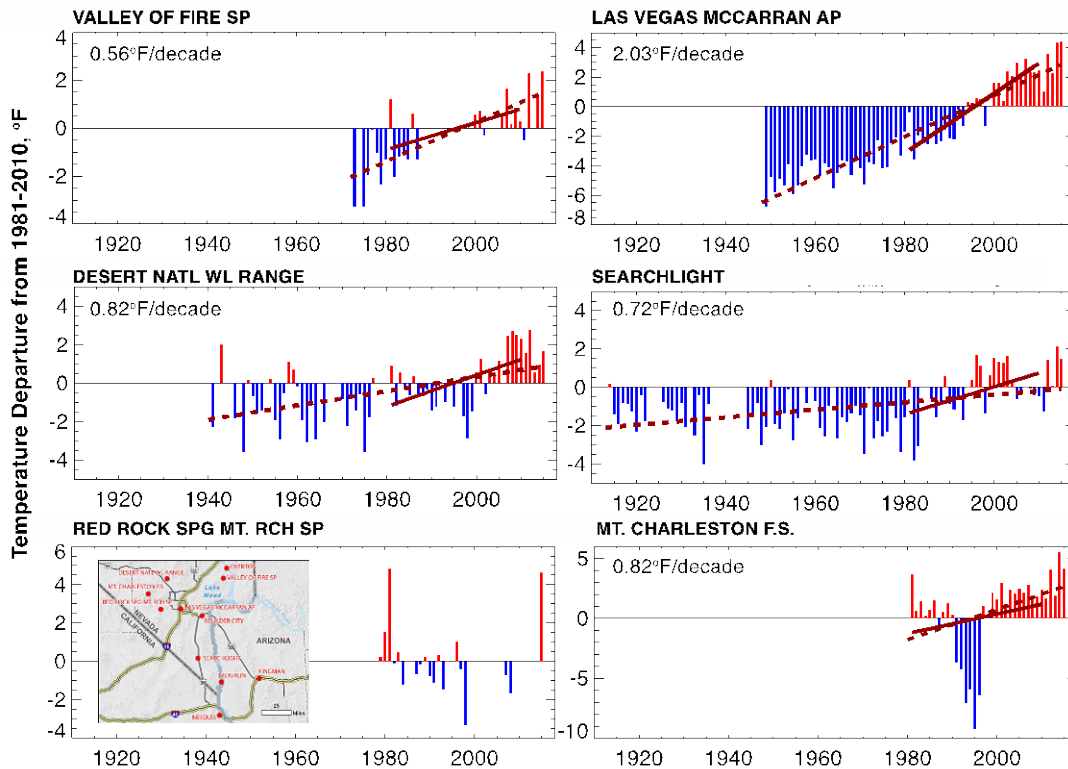
Figure 2-6. Same a Figure 2-5 but for T$_{min}$. Notice that there are more significant trend lines and the rate of change is greater than for T$_{max}$ at most stations.

Table 2-3. The 30-year average of annual average T$_{min}$ (˚F).

Annual Average T$_{min}$ (˚F)				
	1951-1980	1961-1990	1971-2000	1981-2010
VALLEY OF FIRE SP	N/A	N/A	N/A	58.8
MCCARRAN AP	52.9	53.8	55.1	57.0
DESERT NATL WL RANGE	47.1	46.4	46.6	47.4
SEARCHLIGHT	51.4	52.5	51.7	53.2
RED ROCK SPG	N/A	N/A	N/A	48.0
MT. CHARLESTON	N/A	N/A	N/A	31.8

Beyond understanding general temperature trends, there is value in understanding the frequency at which certain thresholds are reached and if these are changing. For instance, extreme high temperatures can decrease power transmission efficiency and production, decrease the lifespan of an asset, increase water needs for outdoor irrigation, or jeopardize the health of SNWA's outdoor workforce. In contrast, temperatures below freezing can cause pipe failures. To determine if there is a trend in extreme heat the number of days per year from May-Sept above 100ºF, 105ºF, 110ºF, and 115ºF are plotted for each station in Figure 2-7. There are no significant trends in the station data using data from May-Sept. In a separate

19

analysis that only evaluates days in July at McCarran, revealed a statistically significant decline in the number of days above 100°F at McCarran, and a non-statistically significant increase in the number of 105ºF days (see appendix).

Examining the low temperature thresholds, downward trends in the number of days below a threshold are visible for all stations except Red Rock Springs (Figure 2-8) which shows the number of days from Nov-Mar that are below 32ºF, 40ºF, and 50ºF. The number of days below 32ºF is particularly important in the high elevation Mt Charleston region because of the potential to impact whether precipitation falls as snow or rain and how late into the season the snow pack remains. Changes in snow pack may impact groundwater recharge given that snow contributes disproportionally more to groundwater recharge than to surface run-off in the Spring Mountains (Earman et al., 2006). The freezing elevation between Nov-March in the Spring Mountains has a statistically significant increasing trend over the time period of 1949-2016 (WRCC, North American Freezing Level Tracker, www.wrcc.dri.edu/cwd/products/), suggesting that snow pack in the region may already be affected by warming.
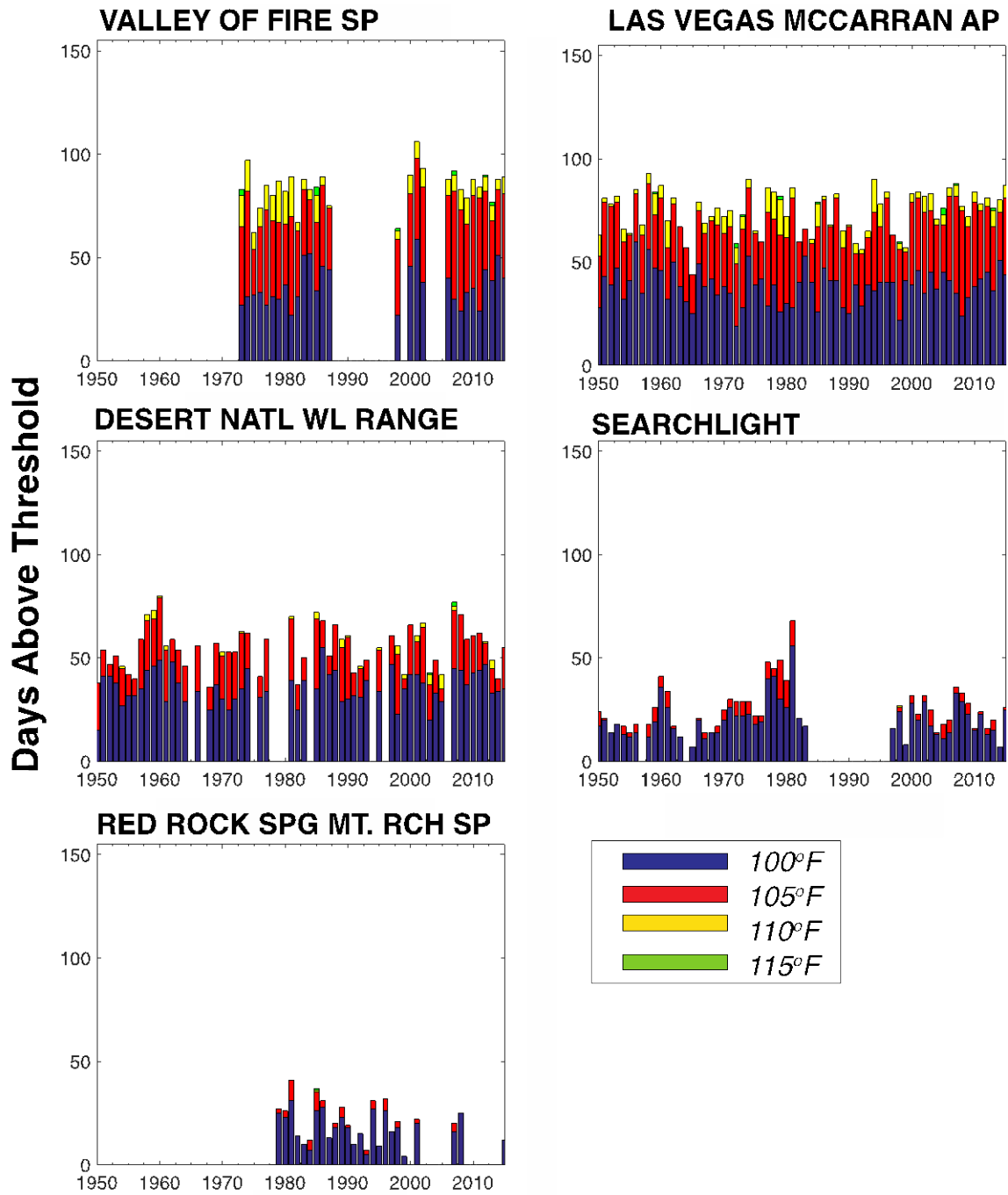
Figure 2-7. The bars illustrate the number of days above a temperature threshold in May, June, July, August and September of a given year. Purple is the number of days above 100˚F, the red is the additional number of days above 105˚F, the yellow is the additional number of days above 110˚F and the green is the additional number of days above 115˚F. Mt Charleston does not have any days above 100 ˚F and is not shown. Similar figures for each station and each month, May-September, are in the appendix.
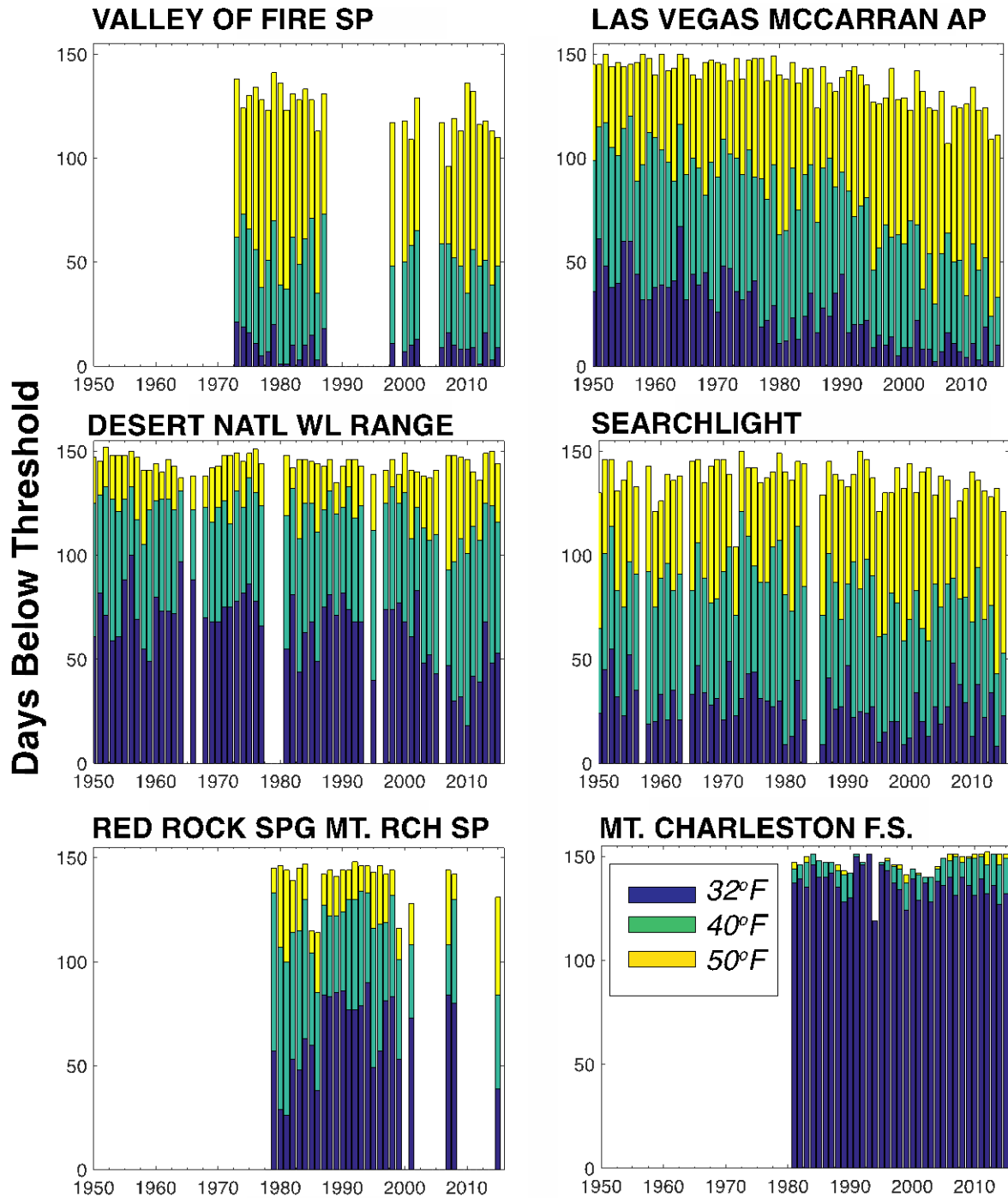
Figure 2-8. The bars illustrate the number of days below a temperature threshold in November, December, January, February and March of a given year. Purple represents the number of days below 32˚F, the green represents the additional number of days below 40˚F, and yellow is the additional number of days below 50˚F. Similar figures for each station and each month, November-March, are in the appendix.

In addition to looking at temperature values, temperature variability was also examined to understand how variable temperature in a given month has been over the historical record. Temperature variability places bounds on the expected temperature range. For example, although July and August are warmer than June, most stations have a larger historical range in June (Figure 2-9, Figure 2-10) indicating that June temperature is less predictable using climatology. The possible temperature range is the largest, for the spring and fall months. For example, the difference between the maximum and minimum April T_{max} differs by over 20˚F in some cases (Figure 2-9). T_{min} values show similar behavior in the shoulder seasons, spring and fall, as having the largest temperature range (Figure 2-10). Examining the range of average winter months' temperature provides information as to what months at a given station are likely to have temperatures regularly below freezing. The variability of maximum daily temperature in any given month was examined further (and is shown for McCarran Airport, and in the appendix for other stations) (Figure 2-11). The monthly variance plots also indicate that May and October are the most variable months at McCarran and that there was no statistically significant trend in the change of monthly variability for any of the months at McCarran.
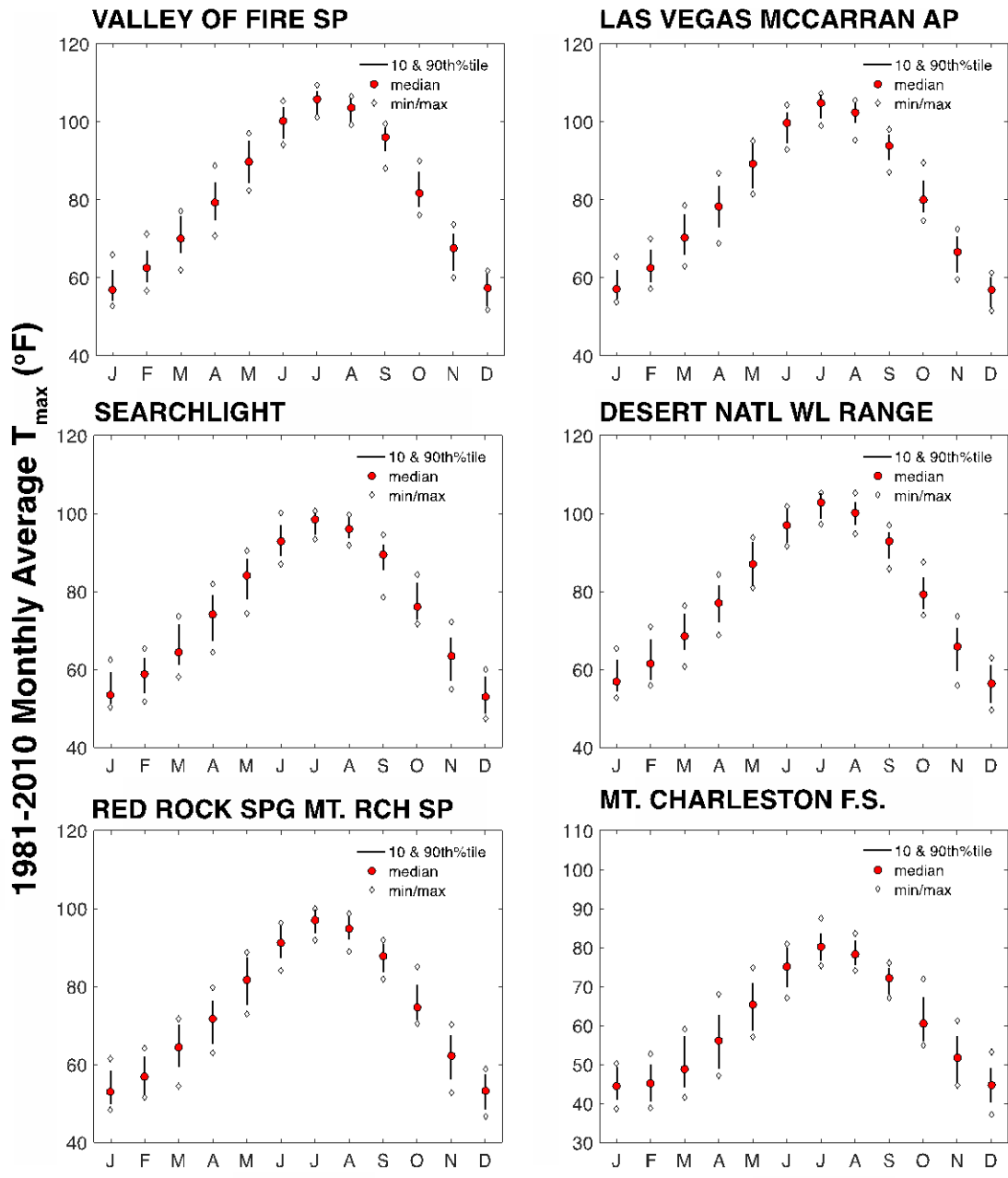
Figure 2-9. For each month (January to December) from 1981-2010, the mean monthly T_{max} (^oF) is represented by the red circles whereas the line illustrates the range of temperatures in the 10th to 90th percentiles. The diamonds represent the maximum and minimum T_{max} values over the 1981-2010 time period. The shoulder seasons, Spring (MAM) and Fall (SON) have a large range of values.
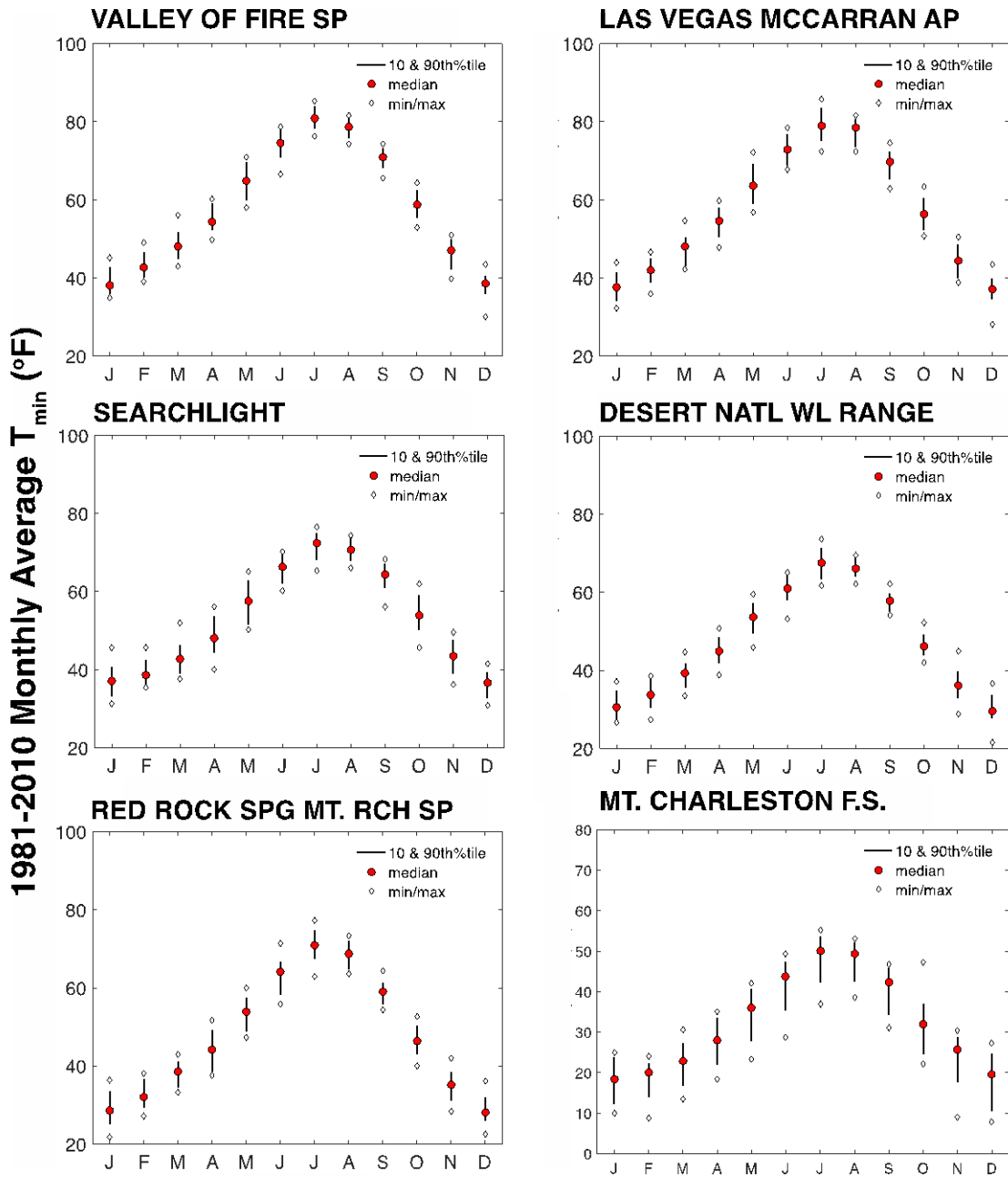
Figure 2-10. Same as previous figure but for T_{min}. Patterns are similar to T_{max}.
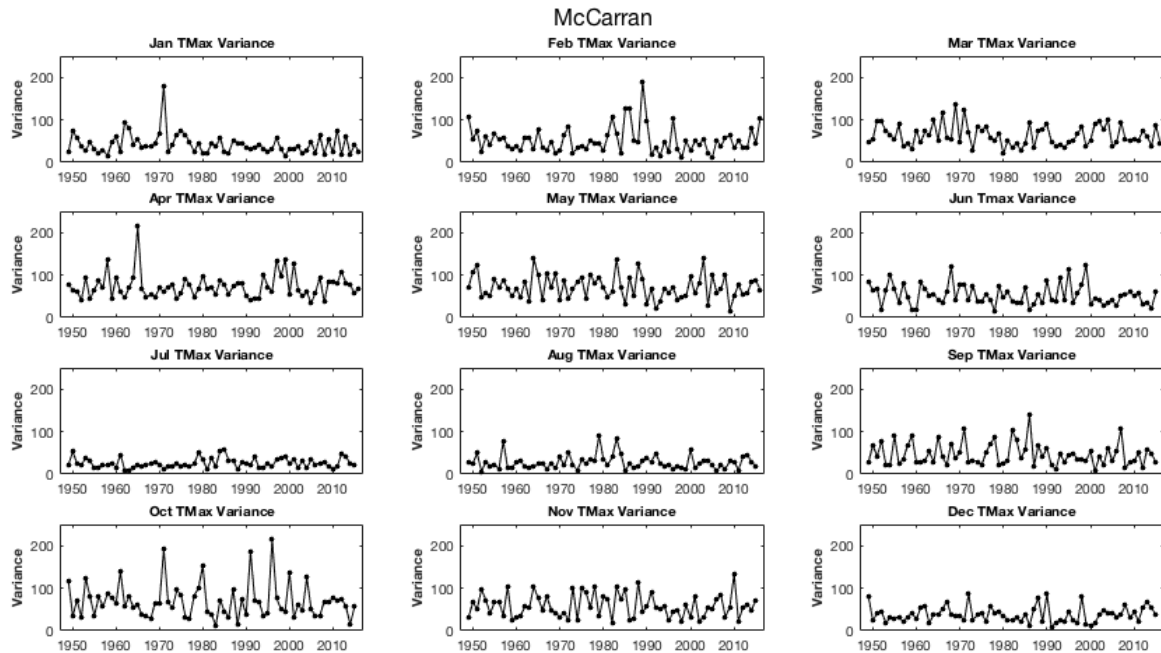
Figure 2-11. Each circle indicates how variable the days of that month were in a given year. The time series allows for an examination of how variability in a given month may have changed over time. This figure is for T_{max} at McCarran Airport, but the variance for all stations and for T_{min} is in the appendix.

The previous sections examined the temporal variability of temperature at the various stations, however, understanding the spatial coherency of the region is needed given the use of McCarran for weather and climate information. As mentioned in the Methodology section (Section 2.2), SNWA's primary source of weather and climate information is from the National Weather Service's McCarran Airport station due to the long history of a quality record. Given its placement in the urban center of Las Vegas, it is likely the McCarran record incorporates the imprint of the urban heat island effect. Seasonal correlations of T_{max} and T_{min} anomalies address this question of regional spatial variability. T_{max} has higher correlations at all stations as compared to T_{min}, with most correlations being above 0.7 for T_{max} and above 0.6 for T_{min} (Figure 2-12 and Figure 2-13). Further study is needed to determine what factors are driving the correlations, such as land surface, elevation, cloud cover, aerosol and air mass homogeneity, which are linked to winter storm systems, the monsoon, and desert conditions, or combination of these factors.
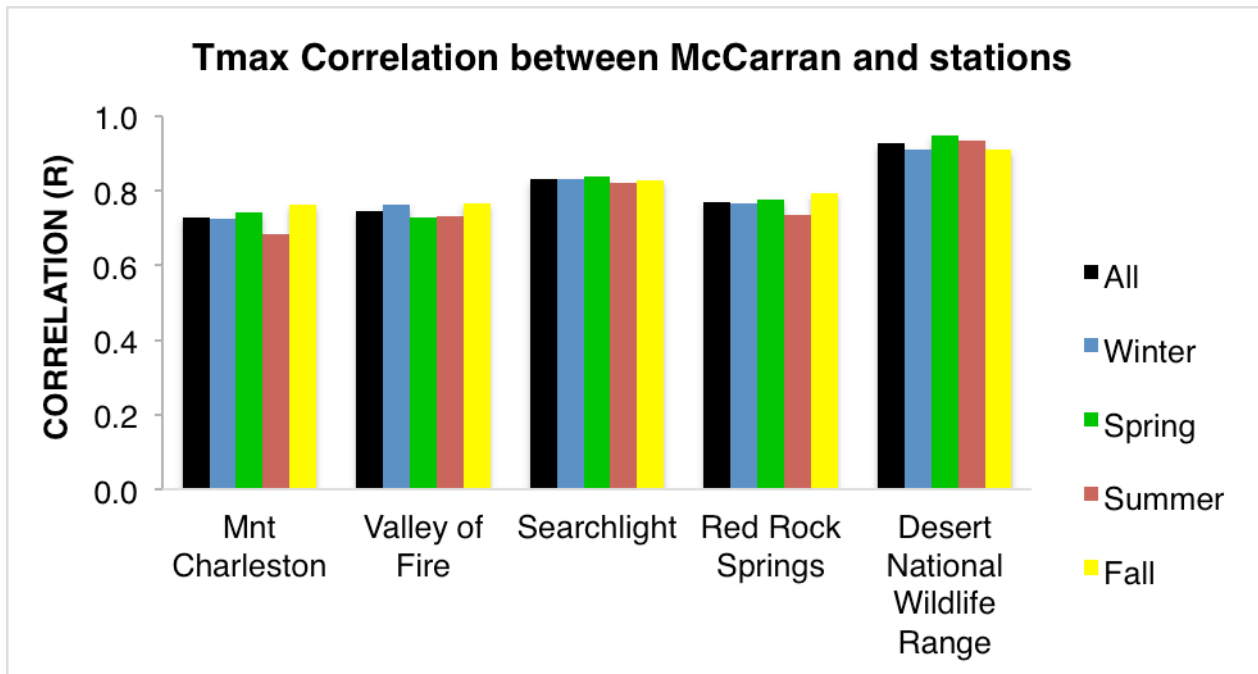
Figure 2-12. The correlations for the entire year and by season between McCarran Airport and the listed station for the time period 1981-2010 for T_{max}.
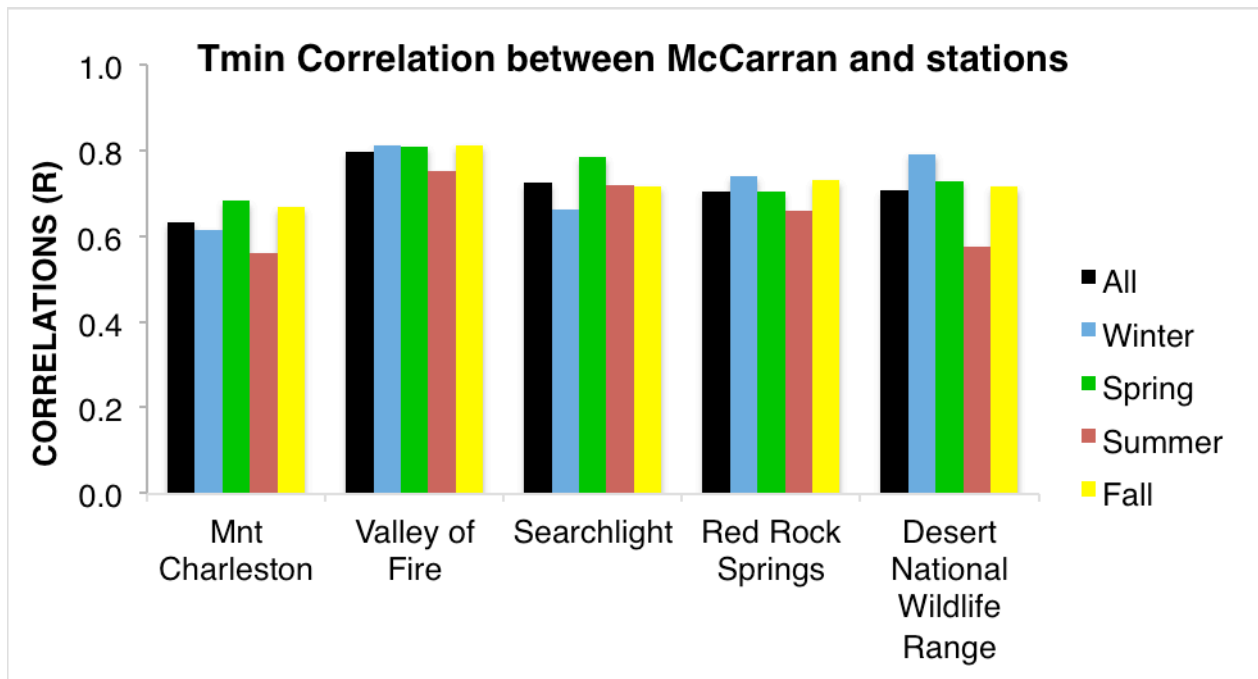

Figure 2-13. The correlations for the entire year and by season between McCarran Airport and the listed station for the time period 1981-2010 for T_{min}.

2.3.2 Precipitation

Precipitation throughout Clark County is highly variable year-to-year, with annual variability a third to half the annual average (Figure 2-14). The two most variable stations are Desert National Wildlife Range (DNWR) and McCarran Airport (McCarran). The trends at these stations are less than 0.01 inch per decade (not shown), suggesting that year-to-year variability is the dominant factor, not a decreasing or increasing trend. Previous research has shown that rare precipitation events, defined as the 95th percentile event explain 79% of the year-to-year variability in southern Nevada (Dettinger, Nevada Water Resources Association Meeting, 2015). Thus, these large, relatively infrequent precipitation events contribute an important fraction of the total precipitation. Over the 1981-2010 period, the 95th percentile storms (red portion of the bar graph in Figure 2-14) contribute between 25-35% of the annual precipitation at the six stations. Annual precipitation totals are available from before 1951 through 2010 for stations McCarran, DNWR, and Searchlight (Table 2-4). Where this data exists, small increases in the 30 year average annual precipitation has occurred through time. More long term monitoring is needed to confirm if this is a statistically significant trend for the region.
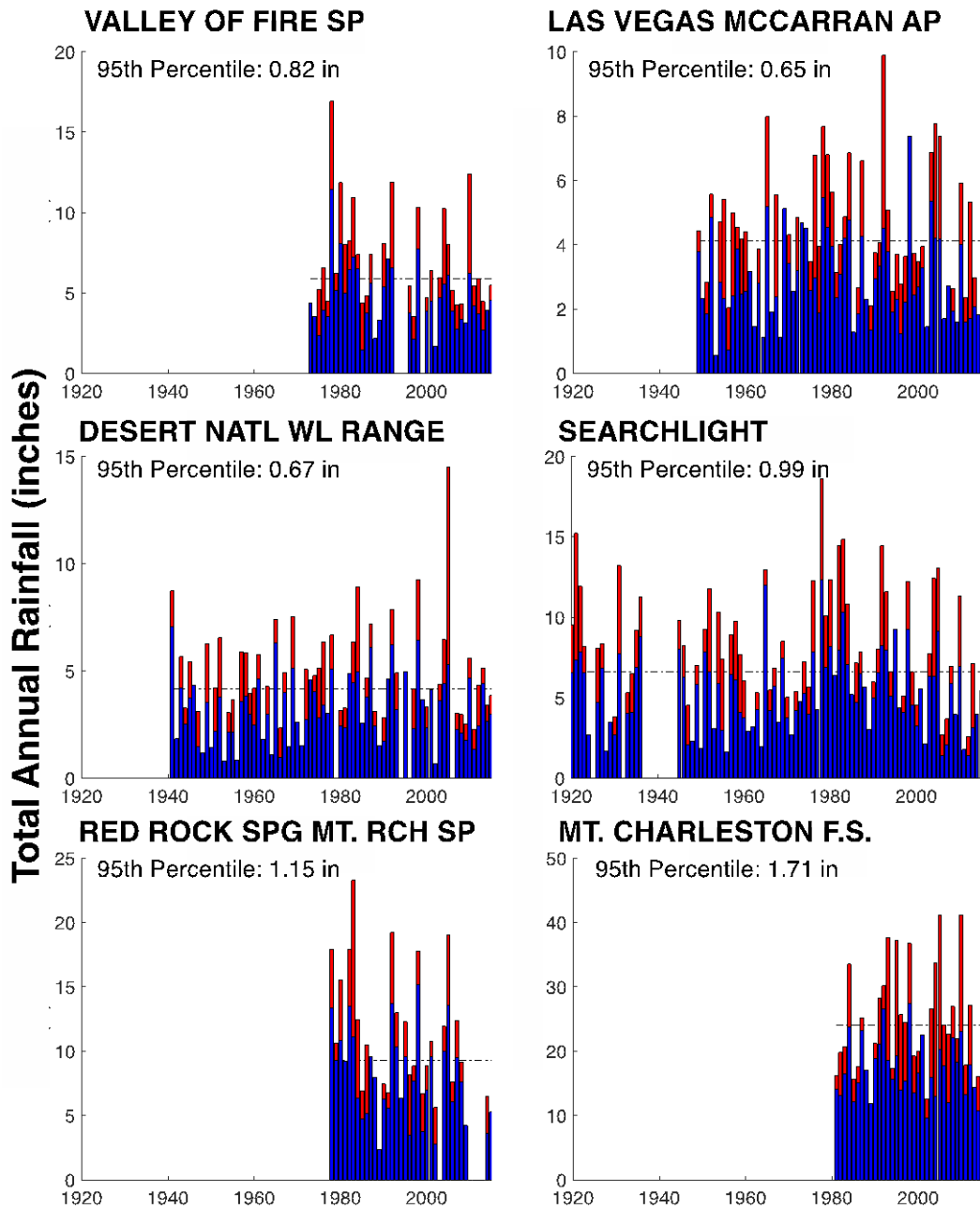
Figure 2-14. The total annual rainfall (inches) at each station. The dashed line is the average annual rainfall over the entire period-of-record. The height of the entire bar represents the total annual precipitation and the red portion is the contribution from events at or exceeding the 95th percentile. The 95th percentile threshold at each station is written in each panel. Note the scale change on the y-axis.

Table 2-4. The 30-year average of annual accumulated precipitation (in).

Annual Accumulated Precipitation (in)				
	1951-1980	1961-1990	1971-2000	1981-2010
VALLEY OF FIRE SP	N/A	N/A	N/A	5.99
MCCARRAN AP	4.19	4.14	4.49	4.20
DESERT NATL WL RANGE	4.24	4.01	4.38	4.73
SEARCHLIGHT	6.17	7.22	7.50	8.94
RED ROCK SPG	N/A	N/A	N/A	9.79
MT. CHARLESTON	N/A	N/A	N/A	23.45

Climate and weather extremes, particularly precipitation, are garnering attention recently, given recent tropical storms, Harvey, Maria and Irma in 2017. Some studies indicate that extreme precipitation intensities have already increased across the contiguous U.S. (Kunkel et. al. 2013), and a 2016 study suggests that both frequency and intensities will continue to increase with warming (Prein et al., 2017). These high intensity, but rare precipitation events are those most likely to lead to flooding - and costly damage. In the case of societal costs related to climate and weather- it is those rare extreme events that cause the majority of those costs (Peterson et al. 2008). Understanding if the occurrence of extreme events locally has changed historically, and whether we should expect their occurrence to change in the future is an essential step for planning. For the purpose of this report, identification of an extreme event is based only on precipitation amounts, not on the total monetary loss from events, which is influenced by the density and structural integrity of the built environment where the extreme event occurs.

Warmer temperatures cause more water vapor to be evaporated and held in the atmosphere. Globally, there has been an increase in water vapor of 3-5% since 1970s (IPCC 2013). At the local scale, it is unclear if that increased water vapor is translated into more frequent heavy or extreme precipitation events. Here the definition of "extreme event" includes all events with magnitudes greater than or equal to the 99th percentile of wet days at a given station over the 30-year period. By definition, these events are rare with 8-10 events during 1981-2010, with the exception of Mt. Charleston, which had 16 events. Mt. Charleston also has the highest threshold for a 99th percentile event, 3.24 inches of precipitation falling in a 24-hour period. McCarran has the smallest threshold, 0.96 inches.

In Figure 2-15, the number of 99th percentile precipitation events, or extreme precipitation events, is plotted against the backdrop of percent contribution of each month to total annual accumulation. Of all months, the occurrence of extreme precipitation events was greatest in December followed by February (Figure 2-15). These events, and other winter extremes are possibly related to inland penetrating atmospheric rivers, as 35-55% of the top 10% of 24-hour precipitation events during the winter months are associated with atmospheric rivers in this region (Rutz et al. 2014). Currently there is a research effort to improve the forecasts of these

extreme events and the inland penetration of the events to help emergency managers. The July and August events in summer are related to the Monsoon. It is also important to note the absence of these events. There are no 99th percentile events from 1981-2010 in April, May or June. Further analysis indicated the 99th percentile events are not becoming more frequent in the most recent decade relative to historic decades.
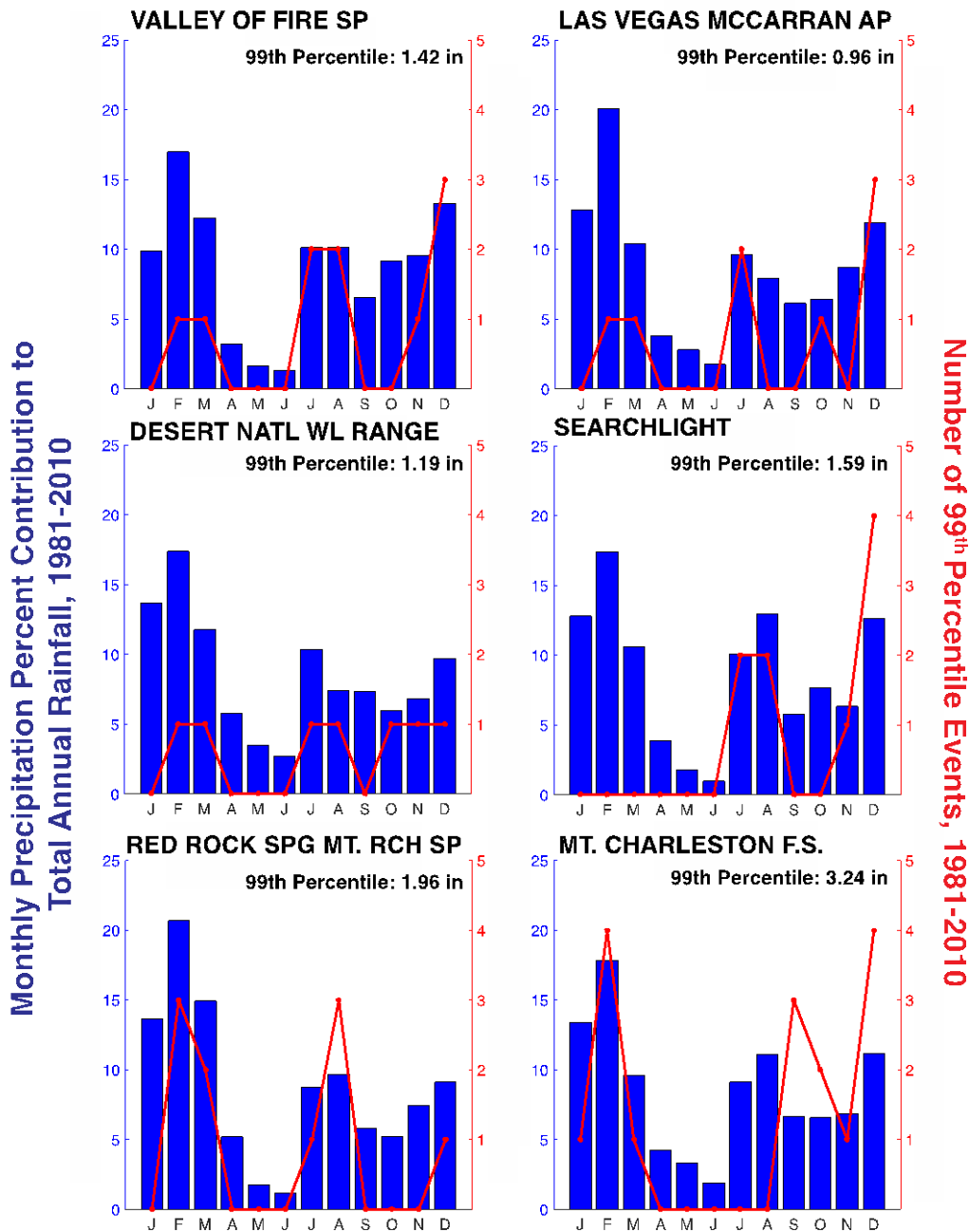

Figure 2-15. The blue bars depict the average monthly percent contribution of all precipitation to the total annual rainfall. Thus all 12 bars total 100%. As noted previously, at all six stations, February has the largest contribution to total annual precipitation. The red line is the number of extreme precipitation events, or 99th percentile events over 1981-2010.

Similar to temperature, understanding the spatial variability of precipitation is important. Figure 2-16 compares the number of days it rained at a specific station to when it rained at McCarran. This is represented as a fraction of the total raining days at McCarran. Approximately 50-67% of the days it rained at McCarran Airport it also rained at the other stations. During winter and spring the shared fraction of days are higher suggesting that winter and spring precipitation events are a result of larger regional storm systems. Summer months have the lowest fractions, presumably reflecting the more spatially spotty nature of the convective precipitation during the warm season. Mt. Charleston has the highest shared fractions for all seasons, which is likely a result of the fact that of all the stations it has the greatest number of days with precipitation resulting in increased common fractions with McCarran.
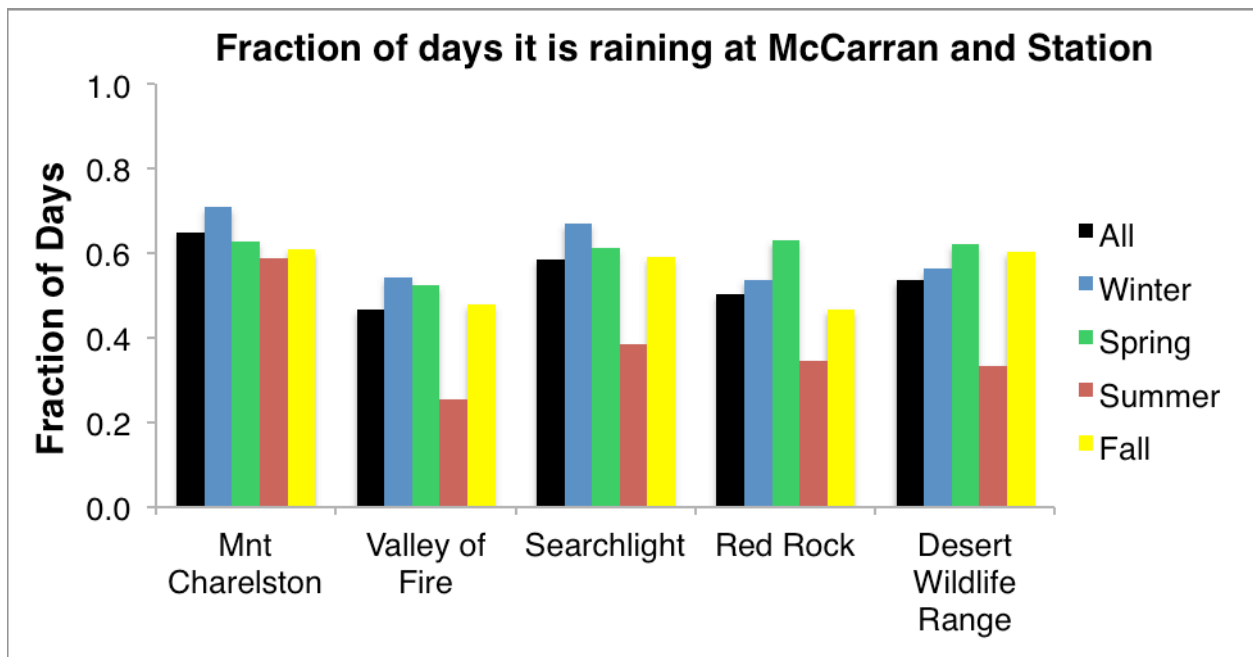
Figure 2-16. The fraction (or percentage) of time that if it is raining at McCarran it is also raining at the listed station using data from 1981-2010. The lowest percentage is during the summer, monsoon season, when the precipitation events are not spatially coherent.

2.3.3 Climate Oscillations

The El Niño - Southern Oscillation (ENSO) is a climate oscillation, or periodic fluctuation, that occurs in the Equatorial Pacific approximately every 2-7 years. ENSO is an interaction between the tropical atmosphere and ocean in which the winds affect Pacific Ocean temperatures which in return affects the strength of the winds creating a positive feedback. During El Niño events, the winds across the tropical Pacific are weaker and sea surface temperatures (SSTs) in the eastern tropical Pacific are warmer. In contrast, during a La Niña event, the winds are stronger and the SSTs along the west coast of the U.S. are cooler. The presence of an El Niño, or La Niña, can modify the atmosphere such that it affects typical

weather patterns throughout the world. Because an ENSO phase in the tropical pacific can be predicted 3 or more months in advance of onset (Jin et al., 2008) the relationship between ENSO phase (El Niño, La Niña or neutral) and precipitation and temperature are often used for seasonal forecasts across the U.S.

Using the Oceanic Nino Index (ONI), which is a three-month running mean of SST anomalies in the Niño 3.4 region (5°N-5°S, 120°-170°W), the precipitation-ENSO relationships for Clark County using data from Searchlight, McCarran Airport and Desert National Wildlife Range from 1950-2015 were examined. ONI anomalies with values greater than 0.5 define El Niño conditions and values less than - 0.5 signify La Niña conditions. Here, ONI values are averaged over January, February and March (JFM) because this provided the strongest correlation. For December – April precipitation, JFM ONI values explain about 18% of the variability (r^2 =0.18) (Figure 2-17, top). All December-April periods with more than 5 inches of precipitation occurred when the ONI index was 0.3 or above, suggesting that an El Niño is not necessary to have a wet winter; however, historically there is no precedent for a wet winter if the ONI value is below 0.3 (i.e. neutral or La Niña conditions).

The wettest winters did occur when the ONI values were between 0.3 and 0.6 indicating that a strong El Niño does not necessarily mean a very wet atmospheric response over southern Nevada. Further, in all cases when the ONI is above 1, the region received 2 inches of rain or more suggesting that very dry winters are not likely to occur during moderately strong El Niño events. There is a weak relationship with T_{max}, but similar to precipitation in that the ENSO strength provides some bounds on the expected seasonal conditions (Figure 2-17, bottom). For example, the coldest winters do not occur during La Niña events over 1.0 and the warmest winters do not occur during El Niño events over 1.0. There is no relationship with T_{min}.

In addition to ENSO, it was previously shown that the Pacific Decadal Oscillation, a pattern of Pacific climate variability similar to ENSO in character but oscillates on a much longer time scale, 10-30 years, can affect the amount of precipitation in southern Nevada (Dettinger, Nevada Water Resource Association Meeting, 2015).
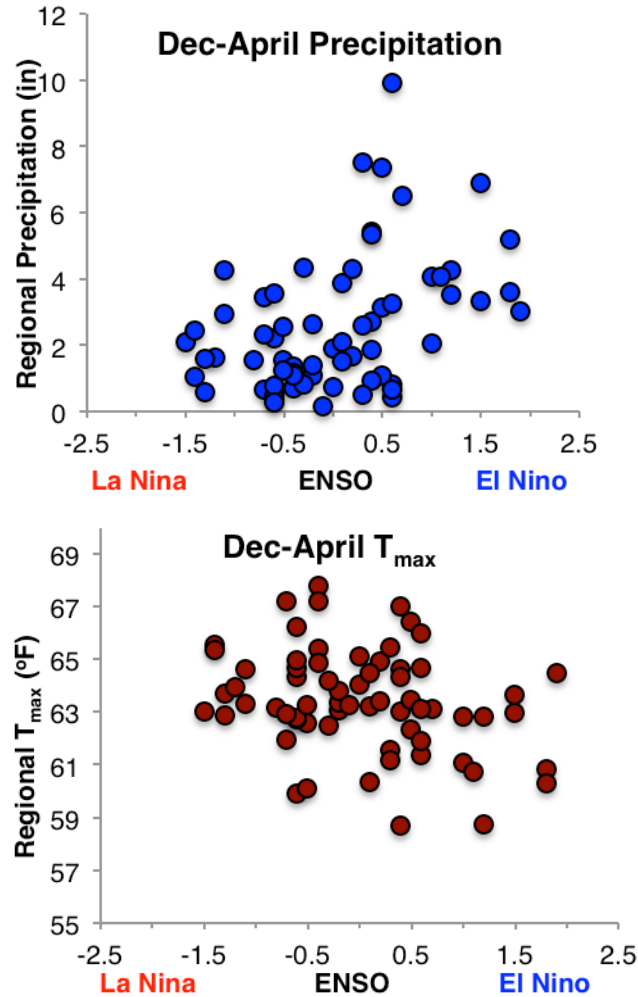
Figure 2-17. (Top) December -April precipitation (averaged from Searchlight, McCarran Airport, and Desert National Wildlife Range) plotted against the January-March ONI values, or sea surface temperature anomalies in the tropical Pacific. More negative ONI values correspond to cooler ocean temperatures that define La Niña events. (Bottom) Same as top, but for T_{max}.

2.3.4. Atmospheric Patterns for Wet Months, Cold Months and Heat Waves

To understand what atmospheric patterns are driving monthly variability in the Clark County region, the wettest months over the period 1981-2010 were identified for both the warm and cool seasons, and the coldest months and the most significant heat waves were identified for the same period. For each month that produced these end member climate conditions, the atmospheric setup over the equatorial Pacific and western U.S. were evaluated. The objective was to determine if there was a common atmospheric synoptic scale set up, that led to each of these anomalous inland conditions. The results from this analysis will be used in the model selection process in Chapter 3.

The four analyses of atmospheric patterns leading to outlier climate conditions in Clark County over the period 1981-2010 are displayed in Figure 2-18 through Figure 2-21. Figure 2-18 displays the 10 winter months with the coldest average T_{min} value at McCarran. Every 1981-

2010 cool season month (DJF) was evaluated to see which month and year produced the most number of wet days (Figure 2-19). The number of wet days was used rather than the total precipitation because the number of wet days in a given period generally has a greater impact on water demand.

In contrast, Figure 2-20, displays the 11 months of the 1981-2010 summer season months (JAS) with the most number of wet days in Clark County. Figure 2-20 indicates the 10 hottest heat waves that occurred in the region from 1981-2010. Heat waves were examined rather than the hottest 10 months, because when the hottest 10 summer months were determined, they all occurred in July and likely were a reflection of the long, hot days during this month rather than an anomalous feature. Heat waves were determined using the same method as Gershunov et al. (2009), which counts the degrees above the 95th percentile for a given day at a given station. The total degrees above this threshold for each station were then summed to determine the severity of the heat waves regionally. All of the "top 10 analyses" were done from 1981-2010. All synoptic patterns are showing the 500 millibar height anomalies using NCEP/NCAR reanalysis (Kalnay et al. 1996), with warm colors indicative of a high pressure and cool colors indicative of low pressures.

In examining the cases in more detail, there are some atmospheric patterns that emerge for the coldest months, wettest winter months and heat waves, however no patterns are apparent for the wettest summer months. Even in cases where there are common patterns in the "top 10", there is still much variability between each month as would be expected. In 8 of the coldest months, there is a high-pressure system off the coast of North America with an adjacent low-pressure system bringing cold air from the north which causes these cold months, although the intensity and exact location of the low-pressure system varies (Figure 2-18). For most of the 10 wettest winter (DFJ) months in the region, a low-pressure system is located off the coast of North America which leads to an atmospheric circulation that brings in moisture from the Pacific (Figure 2-19). Of these 10 months, 7 of them are also the 10 wettest months using the total precipitation in the region. No clear pattern emerges during the top 11 wettest summer months (not shown). Of these 11 months, 6 of them are also on the list of the top 10 wettest summer months if total precipitation was used rather than the number of wet days per month.

In a brief comparison, we examined the cloud albedo, an indicator for cloudiness, during the 6 wet months from 1996 onward (not shown). Of the 6 months, 5 months had an anomalously high cloud coverage over the southern half of Nevada while much of the Pacific Northwest and the coastal ocean had anomalously low cloud cover. Further analysis is needed to better understand this relationship between cloudiness, wet summer months and potential temperature variability throughout the region. The 10 most extreme heat waves in the region show a high-pressure system over much of the southwest with anomalies typically greater than 50 millibars (Figure 2-20). The locations of the surrounding low-pressure systems are highly variable.
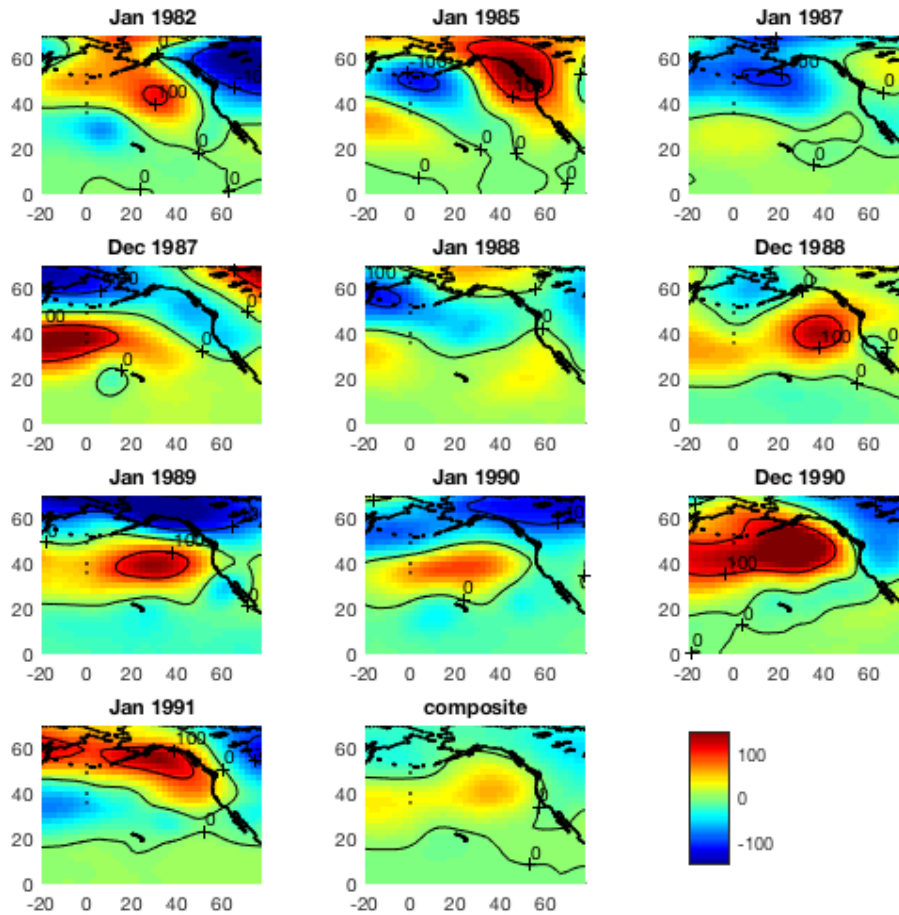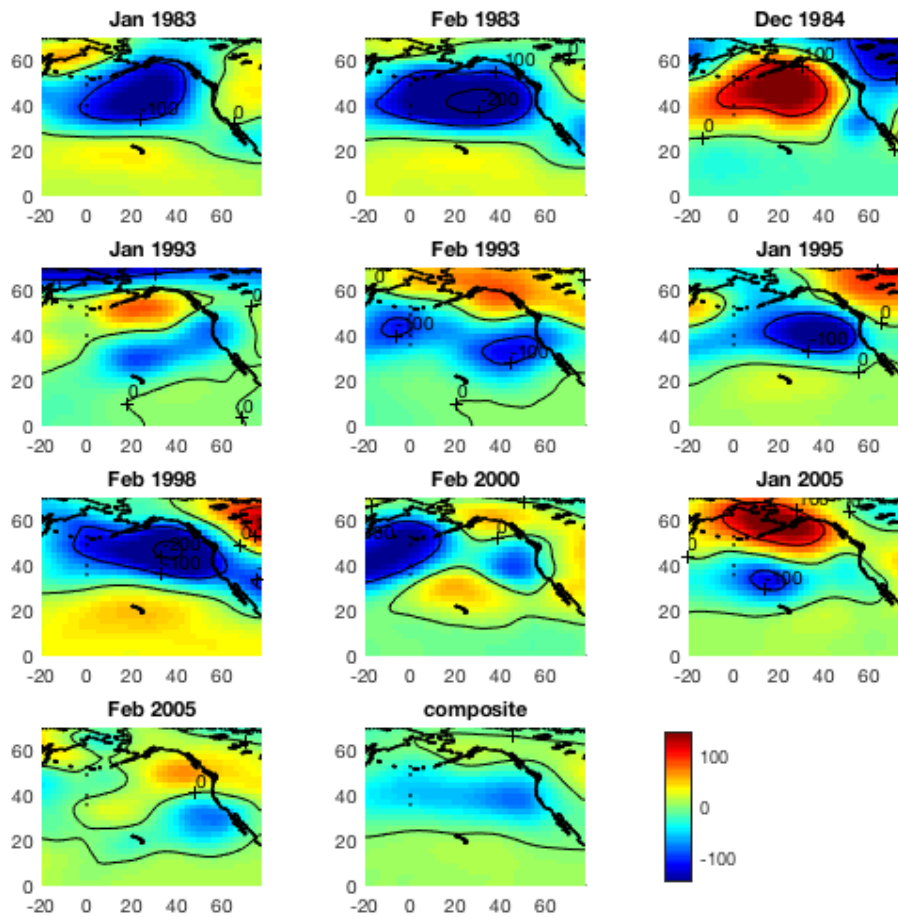
Coldest 10 Months

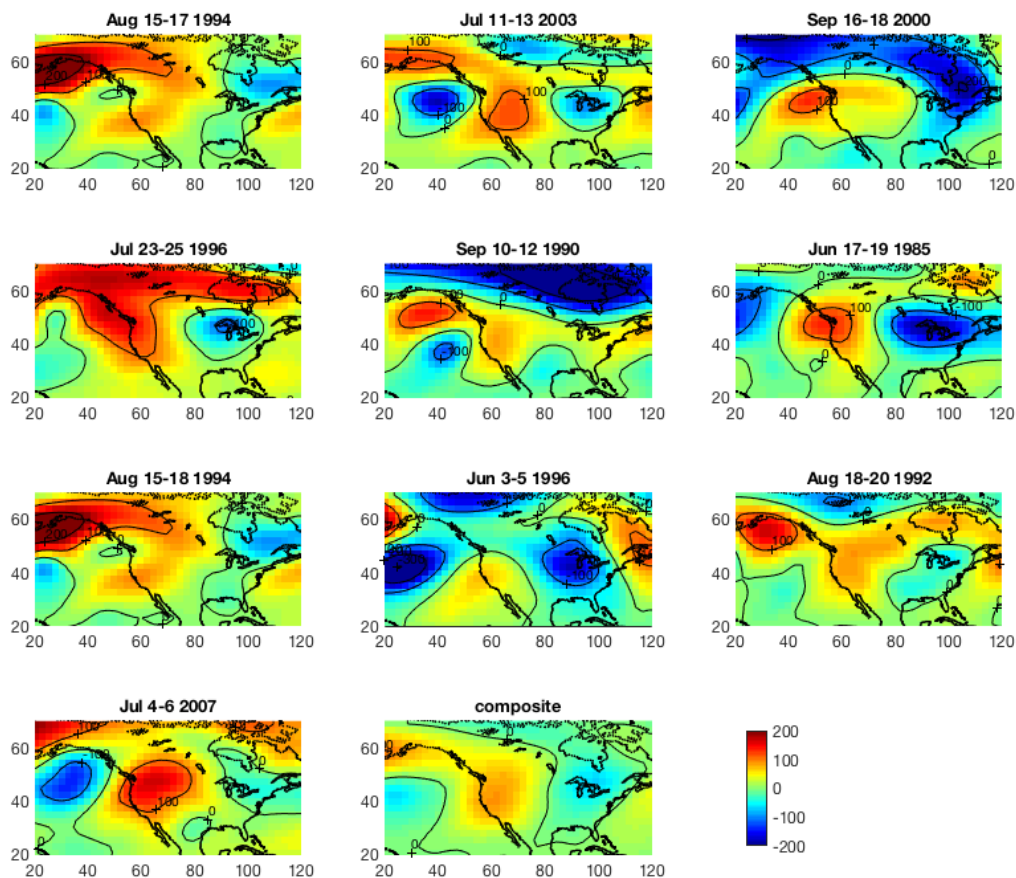*Figure 2-18. Atmospheric circulation (500 millibar height anomalies) for the 10 coldest months at McCarran Airport for the time period between 1981-2010 are illustrated here. The last is the composite, or average, of all 10. Generally, the high-pressure system off the coast of North America and low-pressure to its east results in northerly wind flows which advects cold winter continental air into southern Nevada.*

Wettest 10 Winter Months

Figure 2-19. Atmospheric circulation (500 millibar height anomalies) for the 10 months with the greatest number of wet days in December-January-February at McCarran Airport for the time period between 1981-2010. The last is the composite, or average, of all 10. Generally, when there is low-pressure from the North Pacific across the west coast of North America, North Pacific storms are able to penetrate inland to the Clark County region.

Heat Waves

Figure 2-20. Atmospheric circulation (500 millibar height anomalies) for the 10 most extreme 3 and 4-day heat waves at McCarran Airport for the time period between 1981-2010. The last is the composite, or average, of all 10. During these events, there is an extensive high-pressure system over much of the Southwest. These conditions usually create clear skies and sinking motions over the region which result in high daytime temperatures.

2.4. Summary

The historical summary supports many observations that have previously been noted, as well as bringing to light some new observations particularly with a broader spatial view of the region. The increase in T_{min} was previously noted by SNWA at McCarran, and although it is the strongest at McCarran, the stronger trend in T_{min} relative to T_{max} is documented throughout the region. Unlike temperature, there are no significant trends in precipitation and the large events have occurred sporadically throughout the historical record. El Nino-Southern Oscillation (ENSO) explains 18% of the precipitation variability and places some bounds on what to expect for winter (December-April) precipitation and T_{max} for the region. Specifically, the region tends to be warmer and drier during La Nina events, and cooler and wetter during El Nino events.

Lastly, the wet winter months and cold winter months often have signature atmospheric patterns, with low-pressure systems present over the region. Similarly, heatwaves typically are associated with high-pressure systems over the Clark County region. The observations and analyses in this section will be used and referred to in the model selection and future projections chapters (Chapter 3 and Chapter 4).

3. Global Climate Model Selection

3.1 Introduction

Global Climate Models (GCMs) provide simulations of how the Earth's climate evolves under different conditions, such as different atmospheric concentrations of greenhouse gas emissions (GHGs), and are currently the best tool for examining potential future climate scenarios. GCMs are mathematical representations of the Earth system and simulate the complex interaction between the atmosphere, the oceans, the land surface, glaciers, and sea ice. In addition to simulating climate conditions through the end of the 21st century, the same models simulate climate conditions for the historical period using observations of solar radiation, volcanic eruptions, greenhouse gas and aerosol emissions, and land use (Taylor et al., 2012). Historical simulations can be compared to observations to determine how well the model represents past climate (Gleckler et al., 2008; Pierce et al., 2009; Sillmann et al., 2013). There are over 30 GCMs, developed at numerous international research institutions, used to project how climate may evolve through time. All of these models are run under an agreed upon set of scenarios to facilitate the comparison between the models and present a range of future outcomes. This range or difference in model simulations is one type of "uncertainty."

Individual GCM results differ for numerous reasons, including the resolution of the model (the distance between grid cells), the unique parameterizations each model uses, the external forcing used, and natural climate variability. Parameterization mathematically simplifies processes through the use of equations and applies it over a larger scale. Parameterizations are used when physical processes, such as the treatment of ice crystals in clouds, occur at smaller scales than the grid resolution and cannot be properly modelled. External forcing, or perturbations, refers to different factors that affect the Earth's climate and "force" or drive the climate system to change. External forcing's include solar variations, volcanic eruptions, greenhouse gas emissions, and aerosols. Natural climate variability refers to the range in outcomes from internal interactions between components of the climate system, and is built into the models (Deser et al., 2012). Despite these components of modeling, uncertainty in how much climate will change by the end of the century is dominated by what, if anything, people do to address rising GHG concentrations in the atmosphere (Hawkins and Sutton, 2009).

There is no perfect model, but modeling the Earth system has improved steadily over the years (IPCC, 2013, Knutti et al., 2013). Some models do a better job of representing parts of the climate system than others. The objective of the climate model selection process was to derive a practical number of GCMs that best capture historical climate variability in southern Nevada. The approach was based on previous research that applied a similar methodology to provide guidance on the most representative models for California (Cayan and Tyree, 2015).

3.2 Methodology

The most recent Coupled Model Intercomparison Project (CMIP5) provides more than 30 GCM simulations forced using multiple greenhouse gas and aerosol emission scenarios allowing for a comparison of future climate projections. The 30 historical model runs were evaluated on how well they represented observed climate variables. The evaluation process used here was similar to that used in Cayan et al., (2015) and began with a global perspective, stepping down to the southwest and finally southern Nevada (Figure 3-1, Table 3-1 and Table 3-3).

Choosing Global Climate Models for Southern Nevada Water Authority

Criteria
- Scientists recommend using information from several Global Climate Models
- Using information from all available GCMs isn't practical
- Remove GCMs that fall short in representing historical climate and hydrologic processes important for Southern Nevada

Method

Global

Western U.S.

Southern Nevada

6 GCMs

Start with 31[1] GCMs

Global Climate Evaluation[2,3]
Evaluate how each GCM represents global historical
- Solar Radiation
- Air Temperature
- Atmospheric Pressure, Wind

Remove ~12 GCMs

Western U.S. Climate Evaluation[4]
Evaluate how each GCM represents Western US historical
- Air temperature & Precipitation
- Atmospheric Pressure Patterns
- El Nino Southern Oscillation Patterns

Remove ~4 GCMs

Southern Nevada Climate & Extremes Evaluation
Evaluate how each GCM represents Southern Nevada historical
- Air Temperature
- Precipitation
- Atmospheric Circulation Patterns

Remove 9 GCMs

GCM Recommendations for Southern Nevada
The remaining 6 GCMs are recommended for SNWA because they represent important components of historical climate at global, regional, and statewide scales.

References:
[1]Available GCMs at the start of the investigation period and similar to Cayan et al. (2015).
[2]Gleckler, P. J., K. E. Taylor, and C. Dourtriaux: Performance metrics for climate models, J. Geophys. Res.-Atmos (2008).
[3]IPCC, Climate Change 2013: The Physical Science Basis, Cambridge University Press, Cambridge, UK and New York (2013).
[4]Rupp, D. E., J. T. Abatzoglou, K. C. Hegewisch, P. W. Mote: Evaluation of CMIP5 20th century climate simulations for the Pacific Northwest USA, J. Geophys. Res.-Atmos (2013).

Figure 3-1. A flow chart representing the model selection process. Note that the first two steps and results from this analysis are described in more detail in Cayan and Tyree, 2015. The figure is modified from Cayan and Tyree, 2015.

The initial elimination of lower-performing global climate models was based on the work of Gleckler et al. (2008), which evaluated the global climatology of atmospheric variables in historical GCM runs to reanalysis data sets. This process eliminated 12 GCMs. The next round of model eliminations was based on the methods used in Rupp et al. (2013), which evaluated models for the Pacific Northwest against historical data, but was done for the Southwest (including Clark County). The models were evaluated on their representation of historical Southwestern temperature and precipitation, including the diurnal temperature range, the seasonal cycle, annual temperature variability, and the coefficient of variation and correlation of winter temperature and precipitation with a measure of the El Nino/La Nina cycle, the Nino3.4 index (Figure 3-1, Table 3.1 and Table 3.3). This eliminated an additional 4 GCMs. The remaining 15 models were then examined regionally against historical data, specifically McCarran station, for southern Nevada, which is the focus of this section.

To impartially compare the 15 GCM historical simulations with different model resolutions, each GCM's data was interpolated to the same 2° x 2° grid using bilinear interpolation (Adams, 1994). The various GCMs use different grids and because of this, interpolating or regridding is necessary to compare the same spatial domain. The regridding process resulted in four grid boxes over southern Nevada (Figure 3-2), each representing climate in four sub-regions near southern Nevada.
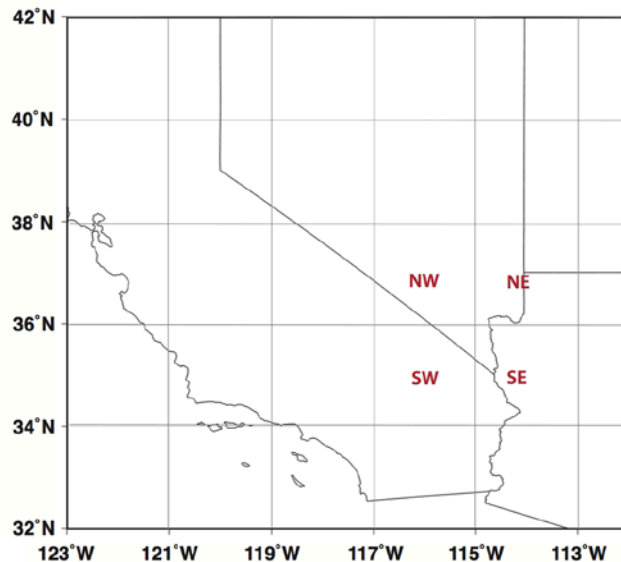
Figure 3-2. Map of location of four GCM interpolated grid boxes (2° x 2°) used in this report over southern Nevada for GCM evaluation and future climate projections.

Based on historical observations (Chapter 2) several climate variables were used to identify which of the 15 GCMs best represent Clark County climate. The variables used for the selection were based on the relevance to water management in the region, what variables were not already considered in the prior evaluations (Figure 3-1, Table 3-1), and what variables would be readily improved through bias correction. A simple example of a bias correction is if the model is always 2°F warmer than historical, then bias correcting the model would mean subtracting

2˚F from the final value. Based on these guiding principles, the following variables were selected:

    a. Standard deviation in daily T_{max} during four seasons: April-May, June-July-August-September, October-November, and December-January-February-March. This was calculated separately for each seasonal period and year.

    b. Number of wet days during July-August-September and December-January-February-March

    c. Atmospheric circulation patterns based on 500 hPa geopotential height anomalies for:
- 10 Coldest Months
- 10 Wettest Months (based on number of wet days, and then precipitation total)
- Top 10 3-day Heat Waves

Standard deviation of T_{max} was selected because periods of anomalously high maximum temperatures represent periods of high water consumption particularly for outdoor irrigation. As a result, how well models do in representing the T_{max} variability and in different seasons is important for considering future conservation efforts.

The second selection criteria were the number of wet days in southern Nevada's two primary precipitation seasons, winter (December-March) and the summer monsoon (July-September). In this study, for a day to be considered a precipitation day, the total daily precipitation had to exceed 1 mm/day because GCMs have a tendency to over produce small amounts of precipitation (Pendergrass and Hartmann, 2014). The number of wet days was used rather than total precipitation because a wet day and the associated cloud cover reflect days of lower water consumption, particularly in summer months.

Both the standard deviation of T_{max} and the number of wet days in the historical runs were compared against daily temperature and precipitation observation from McCarran. The difference between the models and McCarran for the mean and standard deviation were considered for the four grid boxes and for the aforementioned seasons.

Note that the months included in each season for the selection criteria differs between temperature and precipitation. This was done based on the results from the historical analysis. For T_{max}, the shoulder seasons in the model selection process were defined as April-May and October-November. This was done because these seasons have the largest range of temperatures (Figure 2-9), and typically demonstrate the largest variability in water use year-to-year. The precipitation seasons, winter (December – March) and summer (July-September), were based on the winter and summer months that receive the most amount of precipitation (Figure 2-15).

Another selection criterion was based on the models' ability to represent atmospheric circulation patterns that are historically associated with extremes. The climate extremes chosen were the coldest winter months, the wettest winter months, and 3-day heatwaves. The

underlying assumption is that models that produce climate extremes for the right atmospheric reasons are more reliable for the future projections. For each of the 15 models, the atmospheric circulation patterns associated with the ten coldest winter months, wettest winter months, and heatwaves were compared to the corresponding observed composites in Chapter 2 (Figure 2-18 through Figure 2-20). The comparison used the dot product (similar to a pattern correlation) for a quantitative evaluation. Two of the models, CESM1-BGC and CESM1-CAM5, did not have the necessary atmospheric variables to do this analysis and therefore were only evaluated on the T_{max} standard deviation and number of wet days.

Lastly, the final selection criteria were "model genetics", or if the model was developed by the same institution and had similar internal structure (Knutti et al., 2013). For example, although two models from the UK Hadley center, HadGEM2-ES and HadGEM2-CC, ranked highly, only one of the HadGEM2 models were selected. Selecting models from different lineages increases the likelihood that a wide range of solutions are included in the selection. Further consideration was given to what models are being used in other regional studies such as the National Climate Assessment Report 4 in order to better leverage the results from these on-going studies.

Table 3-1. The metric and description of the variables used to select models at the different spatial scales

Metric	Description
Global Metrics (Glecker et al. 2008)	
LW CRE, SW CRW	Longwave (LW) or Shortwave (SW) Cloud Radiative Effects
RSUT RLUT	Top of the Atmosphere Reflected Shortwaves (S) and Longwave (L) Radiation
PR	Total Precipitation
TAS	Surface Air Temperature
ZG (500 hPA)	Geopotential height
VA & UA (200 hPa) VA & UA (850 hPa)	Meridional (VA, North-South) and Zonal (UA, West-East) wind speeds at two different levels in the atmosphere 200 hPA and 850 hPa
TA (200 hPA), TA (850 hPA)	Temperature at two different levels in the atmosphere, 200 hPA and 850 hPa
Western United States Metrics (Rupp et al., 2013)	
Mean-T and Mean-P	Mean Annual Temperature (T0 and Precipitation (P), 1960-1999
DTR-MMM	Mean diurnal temperature range, 1950-1999
SeasonAmp-T SeasonAmp-P	Mean amplitude of seasonal cycle as the difference between the warmest and coldest month (T) or between the wettest and driest month (P), 1960-1999. Monthly precipitation calculated as percentage of mean annual total
SpaceCor-MMM*-T SpaceCor-MMM*-P	Correlation of simulated with the observed the mean spatial pattern of temperature and precipitation, 1960-1999
SpaceSD-MMM*-T SpaceSD-MMM*-P	Standard deviation of the mean spatial pattern of temperature and precipitation, 1960-1999
TimeVar.1-T to TimeVar.8-T	Variance of temperature calculated at frequencies (time periods of aggregation) ranging for N=1 and 8 years, 1901-1999
TimeCV.1-P to TimeCV.8-P	Coefficient of variation (CV) of precipitation calculated at frequencies (time periods of aggregation) ranging for N=1 & 8 water years**, 1902-1999
Trend-T and Trend-P	Linear trend in annual temperature and precipitation, 1901-1999
ENSO-T and ENSO-P	Correlation of winter temperature and precipitation with Niño 3.4 index, 1901-1999
Hurst-T and Hurst-P	Hurst exponent using monthly difference anomalies (t) of fractional anomalies (p), 1901-1999.
Southern Nevada Metrics	
Seasonal-T_{max}Stdev	T_{max} standard deviation seasonally (DJFM, AM, JJAS, ON) relative to McCarran
WetDays-Winter, WetDays-Summer	Number of wet days in winter (DJFM) and summer (JA) relative to McCarran
Atmospheric circulation patterns associated with extremes	Compare the atmosphere circulation patterns (500 mbar height anomalies) during wettest winter months, coldest months and 3-day heat to a composite from reanalysis data
Miscellaneous	
Model genetics	Only one model from the same model family was included in the selected models to represent model diversity.

3.3 Results

The paragraphs below discuss the analysis and the results of comparing the historical runs (1950-2000) for the 15 models to observations, which in this case was McCarran station. Based on the results presented below, 6 models: ACCESS1-0, CCSM4, CMCC-CMS, CNRM-CM5, HadGEM2-ES, and MPI-ESM-LR, were chosen for southern Nevada.

3.3.1 Annual Seasonal Number of Wet Days

As discussed, one of the evaluation criteria for selecting the GCMs, was the number of wet days in winter and summer. The two seasons were examined separately because precipitation in each season is generally caused by different weather patterns, and the skill of each individual GCM to represent the two seasons varied. The GCMs better represent the mean observed McCarran Airport number of wet days in summer than winter (Figure 3-3 and Figure 3-4). Most of the GCMs overproduce the number of wet days during winter and have a larger interannual variability than McCarran as demonstrated by the standard deviation of the number of wet days (Figure 3-5). More specifically, CNRM-CM5, HadGEM2-ES, CMCC-CM (not included in the final 6), and CanESM2 were the GCMs that were the most similar to McCarran, while BCC-CSM1-1 and GFDL models were the least similar (Table 3-2). This remained largely true in summer, with the exception of the CanESM2 model, which did not perform as well during summer. Both ACCESS1-0 and MPI-ESM-LR models were moderately successful when compared to observations. Differences in the GCM rankings varied across the 4 grid boxes, as inherently some grid boxes were in drier locations and the latitude of the storm tracks varied in the GCMs.
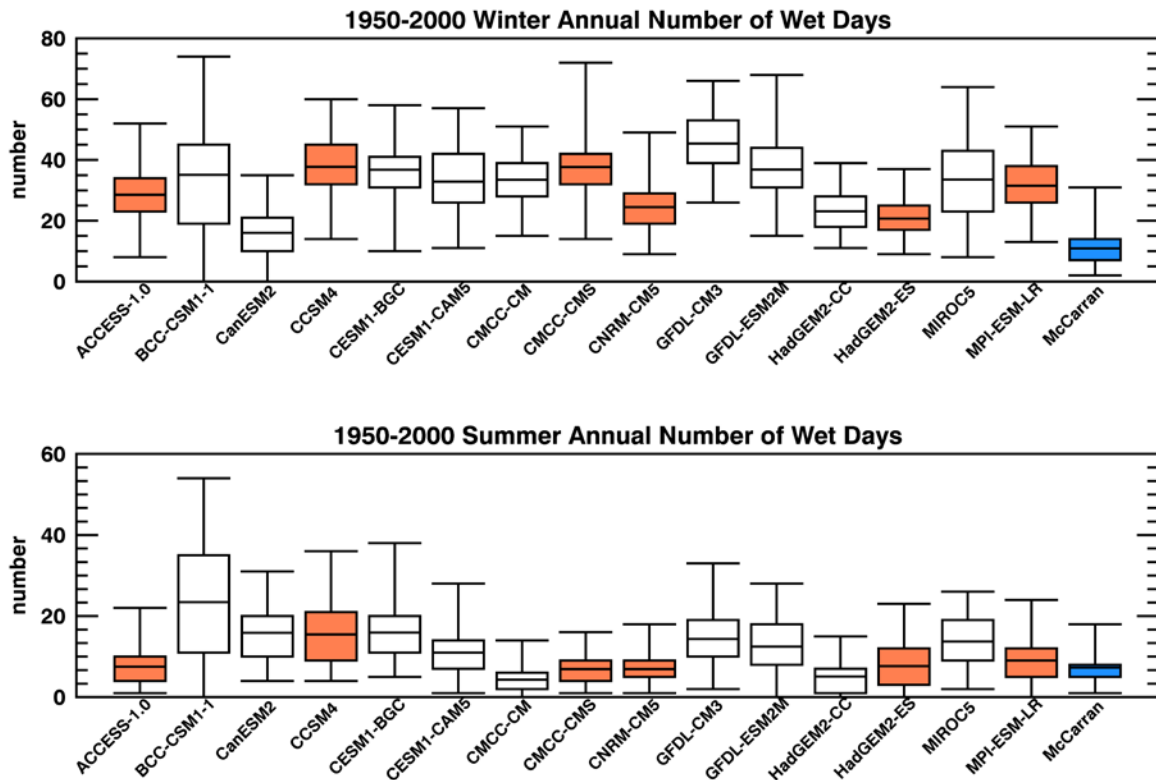
Figure 3-3. The range in annual number of wet days in (top) December-January-February-March & (bottom) July-August-September for 15 GCMs from the NE grid box. The middle line is the mean, the top and bottom of the box are the 25th and 75th percentiles and the outer bounds are the maximum and minimum values. The orange models are the selected models and blue is McCarran for reference.
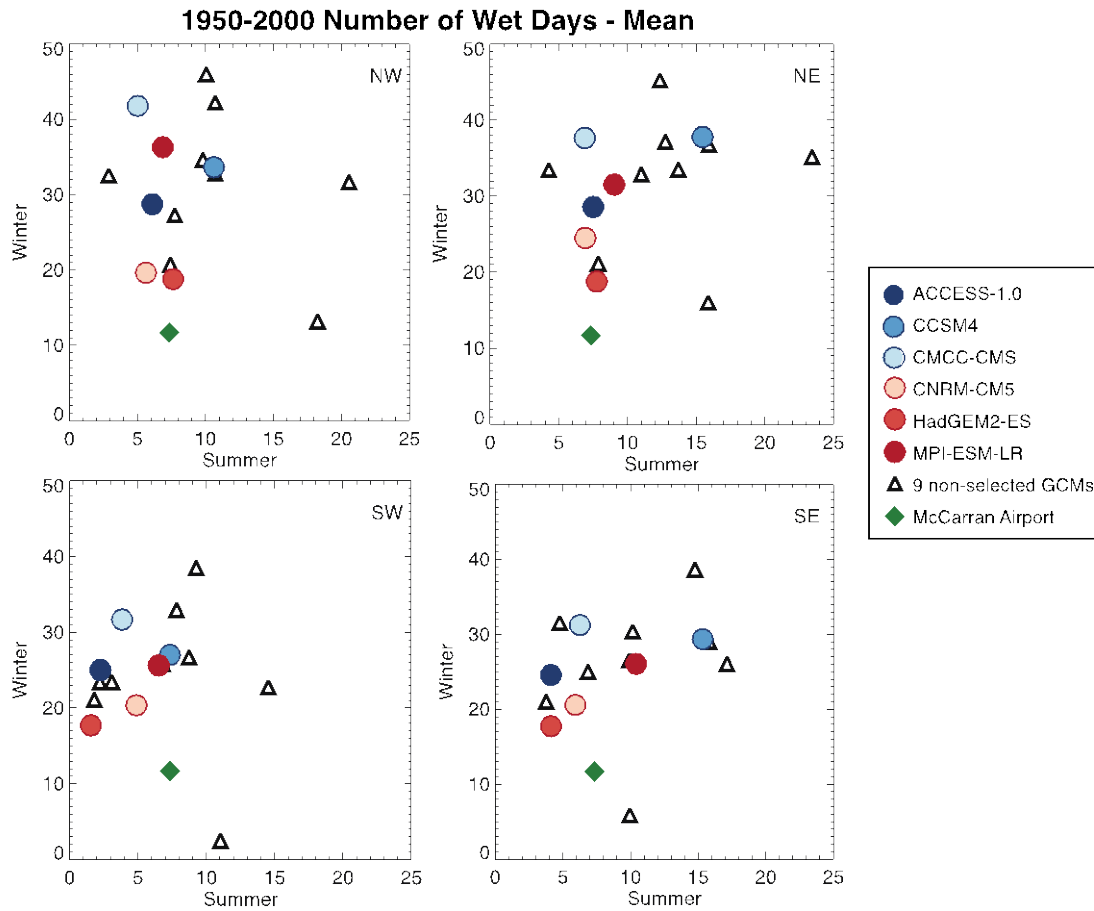
Figure 3-4. The mean number of wet days during winter (y-axis) and summer (x-axis) relative to the observed at McCarran for the 15 models analyzed for southern Nevada. The colored circles are the selected models and the open triangles are the models that were not selected. The green diamond represents McCarran. Most models had more wet days during winter than McCarran.
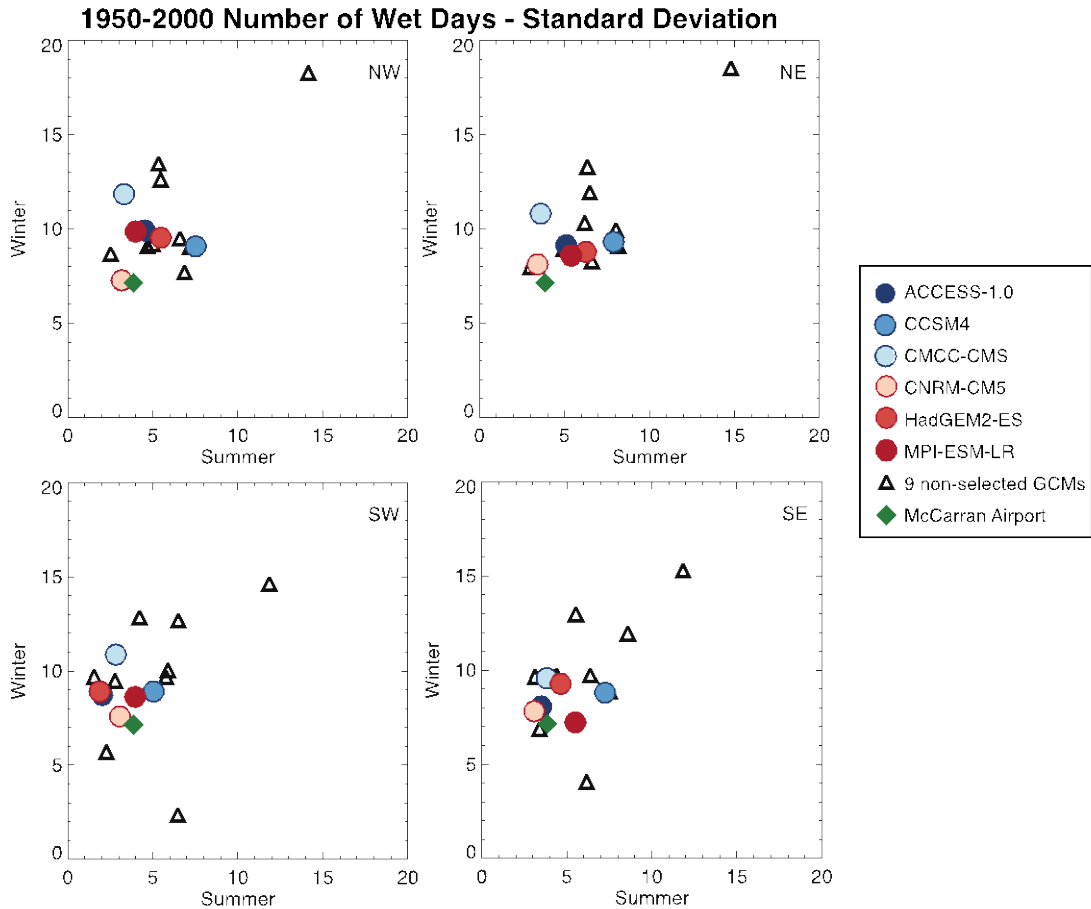
Figure 3-5. Same as Figure 3-4, but for the standard deviation of the number of wet days. Models generally had high winter variability relative to McCarran.

3.3.2 T_{max} Standard Deviation

In comparing the 15 climate models to McCarran over the historical range 1950 to 2000, the year-by-year standard deviation of daily T_{max} range for fall (October- November) most closely represented the McCarran range. During the other seasons, the models generally overestimate the range across the years of daily T_{max} standard deviation. (Figure 3-6 and Figure 3-7). This is generally true for all four of the grid-boxes, though only the NE gridbox is shown. The four models that did the best job of capturing the historical variability were HadGEM2-CC, HadGEM2-ES, CMCC-CM and CMCC-CMS, however there is little agreement between what models did best for each season. The models that were in the mid-range include ACCESS1-0, CCSM4, CESM1-BGC and MPI-ESM-LR. The models that poorly represented T_{max} standard deviation for all grids were CanESM2 and MIROC5.

50
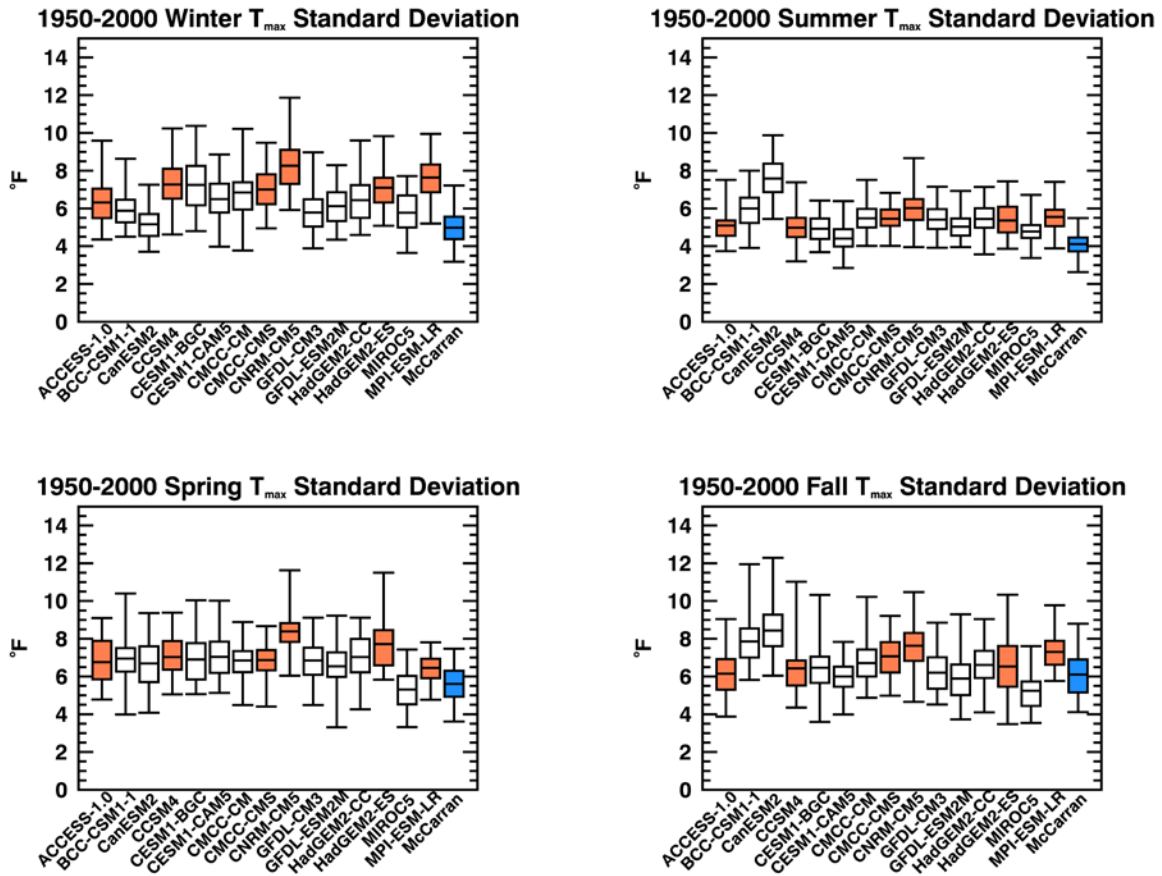
Figure 3-6. The range in year-by-year standard deviation of daily T_{max} for the four seasons for 15 GCMs from the NE grid box. The middle line is the mean, the top and bottom of the box are the 25th and 75th percentiles and the outer bounds are the maximum and minimum values. The orange models are the selected models and blue is McCarran for reference.
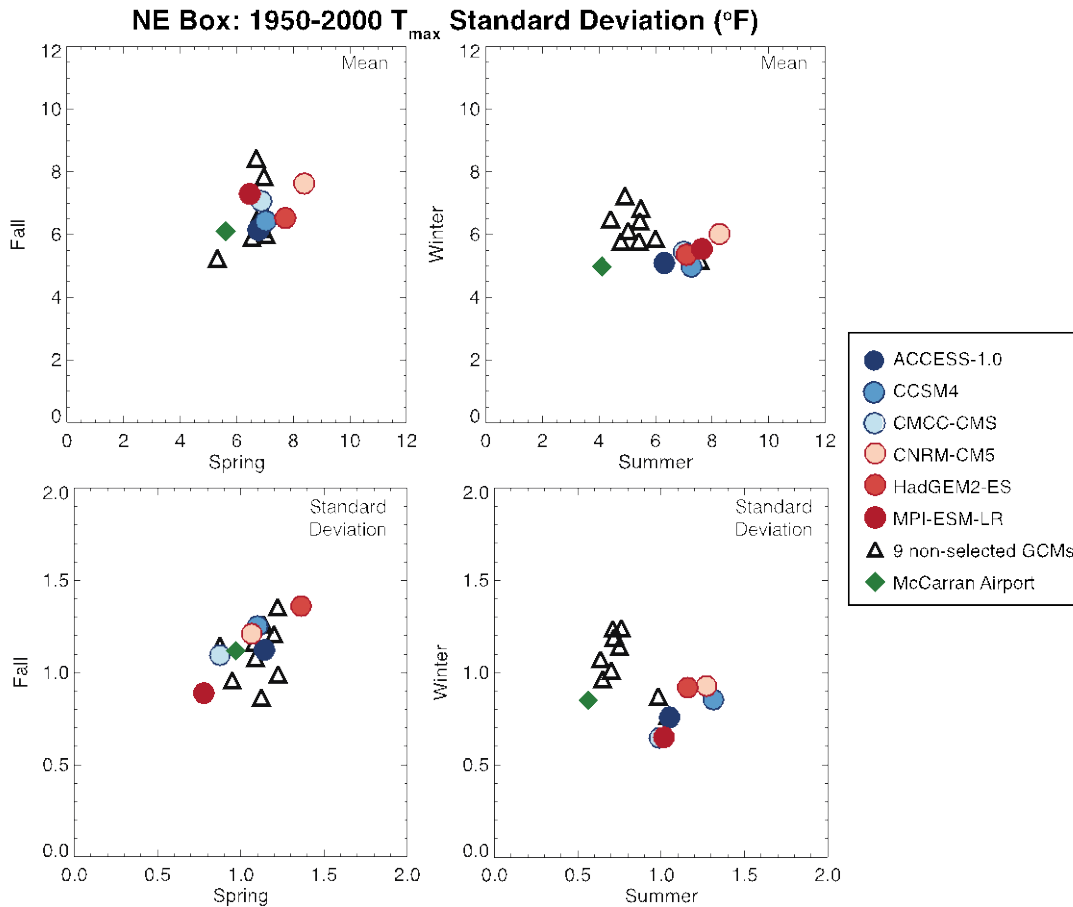
Figure 3-7. Top: the mean, across all years, of daily T_{max} standard deviation calculated separately for each season and year. Bottom: the standard deviation of the time series of yearly values for the NW grid box. The figures on the left show the results for spring and fall and the figures on the right show the results for winter and summer.

3.3.3 Climate Maps

For each of the three extremes that were examined (the coldest winter months, the wettest winter months and heat waves), the models represented the observed atmospheric patterns better overall for the heatwaves and wet winter months, relative to the cold winter months. The performance amongst the models in capturing the atmospheric set-up was generally consistent amongst the extremes. The models that always ranked in the top 6 were ACCESS1-0, CCSM4, CMCC-CM, CMCC-CMS and GFDL-CM3. The models CanESM2, BCC-CSM1, and MIROC5 consistently did poorly.

3.3.4 Model Genetics and Other Considerations

Table 3-2 shows the results of the selection criteria applied to the 15 models evaluated over southern Nevada. The final 6 selected models are shown in bold. Cases where a model was rejected due to having model genetics similar to another selected model are noted. The other consideration was the preference for models used in the 4th National Climate Assessment (USGCRP, 2018) because common models will allow for a comparison between the federal

project and this local focus. The models that were selected for this reason are noted as "Part of 4th NCA."

Table 3-2. The results of the evaluation of based on the different variables. The models that did poorest are indicated by a blue shading, the best by a dark gold and the mid-range models by a light gold.

Global Climate Model	Wet Winter Months	Wet Summer Months	T_{max} Standard Deviation	Atmospheric Circulation Patterns	Notes
ACCESS1-0	light gold	dark gold	light gold	dark gold	
BCC-CSM1-1	blue	blue	blue	blue	
CanESM2	dark gold	blue			Part of 4th NCA*
CCSM4			light gold	dark gold	Part of 4th NCA*
CESM1-BGC		blue	light gold	No Data	
CESM1-CAM5		light gold		No Data	
CMCC-CM	dark gold	light gold	dark gold	dark gold	model genetics
CMCC-CMS		dark gold	dark gold	dark gold	
CNRM-CM5	dark gold	dark gold			
GFDL-CM3	blue			dark gold	
GFDL-ESM2M	blue				
HadGEM2-CC	light gold	light gold	dark gold		model genetics
HadGEM2-ES	dark gold	light gold	dark gold		Part of 4th NCA*
MIROC5		light gold	blue	blue	Part of 4th NCA*
MPI-ESM-LR	light gold	dark gold	light gold		

*NCA – National Climate Assessment

Table 3-3. The blue highlighted cells indicate the evaluation step each model was eliminated in the evaluation process. The Global and Regional evaluation is explained in more detail in Cayan and Tyree, 2016. The gold highlighted cells indicate the six models selected for this study.

Global Climate Model	Evaluation Step where Model was Removed from Consideration.		
	Global	Regional	Southern Nevada
ACCESS-1.0 *(gold)*			
CCSM4 *(gold)*			
CMCC-CMS *(gold)*			
CNRM-CM5 *(gold)*			
HadGEM2-ES *(gold)*			
MPI-ESM-LR *(gold)*			
BCC-CSM1-1			▓
CanESM2			▓
CESM1-BGC			▓
CESM1-CAM5			▓
CMCC-CM			▓
GFDL-CM3			▓
GFDL-ESM2M			▓
HadGEM2-CC			▓
MIROC5			▓
BNU-ESM		▓	
GFDL-ESM2G		▓	
MRI-CGCM3		▓	
NORESM1-M		▓	
ACCESS1-3	▓		
BCC-CSM1-1-M	▓		
CSIRKO-MK3-6-0	▓		
EC-EARTH	▓		
FGOALS-G2	▓		
INMCM4	▓		
IPSL-CM5A-LR	▓		
IPSL-CM5A-MR	▓		
IPSL-CM5B-LR	▓		
MIROC-ESM	▓		
MIROC-ESM-CHEM	▓		
MPI-ESM-MR	▓		

3.4 Summary

Research shows that as the number of models in an ensemble increases, the more likely the ensemble is to reflect long-term climate change rather than natural variability (Deser et al., 2012; Pierce et al., 2009). "Ensemble" in this report refers to the average of multiple models through time. Using the full suite of available climate models is not realistic for SNWA because for every climate model added the number of analyses increases exponentially. However, selecting enough models, in this case six, was important to average out the natural climate

variability when using an ensemble (averaging of the models). This chapter describes the process used to arrive at a manageable number of models that will be used to characterize the range in future climate conditions in Clark, described in Chapter 4.

The six models that were selected for southern Nevada are ACCESS1-0, CCSM4, CMCC-CMS, CNRM-CM5, HadGEM2-ES, and MPI-ESM-LR. The models were selected based on the three different evaluation components. Consideration was also given to those models used in the 4th National Climate Assessment. None of the models were ranked as "best" in all evaluation components, nor were any of the models selected in the bottom tier in any of the evaluation components.

4. Future Model Projections for Clark County

4.1 Introduction

Using the six global climate models (GCMs) that were previously selected in Chapter 3, this Chapter examines the magnitude and range in future climate projections for Clark County. Remaining consistent with the rest of report, this Chapter focuses on changes in maximum and minimum daily temperature (T_{max} and T_{min}) and precipitation.

4.2 Methodology

Downscaled GCM data, or localized constructed analogues (LOCA) data, is used to characterize a range of possible future Clark County climate conditions (Pierce et al., 2014; loca.ucsd.edu). The method used to develop LOCA data is described in Section 4.2.1 below. Future climate conditions are a function of the concentration of future GHG emissions, which depends on the global efforts to reduce GHG emissions. Two GHG emission scenarios are used to capture the range of possibilities of global GHG emissions. A high emission concentration scenario in which "business as usual" practices continue through the end of the century, and a low concentration scenario in which the world aggressively mitigates GHG emissions resulting in "significant GHG reductions" scenario. This is described in Section 4.2.2. For each emission scenario and each climate variable (e.g. T_{max}, T_{min}, precipitation), the ensemble of the six models selected in Chapter 3 are averaged through time. To show the uncertainty from model selection, the minimum and maximum across the six models for each climate variable for a given year is reported. To estimate the change in each climate variable through time, the change in the model's 1976-2005 average historical simulation is compared to the model's future simulation. The difference between the ensemble mean and natural variability is explained in Section 4.2.3.

4.2.1 Downscaled data

LOCA is a method of statistically downscaling larger GCM grids to 1/16th degree grids, at 6 km or 3.9 mile resolution (Figure 4-1). This method uses historically observed relationships between large-scale and fine-scale weather patterns. Higher resolution downscaled data better captures the sub-regional variability that is a result of topography amongst other attributes including the type of precipitation event (i.e. large spatial storms versus localized thunderstorms produced by the Monsoon). In addition to downscaling, the LOCA methodology also bias corrects the models with respect to both magnitude and frequency. The bias correction used in the LOCA methodology has been shown to better preserve the original GCM projected future change as compared to other bias correction approaches (Pierce et al., 2015). The 4th National Climate Assessment and 4th California Climate Change Assessment are two of the several groups that are basing regional impact assessments on LOCA downscaled data.

For clarification, the LOCA data used here is different from the non-downscaled data used in the Chapter 3. This Chapter and Chapter 3 have different objectives, justifying the use of the different data sets. In the model selection process (Chapter 3), the objective was to determine which models, without any bias correction, best represent Clark County's historical climate.

Thus, data used in Chapter 3 were not bias corrected; they were only regridded to latitude and longitude grid cells of 2˚ by 2˚, similar to the native size GCM grid cells. For this Chapter, the objective is to show future climate projections for the region using the LOCA downscaling method, which represents the latest state of the science.
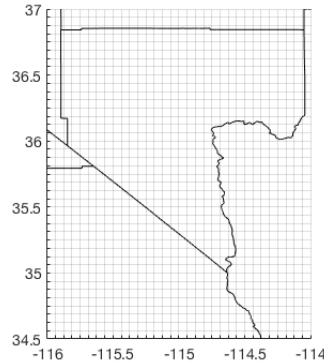
Figure 4-1. Clark County, Nevada. The small squares represent the grid of the LOCA downscaled data set, which are approximately 6 km, or 3.9 miles.

4.2.2 Emission Scenarios

The global modeling community agreed to run each organizations' (i.e. university, national laboratory, government agency) GCM under the same GHG emission scenarios in order to make the model runs, or simulations, comparable. The GHG emission scenarios are called Representative Concentration Pathways (RCP) with the larger numbers indicating more global warming potential (Figure 4-2). For this report, we are using RCP4.5 and RCP8.5, which can be considered a future with "significant GHG reductions" and a "business as usual" scenario, respectively. Current global CO_2 emissions are on a trajectory above the RCP8.5 scenario.
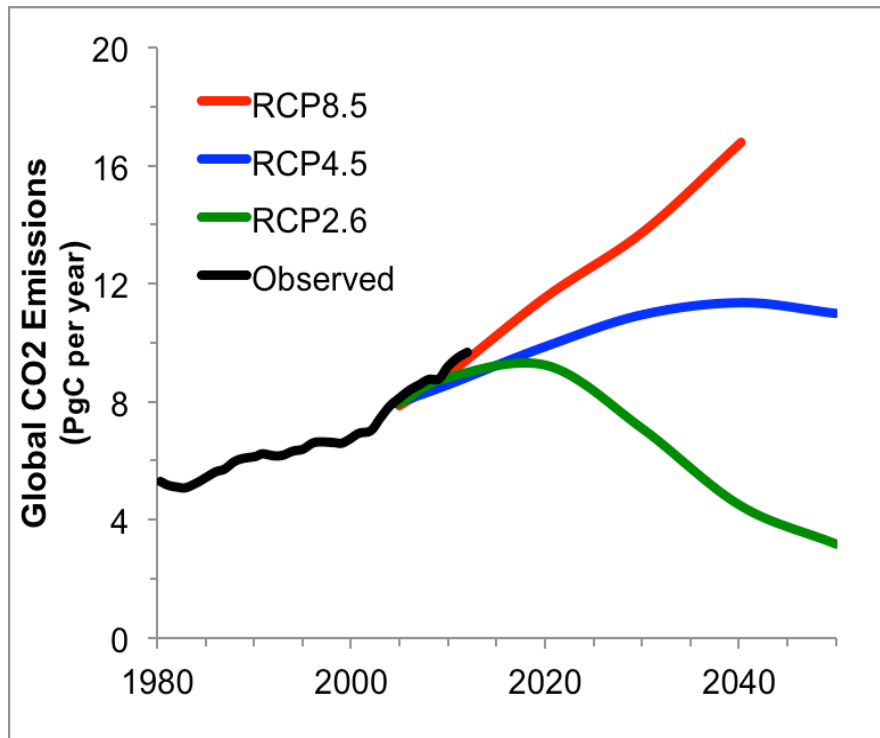
Figure 4-2. Carbon dioxide, or CO_2, annual emission for the different Representative Concentration Pathways (RCPs) or GHG scenarios. The two used in this report are RCP4.5 and RCP8.5. RCP4.5 assumes reductions in GHG emissions in the future, while RCP8.5 is considered the business as usual scenario. Note that the current level of global CO_2 emissions is higher than RCP8.5.

4.2.3 Ensemble Mean versus Natural Variability

Every GCM includes a representation of the natural variability that occurs within the climate system. This variability results from large and small scale climate phenomenon interacting in unexpected ways on different time scales, from interannual, to decadal, to multi-decadal.

Climate oscillations that affect natural variability include ENSO, the Pacific Decadal Oscillation, and the North American Oscillation amongst others. The occurrence of these natural oscillations impact future climate projections. Deser et al. (2012) estimated the uncertainty in natural variability for a given location. The authors ran the same model using the same forcing information 40 different times with slightly different initial atmospheric conditions out to 2060. The projected winter temperatures for Phoenix, AZ varied by ~3˚F by 2060 in the different model runs (Deser et al. 2012). The range in summer temperature was smaller, in large part because summer temperatures are less variable. In contrast, the large interannual variability in precipitation causes an even wider range of projected changes in precipitation, including some runs projecting wetter while other runs projecting drier conditions (Deser et al., 2012).

Using an ensemble average, as is shown below, helps to decrease the influence of natural variability when examining long-term climate change trends as discussed in Chapter 3. The ensemble average, however, does not reproduce possible extreme conditions. Extreme climate

conditions generally result when rare climate phenomenon align and amplify impacts. This is why it is valuable to examine the extremes in individual models.

4.3 Results

4.3.1 Temperature Projections

Daytime (nighttime) high temperature projections for Clark County, represented by T_{max} (T_{min}), are increasing through the end of the century. The simulated ensemble average for T_{max} (T_{min}) through time and each season, is plotted in Figure 4-3 (Figure 4-4). Figure 4-3 (Figure 4-4) illustrates the impact of climate scenarios RCP4.5 and RCP8.5 on T_{max} (T_{min}) in Clark County; specifically, the RCP scenarios diverge only after the middle of the century. The temperature projections for Clark County are generally consistent with projections for the state and southwest (California Fourth Climate Change Assessment, *in prep.*; Runkle et al., 2017).

The average change in T_{max} (T_{min}) across the six GCMs is plotted in Figure 4-5 (Figure 4-6) for each RCP, time period, and season. The minimum and maximum bars represent the range of results from the climate models and indicate the uncertainty due to differences between the models. Generally, the range of model results for T_{min} is smaller than for T_{max} indicating there is more certainty in the projected T_{min} changes. The projected change in the thirty-year average for T_{max} (T_{min}) is greatest during fall (Figure 4-5 (Figure 4-6)) followed by summer, spring and then winter. By the end of the century the ensemble mean annual T_{max} (T_{min}) increase is 5.0˚F (4.7 ˚F) for RCP4.5 and 8.6˚F (8.7 ˚F) for RCP8.5 (Table 4-1(Table 4-2)). The agreement between the models indicates that it is highly likely that annual average T_{min} will warm by at least 2.0˚F relative to the baseline for the period 2010-2039.
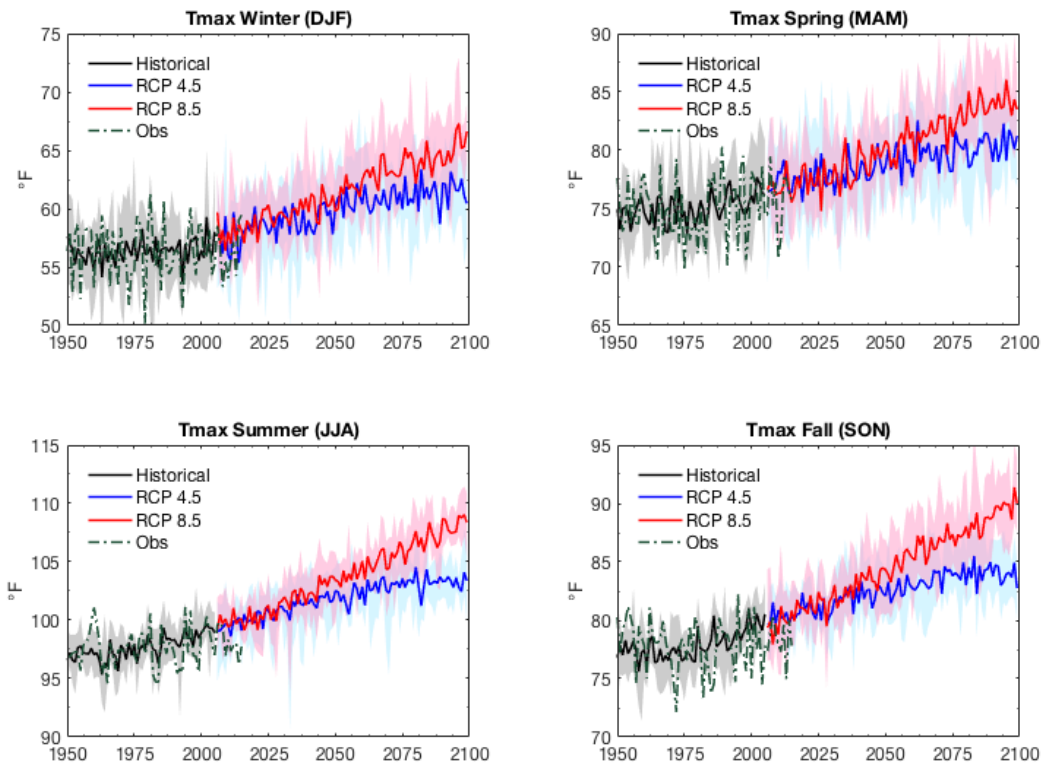
Figure 4-3. The seasonal historical and future projections of T_{max} from the six GCMs selected in the previous section for an area averaged over Clark County. The shaded area represents the window, or range, of the six models and the bold line is the ensemble mean, or average, of the six GCM projections. The black line shows the historical model runs, blue shows RCP4.5 and red shows RCP8.5. The dark green dashed line is the observations from the Livneh gridded data set (Livneh et al., 2015).
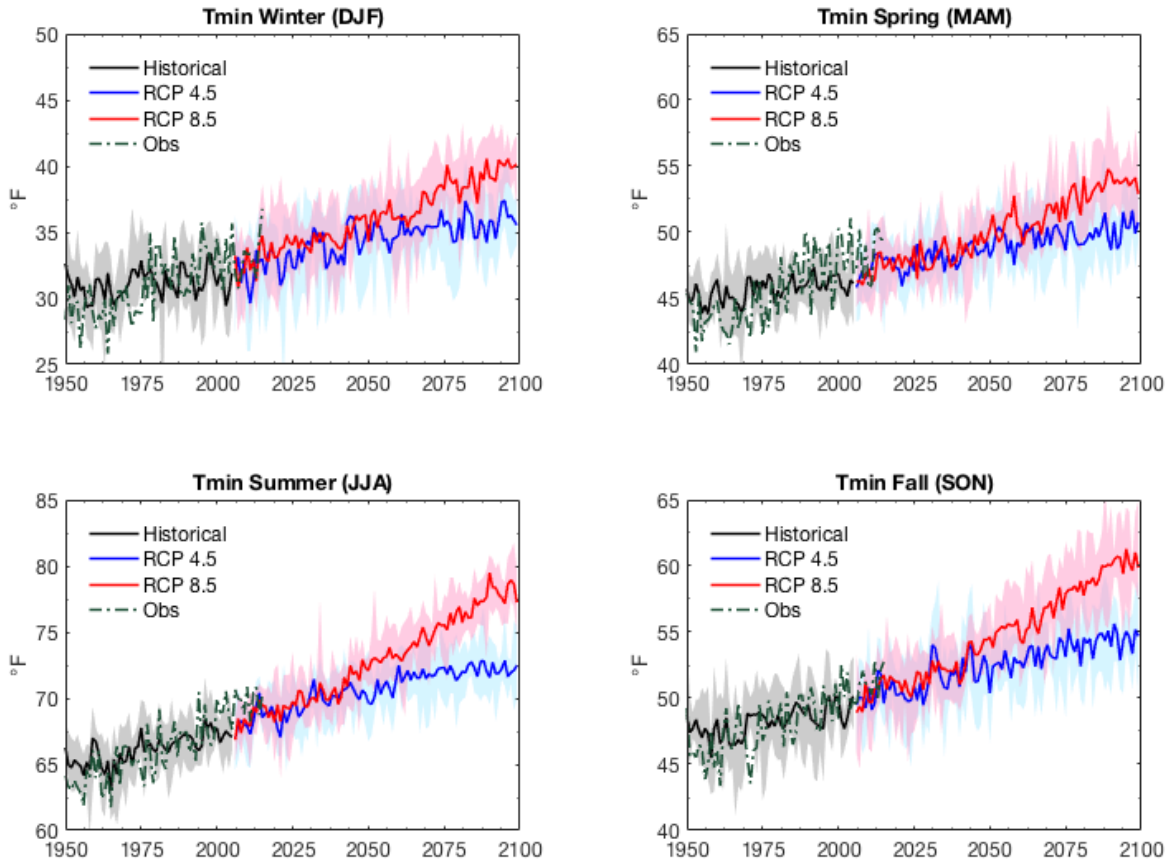
Figure 4-4. Same as Figure 4-3, but for T_{min}.
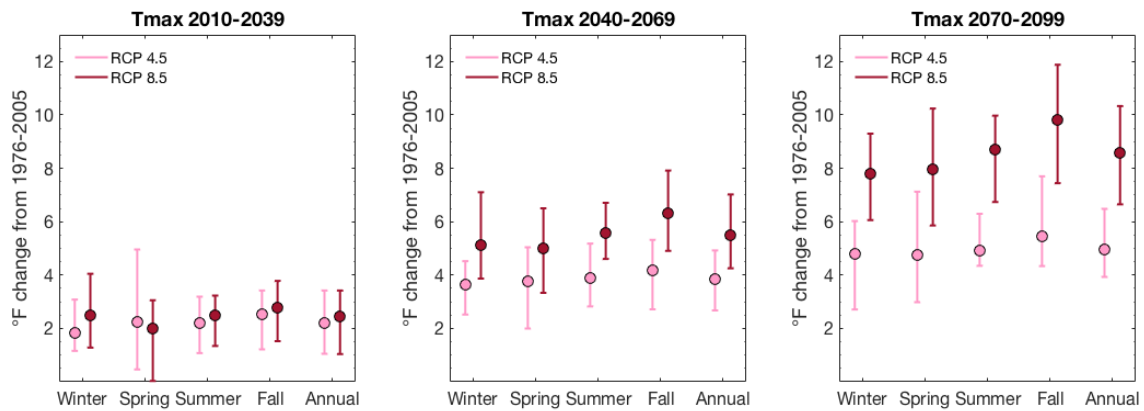
Figure 4-5. Projected change in 30-year average T_{max} relative to the historical period of 1976-2005. The circles represent the ensemble average change, and the lower and upper bounds represent the minimum and maximum projected changes from the six GCM projections. The lighter color shows RCP4.5 and the darker color shows RCP8.5.
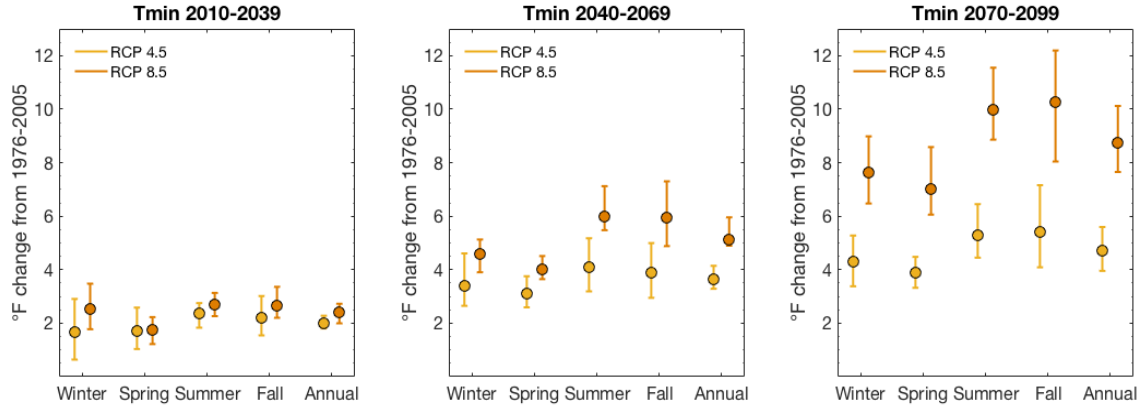
Figure 4-6. Same as Figure 4-5, but for T$_{min}$.

Table 4-1. Changes in T$_{max}$ (˚F) relative to 1976-2005 model historical climatology for Clark County. Only the 30-year ensemble average of all six GCM projections is shown. The first row is the ensemble average value of the historical model runs. Black values are for RCP4.5 and red values are RCP8.5.

30-year Period	Winter	Spring	Summer	Fall	Annual
Historical Model Ave	56.5˚F	75.4˚F	98.3˚F	78.5˚F	77.2˚F
2010-2039	1.8/2.5	2.3/2.0	2.2/2.5	2.5/2.8	2.2/2.4
2020-2049	2.4/3.3	2.6/2.8	2.8/3.5	3.1/3.9	2.7/3.4
2030-2059	3.1/4.0	3.1/3.9	3.4/4.5	3.7/5.1	3.3/4.4
2040-2069	3.6/5.1	3.8/5.0	3.9/5.6	4.2/6.3	3.9/5.5
2050-2079	4.2/6.2	4.2/5.9	4.4/6.5	4.8/7.5	4.4/6.5
2060-2089	4.4/7.1	4.5/7.0	4.8/7.6	5.2/8.6	4.7/7.6
2070-2099	4.8/7.8	4.7/8.0	4.9/8.7	5.4/9.8	5.0/8.6

Table 4-2. Changes in T$_{min}$ (˚F) relative to 1976-2005 model historical climatology for Clark County. Table only shows the 30 –year ensemble average of all six GCMs projections. The first row is the ensemble average value of the historical model runs. Black values are for RCP4.5 and red values are RCP8.5.

30-year Period	Winter	Spring	Summer	Fall	Annual
Historical Model Ave	31.4˚F	46.1˚F	66.8˚F	48.8˚F	48.3˚F
2010-2039	1.7/2.5	1.7/1.8	2.4/2.7	2.2/2.6	2.0/2.4
2020-2049	2.3/3.2	2.0/2.3	2.9/3.6	2.8/3.4	2.5/3.1
2030-2059	3.0/3.9	2.6/3.2	3.5/4.7	3.5/4.8	3.2/4.2
2040-2069	3.4/4.6	3.1/4.0	4.1/6.0	3.9/5.9	3.6/5.1
2050-2079	3.8/5.7	3.5/5.1	4.6/7.3	4.4/7.4	4.1/6.4
2060-2089	4.0/6.5	3.7/5.9	5.1/8.6	5.0/8.7	4.5/7.4
2070-2099	4.2/7.6	3.9/7.0	5.3/10.0	5.4/10.3	4.7/8.7

Historically, southern Nevada experiences more extreme temperatures per year than most places in the U.S. Simulations suggest the preponderance for extreme temperatures will only continue in the future. As T$_{max}$ (T$_{min}$) increases (decreases), the number of days exceeding (below) certain temperature thresholds will also increase (decrease). Figure 4-7 (Figure 4-8) plots the number of days above (below) 100˚F, 105˚F, 110˚F, 115˚F and 120˚F (50˚F, 40˚F and 32˚F) through time for RCP4.5 and RCP8.5. Each color band represents the range in the number

of days exceeding (below) the threshold across the six models. The number of days exceeding 100˚F are projected to increase by approximately 40 days in RCP4.5 and almost double to approximately 160 days in RCP8.5 (Figure 4-7) by the end of the century. According to the historic simulations, only approximately five days per year exceeds 115˚F in Clark County. In RCP8.5 the region could experience extreme temperatures almost 50 days of the year or 14 % of the time by the end of the century. The number of days below 50˚F is projected to decrease by approximately 40 days annually by 2100 under RCP4.5 and by 70 days under RCP8.5. The number of days below freezing are projected to decline from approximately 50 days per year to less than 30 days per year in RCP4.5 and to less than 5 days per year in RCP8.5 (Figure 4.8).
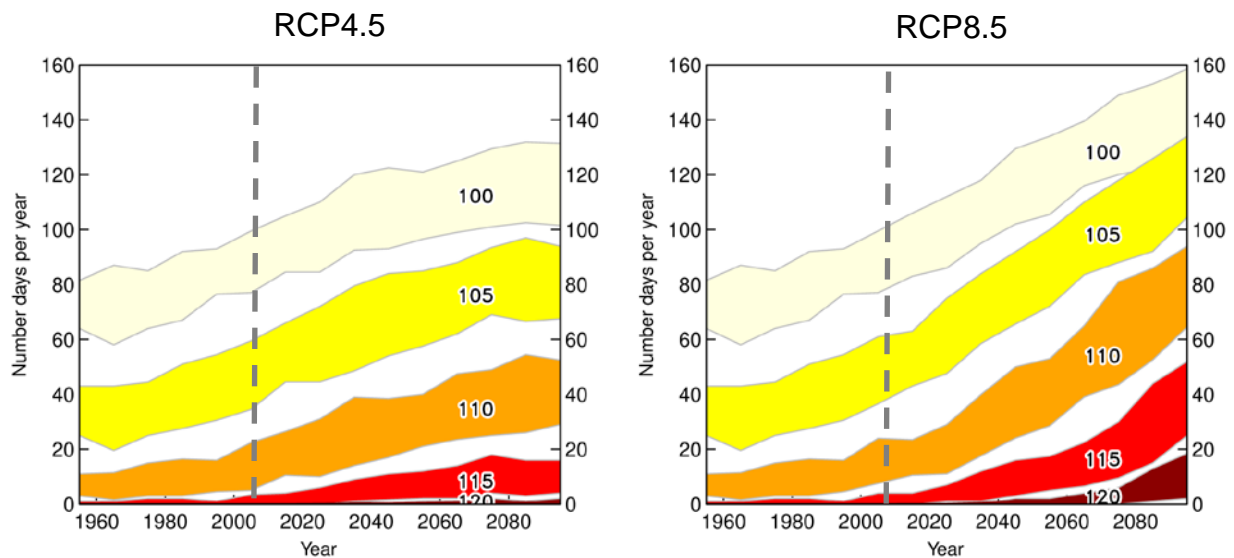
Figure 4-7. Each color band represents the range of the six GCM projections average number of days at or above the indicated temperature threshold (˚F) for RCP4.5 (right) and RCP8.5 (left). The range is calculated for each decade from 1950's to the 2090's. The T_{max} is averaged over Clark County. The dashed line illustrates the division between the historical model scenarios and the future climate scenarios.
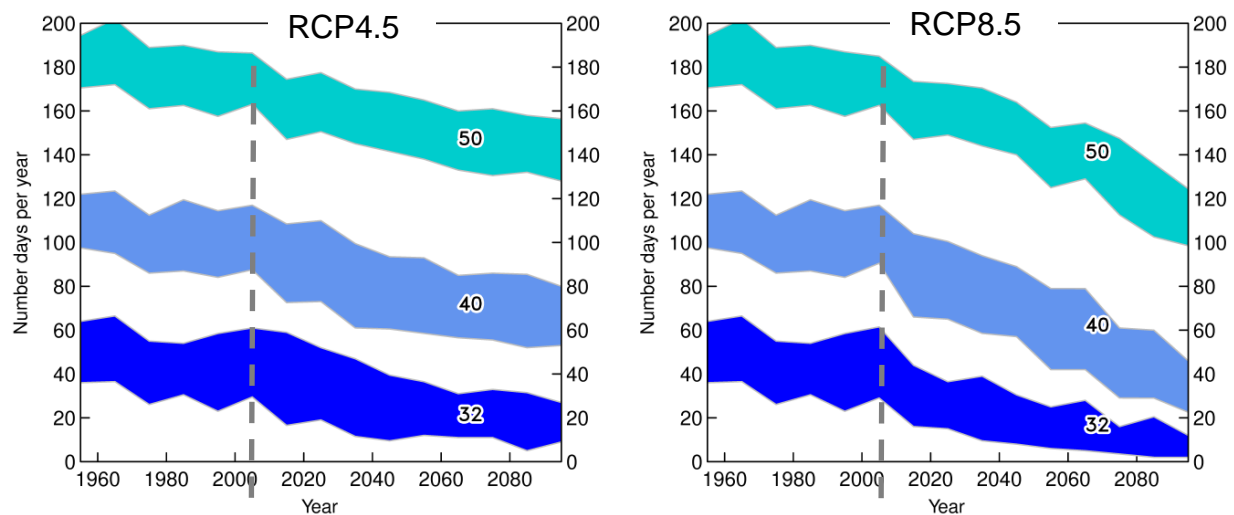
Figure 4-8. Similar to Figure 4-7, but showing the number of days at or below the indicated temperature threshold (T_{min}, ˚F).

4.3.2 Precipitation

Unlike temperature, annual and seasonal precipitation totals are variable among the models and changes in future precipitation are uncertain. The low precipitation totals along with the highly variable precipitation regime of Clark County makes precipitation projections for this region uncertain. This is reflected in the results. Nonetheless, there is some information that

can be gleaned from the projections. Most importantly, is that the precipitation regime will remain highly variable year-to-year and continue to be a primary characteristic of the local climate (Figure 4-9). Relative to the historical simulations (grey lines) future projections indicate more variable precipitation. The models generally agree that spring (March, April, May) precipitation will decrease in the future (Figure 4-10; Table 4-3). The small changes in the ensemble mean precipitation by decade is reiterated in Table 4-3.
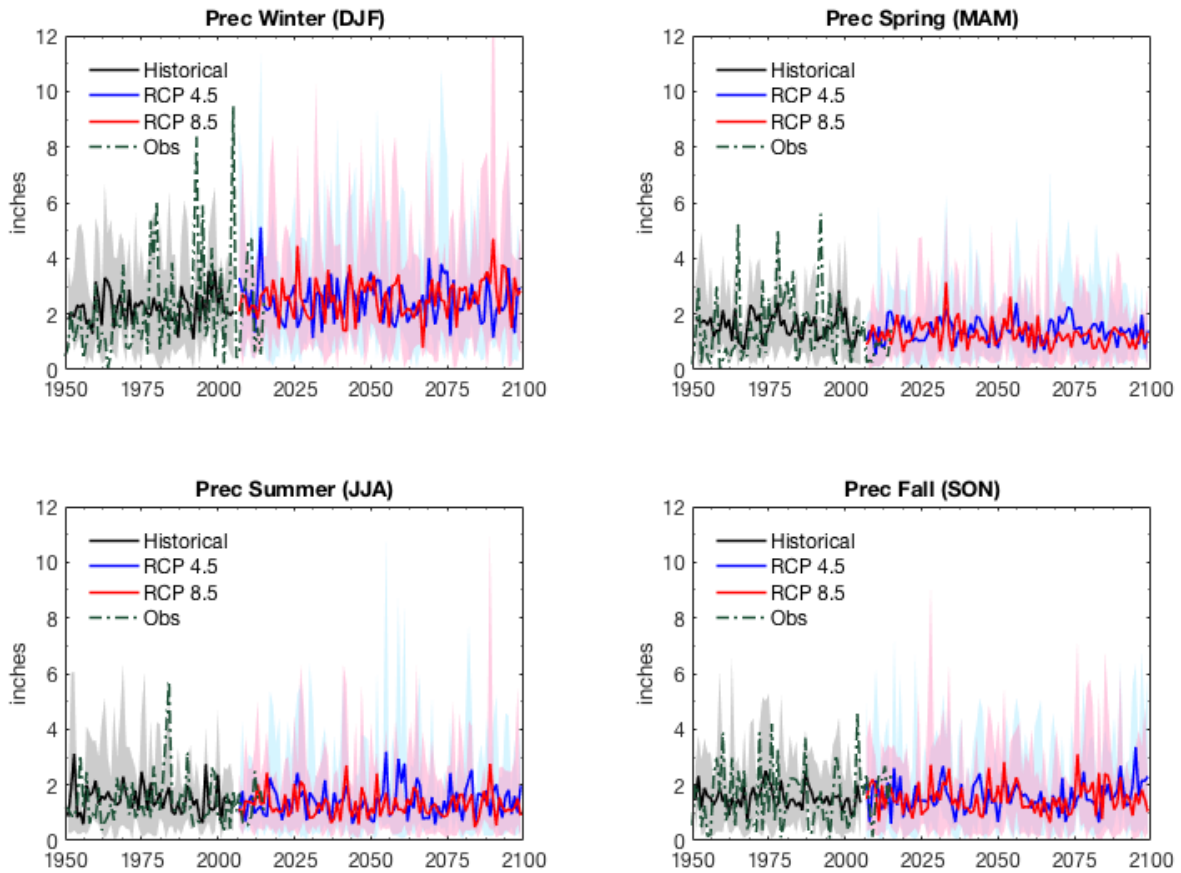
Figure 4-9. Same as Figure 4-3, but for seasonal precipitation totals.
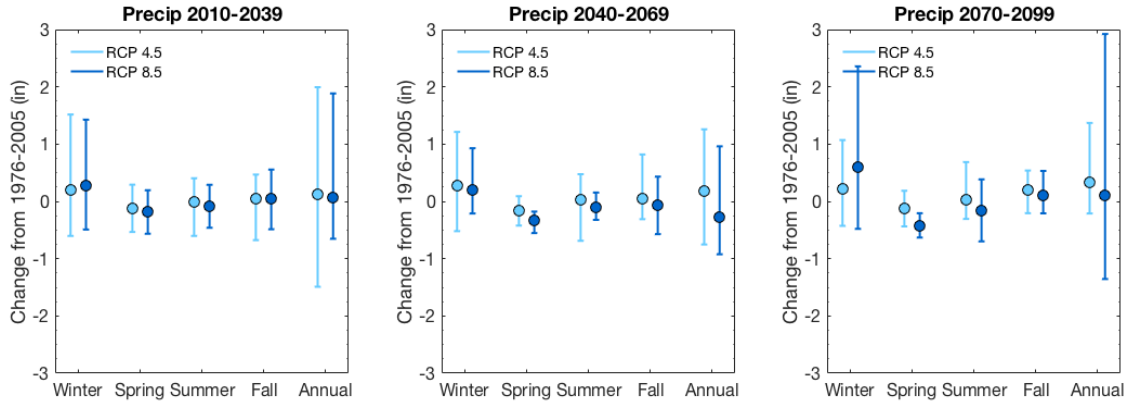
Figure 4-10. Same as Figure 4-5, but for total seasonal precipitation in inches.

Table 4-3. The seasonal precipitation change in inches relative to 1976-2005 model historical climatology for Clark County. Table only shows the 30-year ensemble average of the six GCMs projections. The first row is the ensemble average value of the historical model runs. Black values are for RCP4.5 and red values are RCP8.5.

30-year Period	Winter	Spring	Summer	Fall	Annual
Historical Model Ave	2.2 in	1.6 in	1.4 in	1.5 in	6.7 in
2010-2039	0.2/0.3	-0.1/-0.2	0/-0.1	0/0.1	0.1/0.1
2020-2049	0.2/0.3	-0.1/-0.2	-0.1/-0.1	0/0	0.1/0
2030-2059	0.3/0.3	-0.1/-0.2	0/-0.2	0.1/0.1	0.4/0.1
2040-2069	0.3/0.2	-0.2/-0.3	0/-0.1	0.1/-0.1	0.2/-0.3
2050-2079	0.3/0.2	-0.1/-0.3	0/-0.1	0/0	0.2/-0.2
2060-2089	0.2/0.3	-0.2/-0.4	0/-0.1	0/0	0.1/-0.3
2070-2099	0.2/0.6	-0.1/-0.4	0/-0.2	0.2/0.1	0.3/0.1

Although modeling precipitation totals, especially for the small amounts that fall in this region, is challenging and highly uncertain, days when precipitation occurs within SNWA service area typically have reduced water demand. Therefore, analyzing the change in the number of wet days for each season may provide some information about future conditions for the water utility. Wet days are defined as days with precipitation totals exceeding 0.1 mm/day. Figure 4-11 plots the spatial change in the number of wet days for each season for each RCP by the end of the century. The projections suggest that in general, winter and fall will have a similar number of wet days/year as historical simulations, while the number of wet days in spring and summer for both RCPs may increase by the end of the century.

The change in the number of wet days per year for the fall suggests Clark County will not experience a seasonal shift in the Monsoon to later in the fall, which other studies on the Monsoon have suggested (Cook et al. 2013; Maloney et al. 2014). This inconsistency can be explained by the uncertainty in precipitation totals due to the small amount of precipitation that falls here annually, and the difference between the study locations. The previous work focused on the core Monsoon region, and did not include southern Nevada in the study region.

The discrepancy in the timing of the monsoon and what potentially makes southern Nevada different from the core monsoon regions is a topic that deserves more attention, but is beyond the scope of this study.
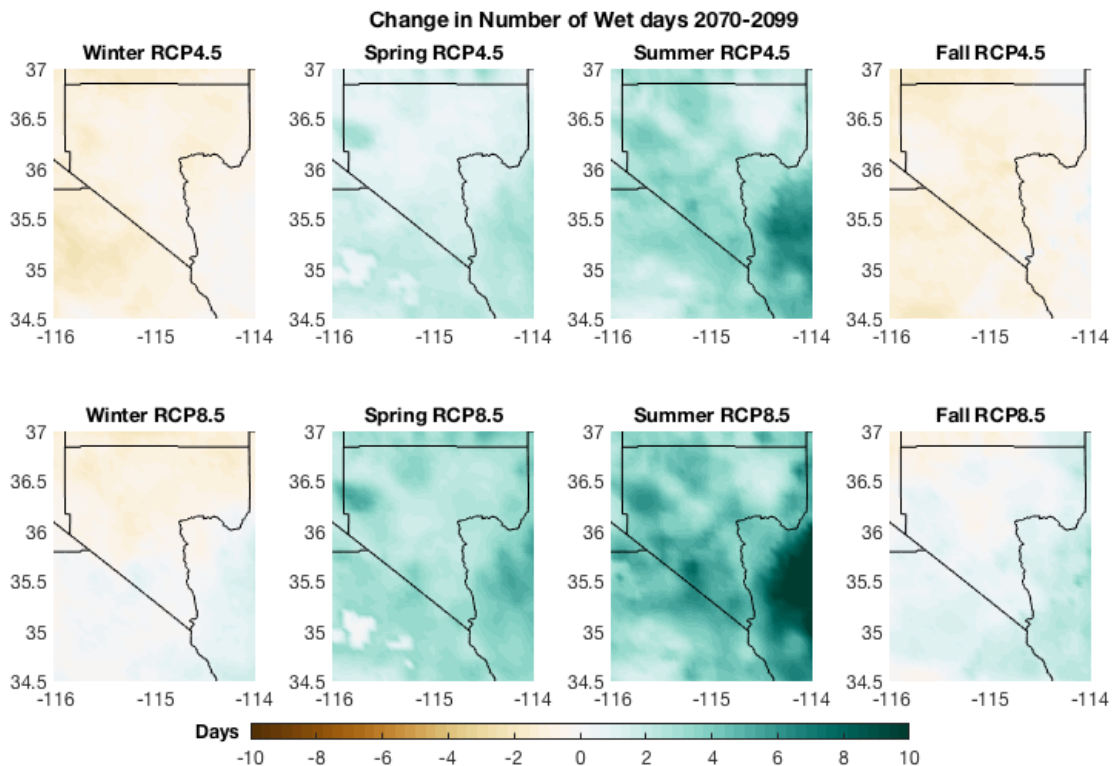
Figure 4-11. The maps show the ensemble mean of the increase or decrease in the number of wet days at the end of the century (2070-2099) by season for RCP4.5 (top row) and RCP8.5 (bottom row). The brown colors indicate fewer wet days relative to the baseline (1976-2005) and the green colors indicate more wet days than the baseline. Similar to Chapter 3, a threshold of >1 mm/day was used to define a wet day.

Despite occurring only infrequently in Clark County, extreme precipitation events were identified in Chapter 2 as being important contributing factors with respect to total precipitation (95th percentile) and flooding (99th percentile). The change in the number of 95th percentile and 99th percentile events relative to the baseline (1976-2005) are plotted in Figure 4-12 and Figure 4-13, respectively. Future projections indicate that approximately 30 more 95th percentile events will occur each year in a 30-year period, or one more extreme event per year (Figure 4-12). For the 99th percentile events, Clark County is expected to see at most 15 more extreme events, depending on location, in a 30-year period (Figure 4-13). It should be noted that in terms of percentages, the change in the number of 95th percentile and 99th percentile events are significant. For example, McCarran historically has on average 41 95th percentile events throughout a 30-year period. This means an increase of 15 events in a 30-year period is an increase of 36%. Similarly, McCarran has approximately 10 99th percentile events over a 30-year period. An increase by 5 events is a 50% increase in the number of extremes.
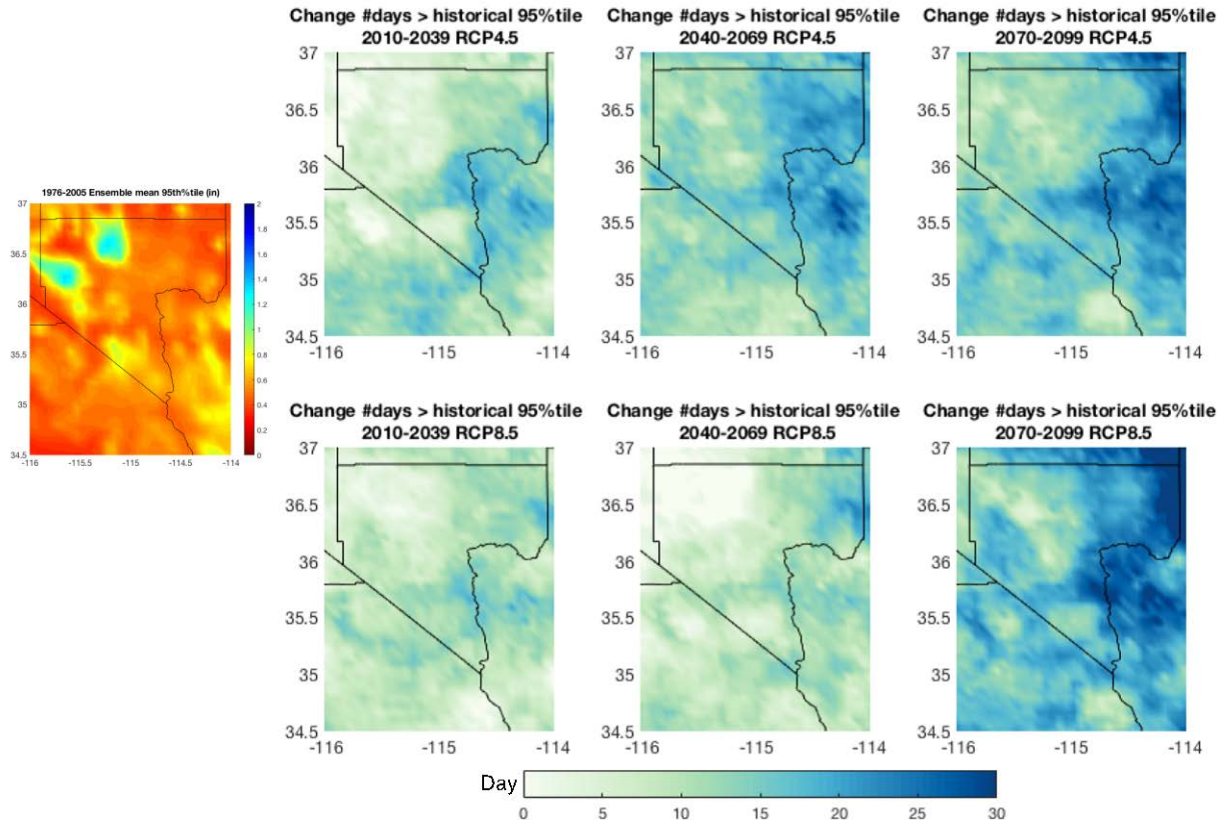
Figure 4-12. The 1976-2005 ensemble mean for the threshold of a 95thpercentile event is on the left. The maps on the right show the increase in number of days over the 30-year period that reach or exceed the threshold indicated on the historical map on the left.
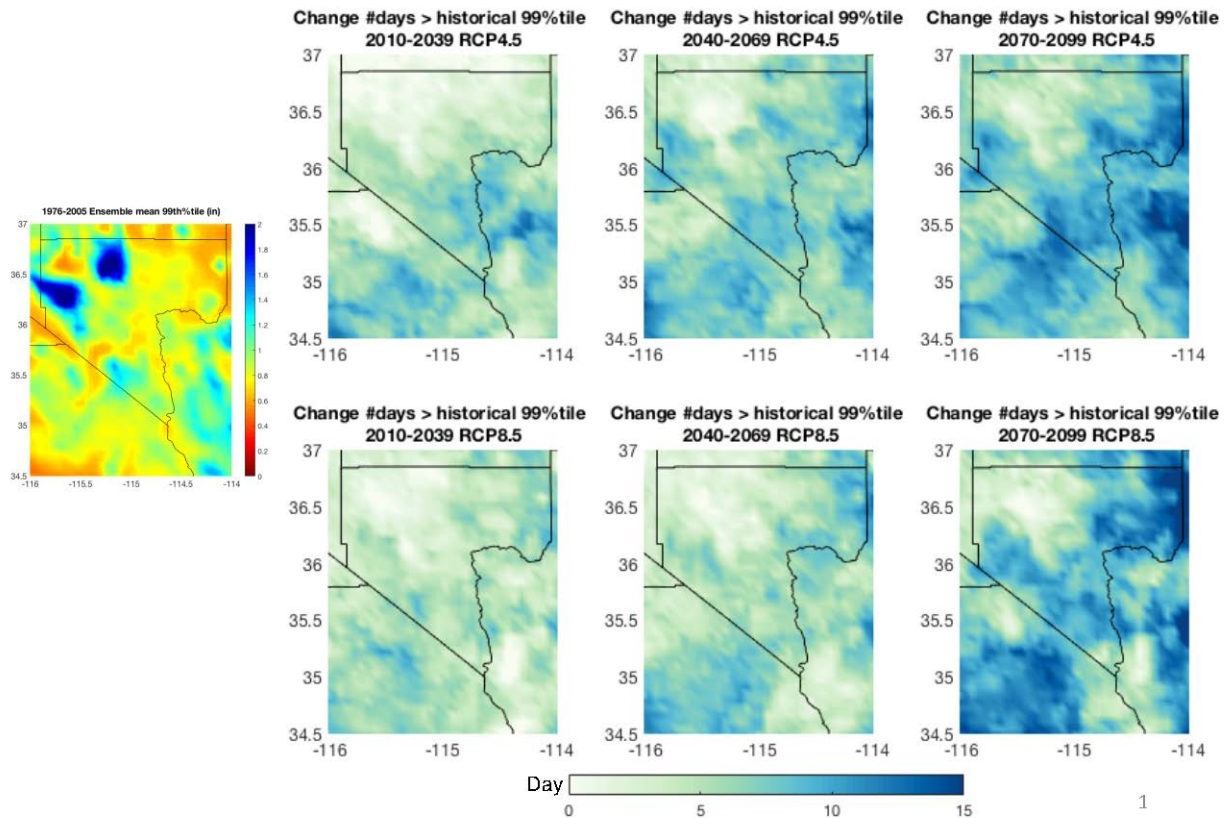
Figure 4-13. Same as Figure 4-12, but for the 99th percentile events. Please note the color bar change in scale from Figure 4-12.

4.3.3 Future Projections of El Niño Southern Oscillation (ENSO)

A weak ENSO signal is identified in Chapter 2 as influencing climate variability in Clark County. Historically, El Niño (La Niña) events are associated with relatively cooler and wetter (warmer and drier) winters (Chapter 2). Changes in the ENSO frequency or intensity has the potential to impact Clark County. An analysis to evaluate relationships between projected temperature and precipitation magnitudes and frequencies relative to ENSO phasing is not conducted here. However, a brief review of literature provides some insight on conditions to expect in the future.

Many GCM's do not accurately represent the ocean-atmosphere relationship in the tropical Pacific Ocean, which makes understanding the future projections of ENSO difficult (Bellenger et al., 2014). Nonetheless, recent work suggests that the most intense El Niño events and La Niña events are projected to become more frequent in the future (Cai et al., 2014; Cai et al., 2015). With increased ENSO variability Clark County could experience more year-to-year variability in precipitation.

4.4 Summary

The projections for Clark County presented here broadly support research studies that have examined regional projections of climate change. The present projections show high certainty

that temperature will increase, though the exact amount is less certain, with the largest uncertainty from the global GHG emissions. Precipitation projections are less certain, in large part due to the high natural variability of the region, however, the projections suggest that the precipitation regime will become even more variable. Below are some key findings from examining the future projections.

Based on the ensemble average projections, results suggest high temperatures in Clark County will warm between 4-10˚F by the end of the century depending on the GHG emission scenario. In the near-term (2010-2039), 2.0˚F or more warming is likely. Seasonally, fall will warm more rapidly than winter and spring, with summer warming almost as quickly. Fall daytime temperatures, in RCP8.5 are projected to increase by as much as 10˚F by the end of the century.

By the end of the century in RCP8.5, the number of days above certain temperature thresholds is expected to increase in Clark County. The number of days exceeding 100˚F is projected to approximately double from 80 to 160 days. Under RCP8.5 models are projecting an approximate 10-fold increase in the number of days above 115˚F to about 50 days, or 14% of the time, on average.

By the end of the century in RCP8.5, the number of days below certain temperature thresholds are expected to decline in Clark County. In RCP8.5, the number of days below 50˚F is projected to decrease by approximately 70 days by the end of the century. When air temperatures are below 50˚F turf grass goes dormant. Turf grass requires less water during dormancy, thus the decrease in days below 50˚F may cause an increase in water use. The number of days below freezing, below which water pipes freeze, are projected to decline by a factor of ten to approximately 5 days per year for RCP8.5.

Precipitation is more uncertain. The projected changes in precipitation are small (on the order of +/- 1-2 inches) and highly variable. The projections indicate some seasonal differences in the future relative the baseline period, in particular that spring will become drier. Additionally, summer and spring indicate more wet days suggesting more days with little precipitation as the change in precipitation is small. This also does not indicate a shift in the monsoon season to later in fall for Southern Nevada.

In Chapter 2, extreme precipitation events were identified as being important both with respect to total contribution to annual precipitation totals (95th percentile) and flooding (99th percentile). Previous research has projected that extreme events regionally and globally will increase because a warmer atmosphere can hold more moisture (Dominguez et al., 2012; Lau et al., 2013). Consistent with this research, the number of extreme precipitation events for Clark County is projected to increase.

5.Conclusions

The SNWA's operations and assets in Clark County could be impacted by changing future climate conditions. This study provides the SNWA with information about past and potential future climates in the Clark County, NV service area. The main conclusions from the study are bulleted below.

Findings based on evaluation of historic station data
- Warming temperatures in Clark County are consistent with warming trends observed nationally and globally. The magnitude and pace of local warming is largely driven by warmer nighttime temperatures, although a weak upward trend in daytime temperatures is also present at some stations.
- The small amount of precipitation that falls in southern Nevada falls primarily during the winter or late summer. At McCarran airport, 43% of the 4.2 inches/year fall during winter storms, while 22% falls during the July through September North American Monsoon season.
- Annual precipitation totals from six weather stations around the region lack any visible or statistically significant trends. Annual precipitation totals vary significantly from year-to-year, although years with an increased frequency of the largest storms (5% wettest days) typically result in wet years.
- Only a weak relationship between ENSO phase and climate in southern Nevada exists. La Niña events tend towards slightly warmer and drier conditions in Clark County, while there is a tendency towards cooler and wetter conditions during El Niño events.
- Wet winter months and cold winter months often occur when a low-pressure system is present over Clark County. In contrast, heatwaves are typically associated with high-pressure systems over the southwestern U.S.

Model selection results based on similarity between historic station data and historic GCM simulations
- The selection methodology follows Cayan et al., (2015) to eliminate models based on Global Climatology, then based on Western U.S. climate. The final selection step uses local criteria to eliminate models down to six models. The local criteria used includes the standard deviation in daily T_{max} by season, the number of wet days during the winter (DJFM) and North American Monsoon (JAS), and the atmospheric circulation patterns based on 500 hPa geopotential height anomalies for the 10 coldest months, the 10 wettest months, and the top 10 3-day heat waves
- The six models used to characterize future climate in Clark County, include: ACCESS1-0, CCSM4, CMCC-CMS, CNRM-CM5, HadGEM2-ES, and MPI-ESM-LR

Findings based on the evaluation of downscaled future climate simulations
- A similar rate of warming is expected in the near term (prior to 2050) regardless of GHG concentrations. It is only after the middle of the century that the benefits of

implementing a strong mitigation policy today would be gained (maximum temperature rise of only 5.0˚F instead of 8.6˚F).

• In the near term (period 2010-2039) nighttime temperatures will very likely warm by 2.0˚F relative to the baseline (1976-2005). This increase can be considered the minimum amount of temperature rise for planning purposes going forward.

• In contrast to the projections for Clark County which warm more in the fall, projections over California and the southwest report greater summer warming in the future compared to other seasons. Future studies to understand the cause for seasonal and regional differences may help us better adapt to potential future changes.

• The number of days exceeding 100˚F are projected to nearly double by the end of the century. Clark county could experience triple digit temperatures approximately 45% of the time. This could have significant impacts on outdoor workforce health. A large number of SNWA's employees work outdoors. SNWA may need to manage outdoor workforce schedules differently.

• By the end of the century Clark County could experience a 10-fold increase in days over 115˚F. Consecutive number of days above 115˚F reduces the efficiency of equipment and the efficiency of power transmission. SNWA requires significant energy to pump, treat and distribute drinking water. These temperatures put critical assets at risk of failure.

• In the future outdoor landscape may require more water than today due to a longer growing season (days above 50 ˚F). Given the magnitude of warming relative to the magnitude of precipitation change, it is likely water demand will be more sensitive to temperatures.

• Projected changes in precipitation are small and highly uncertain, in large part due to the large natural interannual and decadal precipitation variability in the region, but also because this variable is difficult to model given GCM resolution.

• The projections suggest that winter and fall will have a similar number of wet days/year relative to historical simulations, while the number of wet days in spring and summer may increase by the end of the century. If the summer becomes wetter or more humid at the same time it becomes hotter (by as much as 10˚F), cooling units and other electronics may experience more failures or be less efficient.

• Model projections suggest large precipitation events (95th percentile and 99th percentile events) will occur more frequently in the future.

6. Recommended Next Steps

Climate Monitoring Stations
This study relied heavily on the long-term data from the McCarran station, because it was the longest and most complete record available. Additional climate stations in Clark County would provide a broader, long-term data set that could be used for comparison to modeled data, allow for greater trend comparisons and yield enhanced, spatially gridded datasets.

The McCarran data demonstrated a stronger, upward trend in minimum daily temperatures than surrounding stations and is also the only station in the study with a continuous and long-term temperature record in a more urbanized area. As suggested, the increased upward trend in minimum temperatures may be due to urban heat island. Additional high density monitoring will be important to understand how urban heat island may be impacting areas with various development densities, as well as, discerning data biases due to location, shading, surrounding infrastructure, irrigation, etc (Meene et al., 2009). Establishing additional stations now may not provide immediate benefits, but the longer the stations operate, the more useful the data will become –allowing for more comprehensive analyses on how climate is changing locally.

Wind and humidity were two additional climatic variables that were noted to be important to SNWA, though neither were highlighted in the report, due to the reliability of these variables in current GCM models. As GCMs improve, it will be important to have reliable wind and humidity data to evaluate changes in these parameters which are used to compute and evaluate evaporative demand. Enhancing trends and projections of evaporative demand may help SNWA assess changes in vegetation water demands and efficiency of equipment operated by SNWA. Ensuring new stations have humidity and wind sensors will further the understanding of regional microclimates and allow for interpretation of climate variables, not yet modeled consistently.

On-going coordination between CNAP and SNWA
Throughout this research project, SNWA and CNAP have engaged in mutually beneficial information exchanges to better understand how climate may or may not influence SNWA's operations. Several variables that are important to SNWA operations were discussed but extended beyond the scope of the original project. These include relative humidity, an evaporative demand index (exact variable to be determined), and number of days above and below certain operational temperature thresholds, yet to be determined. The CNAP team has additional downscaled data and hydrological runs that SNWA may find useful. Continuing the established dialogue between the two agencies would continue to produce analyses and information that would help SNWA meet its climate resilience objectives.

References

Adams, D. K., and A. C. Comrie (1997), The North American monsoon, *B Am Meteorol Soc*, *78*(10), **2197**-2213, doi: 10.1175/1520-0477.

Albrecht, B. A. (1989), Aerosols, Cloud Microphysics, and Fractional Cloudiness, *Science*, *245*(4923), 1227-1230, doi:10.1126/science.245.4923.1227.

Ault, T. R., J. E. Cole, J. T. Overpeck, G. T. Pederson, and D. M. Meko (2014), Assessing the Risk of Persistent Drought Using Climate Model Simulations and Paleoclimate Data, *Journal of Climate*, *27*(20), 7529-7549, doi:10.1175/jcli-d-12-00282.1.

Ault, T. R., J. S. Mankin, B. I. Cook, and J. E. Smerdon (2016), Relative impacts of mitigation, temperature, and precipitation on 21st-century megadrought risk in the American Southwest, *Science Advances*, *2*(10), doi:10.1126/sciadv.1600873.

Bellenger, H., E. Guilyardi, J. Leloup, M. Lengaigne, and J. Vialard (2014), ENSO representation in climate models: from CMIP3 to CMIP5, *Clim Dynam*, *42*(7), 1999-2018, doi:10.1007/s00382-013-1783-z.

Cai, W., et al. (2014), Increasing frequency of extreme El Niño events due to greenhouse warming, *Nat Clim Change*, *4*, 111, doi:10.1038/nclimate2100.

Cai, W., et al. (2015), Increased frequency of extreme La Niña events under greenhouse warming, *Nat Clim Change*, *5*, 132, doi:10.1038/nclimate2492.

Cayan, D., and M. Tyree (2015), Global Climate Model Selection, in *Perspectives and Guidance for Climate Change Analysis*, edited by E. Lynn and W. O'Daly, California Department of Water Resources.

Cook, B. I., and R. Seager (2013), The response of the North American Monsoon to increased greenhouse gas forcing, *Journal of Geophysical Research: Atmospheres*, *118*(4), 1690-1699, doi:10.1002/jgrd.50111.

Cordero, E. C., W. Kessomkiat, J. Abatzoglou, and S. A. Mauget (2011), The identification of distinct patterns in California temperature trends, *Climatic Change*, *108*(1-2), 357-382, doi:10.1007/s10584-011-0023-y.

Deser, C., R. Knutti, S. Solomon, and A. S. Phillips (2012a), Communication of the role of natural variability in future North American climate, *Nature Clim. Change*, *2*(11), 775-779.

Deser, C., A. Phillips, V. Bourdette, and H. Teng (2012b), Uncertainty in climate change projections: the role of internal variability, *Clim Dynam*, *38*(3), 527-546, doi:10.1007/s00382-010-0977-x.

Dettinger, M. (2015), Droughts, Storms and the Future of Nevada's Water Resources, paper presented at Nevada Water Resources Association.

Dominguez, F., E. Rivera, D. P. Lettenmaier, and C. L. Castro (2012), Changes in winter precipitation extremes for the western United States under a warmer climate as simulated by regional climate models, *Geophys Res Lett*, *39*(5), doi:10.1029/2011GL050762.

Earman, S., A. R. Campbell, F. M. Phillips, and B. D. Newman (2006), Isotopic exchange between snow and atmospheric water vapor: Estimation of the snowmelt component of groundwater recharge in the southwestern United States, *J Geophys Res-Atmos*, *111*(D9).

Easterling, D. R., et al. (1997), Maximum and minimum temperature trends for the globe, *Science*, *277*(5324), 364-367, doi:DOI 10.1126/science.277.5324.364.

Gao, Y., L. R. Leung, J. Lu, Y. Liu, M. Huang, and Y. Qian (2014), Robust spring drying in the southwestern U.S. and seasonal migration of wet/dry patterns in a warmer climate, *Geophys Res Lett*, *41*(5), 1745-1751, doi:10.1002/2014GL059562.

Gershunov, A., D. R. Cayan, and S. F. Iacobellis (2009), The Great 2006 Heat Wave over California and Nevada: Signal of an Increasing Trend, *J Climate*, *22*(23), 6181-6203, doi:10.1175/2009jcli2465.1.

Gleckler, P. J., K. E. Taylor, and C. Doutriaux (2008), Performance metrics for climate models, *J Geophys Res-Atmos*, *113*(D6), doi: 10.1029/2007jd008972.

Hawkins, E., and R. Sutton (2009), The Potential to Narrow Uncertainty in Regional Climate Predictions, *Bulletin of the American Meteorological Society*, *90*(8), 1095-1107, doi:10.1175/2009bams2607.1.

Hoerling, M. P., M. Dettinger, K. Wolter, J. Lukas, J. Eischeid, R. Nemani, B. Liebmann, K. E. Kunkel, and A. Kumar (2013), Present Weather and Climate: Evolving Conditions, in *Assessment of Climate Change in the Southwest United States: A Report Prepared for the National Climate Assessment*, edited by G. Garfin, A. Jardine, R. Merideth, M. Black and S. LeRoy, pp. 74-100, Island Press/Center for Resource Economics, Washington, DC, doi:10.5822/978-1-61091-484-0_5.

IPCC (2007), Climate Change 2007: The Physical Science Basis. Contribution of Working Group I to the Fourth Assessment Report of the Intergovernmental Panel on Climate Change *Rep.*, Cambridge University Press, Cambridge, United Kingdom and New York, NY, USA.

IPCC (2013), Climate Change 2013: The Physical Science Basis. Contribution of Working Group I to the Fifth Assessment Report of the Intergovernmental Panel on Climate Change*Rep.*, Cambridge University Press, Cambridge, United Kingdom and New York, NY, USA.

Jin, E. K., et al. (2008), Current status of ENSO prediction skill in coupled ocean-atmosphere models, *Clim Dynam*, *31*(6), 647-664, doi:10.1007/s00382-008-0397-3.

Kalnay, E., M. Kanamitsu, R. Kistler, W. Collins, D. Deaven, L. Gandin, M. Iredell, S. Saha, G. White, and J. Woollen (1996), The NCEP/NCAR 40-year reanalysis project, *B Am Meteorol Soc*, *77*(3), 437-471.

Karl, T. R., P. D. Jones, R. W. Knight, G. Kukla, N. Plummer, V. Razuvayev, K. P. Gallo, J. Lindseay, R. J. Charlson, and T. C. Peterson (1993), A New Perspective on Recent Global Warming - Asymmetric Trends of Daily Maximum and Minimum Temperature, *B Am Meteorol Soc*, *74*(6), 1007-1023, doi:Doi 10.1175/1520-0477.

Knutti, R., D. Masson, and A. Gettelman (2013), Climate model genealogy: Generation CMIP5 and how we got there, *Geophys Res Lett*, *40*(6), 1194-1199, doi:10.1002/grl.50256.

Lau, W. K. M., H. T. Wu, and K. M. Kim (2013), A canonical response of precipitation characteristics to global warming from CMIP5 models, *Geophys Res Lett*, *40*(12), 3163-3169, doi:10.1002/grl.50420.

Livneh, B., T. J. Bohn, D. W. Pierce, F. Munoz-Arriola, B. Nijssen, R. Vose, D. R. Cayan, and L. Brekke (2015), A spatially comprehensive, hydrometeorological data set for Mexico, the U.S., and Southern Canada 1950–2013, *Scientific Data*, *2*, 150042, doi:10.1038/sdata.2015.42.

Lobell, D. B., and C. Bonfils (2008), The effect of irrigation on regional temperatures: A spatial and temporal analysis of trends in California, 1934-2002, *J Climate*, *21*(10), 2063-2071, doi:10.1175/2007jcli1755.1.

Maloney, E. D., et al. (2014), North American Climate in CMIP5 Experiments: Part III: Assessment of Twenty-First-Century Projections, *Journal of Climate*, *27*(6), 2230-2270, doi:10.1175/jcli-d-13-00273.1.

Pendergrass, A. G., and D. L. Hartmann (2014), Changes in the Distribution of Rain Frequency and Intensity in Response to Global Warming, *Journal of Climate*, *27*(22), 8372-8383, doi:10.1175/jcli-d-14-00183.1.

Peterson, T., D. Anderson, S. Cohen, M. Cortez-Vázquez, R. Murnane, C. Parmesan, D. Phillips, R. Pulwarty, and J. Stone (2008), Why weather and climate extremes matter*Rep.*, 11-33 pp.

Pierce, D. W., D. R. Cayan, E. P. Maurer, J. T. Abatzoglou, and K. C. Hegewisch (2015), Improved Bias Correction Techniques for Hydrological Simulations of Climate Change, *Journal of Hydrometeorology*, *16*(6), 2421-2442, doi:10.1175/jhm-d-14-0236.1.

Pierce, D. W., D. R. Cayan, and B. L. Thrasher (2014), Statistical Downscaling Using Localized Constructed Analogs (LOCA), *Journal of Hydrometeorology*, *15*(6), 2558-2585, doi:10.1175/jhm-d-14-0082.1.

Pierce, D. W., et al. (2013), Probabilistic estimates of future changes in California temperature and precipitation using statistical and dynamical downscaling, *Clim Dynam*, *40*(3), 839-856, doi:10.1007/s00382-012-1337-9.

Prein, A. F., R. M. Rasmussen, K. Ikeda, C. Liu, M. P. Clark, and G. J. Holland (2016), The future intensification of hourly precipitation extremes, *Nat Clim Change*, *7*, 48, doi:10.1038/nclimate3168.

Rizwan, A. M., Y. C. L. Dennis, and C. H. Liu (2008), A review on the generation, determination and mitigation of Urban Heat Island, *J Environ Sci-China*, *20*(1), 120-128, doi:Doi 10.1016/S1001-0742(08)60019-4.

Runkle, J., K. Kunkel, S. Champion, and D. Easterlings (2017), Nevada State Summary*Rep.*, 4 pp.

Rupp, D. E., J. T. Abatzoglou, K. C. Hegewisch, and P. W. Mote (2013), Evaluation of CMIP5 20th century climate simulations for the Pacific Northwest USA, *J Geophys Res-Atmos*, *118*(19), 10884-10906, doi:10.1002/jgrd.50843.

Rutz, J. J., W. J. Steenburgh, and F. M. Ralph (2014), Climatological characteristics of atmospheric rivers and their inland penetration over the western United States, *Mon Weather Rev*, *142*(2), 905-921.

Seager, R., M. Ting, C. Li, N. Naik, B. Cook, J. Nakamura, and H. Liu (2013), Projections of declining surface-water availability for the southwestern United States, *Nature Clim. Change*, *3*(5), 482-486, doi:10.1038/nclimate1787.

Sillmann, J., V. V. Kharin, X. Zhang, F. W. Zwiers, and D. Bronaugh (2013), Climate extremes indices in the CMIP5 multimodel ensemble: Part 1. Model evaluation in the present climate, *Journal of Geophysical Research: Atmospheres*, *118*(4), 1716-1733, doi:10.1002/jgrd.50203.

Twomey, S. (1977), The Influence of Pollution on the Shortwave Albedo of Clouds, *Journal of the Atmospheric Sciences*, *34*(7), 1149-1152, doi:10.1175/1520-0469.

USGCRP (2014), Third National Climate Assessment; Climate Change Impacts in the United States., Washington, D.C., https://nca2014.globalchange.gov/.

USGCRP (2018), Fourth National Climate Change Assessment, *Volume 1 ,* Washington, D.C., https://www.globalchange.gov/nca4.
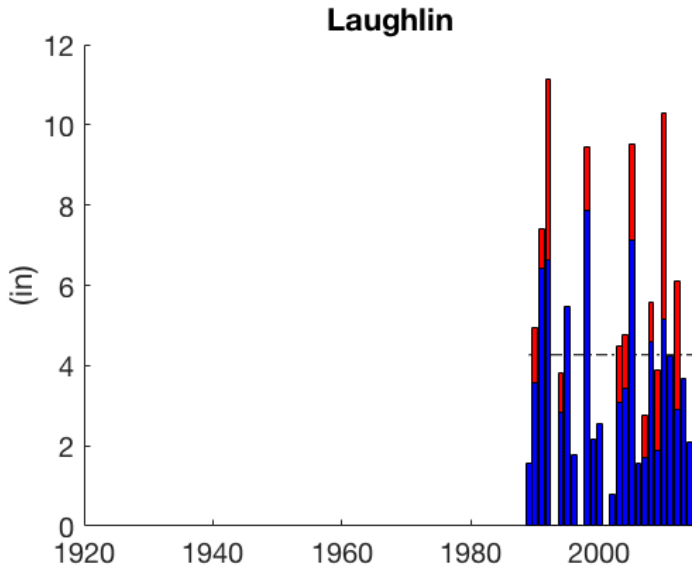
Appendix

1. Boulder City
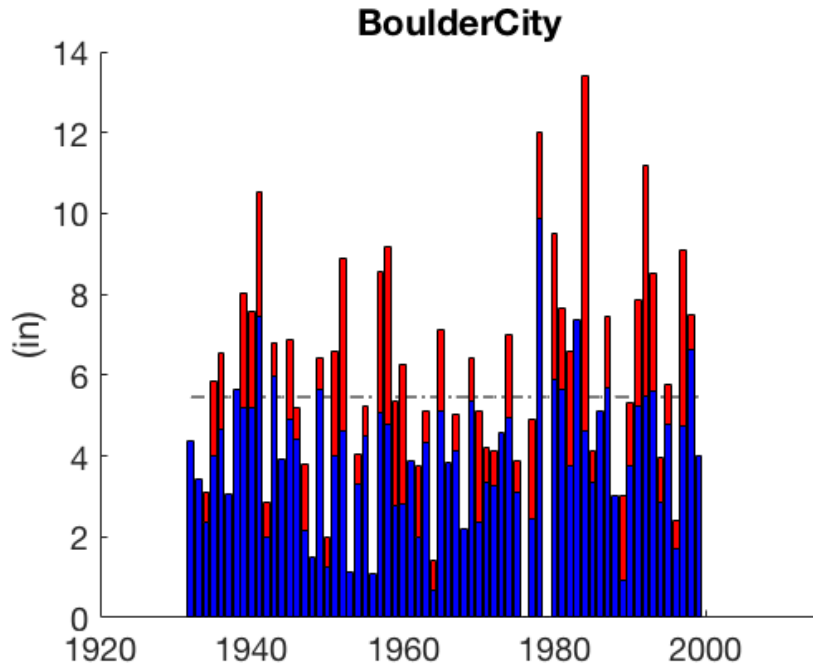
Figure A1-1. The total annual rainfall in inches. The dashed line is the average annual rainfall over the entire period of record. The height of the entire bar represents the total annual precipitation and the red part is the contribution for the 95th percentile events. The 95th percentile event threshold for this location is 0.69 inches.
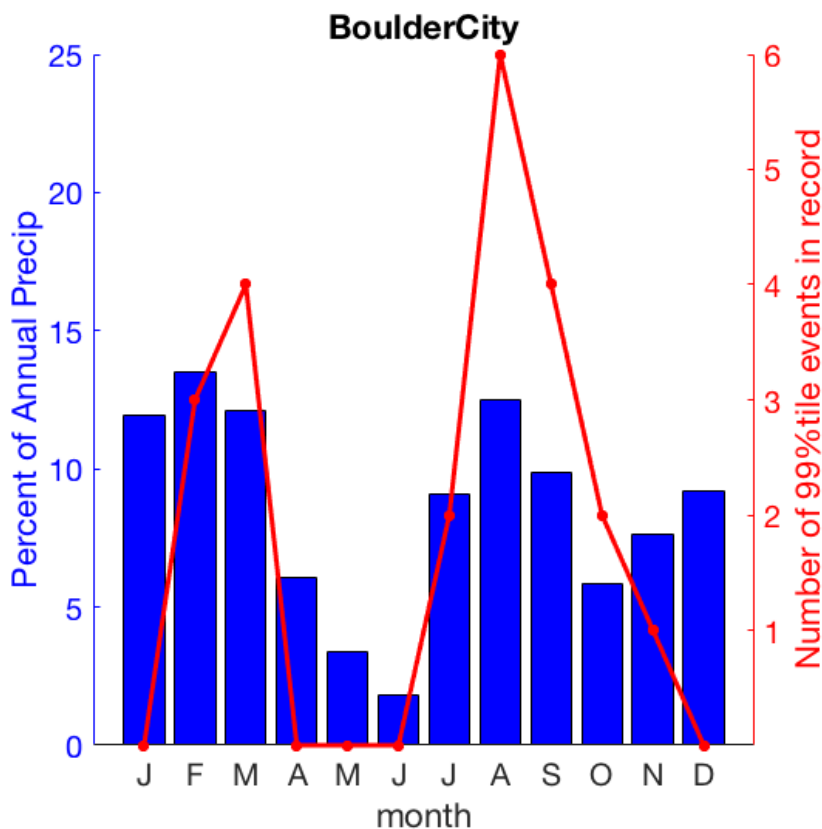
A1-2. The blue bars show the average monthly percent contribution to the total annual rainfall. Thus all 12 bars total 100%. The red line is the number of extreme precipitation events, or 99th percentile events from 1961-1990. The 99th percentile event threshold is 1.13 inches.
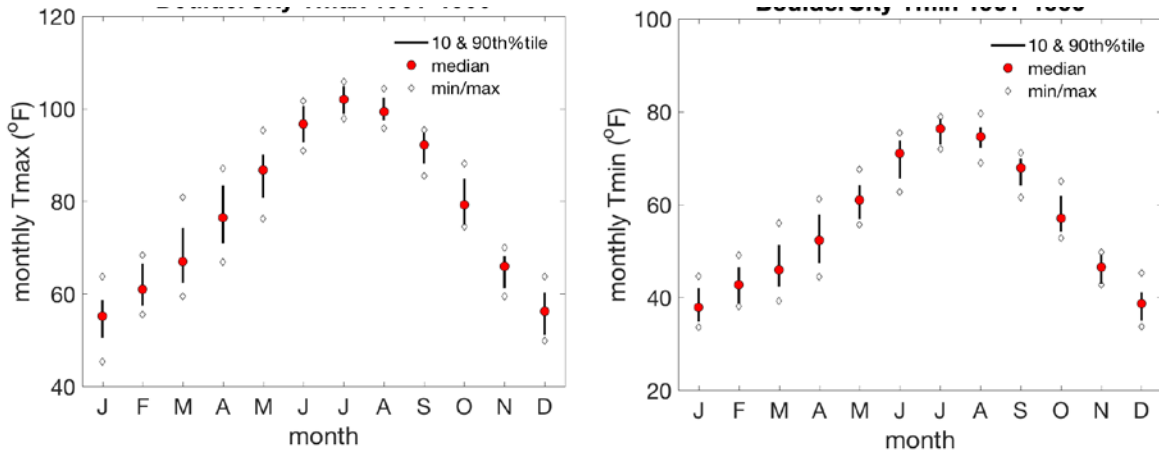
Figure A1-3. The graphs depict the median monthly T_{max} (ºF) (left) and T_{min} (right) at the Boulder City station represented by the circles. Monthly values from 1981-2010 are averaged for each month (January to December). The line illustrates the range of temperatures in the 10th to 90th percentiles. The diamonds represent the maximum and minimum T_{max} values over the 1981-2010 time period.
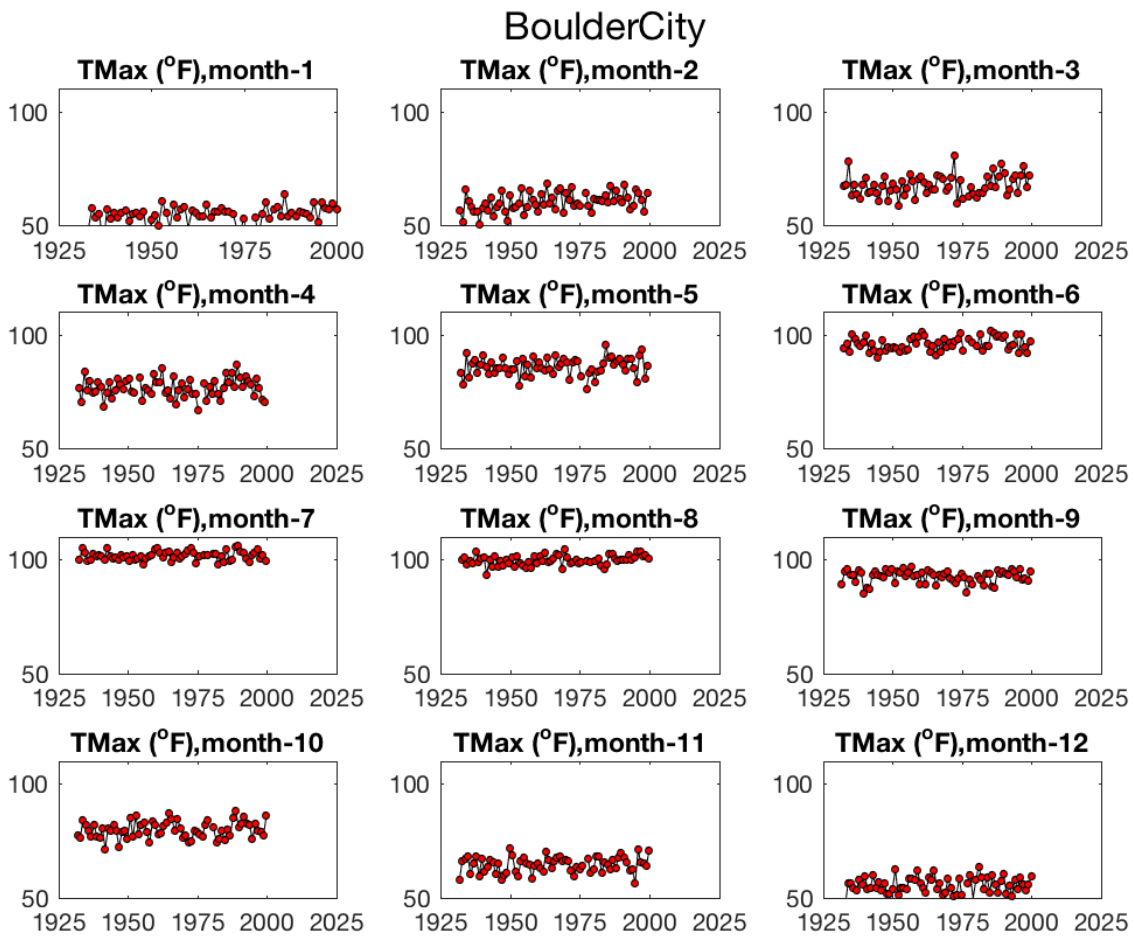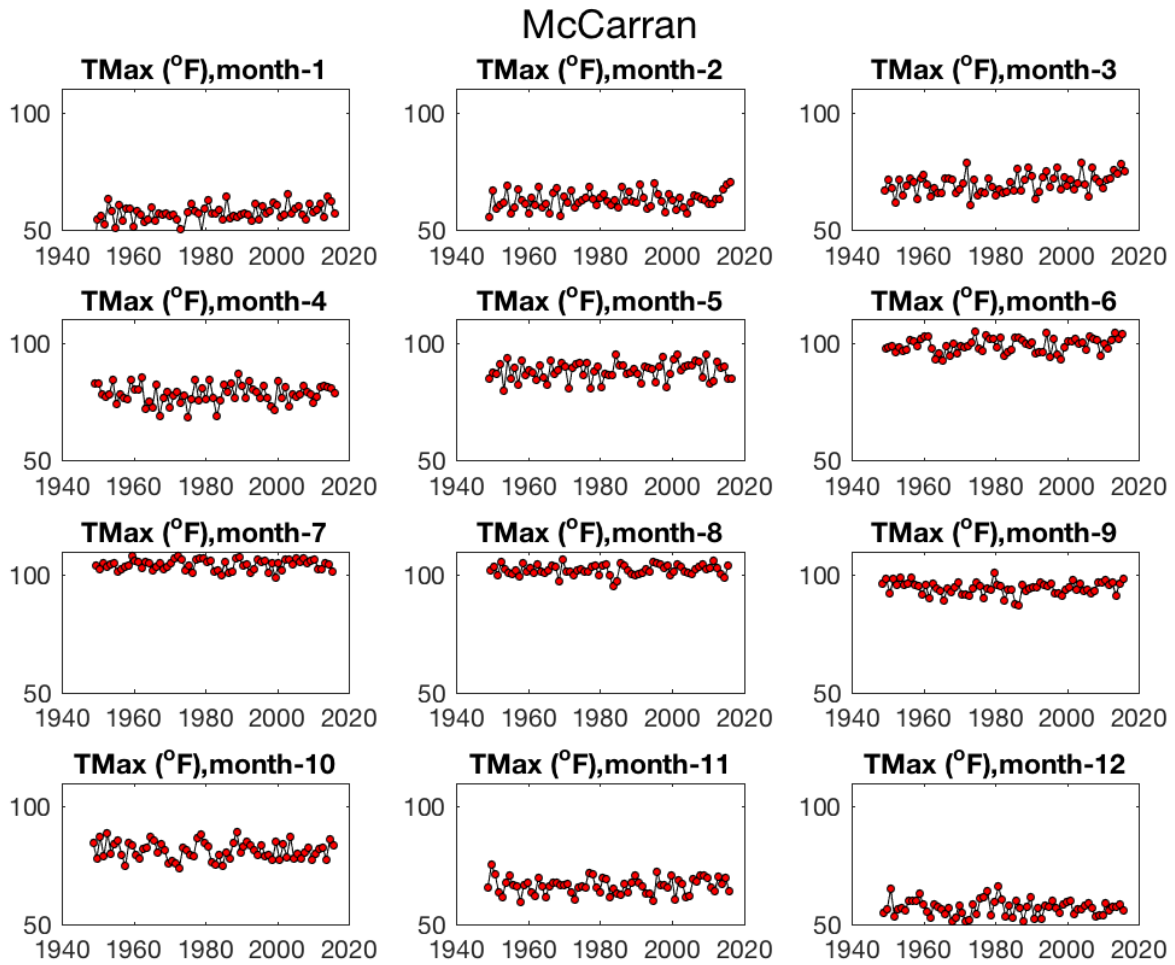

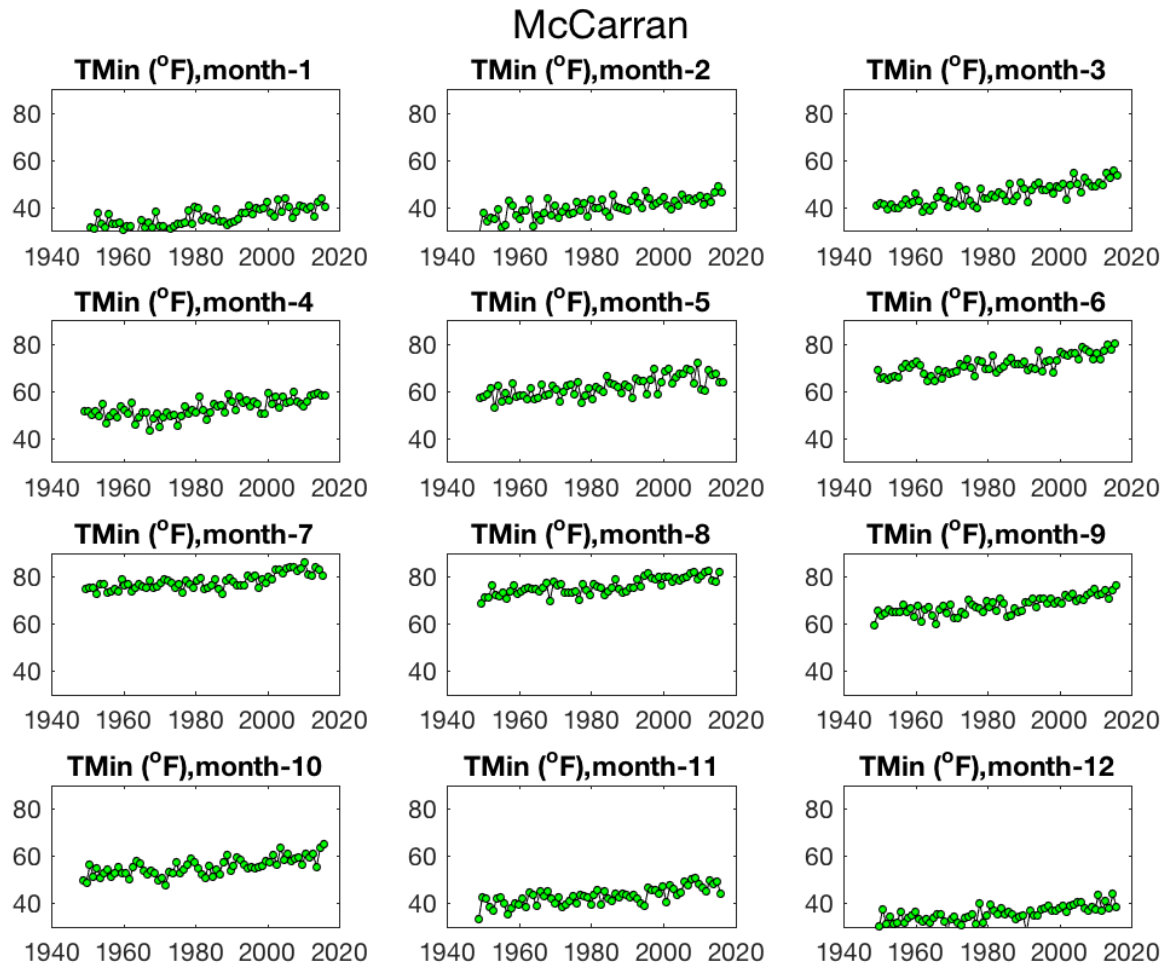Figure A1-4. Each panel shows the monthly average Tmax (˚F) for each year of record at Boulder City.
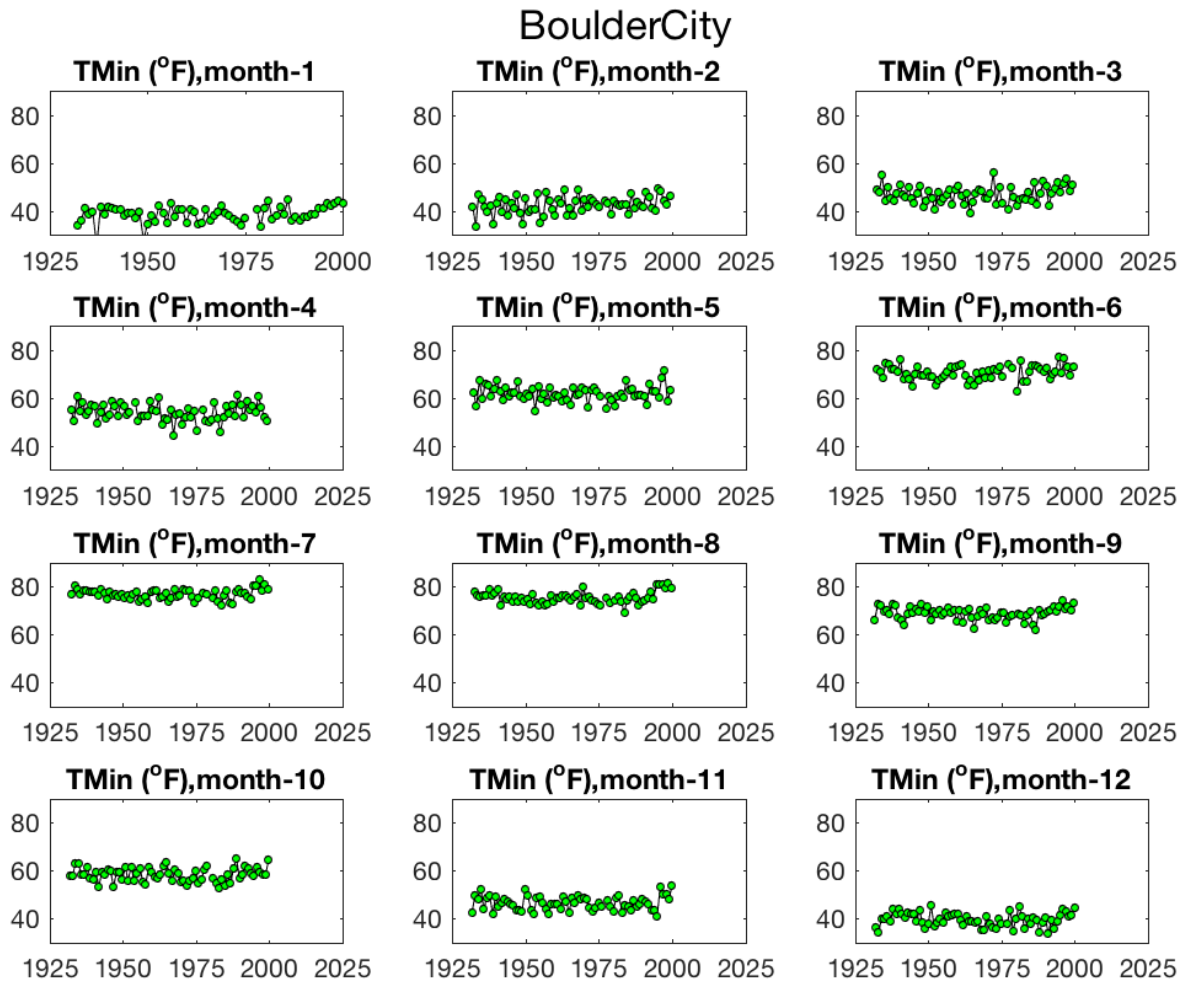
Figure A1-5. Each panel shows the monthly average Tmin (˚F) for each year of record at Boulder City.
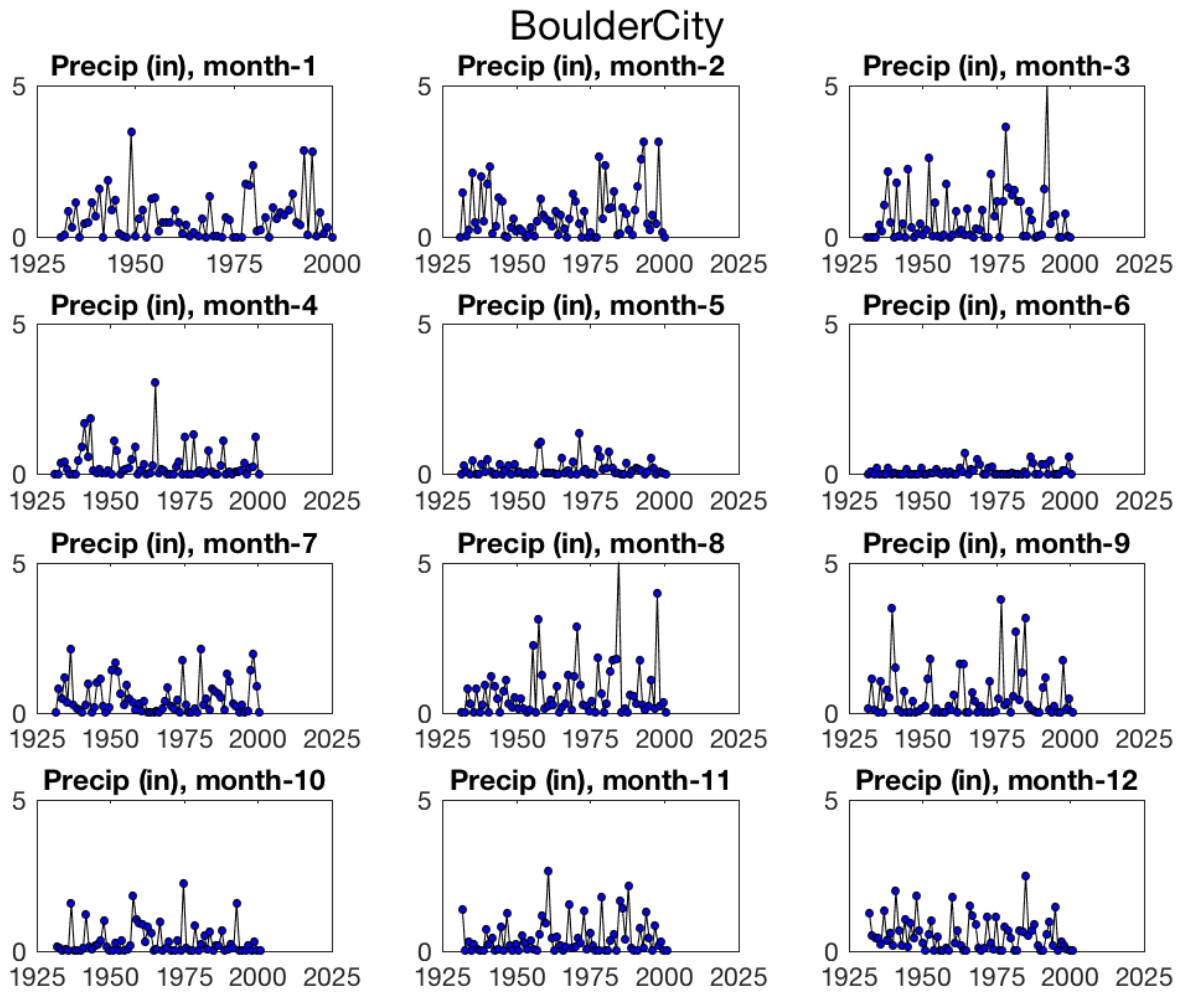
Figure A1-6. Each panel shows the accumulated precipitation (in) for each year of record at Boulder City.

BoulderCity
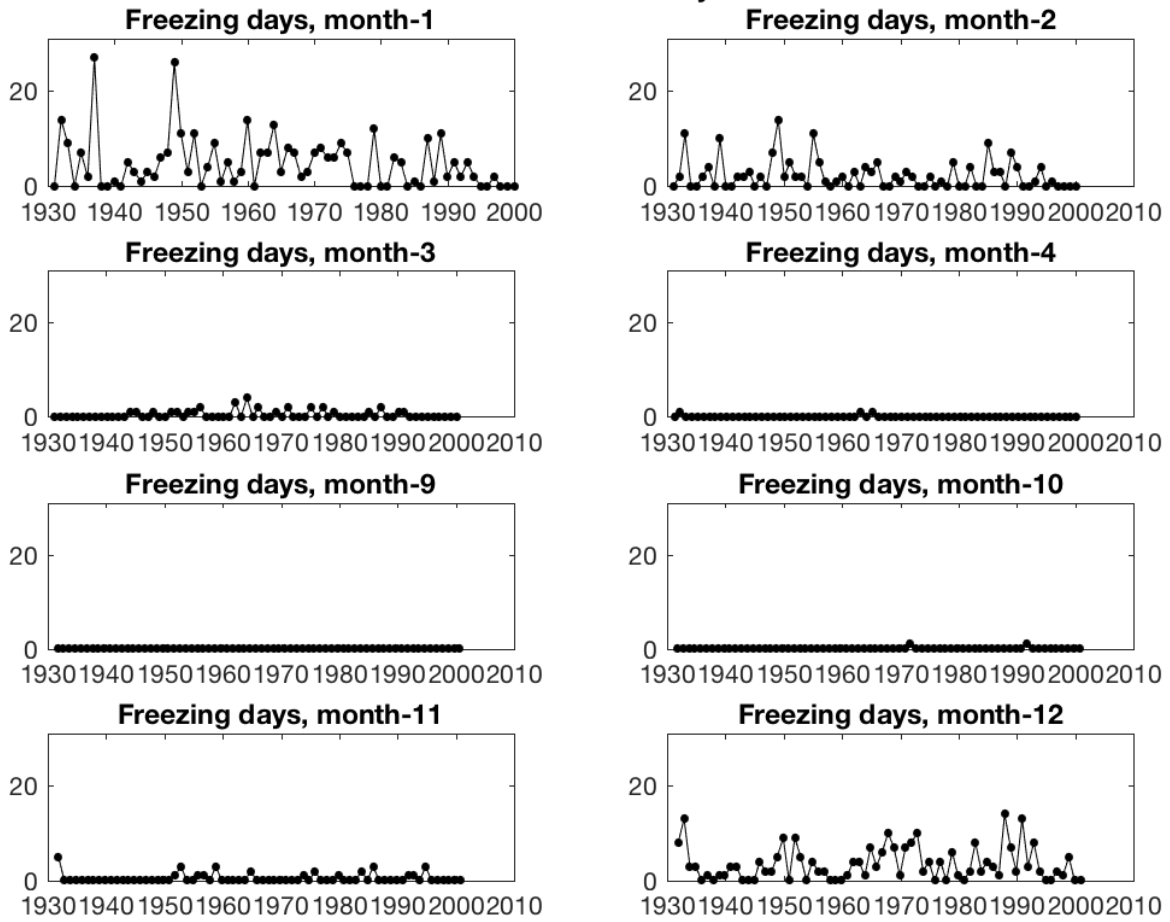
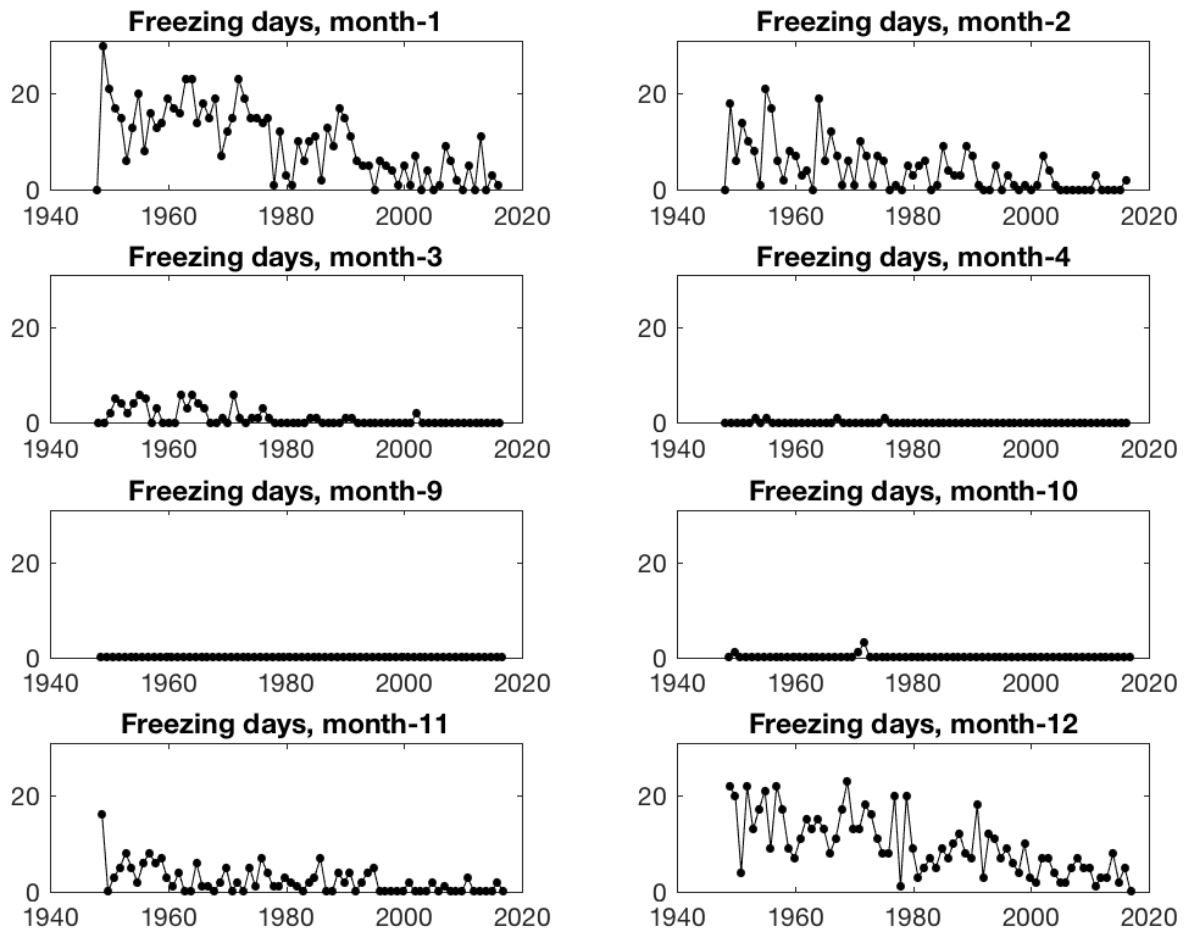Figure A1-7. Each panel shows the monthly sum of the total number of freezing days for each year of record at Boulder City. The maximum in Jan, March, October, and December is 31 days.
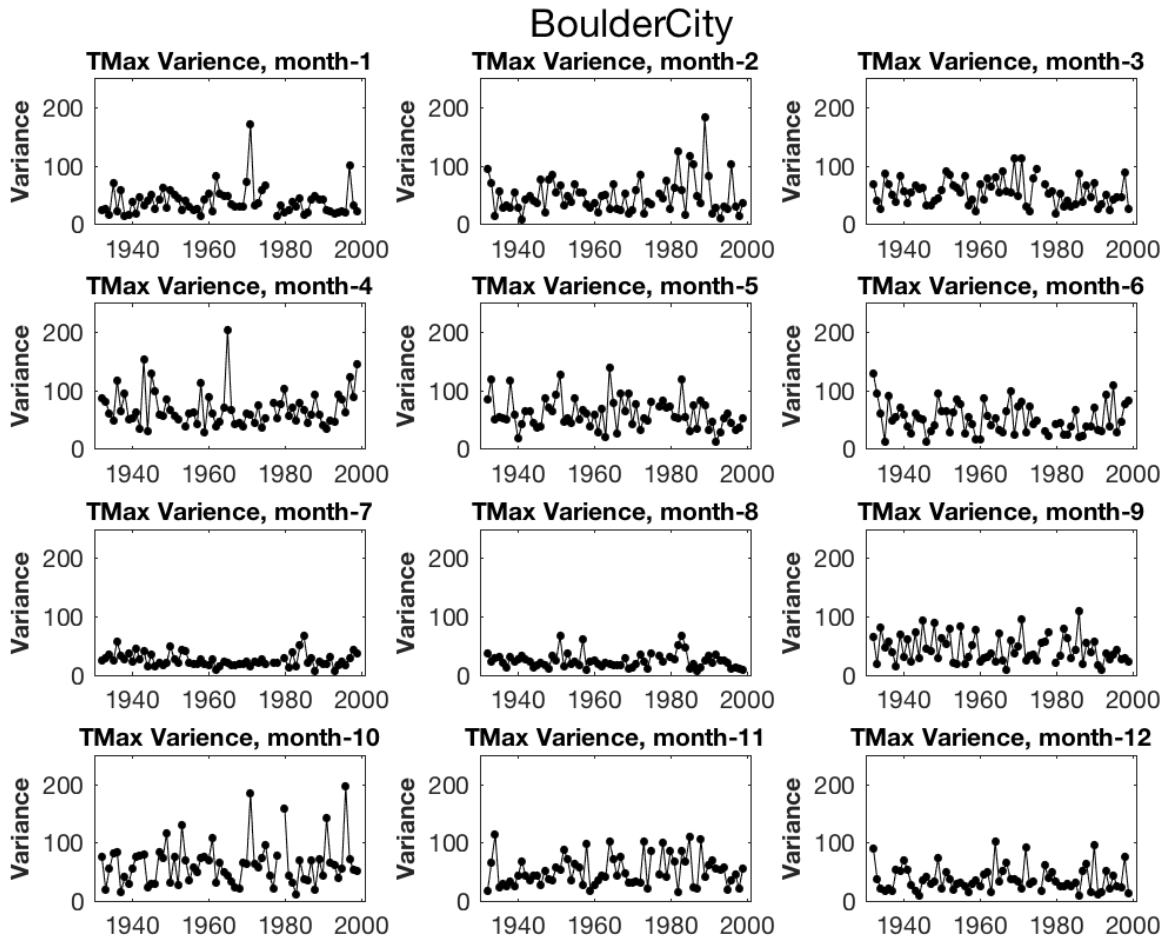
Figure A1-8. Each panel shows the variance (standard deviation squared) in Tmax during a given month at Boulder City.
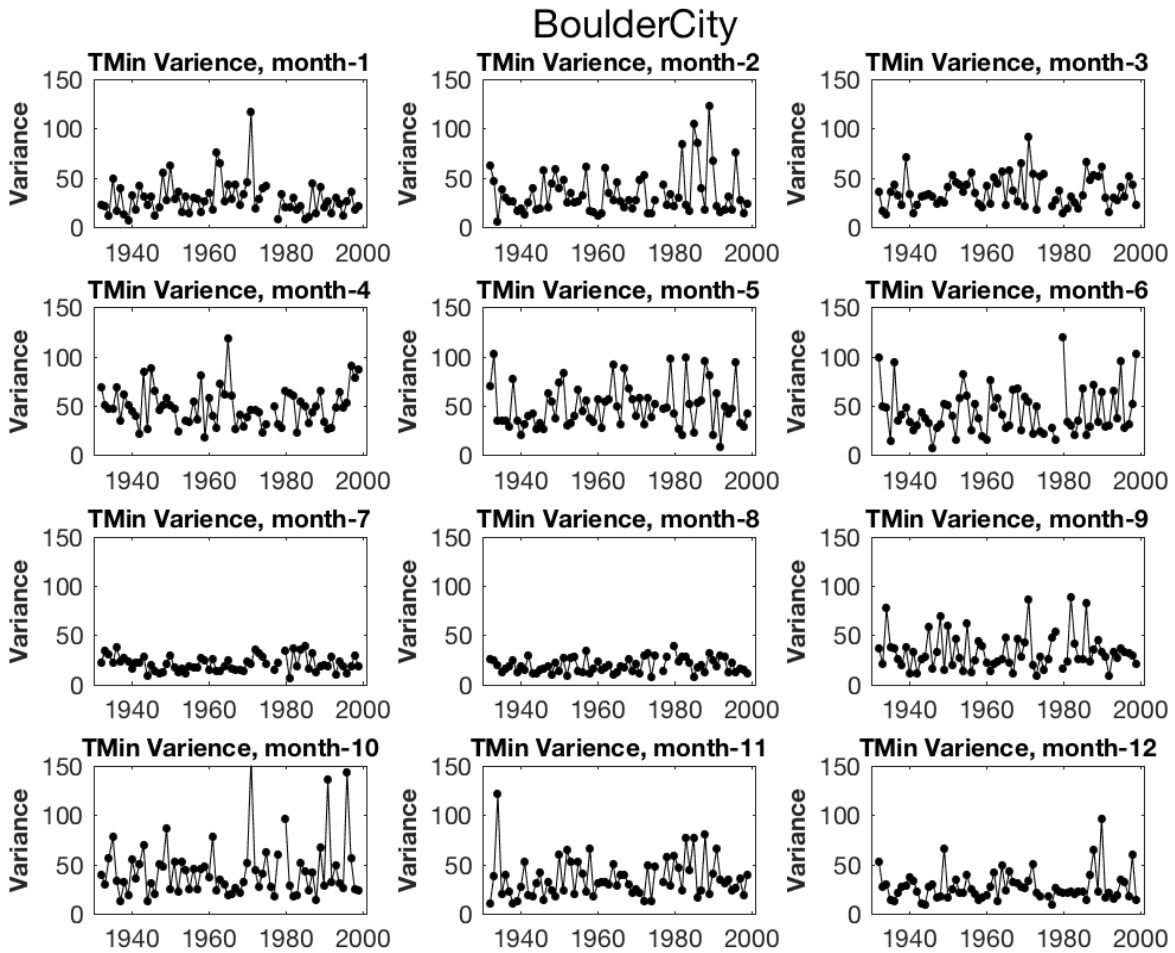
Figure A1-9. Each panel shows the variance (standard deviation squared) in Tmin during a given month at Boulder City.
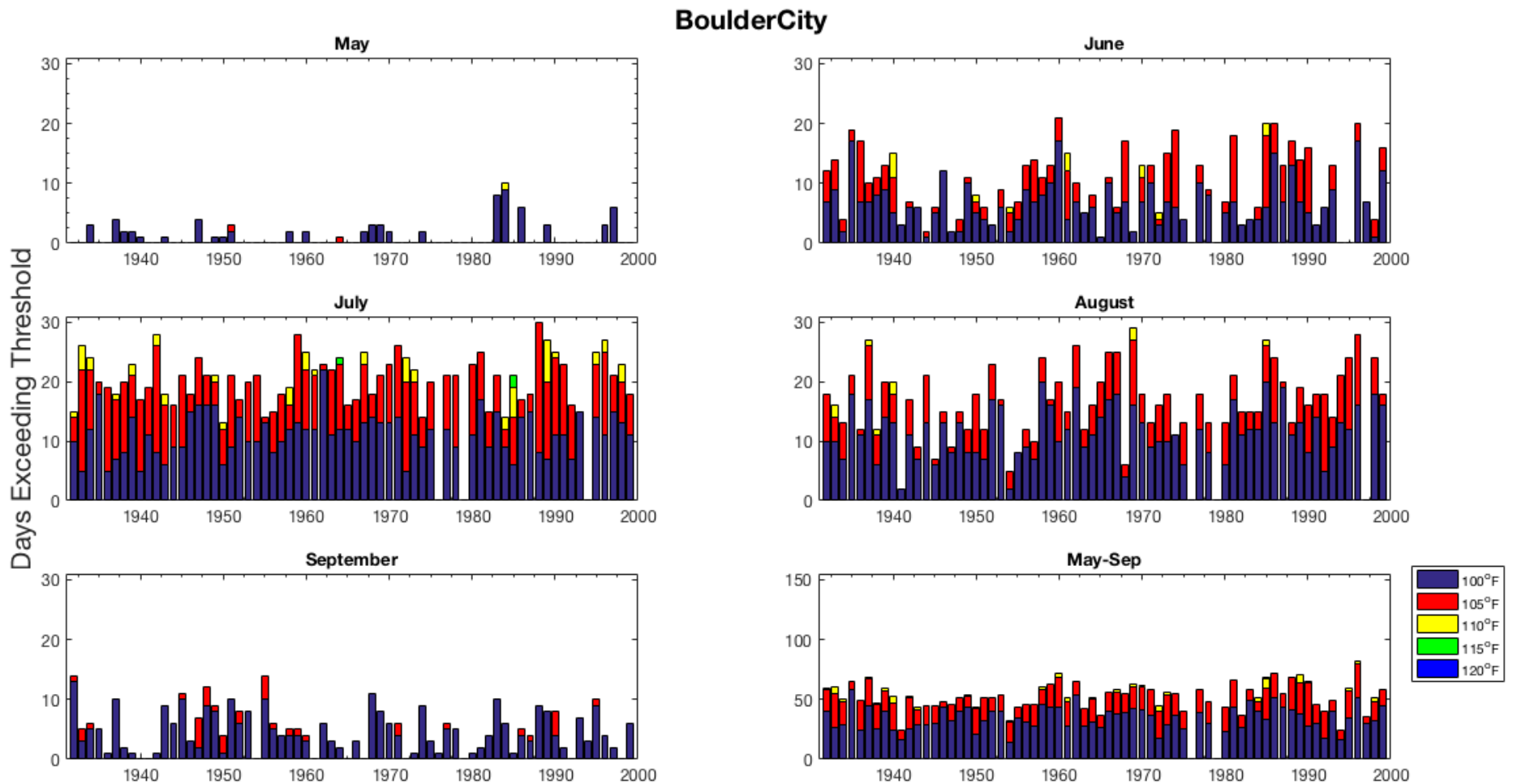
A1-10. The bars illustrate the number of days above a temperature threshold in May, June, July, August and September of a given year. The purple bar indicates the number of days above 100˚F, the red bar is the number of days above 105˚F, the yellow bar is the number of days above 110˚F and the green is the number of days above 115˚F. The last panel depicts the number of days above these thresholds from May through September through time.
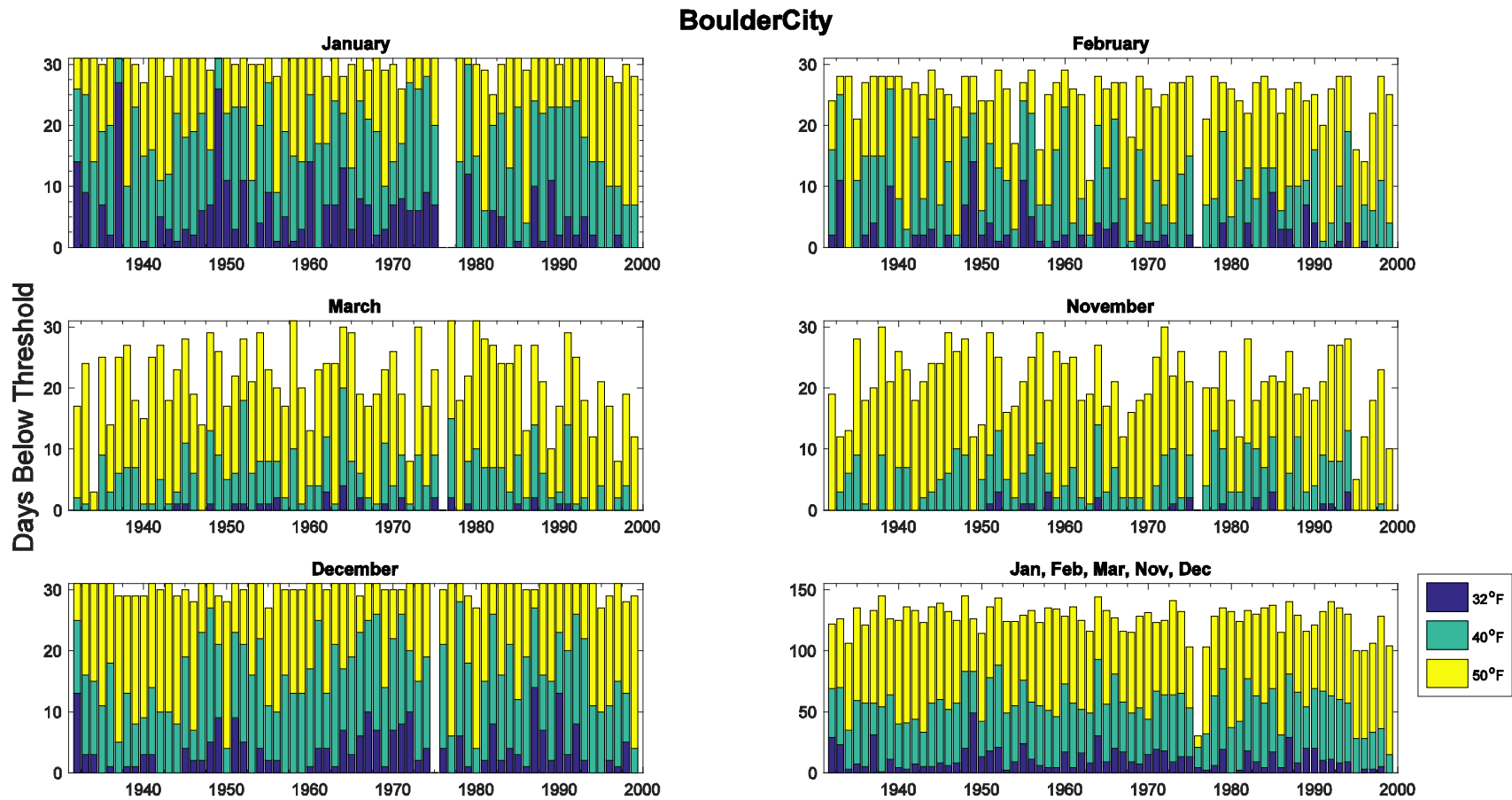
Figure A1-11. The bars illustrate the number of days below a temperature threshold in November, December, January, February and March of a given year. The purple bar represents the number of days below 32˚F, the green bar represents number of days below 40˚F, the yellow bar is the number of days below 50˚F. The maximum number of days for January, March and December is 31.

2. Desert National Wildlife Range
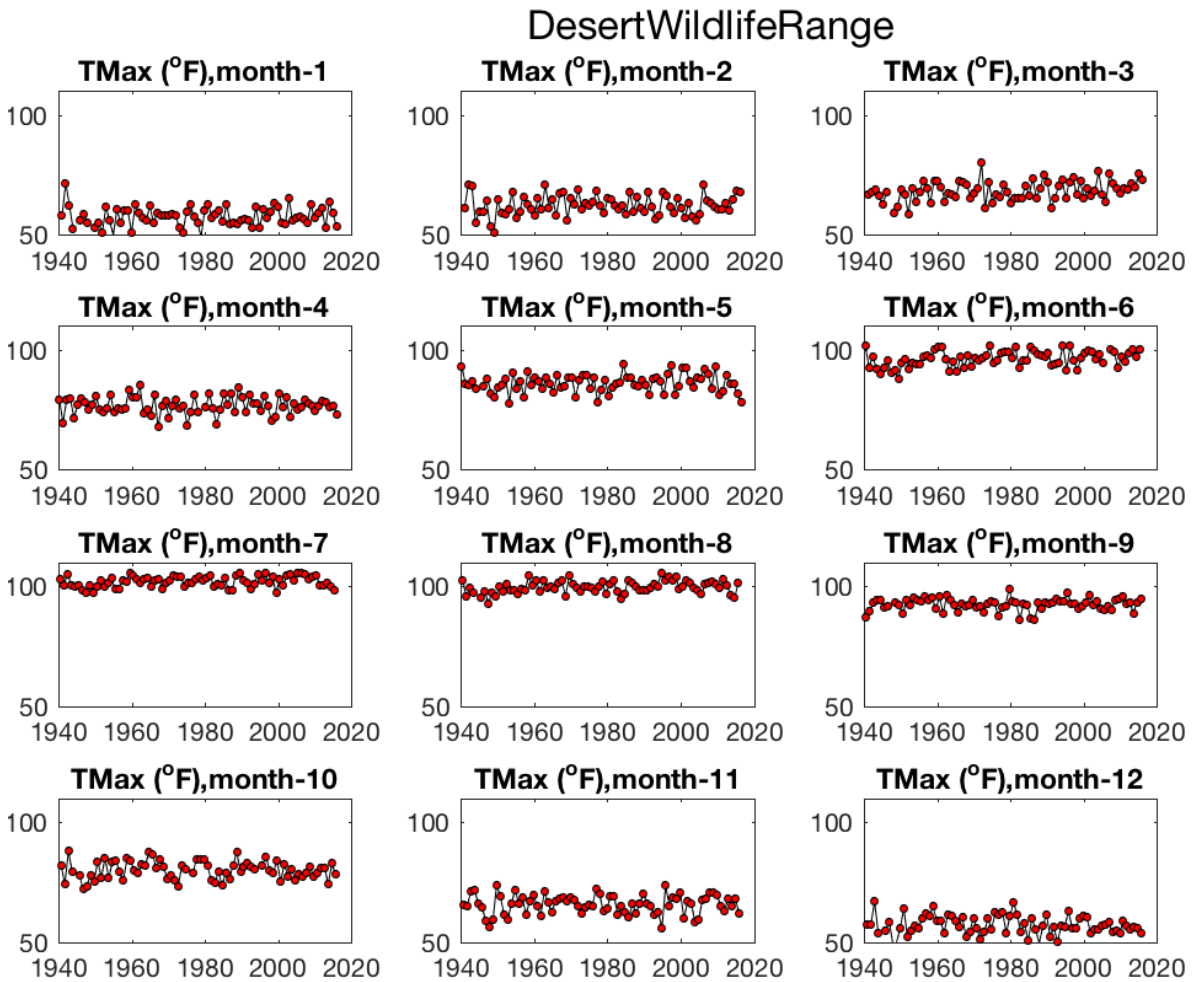
Figure A2-1. Each panel shows the monthly average Tmax (˚F) for each year of record at Desert National Wildlife Range.

DesertWildlifeRange
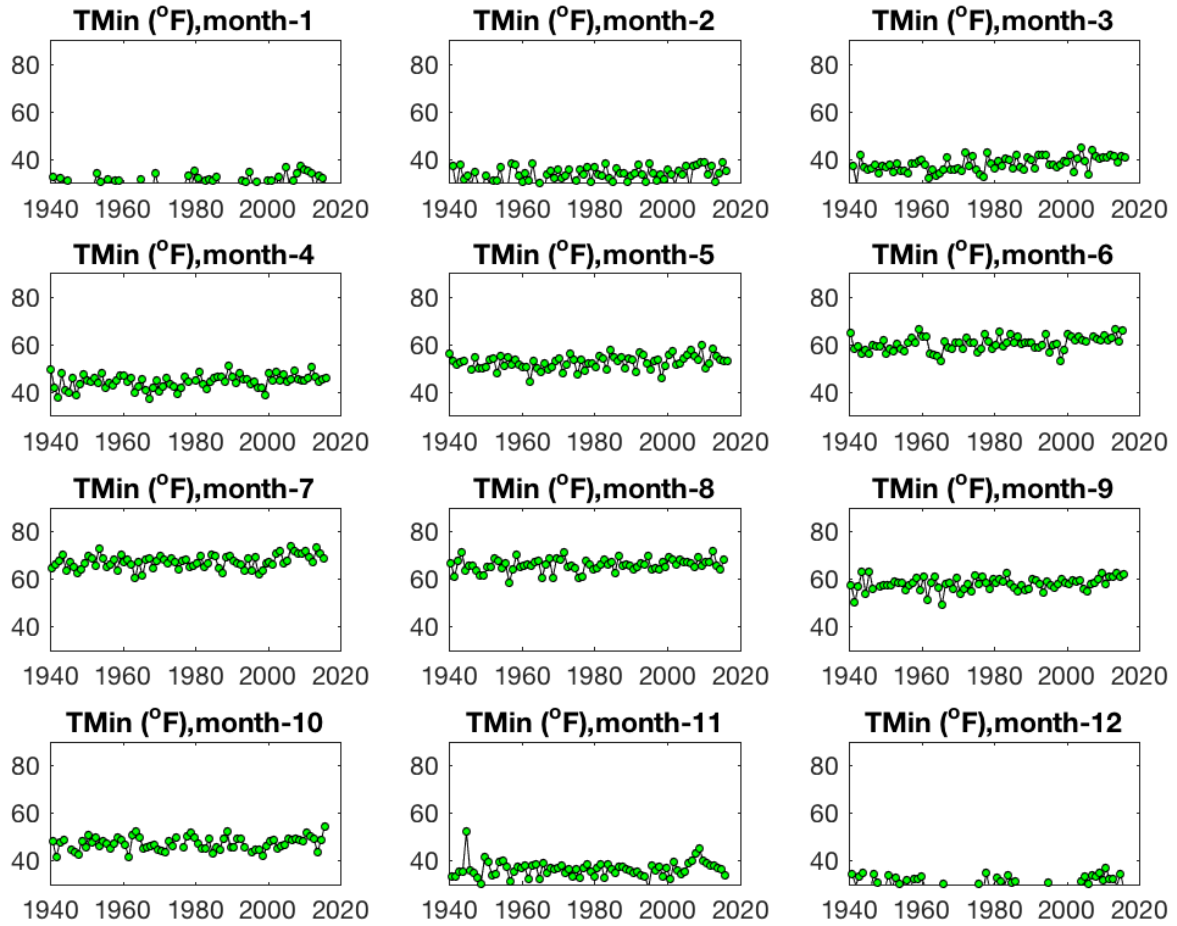
Figure A2-2. Each panel shows the monthly average Tmin (˚F) for each year of record at Desert National Wildlife Range.
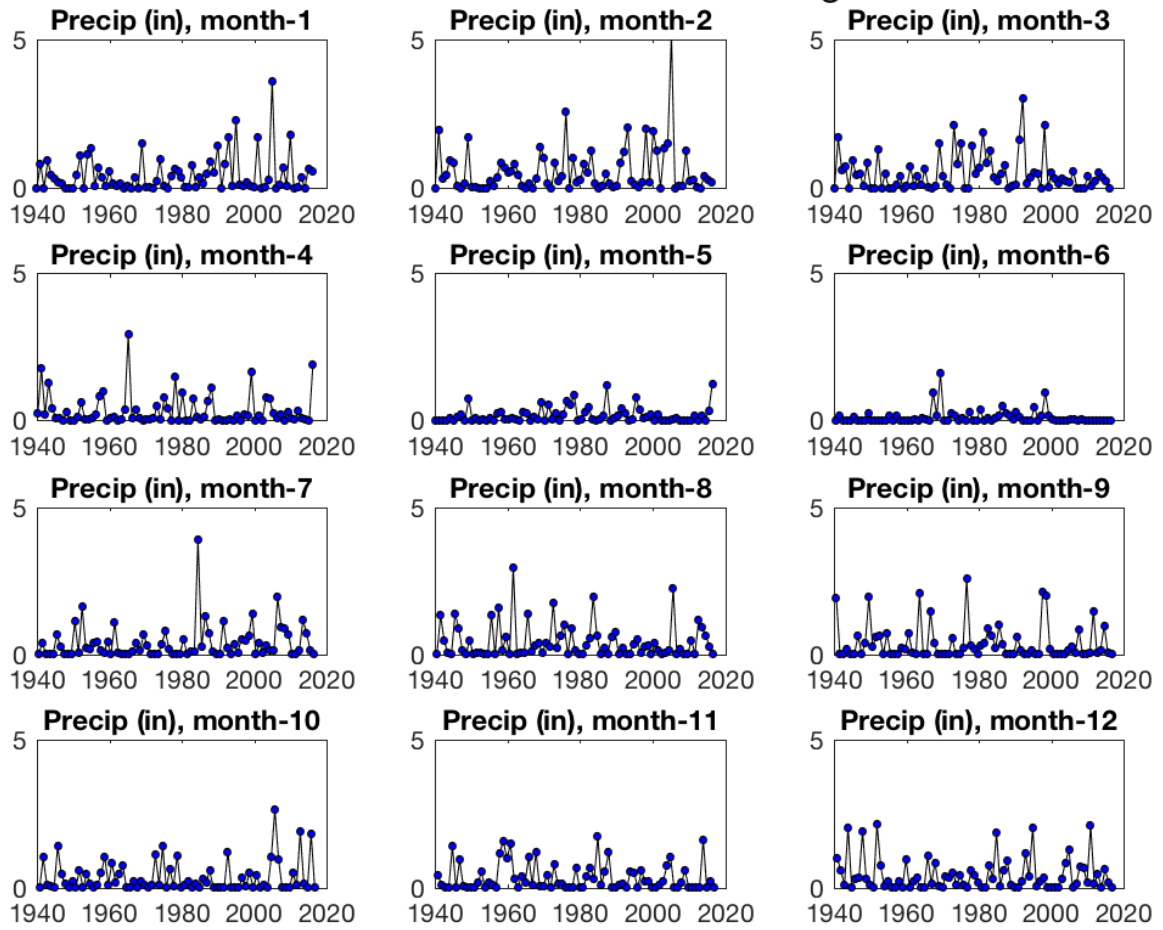
Figure A2-3. Each panel shows the monthly sum of precipitation (in) for each year of record at Desert National Wildlife Range.
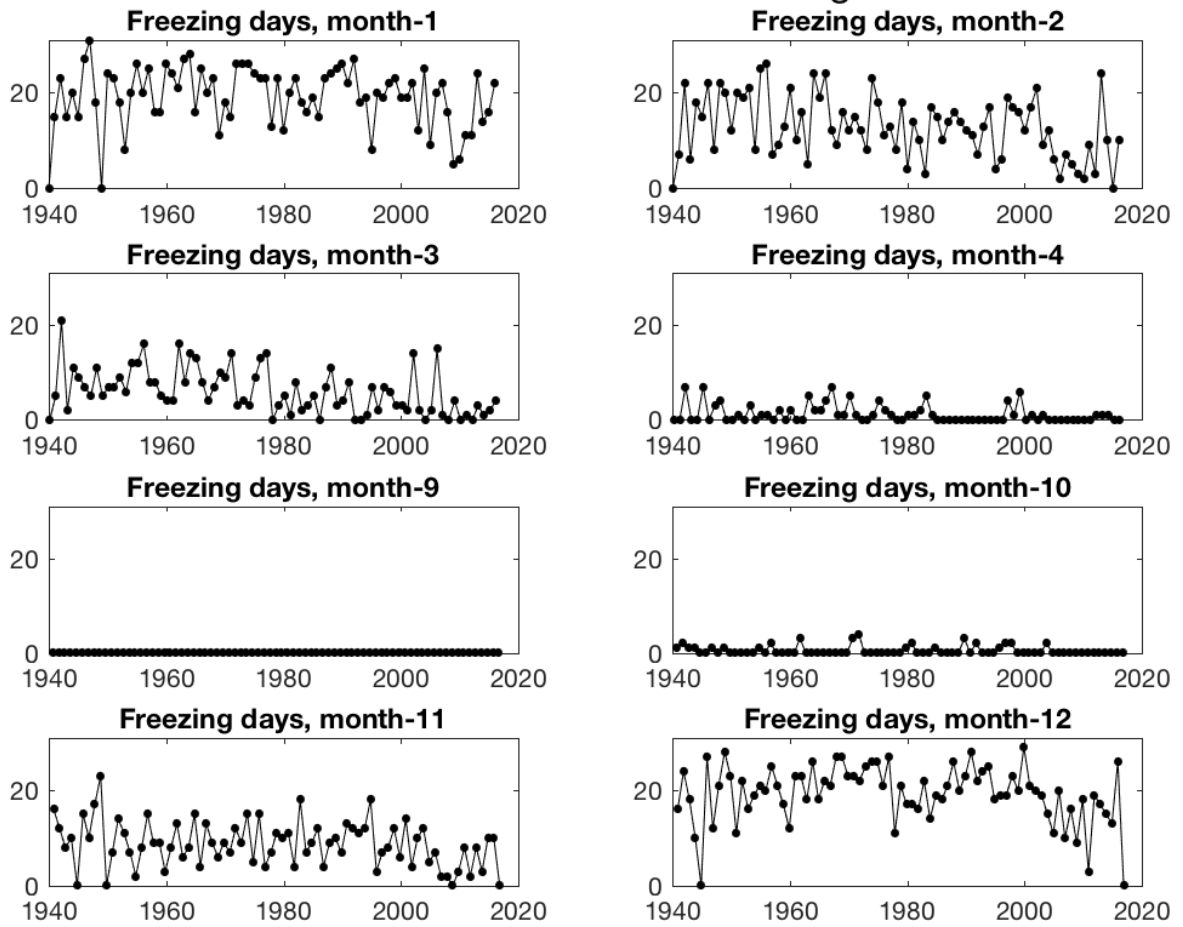
Figure A2-4. Each panel shows the monthly sum of the total number of freezing days for each year of record at Desert National Wildlife Range. The maximum in Jan, March, October, and December is 31 days.
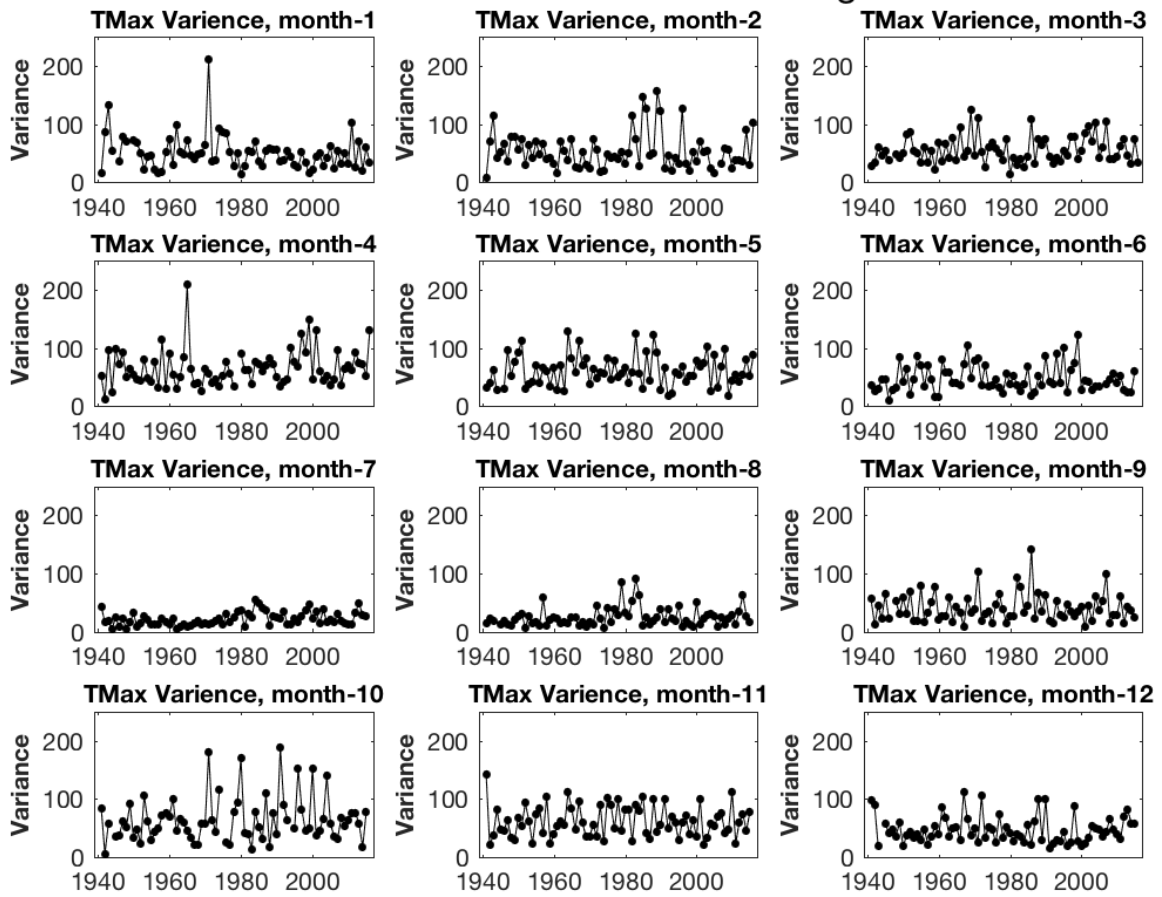
Figure A2-5. Each panel shows the variance (standard deviation squared) in Tmax during a given month at Desert Wildlife Range.
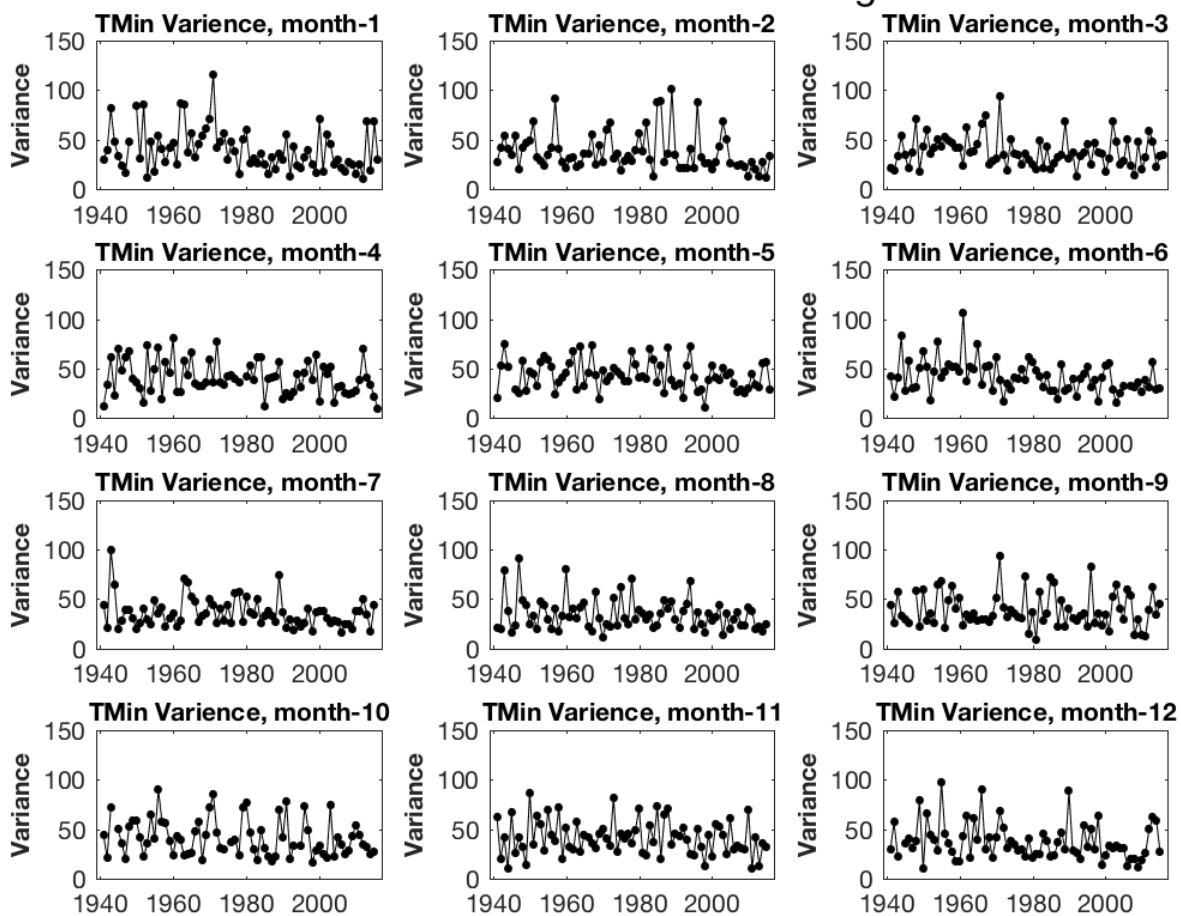
Figure A2-6. Each panel shows the variance (standard deviation squared) in Tmin during a given month at Desert Wildlife Range.
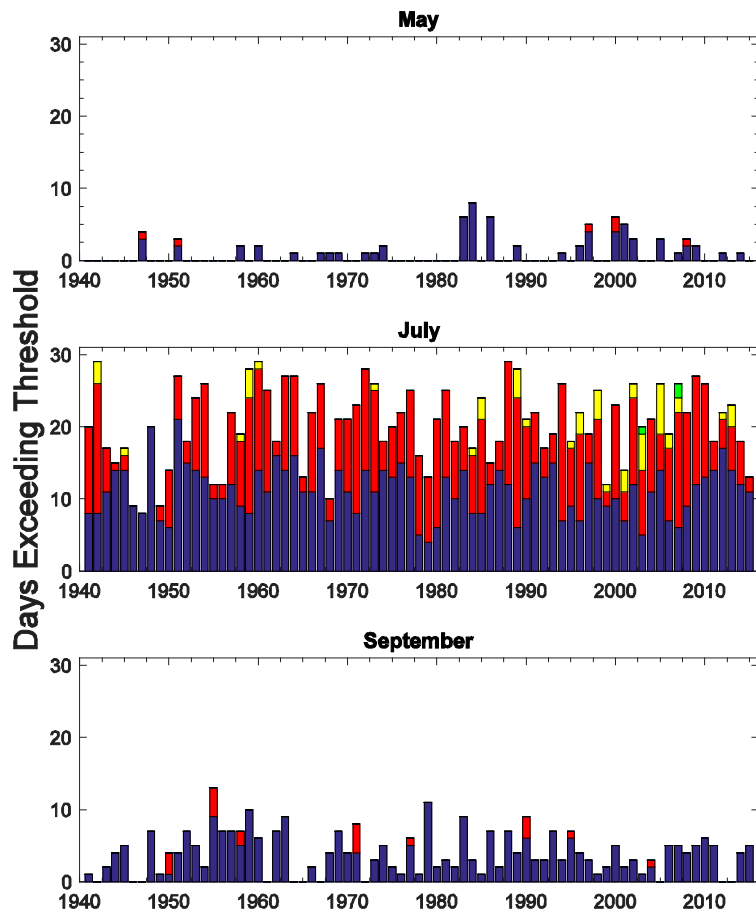
DesertWildlifeRange
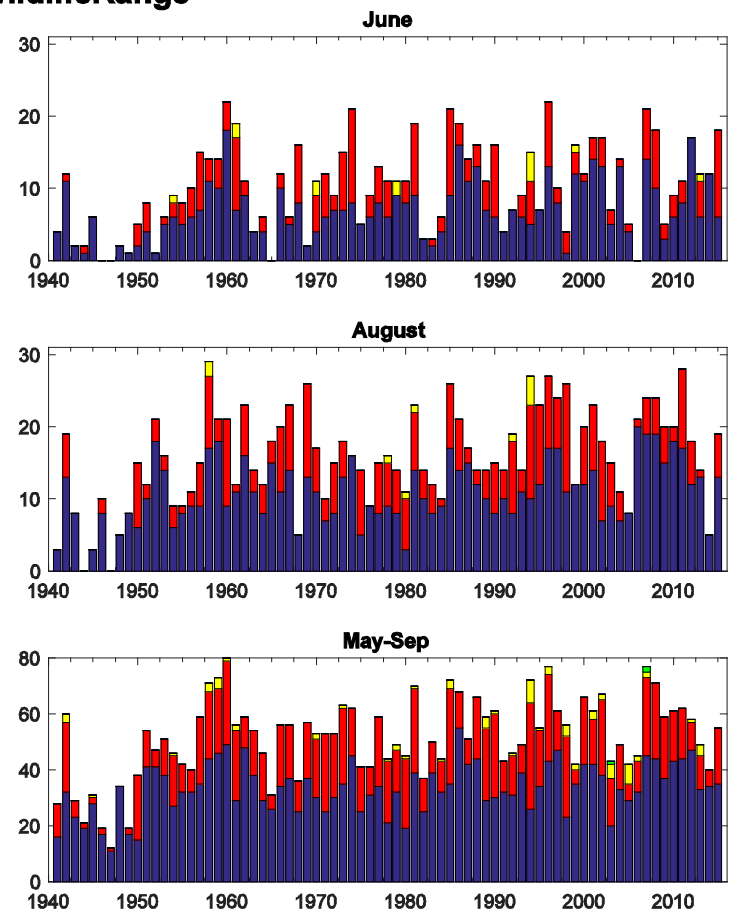
A2-7. The bars illustrate the number of days above a temperature threshold in May, June, July, August and September of a given year. The purple bar indicates the number of days above 100˚F, the red bar is the number of days above 105˚F, the yellow bar is the number of days above 110˚F and the green is the number of days above 115˚F. The last panel depicts the number of days above these thresholds from May through September through time.
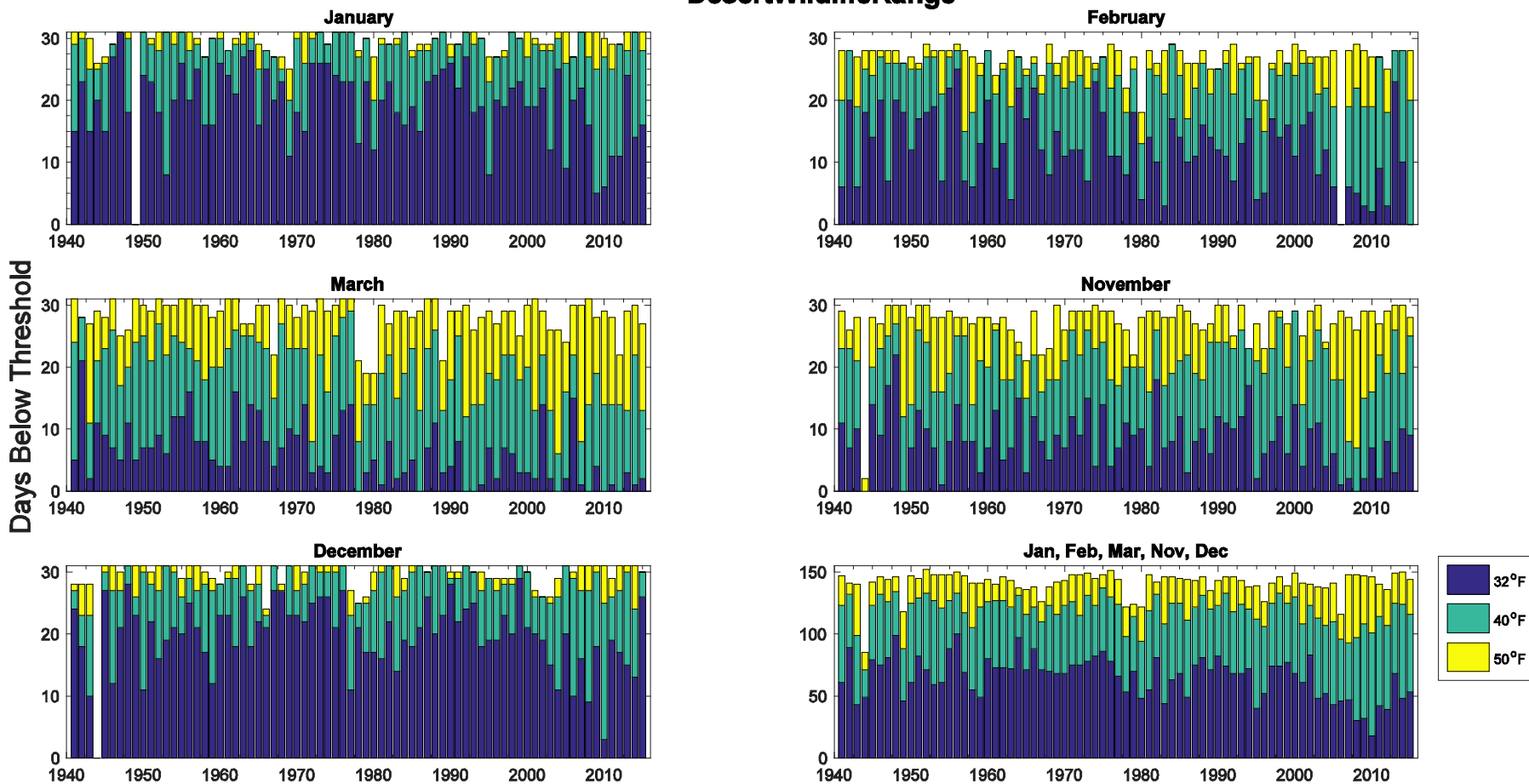
Figure A2-8. The bars illustrate the number of days below a temperature threshold in November, December, January, February and March of a given year. The purple bar represents the number of days below 32˚F, the green bar represents number of days below 40˚F, the yellow bar is the number of days below 50˚F. The maximum number of days for January, March and December is 31.

3. Kingman
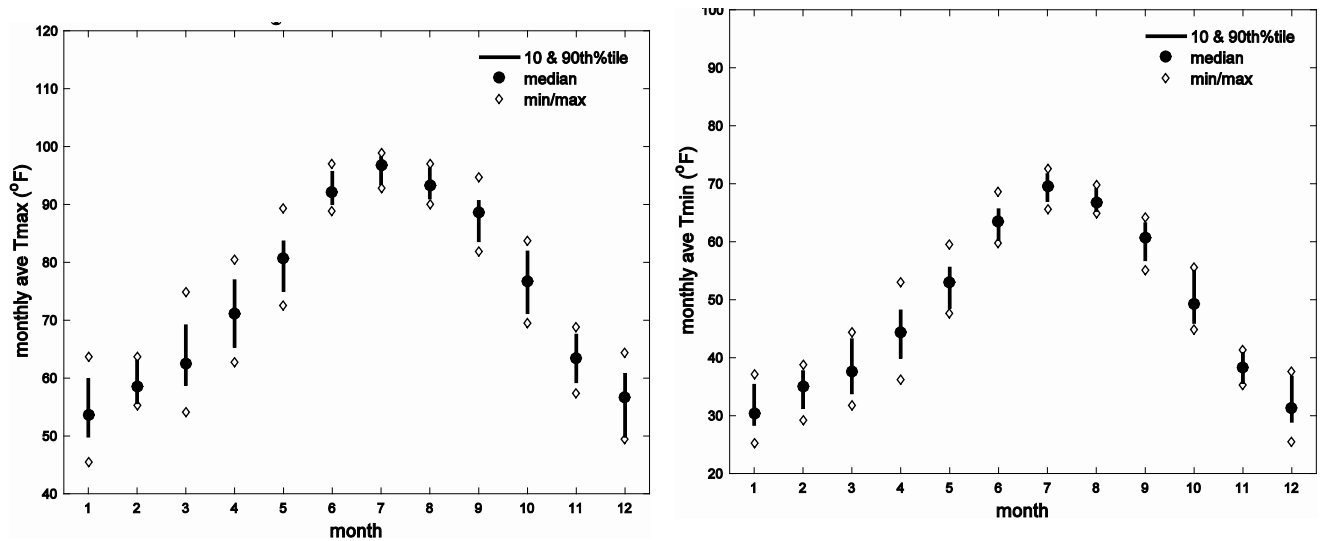
Figure A3-1. The graphs depict the median monthly T_{max} (°F) (left) and T_{min} (right) at the Kingman station represented by the circles. Monthly values from 1981-2010 are averaged for each month (January to December). The line illustrates the range of temperatures in the 10th to 90th percentiles. The diamonds represent the maximum and minimum T_{max} values over the 1981-2010 time period.
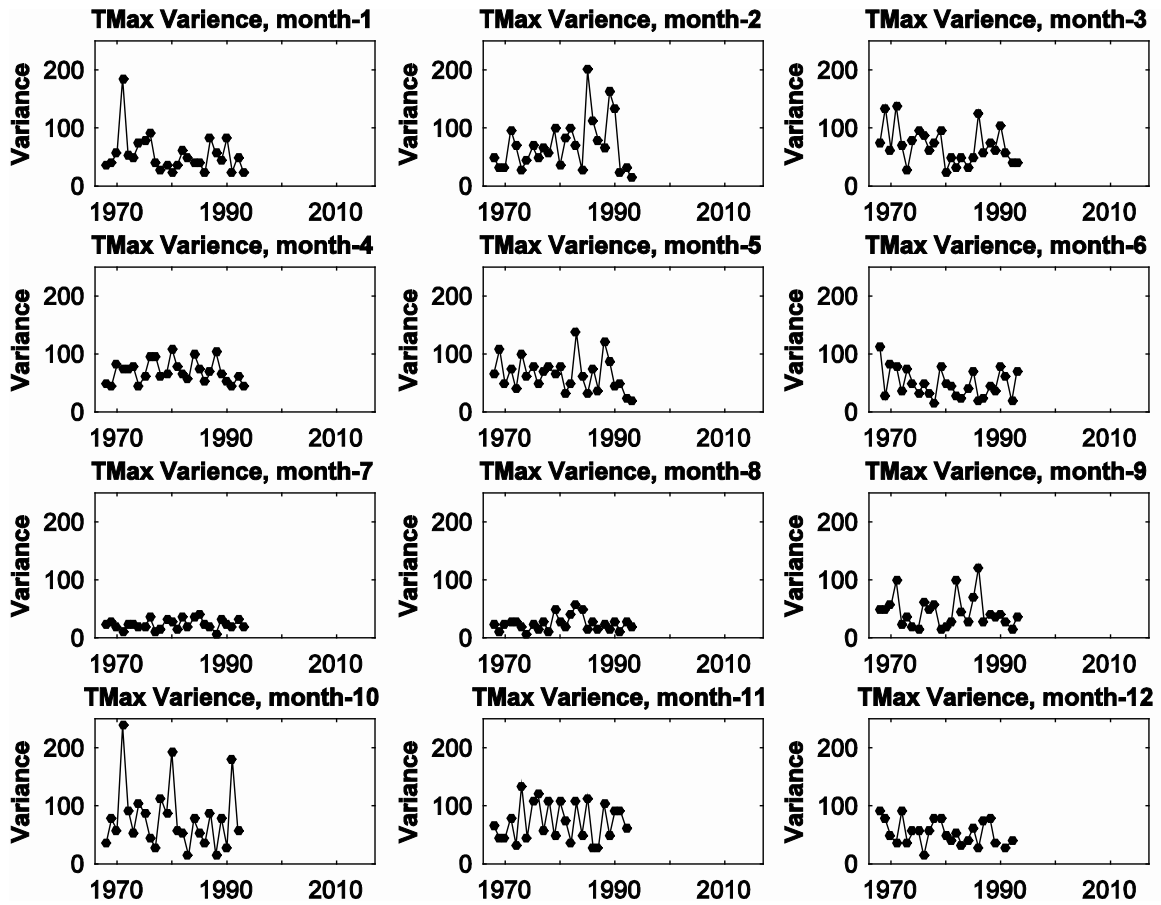
Figure A3-2. Each panel shows the monthly average Tmax (˚F) for each year of record at Kingman.
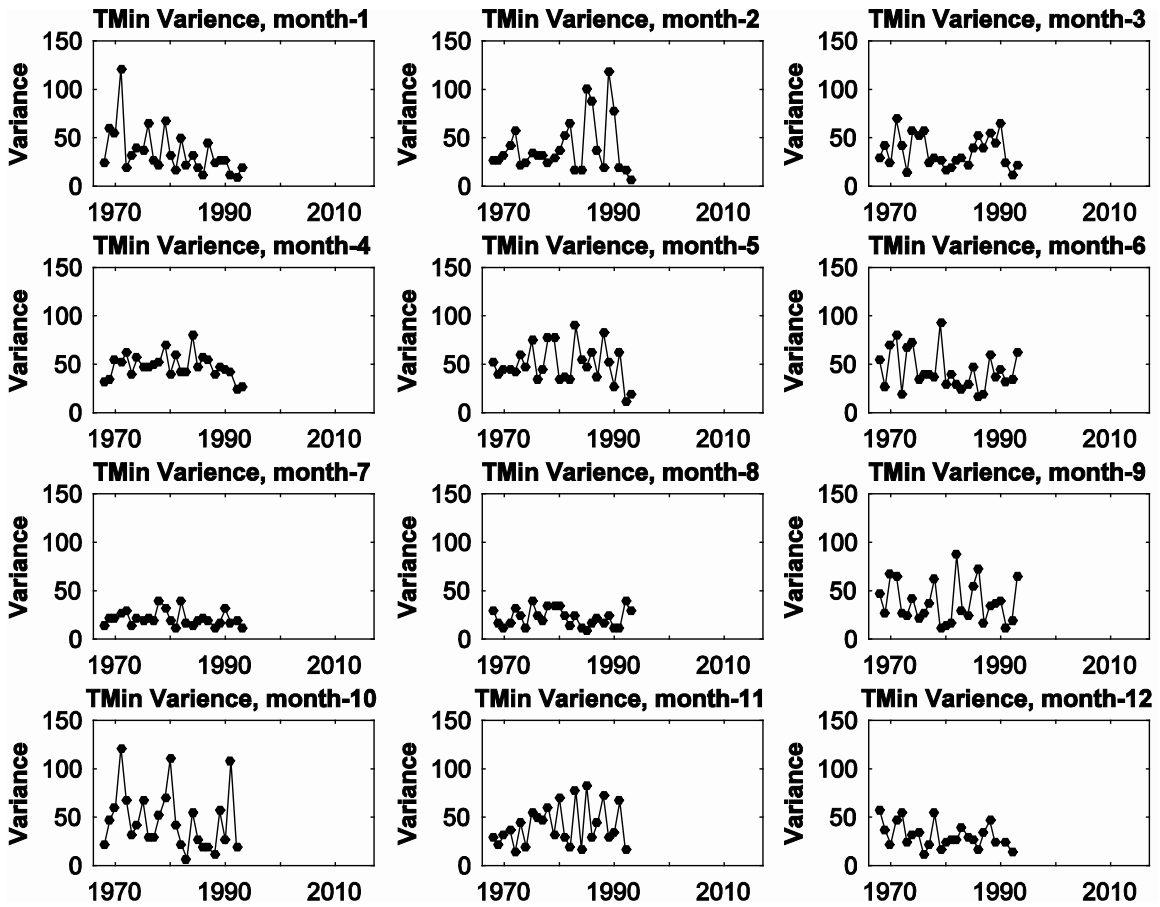
Figure A3-3. Each panel shows the monthly average Tmax (˚F) for each year of record at Kingman.
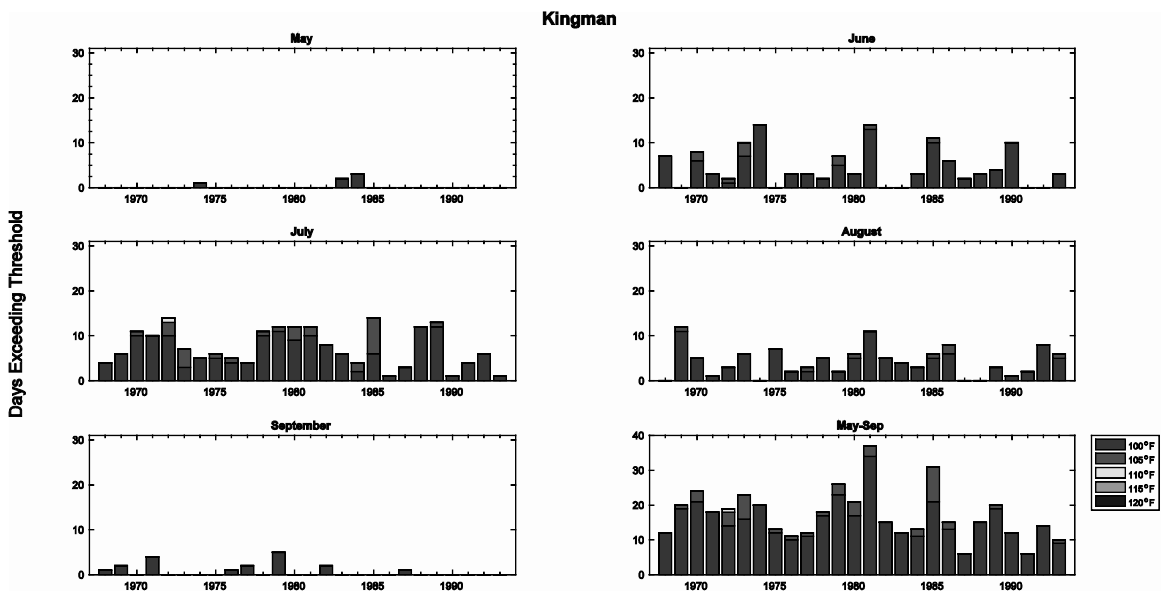
Figure A3-4. The bars illustrate the number of days above a temperature threshold in May, June, July, August and September of a given year. The purple bar indicates the number of days above 100°F, the red bar is the number of days above 105°F, the yellow bar is the number of days above 110°F and the green is the number of days above 115°F. The last panel depicts the number of days above these thresholds from May through September through time.
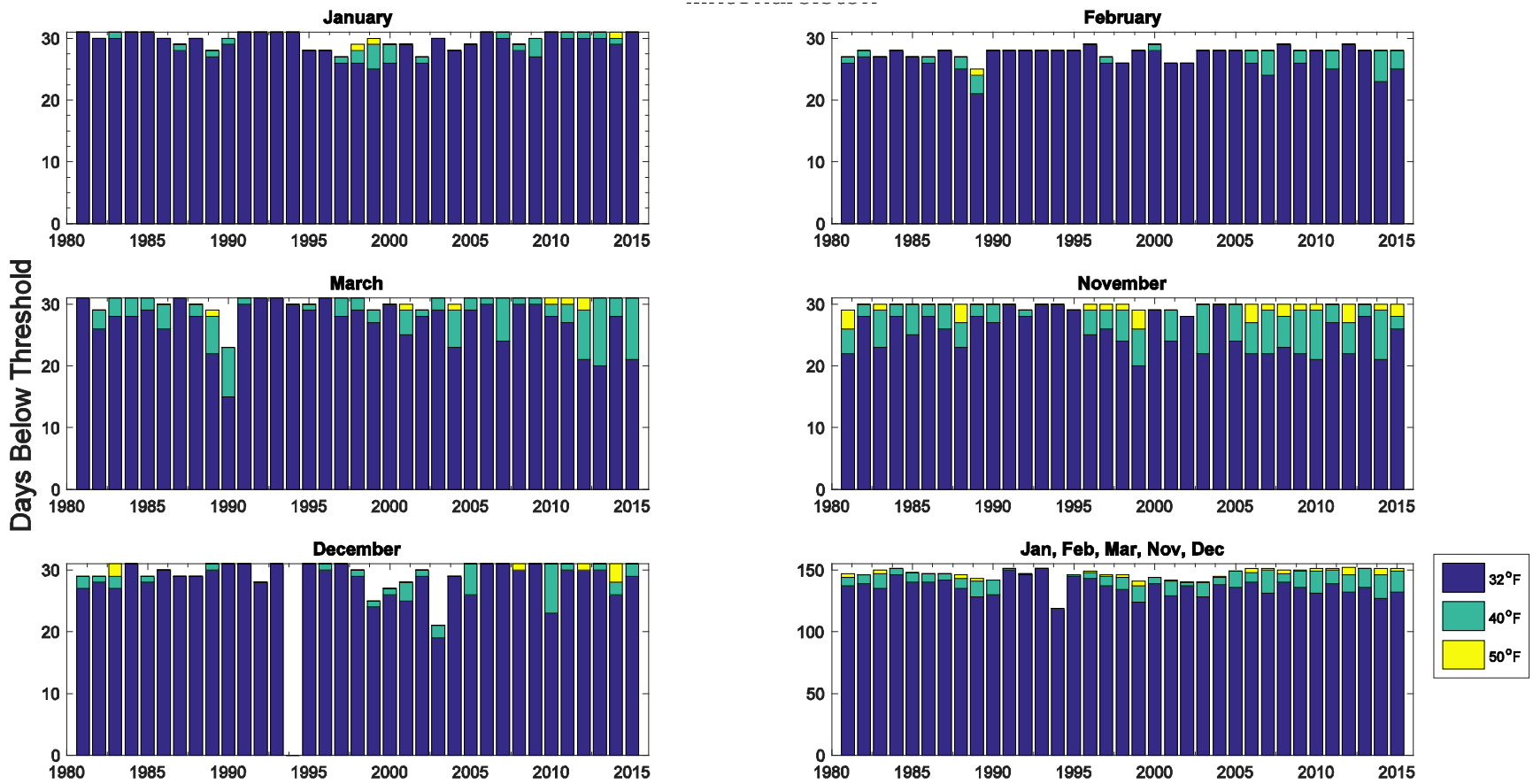

Figure A4-11. The bars illustrate the number of days below a temperature threshold in November, December, January, February and March of a given year. The purple bar represents the number of days below 32°F, the green bar represents number of days below 40°F, the yellow bar is the number of days below 50°F. The maximum number of days for January, March and December is 31.
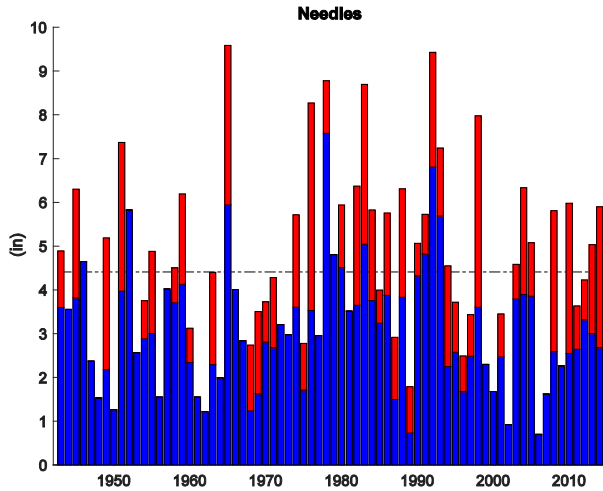
4. Laughlin

Figure A4-1. The total annual rainfall in inches. The dashed line is the average annual rainfall over the entire period of record. The height of the entire bar represents the total annual precipitation and the red part is the contribution for the 95%tile events. The threshold of what the 95%tile event is 0.97 inches.
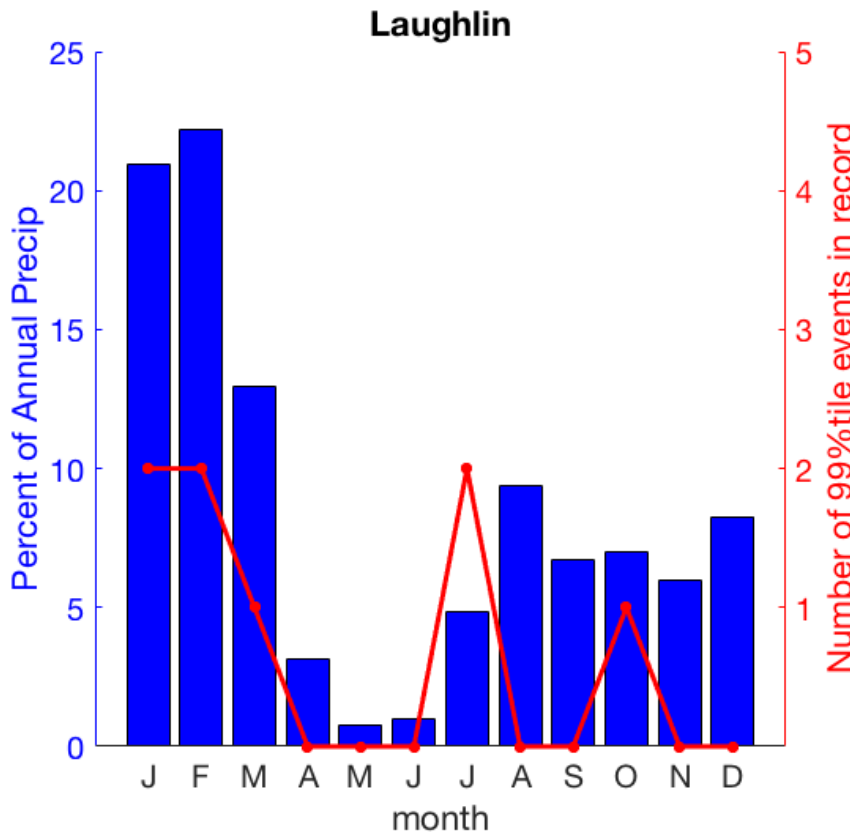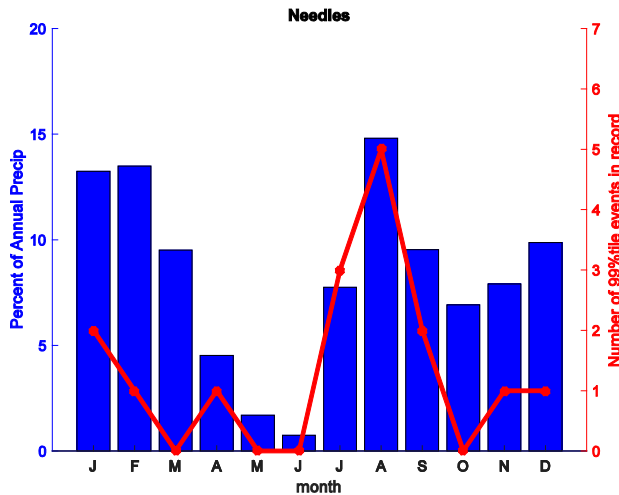

A4-2. The blue bars show the average monthly percent contribution of all precipitation, to the total annual rainfall. Thus all 12 bars total 100%. The red line is the number of extreme precipitation events, or 99th percentile events from 1961-1990. The 99th percentile threshold is 1.48 inches.
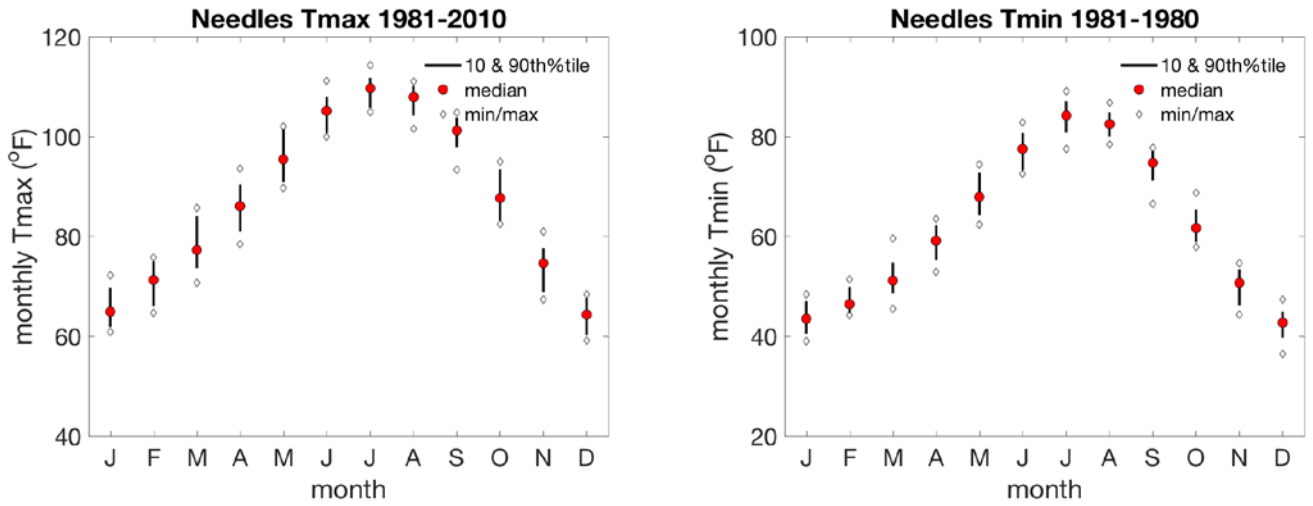
98
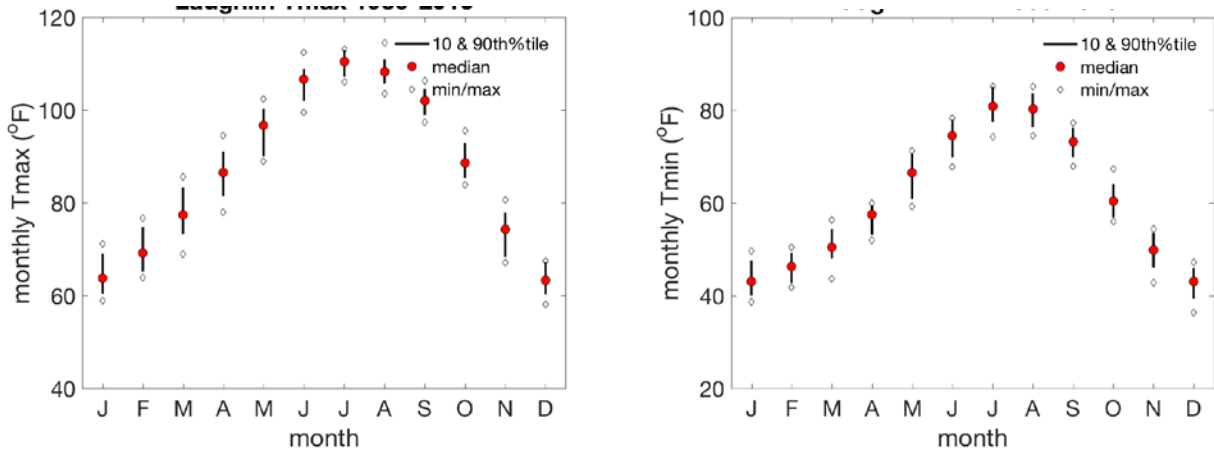
Figure A4-3. The graphs depict the median monthly T_{max} (°F) (left) and T_{min} (right) at the Laughlin station represented by the red circles. Monthly values from 1981-2010 are averaged for each month (January to December). The line illustrates the range of temperatures in the 10th to 90th percentiles. The diamonds represent the maximum and minimum T_{max} values over the 1981-2010 time period.
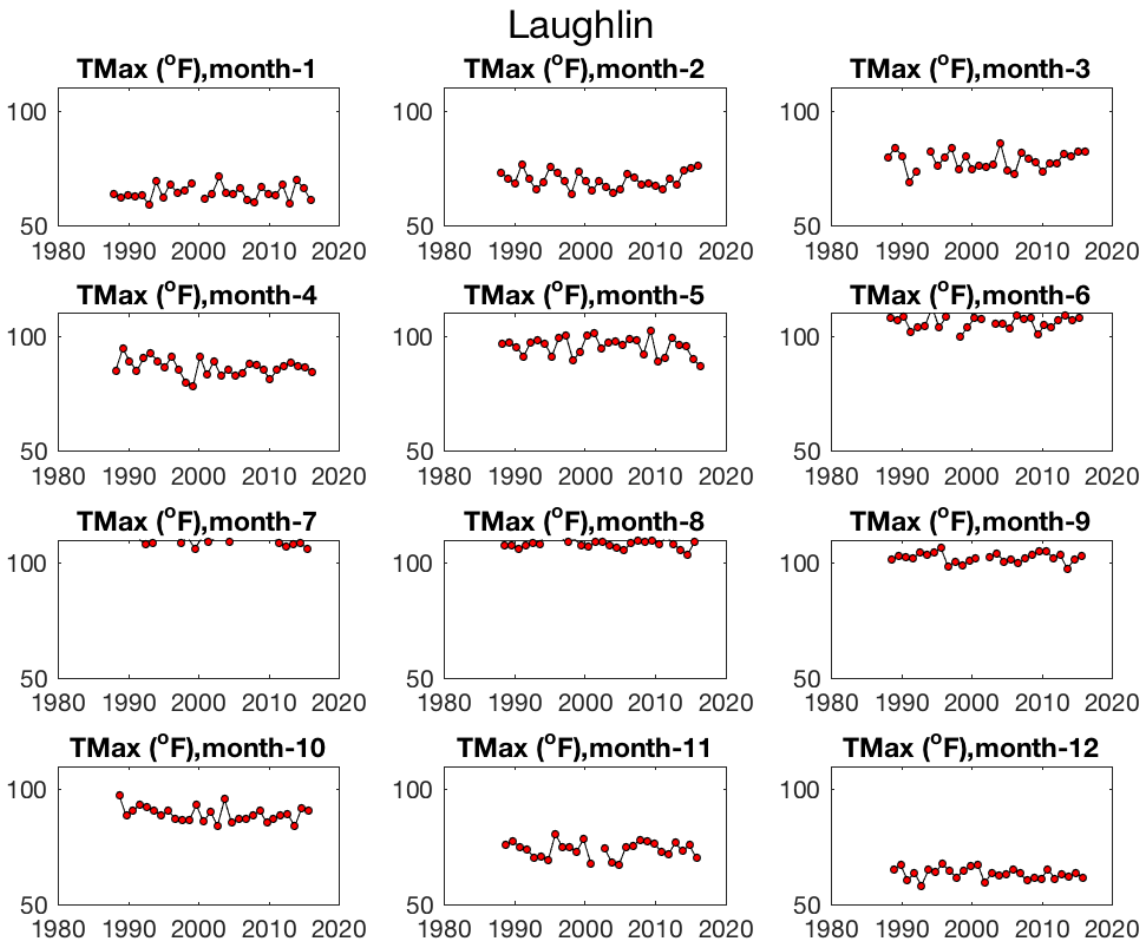
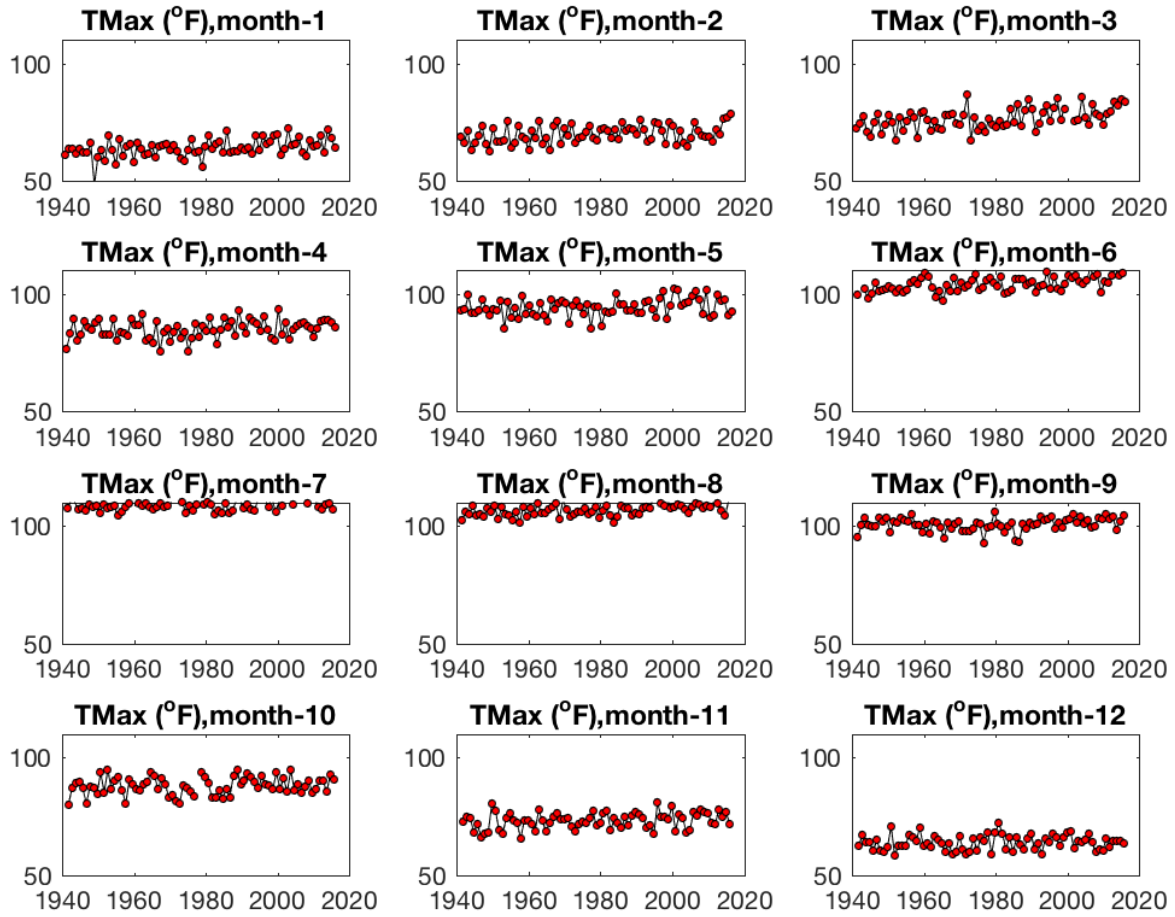Figure A4-4. Each panel shows the monthly average Tmax (°F) for each year of record at Laughlin.
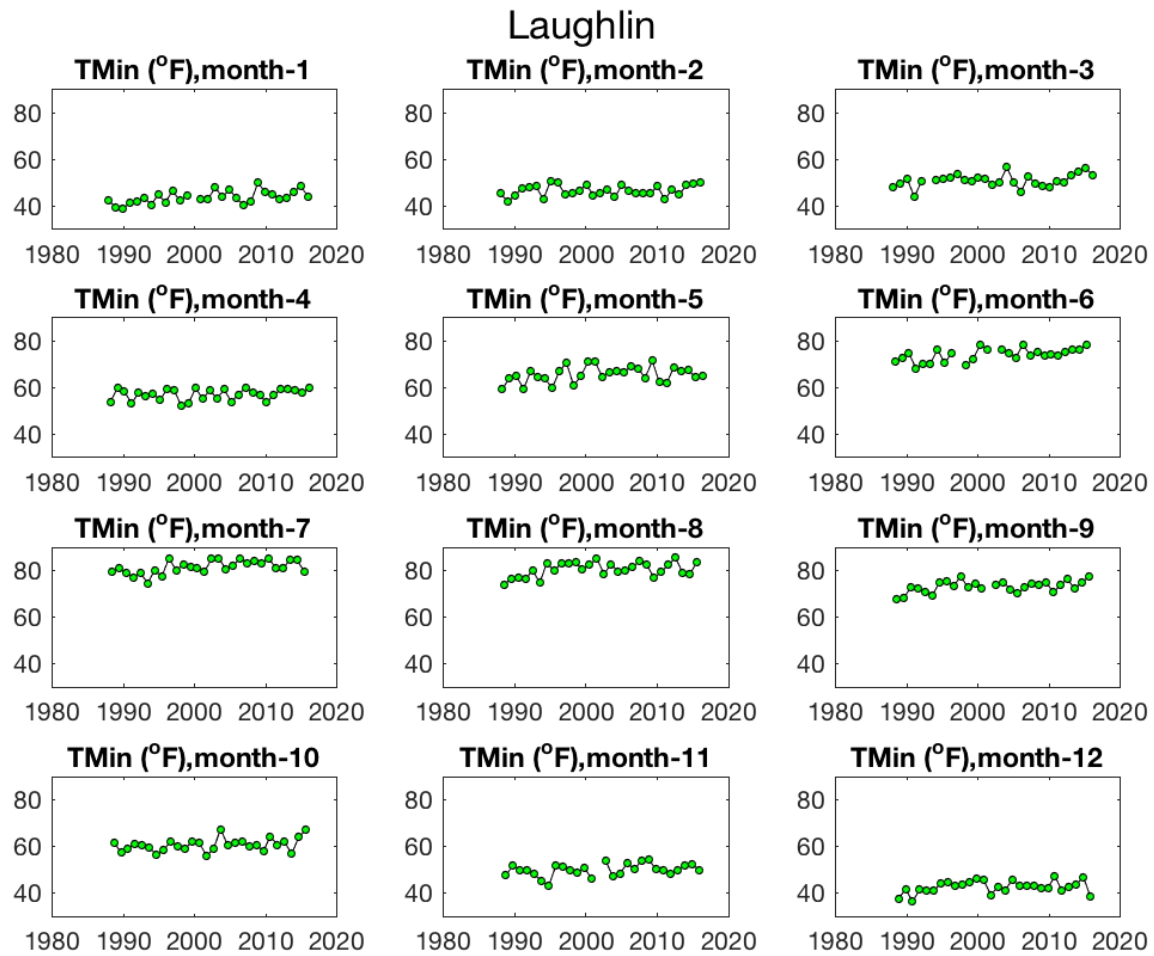
Figure A4-5. Each panel shows the monthly average Tmin (˚F) for each year of record at Laughlin.
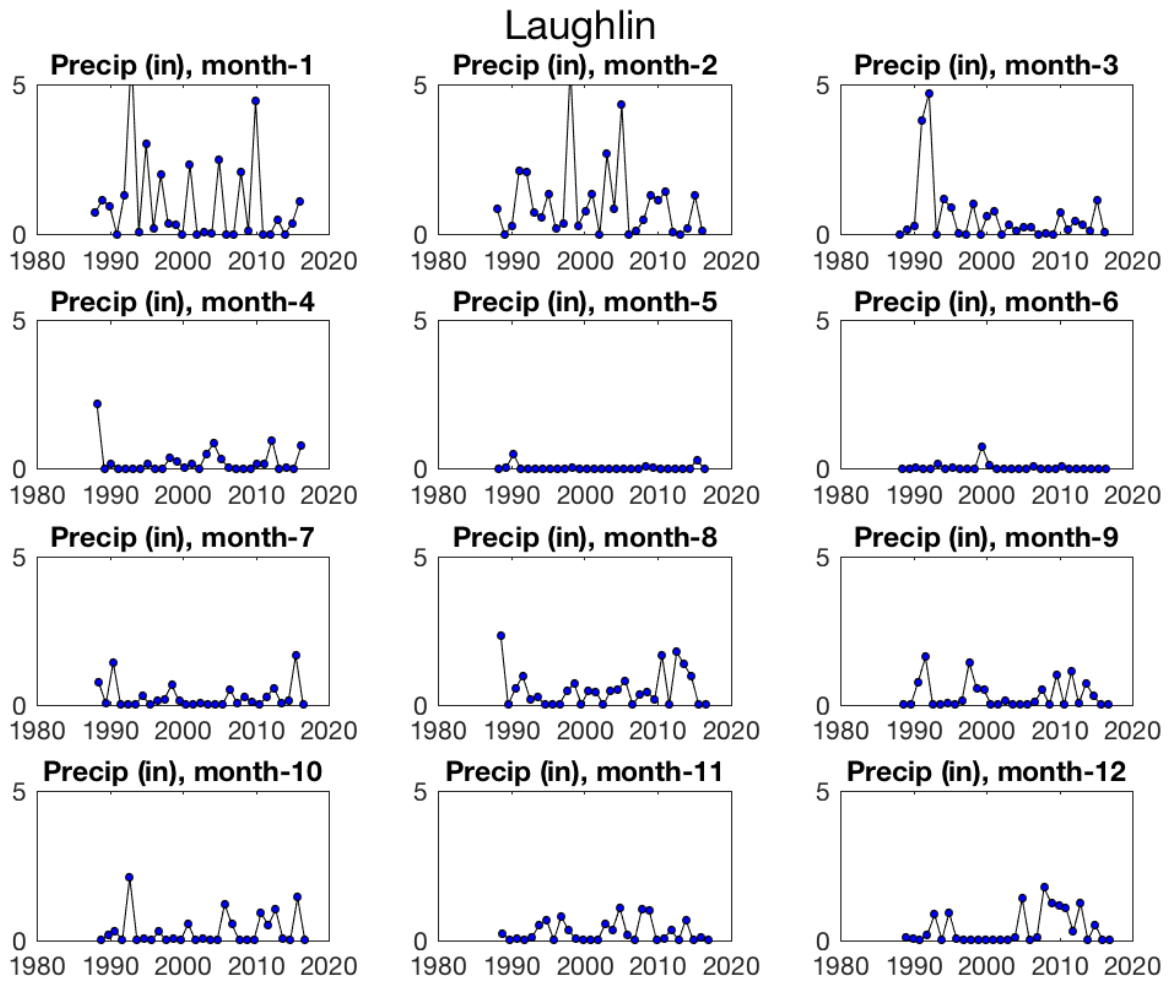
Laughlin

Figure A4-6. Each panel shows the monthly average precipitation (in) for each year of record at Laughlin.
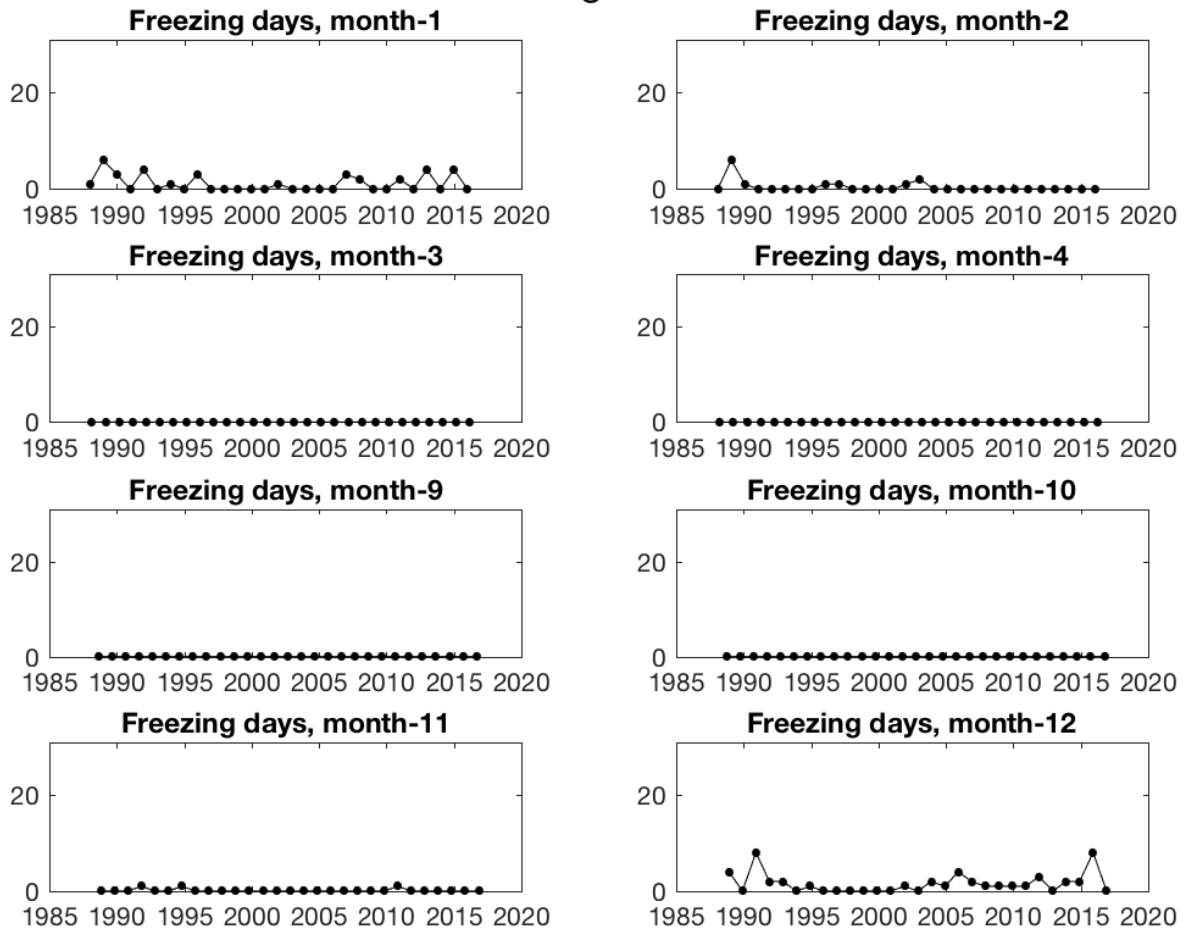
Laughlin

Figure A4-7. Each panel shows the monthly sum of the total number of freezing days for each year of record at Laughlin. The maximum in Jan, March, October, and December is 31 days.
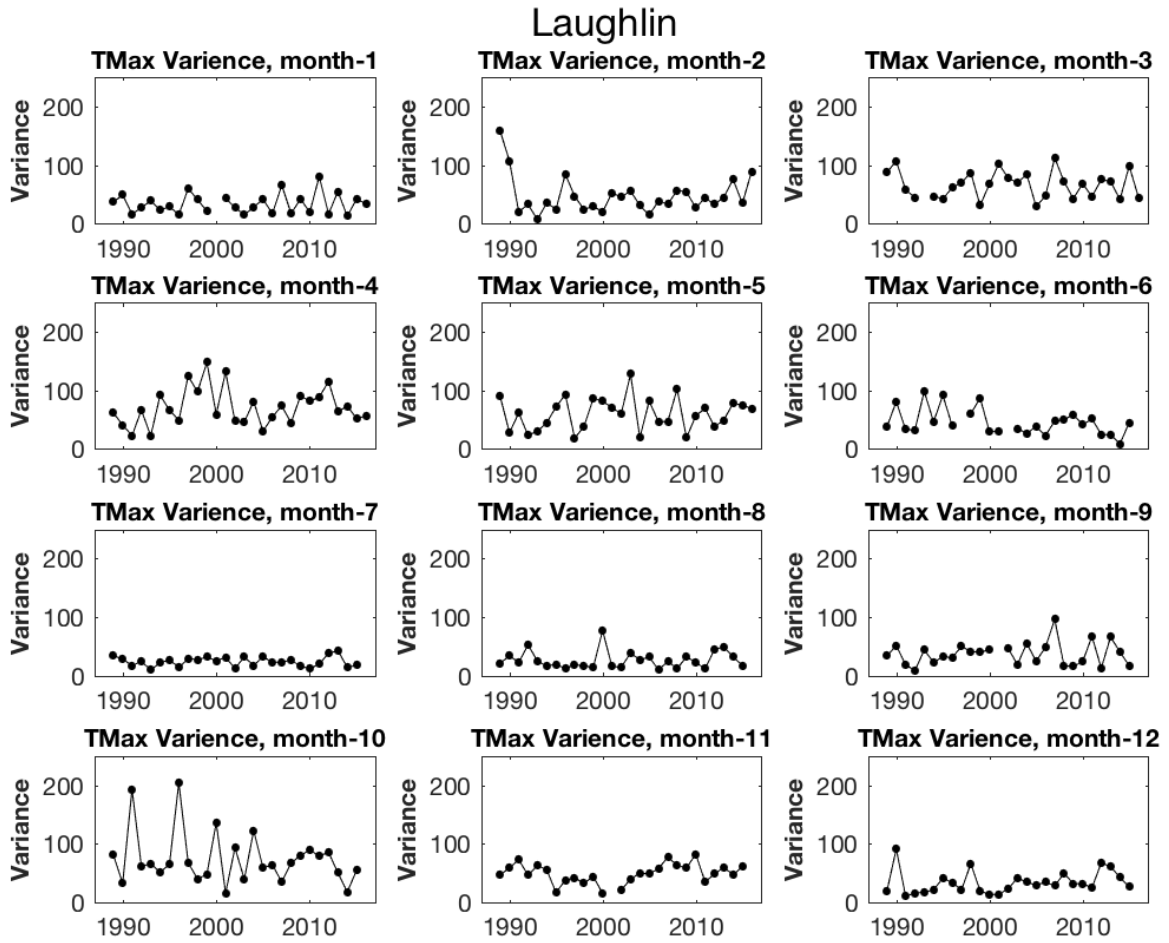
Laughlin

Figure A4-8. Each panel shows the variance (standard deviation squared) in Tmax during a given month at Laughlin.
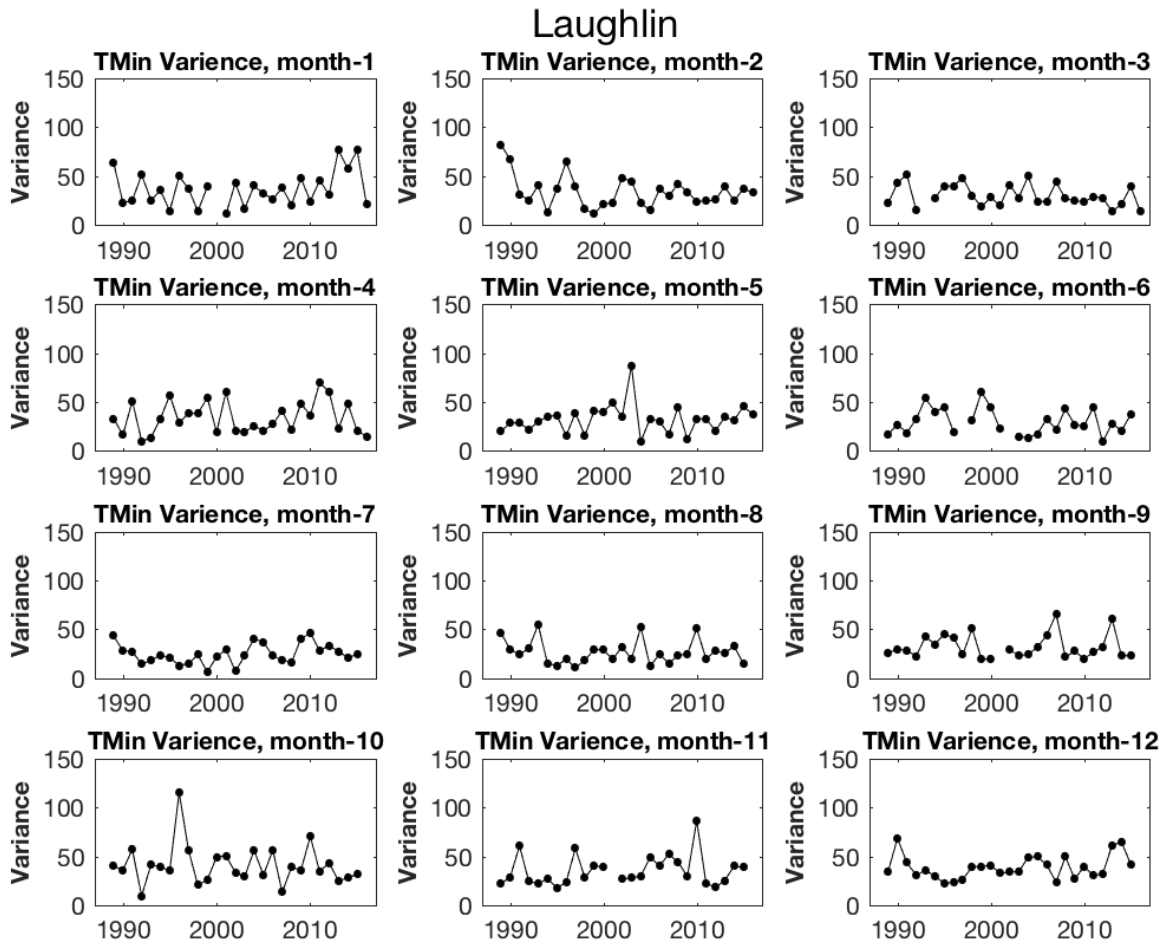
Figure A4-9. Each panel shows the variance (standard deviation squared) in Tmin during a given month at Laughlin.
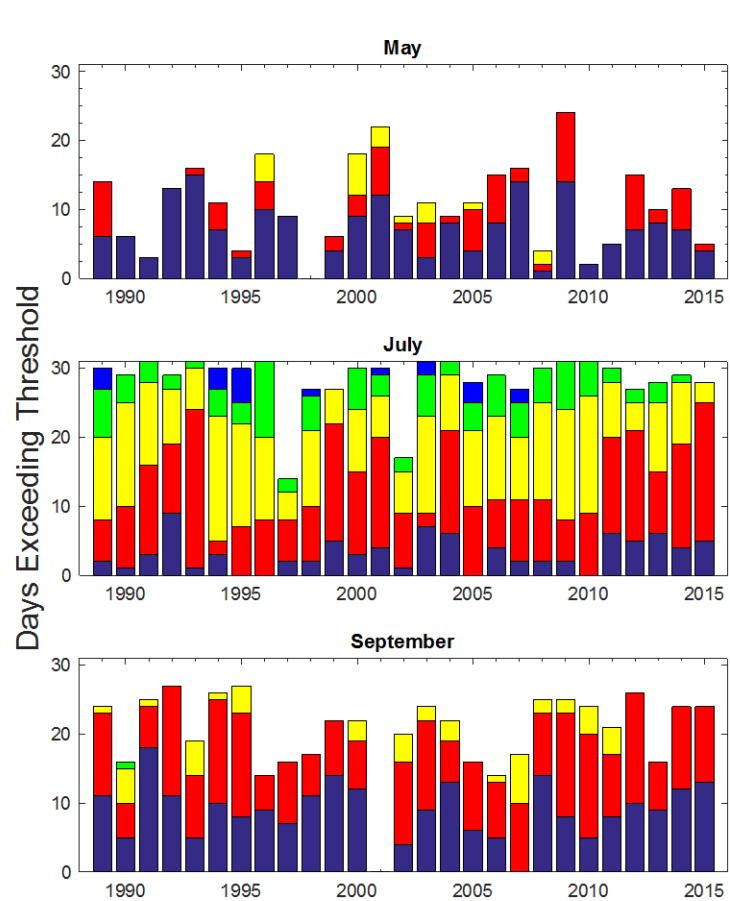
Laughlin

A4-10. The bars illustrate the number of days above a temperature threshold in May, June, July, August and September of a given year. The purple bar indicates the number of days above 100˚F, the red bar is the number of days above 105˚F, the yellow bar is the number of days above 110˚F and the green is the number of days above 115˚F. The last panel depicts the number of days above these thresholds from May through September through time.

Figure A4-11. The bars illustrate the number of days below a temperature threshold in November, December, January, February and March of a given year. The purple bar represents the number of days below 32˚F, the green bar represents number of days below 40˚F, the yellow bar is the number of days below 50˚F. The maximum number of days for January, March and December is 31.

5. McCarran

McCarran

Figure A5-1. Each panel shows the monthly average Tmax (˚F) for each year of record at McCarran.

Figure A5-2. Each panel shows the monthly average Tmin (˚F) for each year of record at McCarran.
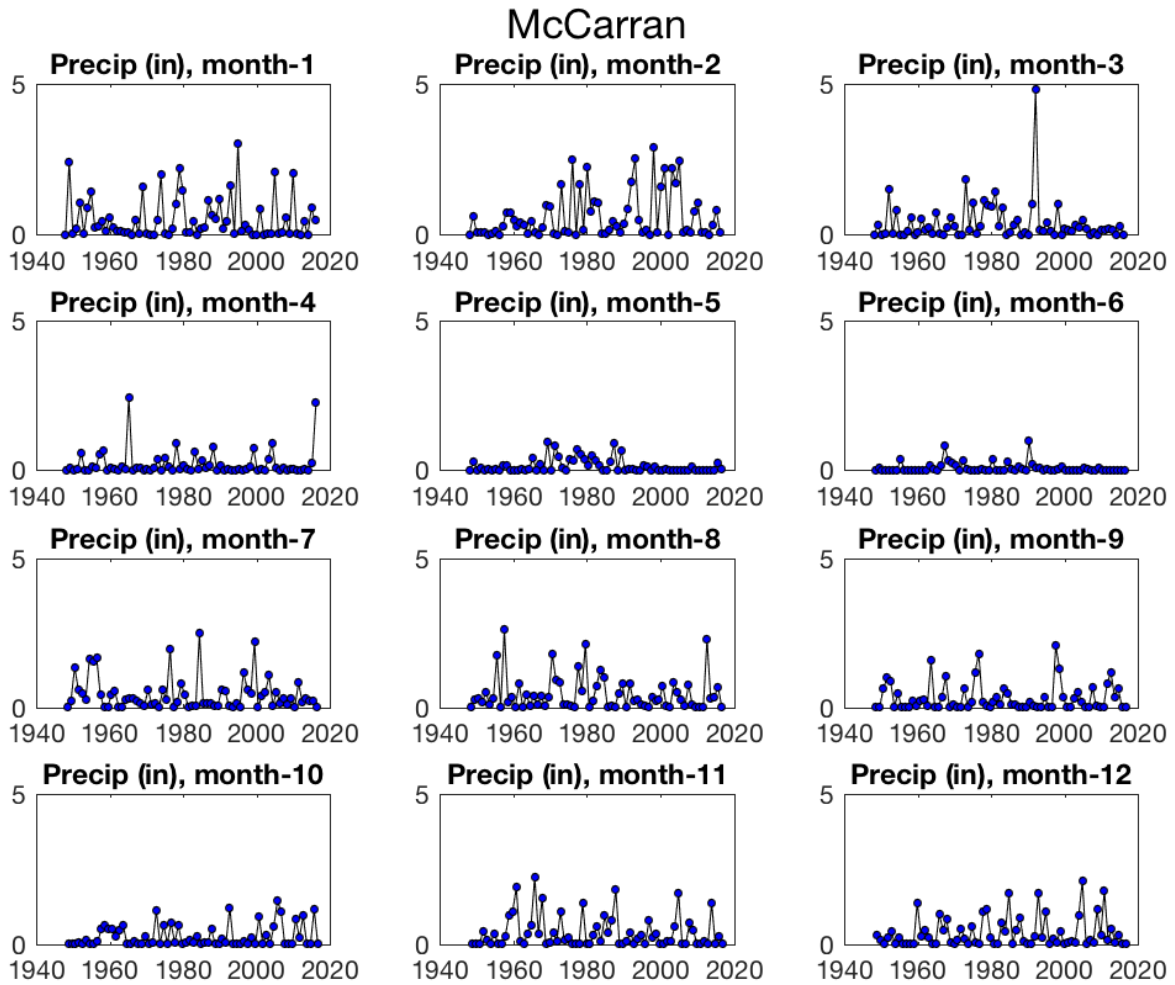
McCarran

Figure A5-3. Each panel shows the monthly accumulated precipitation (in) for each year of record at McCarran.

McCarran

Figure A5-4. Each panel shows the monthly sum of the total number of freezing days for each year of record at McCarran. The maximum in Jan, March, October, and December is 31 days.
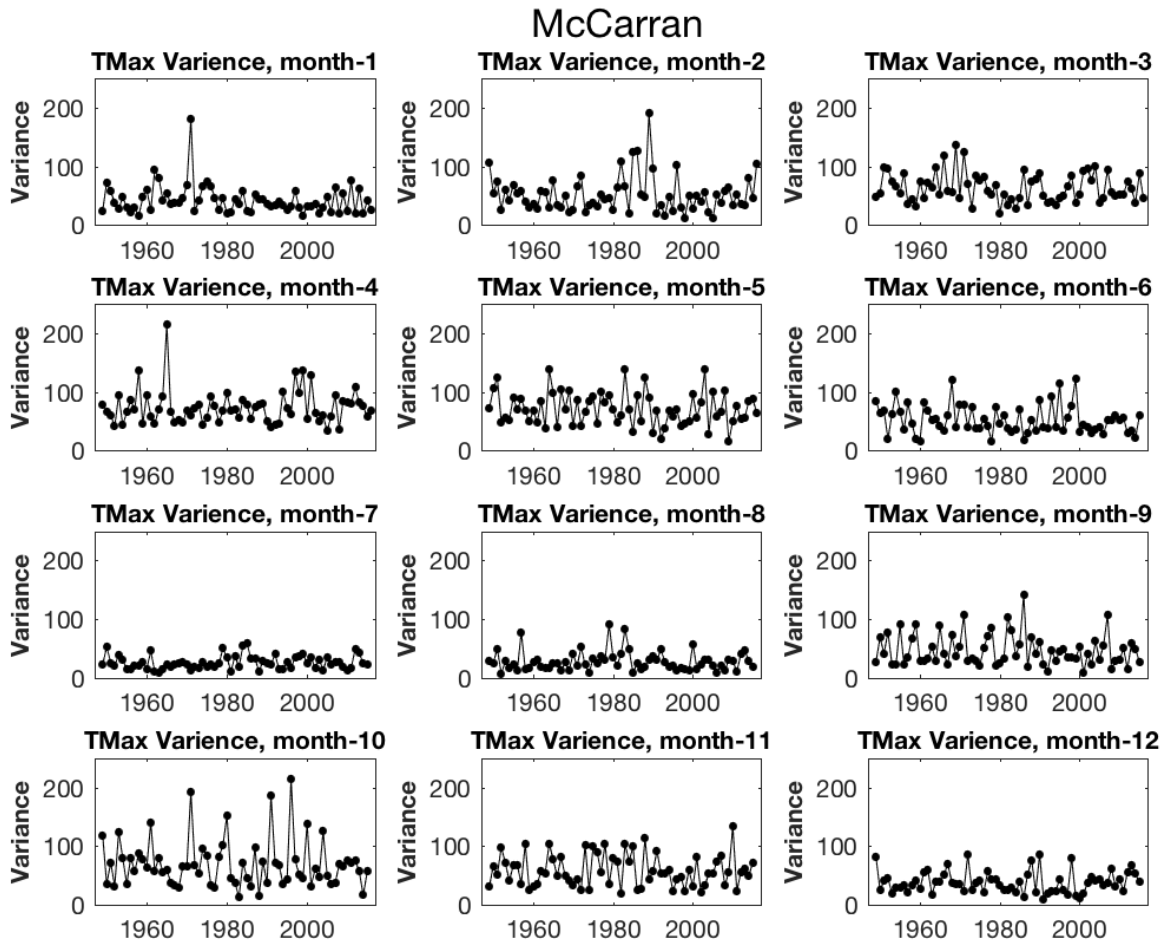
McCarran

Figure A5-5. Each panel shows the variance (standard deviation squared) in during a given month for the McCarran for Tmax.
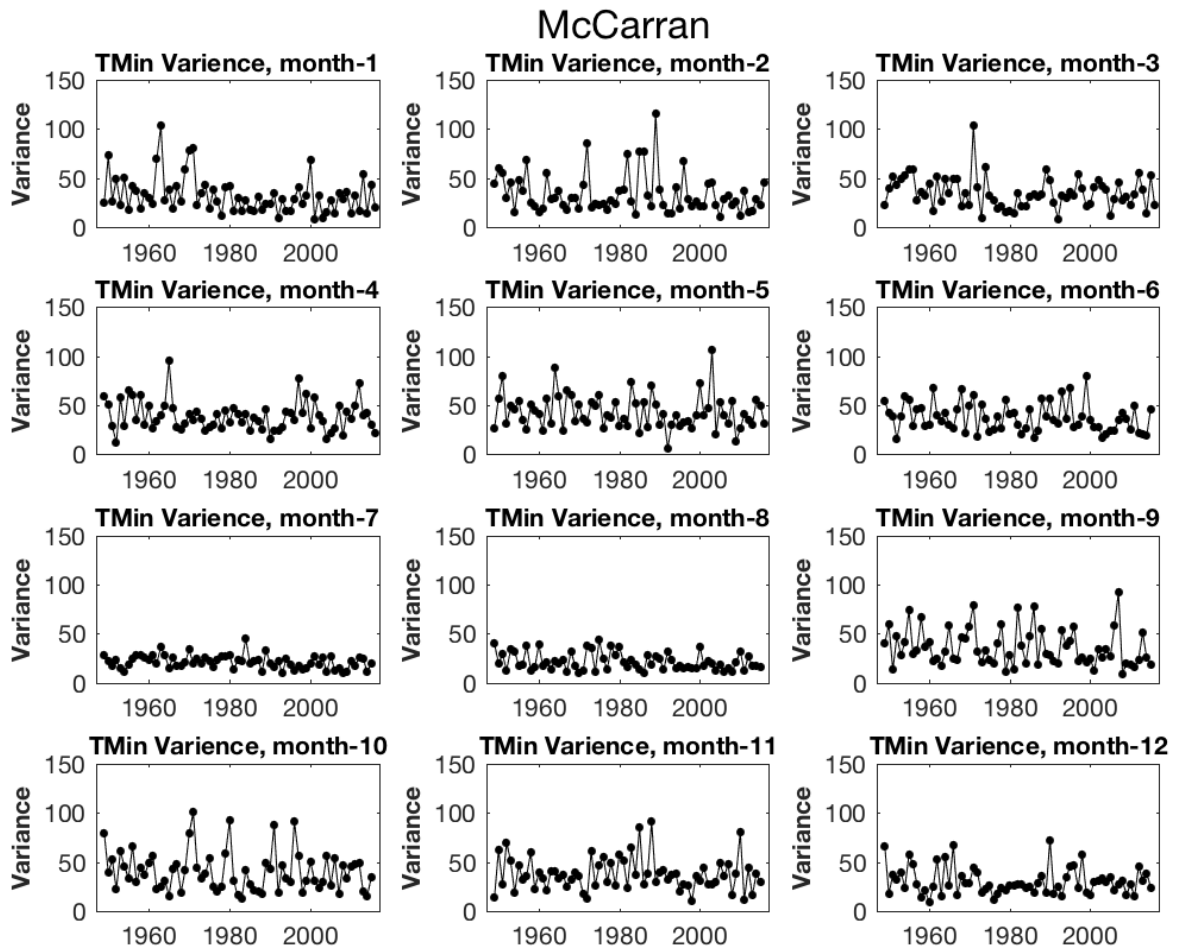
McCarran

Figure A5-6. Each panel shows the variance (standard deviation squared) in Tmin during a given month at McCarran.
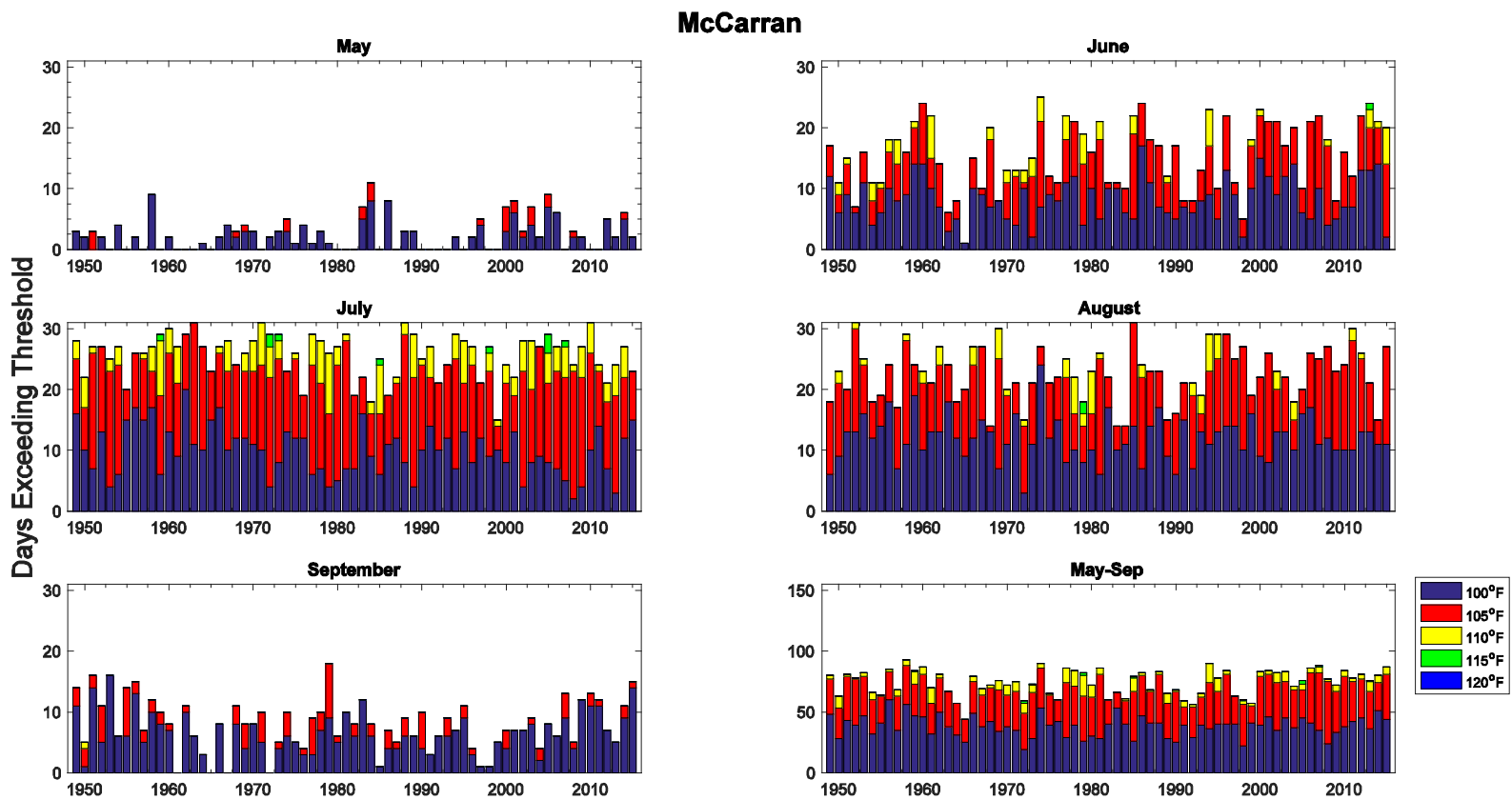
Figure A5-7. The bars illustrate the number of days above a temperature threshold in May, June, July, August and September of a given year. The purple bar indicates the number of days above 100˚F, the red bar is the number of days above 105˚F, the yellow bar is the number of days above 110˚F and the green is the number of days above 115˚F. The last panel depicts the number of days above these thresholds from May through September through time.
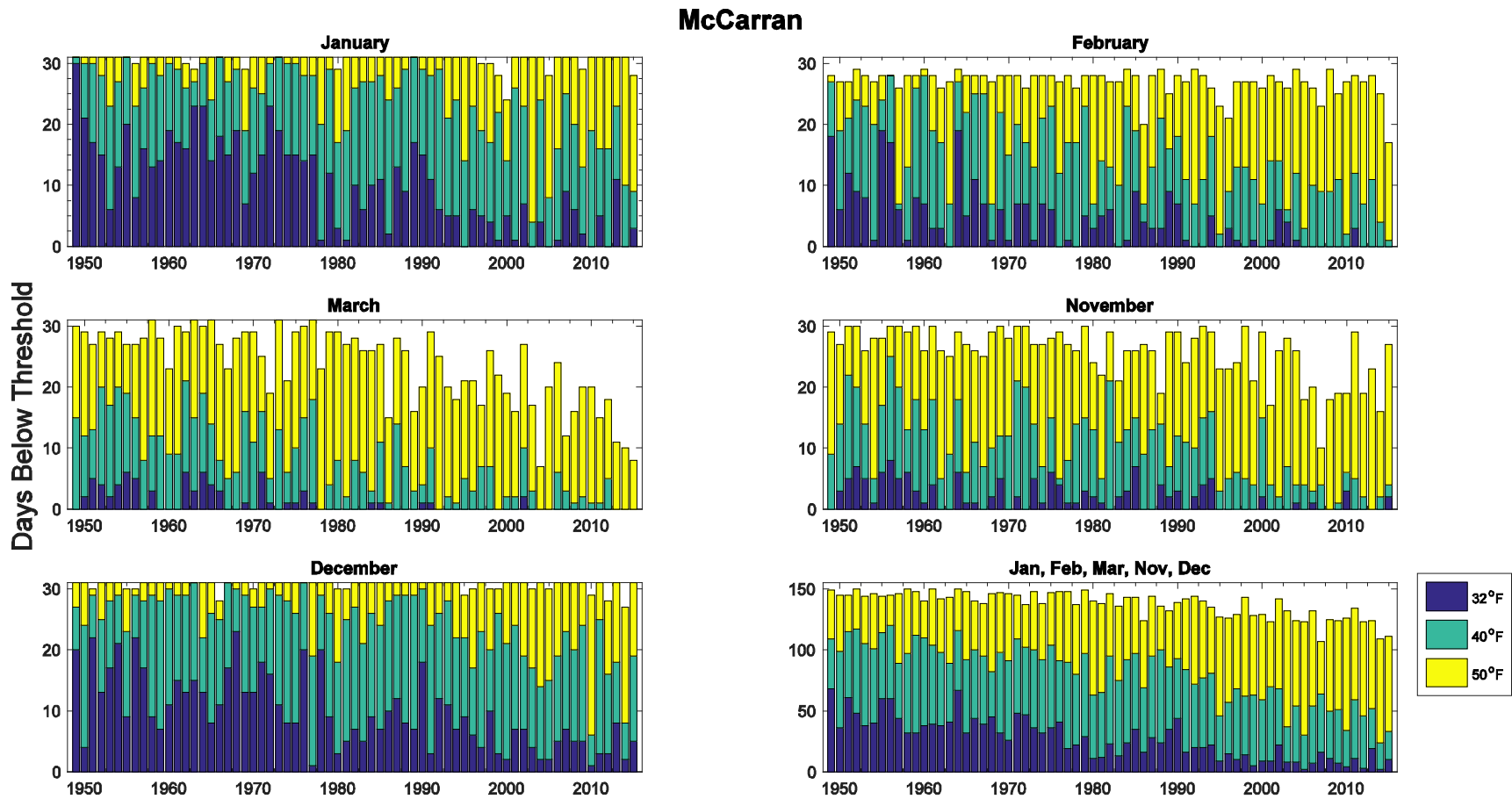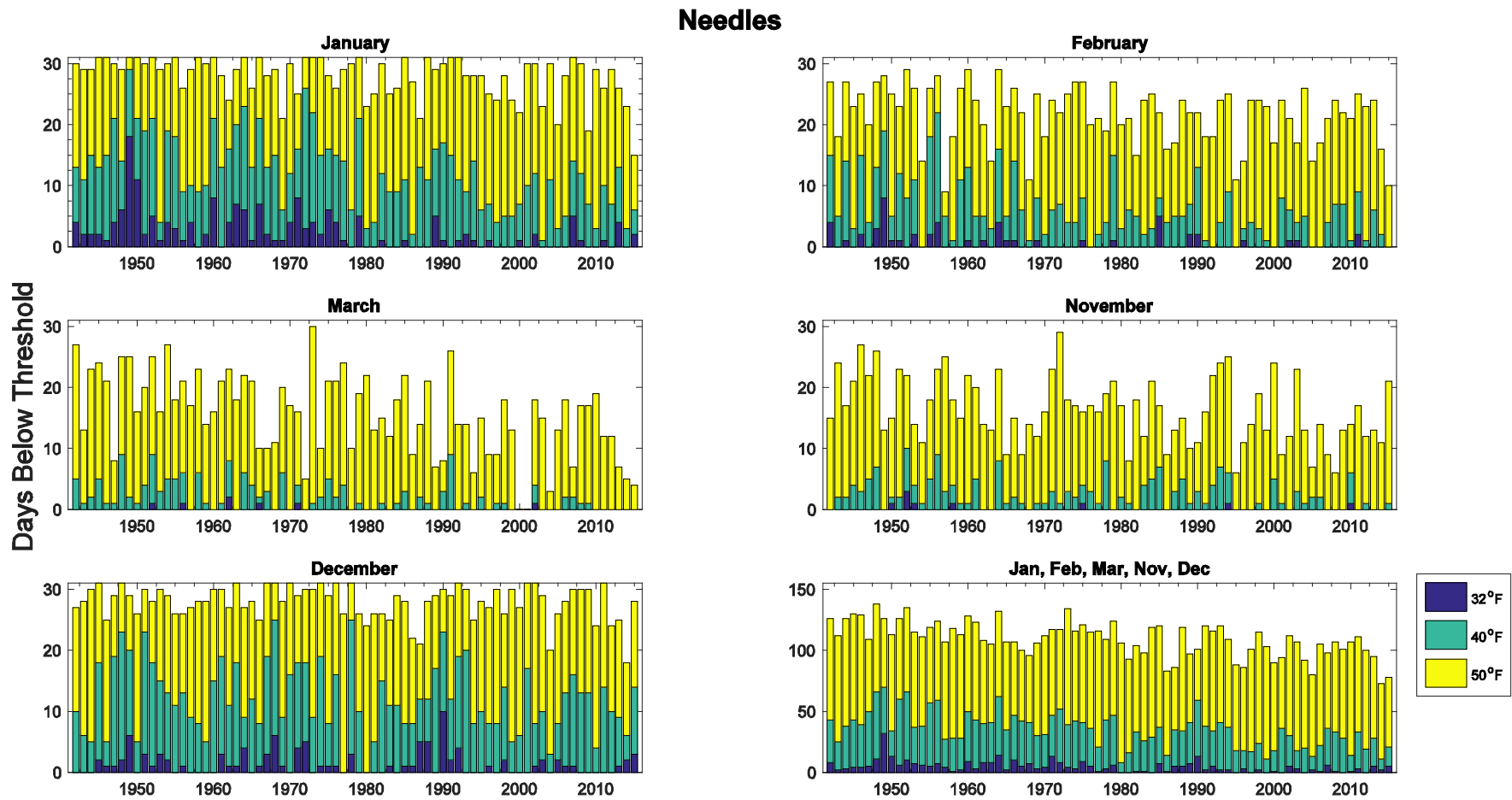
Figure A5-8. The bars illustrate the number of days below a temperature threshold in November, December, January, February and March of a given year. The purple bar represents the number of days below 32°F, the green bar represents number of days below 40°F, the yellow bar is the number of days below 50°F. The maximum number of days for January, March and December is 31.

6. Mount Charleston
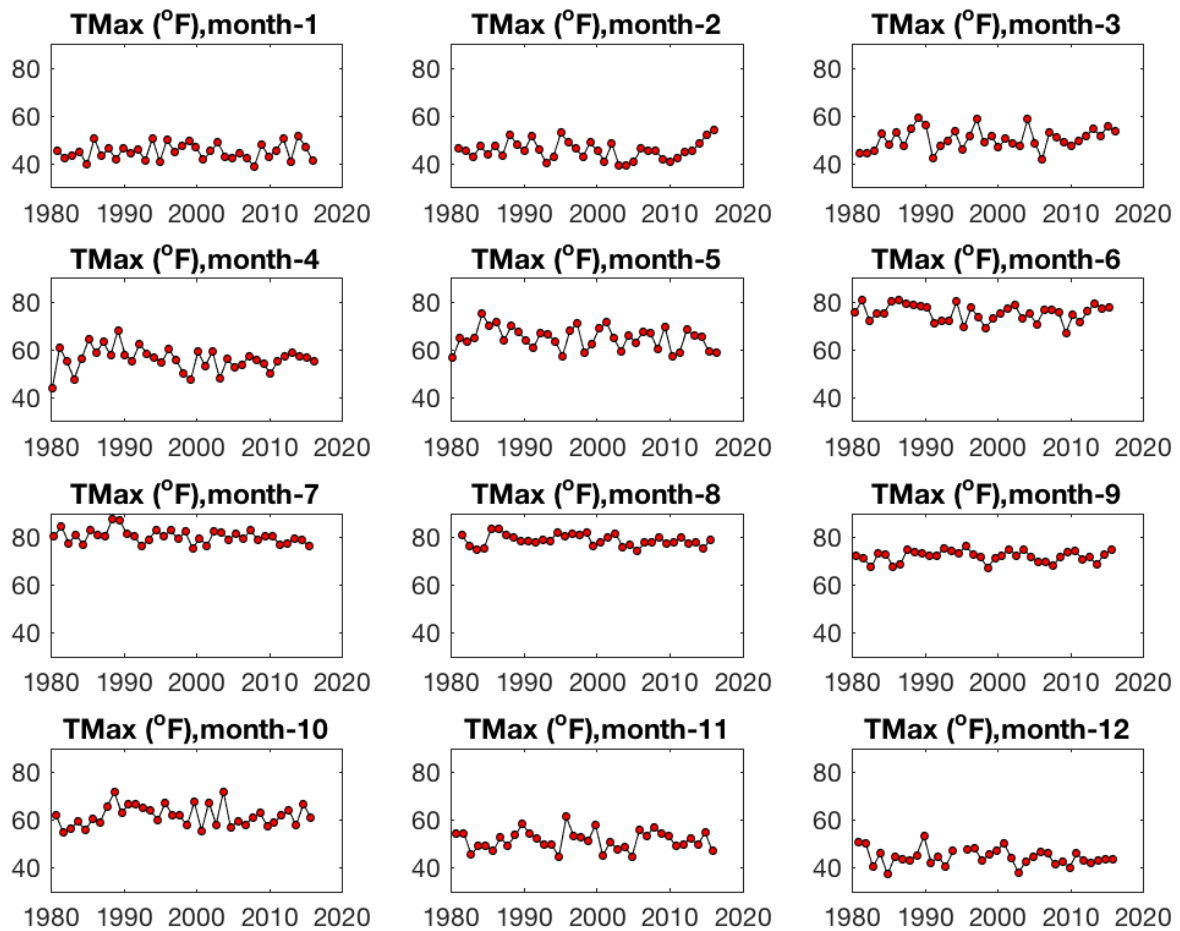
Figure A6-1. Each panel shows the monthly average Tmax (˚F) for each year of record at Mount Charleston.
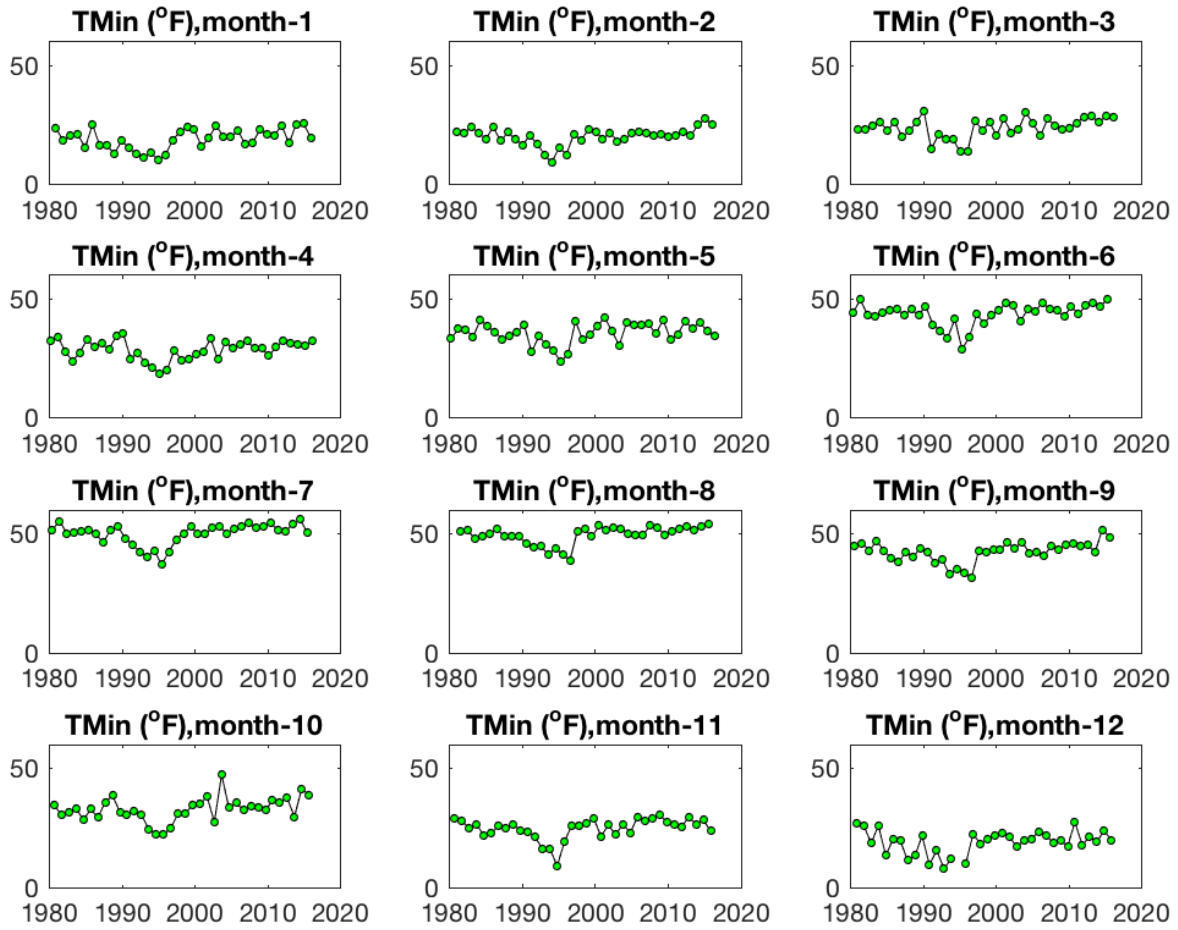
Figure A6-2. Each panel shows the monthly average Tmin (˚F) for each year of record at Mount Charleston.
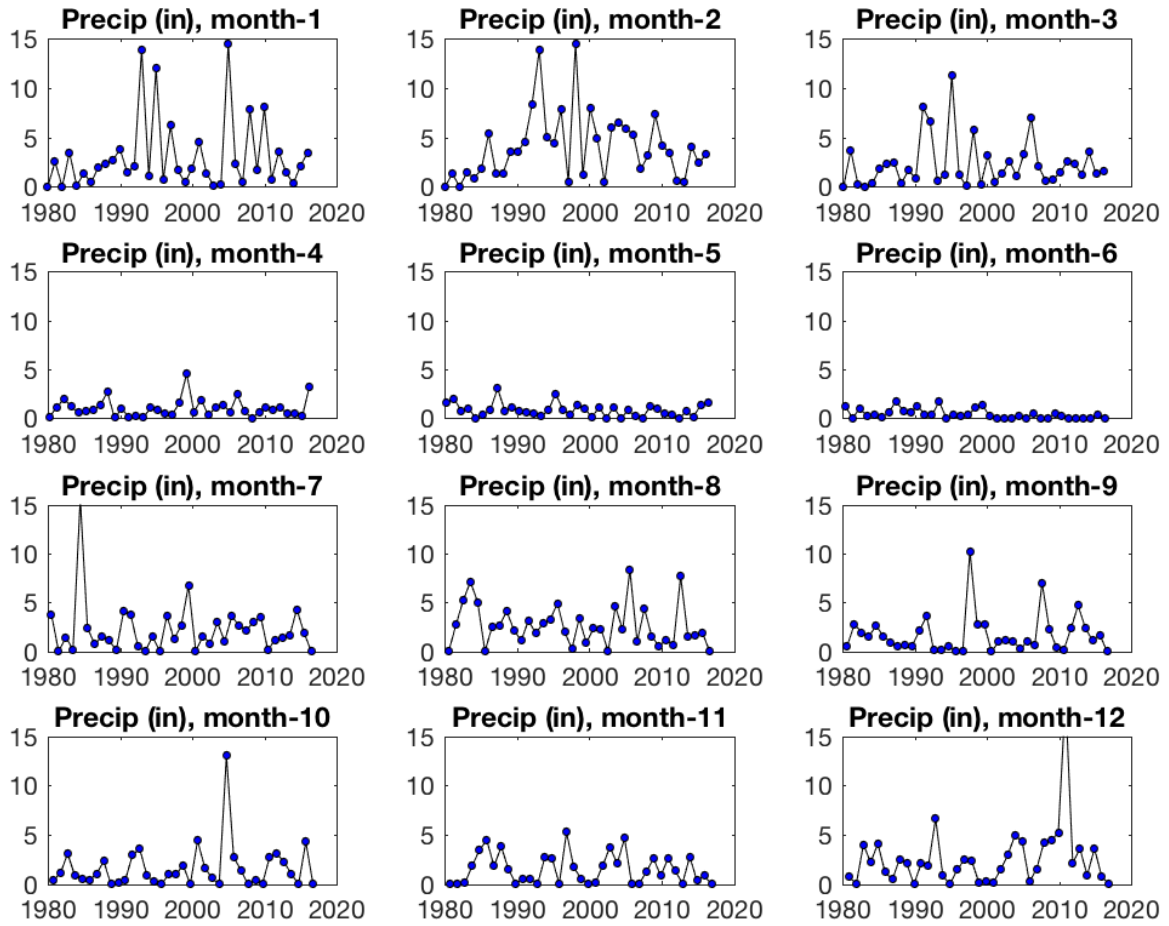
Figure A6-3. Each panel shows the monthly average precipitation (in) for each year of record at Mount Charleston.
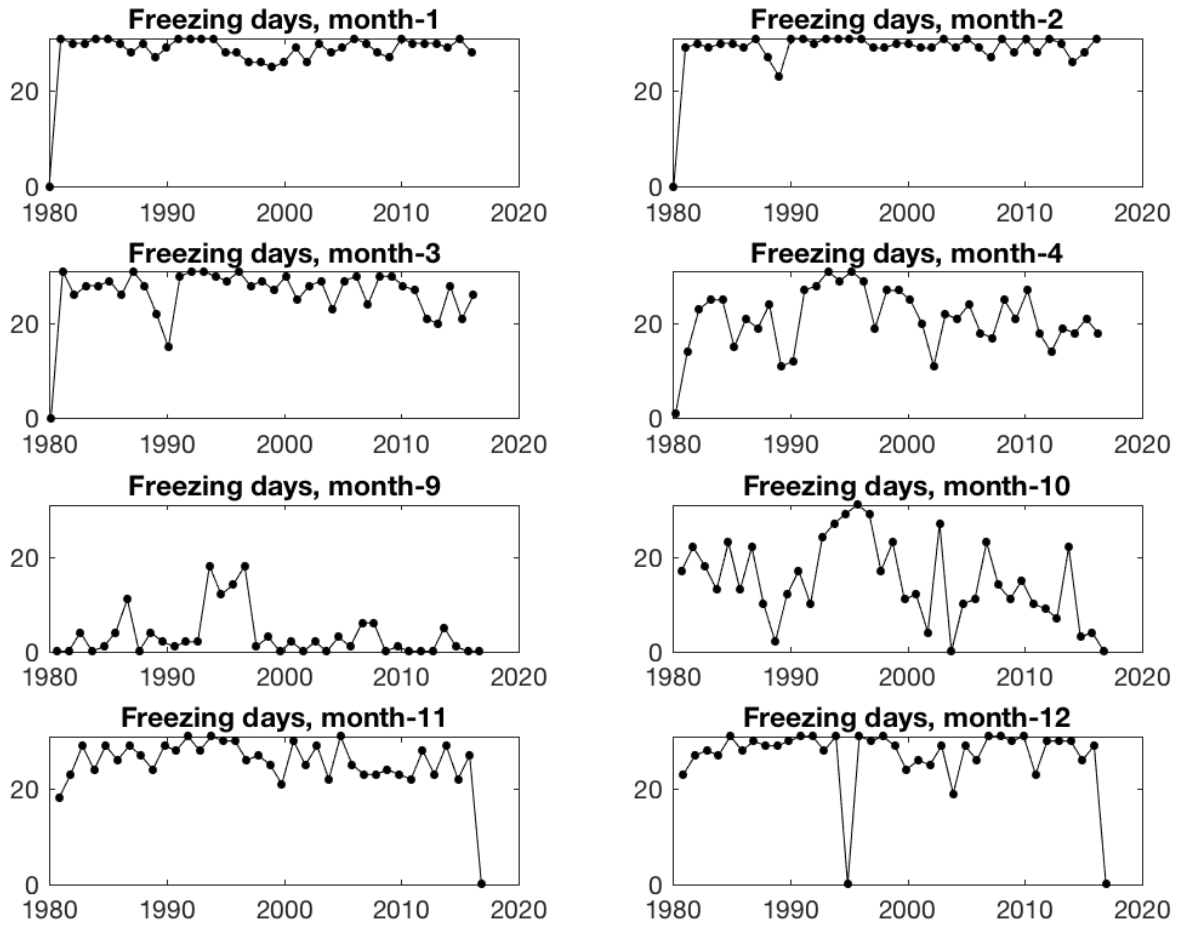
Figure A6-4. Each panel shows the monthly sum of the total number of freezing days for each year of record at Mount Charleston. The maximum in Jan, March, October, and December is 31 days.
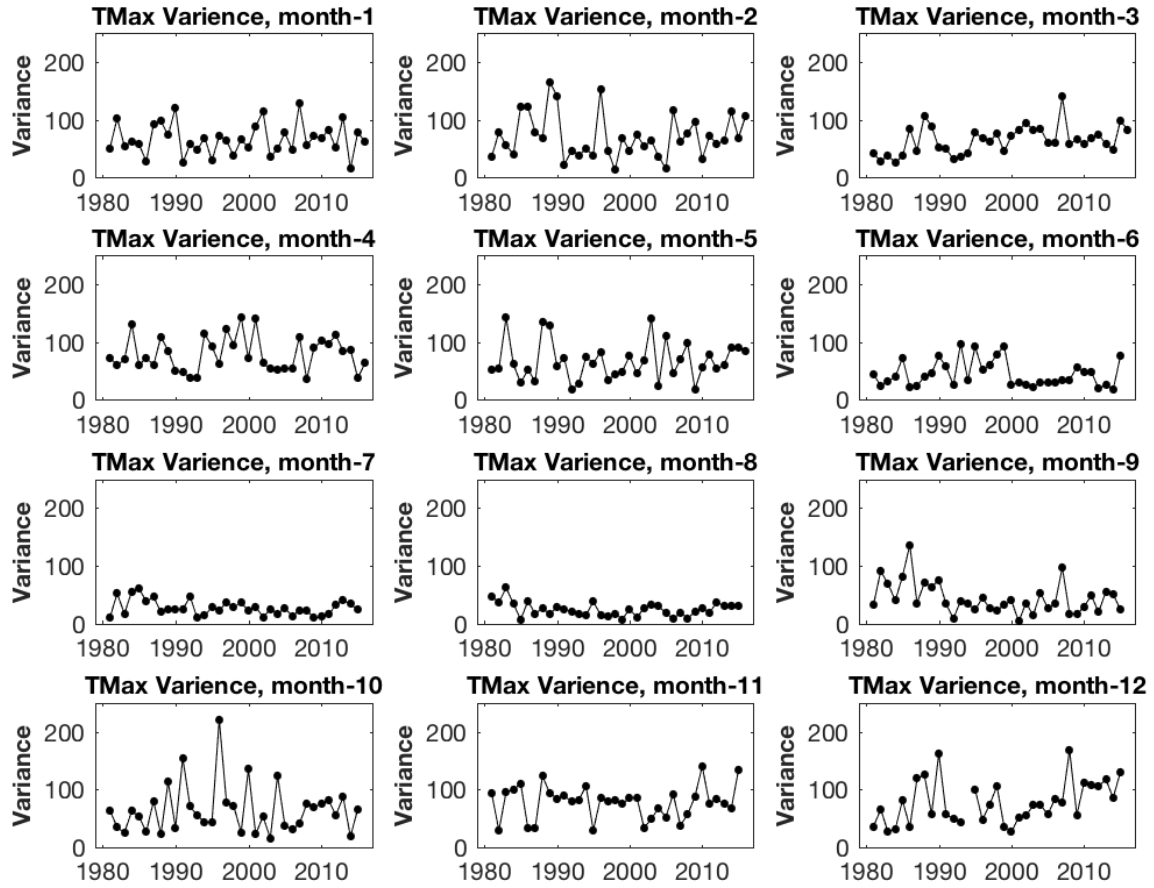
Figure A6-5. Each panel shows the variance (standard deviation squared) in Tmax during a given month at Mount Charleston.
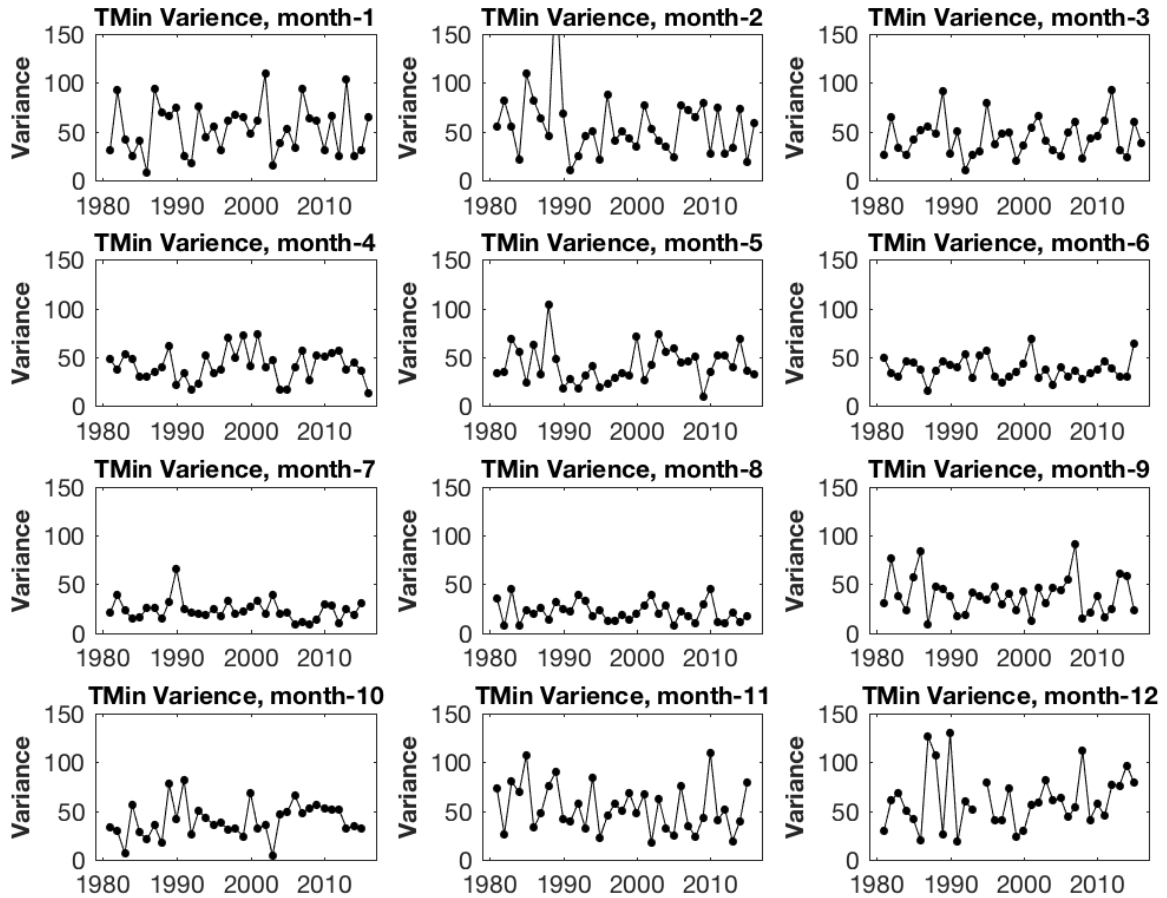
Figure A6-6. Each panel shows the variance (standard deviation squared) in Tmin during a given month at Mount Charleston.

Figure A6-7. The bars illustrate the number of days below a temperature threshold in November, December, January, February and March of a given year at Mount Charleston. The purple bar represents the number of days below 32˚F, the green bar represents number of days below 40˚F, the yellow bar is the number of days below 50˚F. The maximum number of days for January, March and December is 31.

7. Needles

Figure A7-1. The total annual rainfall in inches. The dashed line is the average annual rainfall over the entire period of record. The height of the entire bar represents the total annual precipitation and the red part is the contribution for the 95th percentile events.

Figure A7-2. The blue bars show the average monthly percent contribution to the total annual rainfall. Thus all 12 bars total 100%. The red line is the number of extreme precipitation events, or 99th percentile events from 1961-1990.

Figure A7-3. The graphs depict the median monthly T_{max} (°F) (left) and T_{min} (right) at the Needles station represented by the circles. Monthly values from 1981-2010 are averaged for each month (January to December). The line illustrates the range of temperatures in the 10th to 90th percentiles. The diamonds represent the maximum and minimum T_{max} values over the 1981-2010 time period.

Figure A7-4. Each panel shows the monthly average Tmax (˚F) for each year of record at the Needles station.
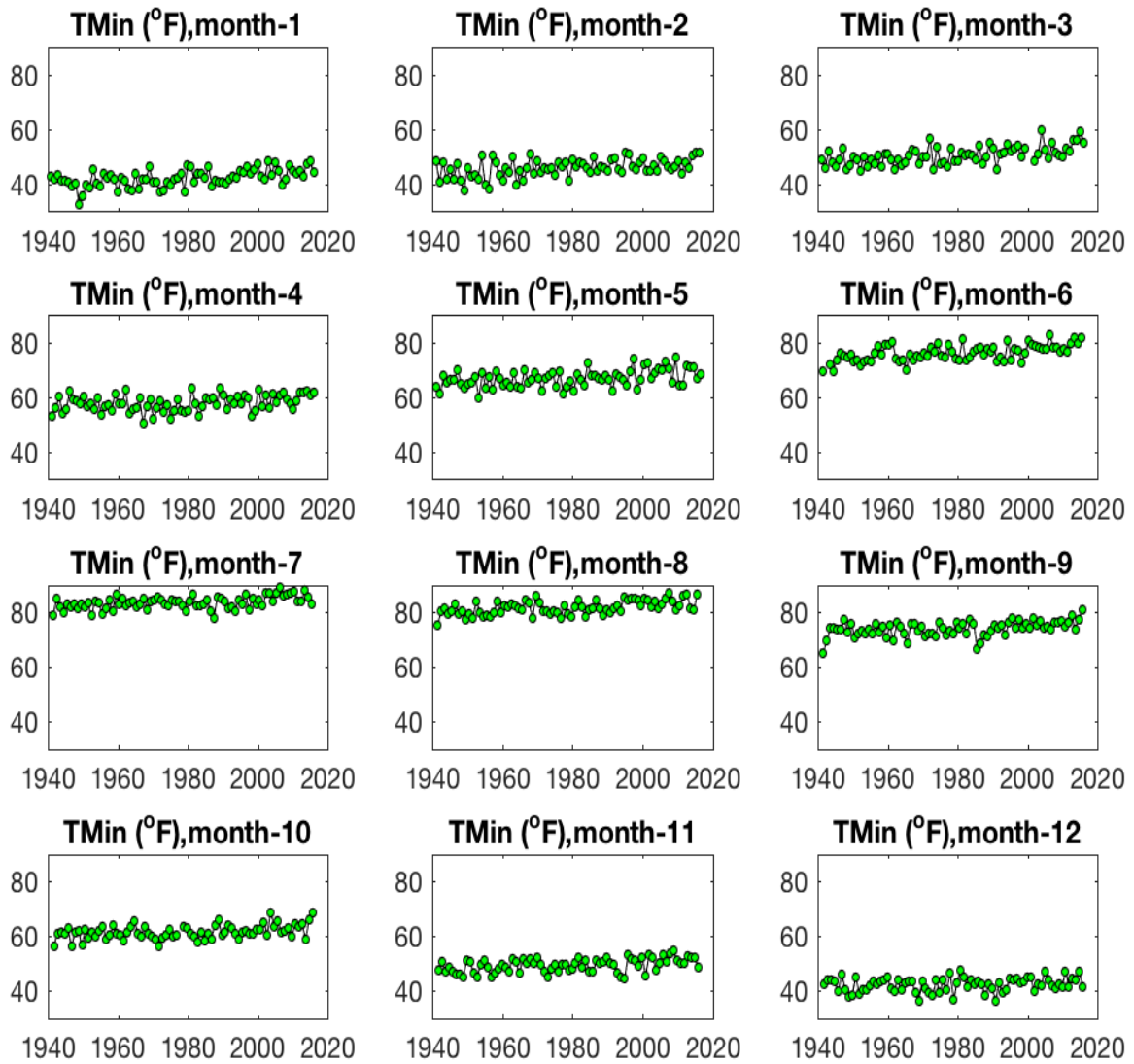
Needles

Figure A7-5. Each panel shows the monthly average Tmin (˚F) for each year of record at the Needles station.
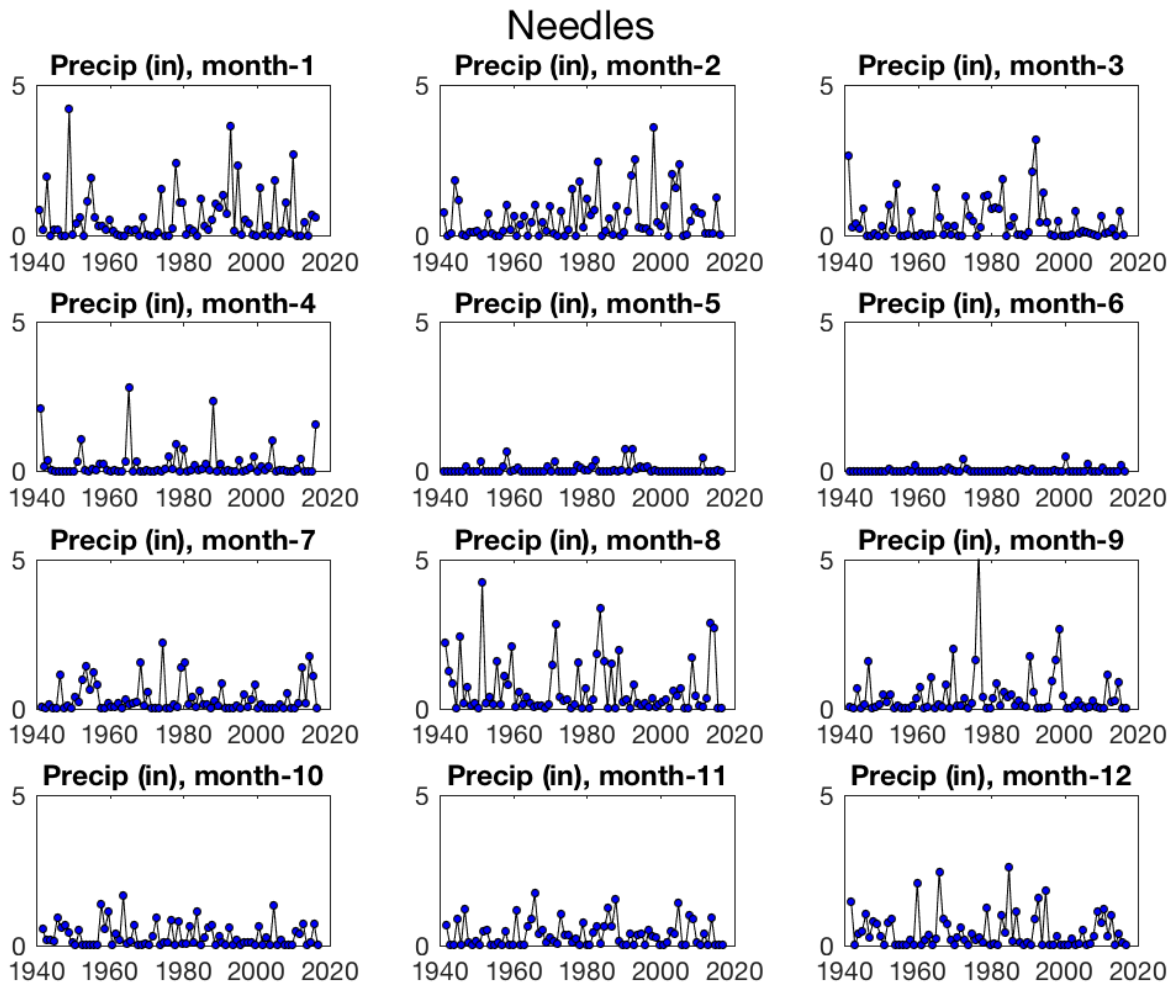
Figure A7-6. Each panel shows the monthly average precipitation (in) for each year of record at the Needles station.
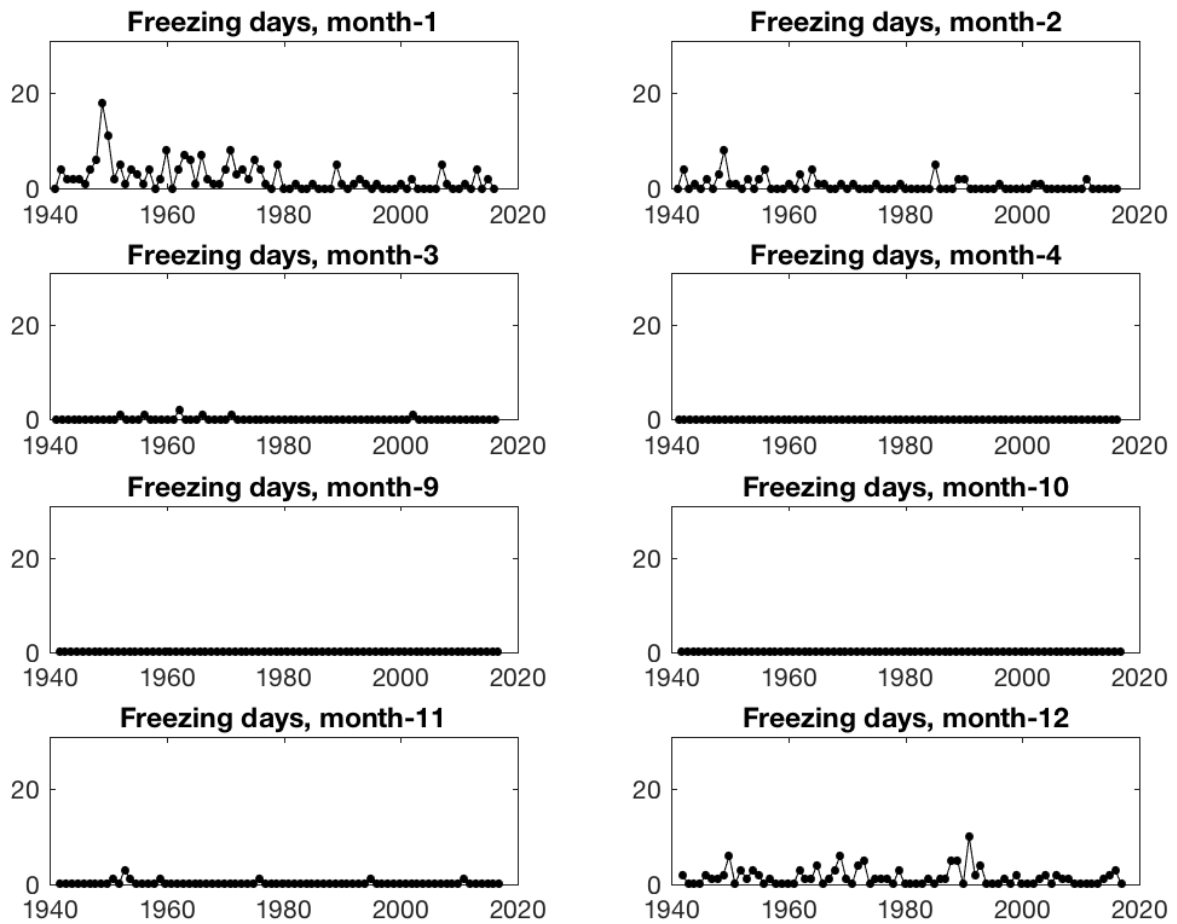
Needles

Figure A7-7. Each panel shows the monthly sum of the total number of freezing days for each year of record at the Needles station. The maximum in Jan, March, October, and December is 31 days.
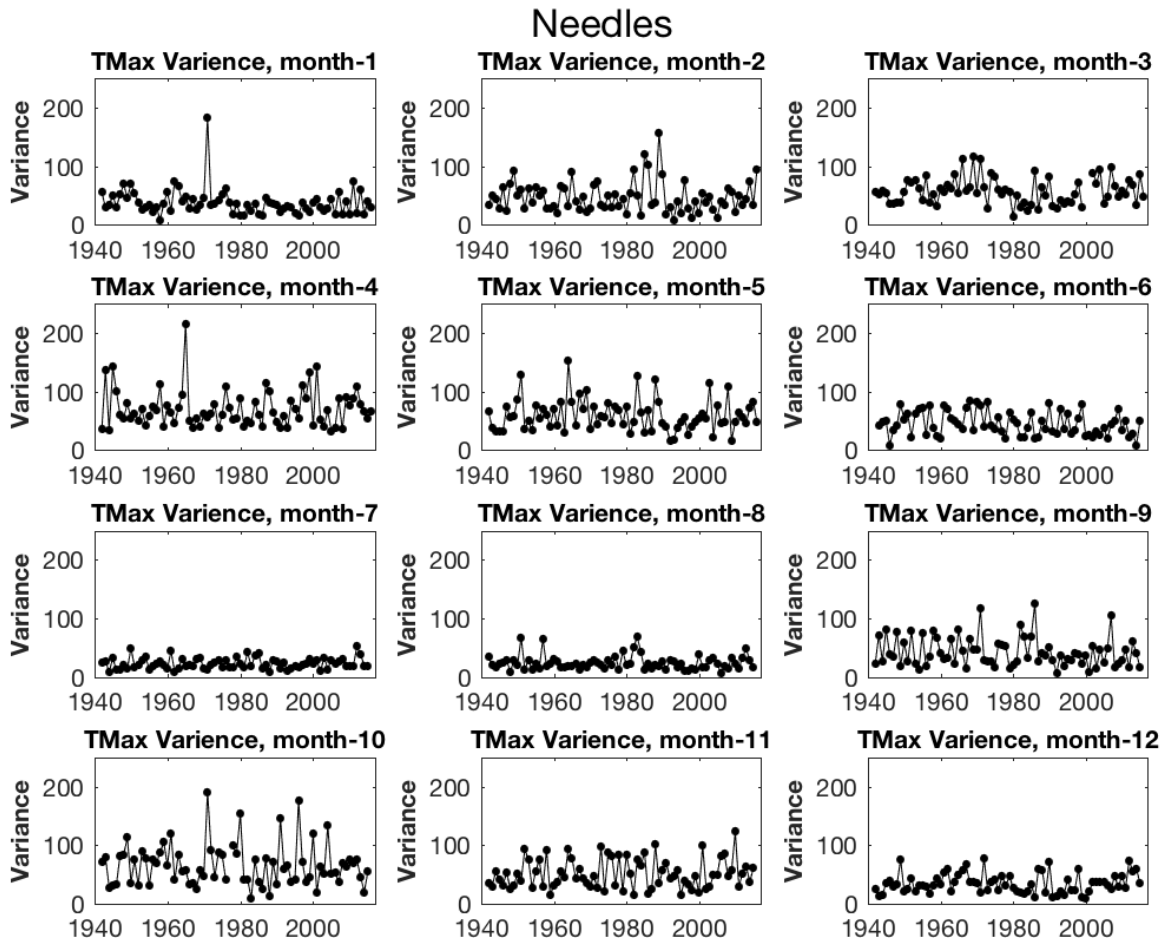
Needles

Figure A7-8. Each panel shows the variance (standard deviation squared) in Tmax during a given month at the Needles station.
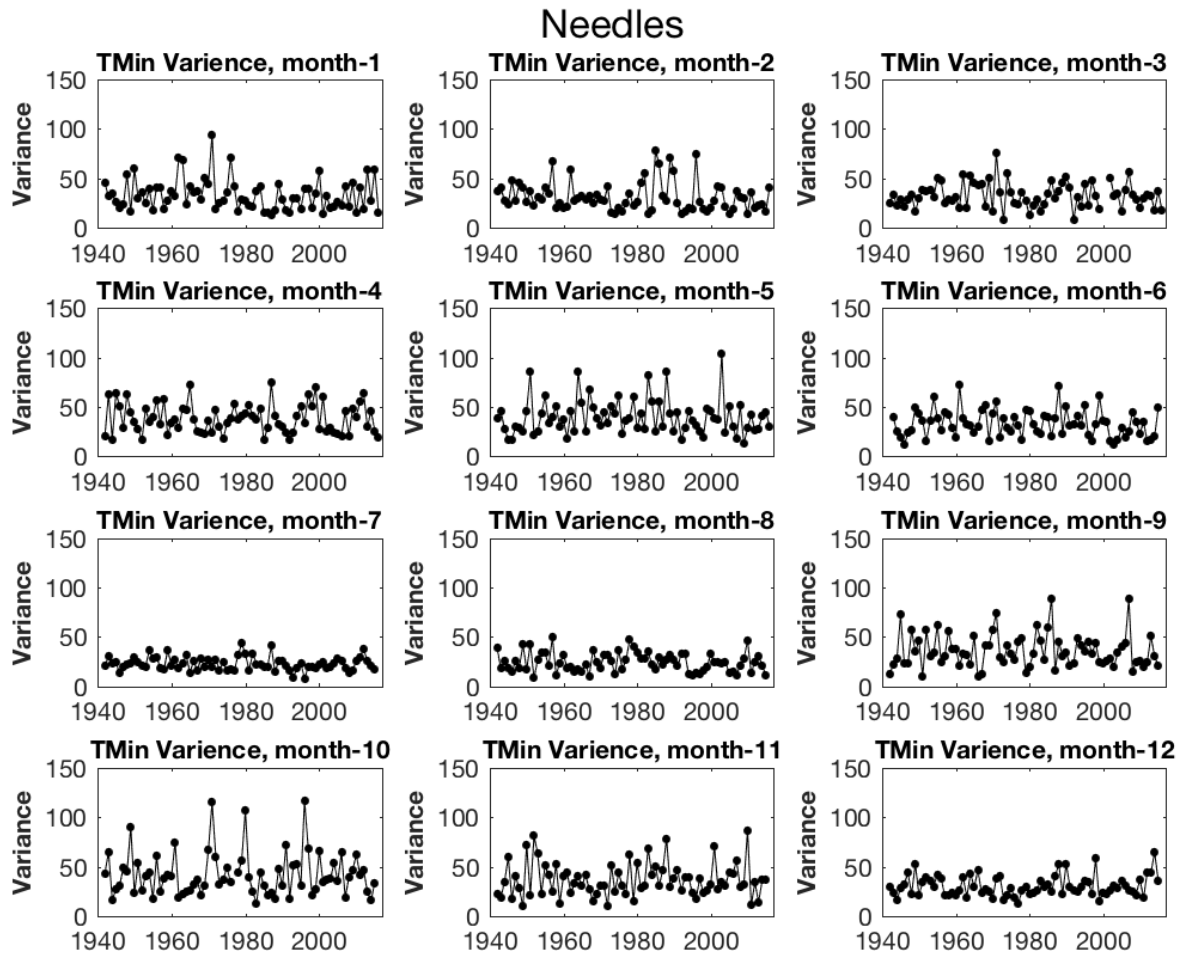
Figure A7-9. Each panel shows the variance (standard deviation squared) in Tmin during a given month at the Needles station.
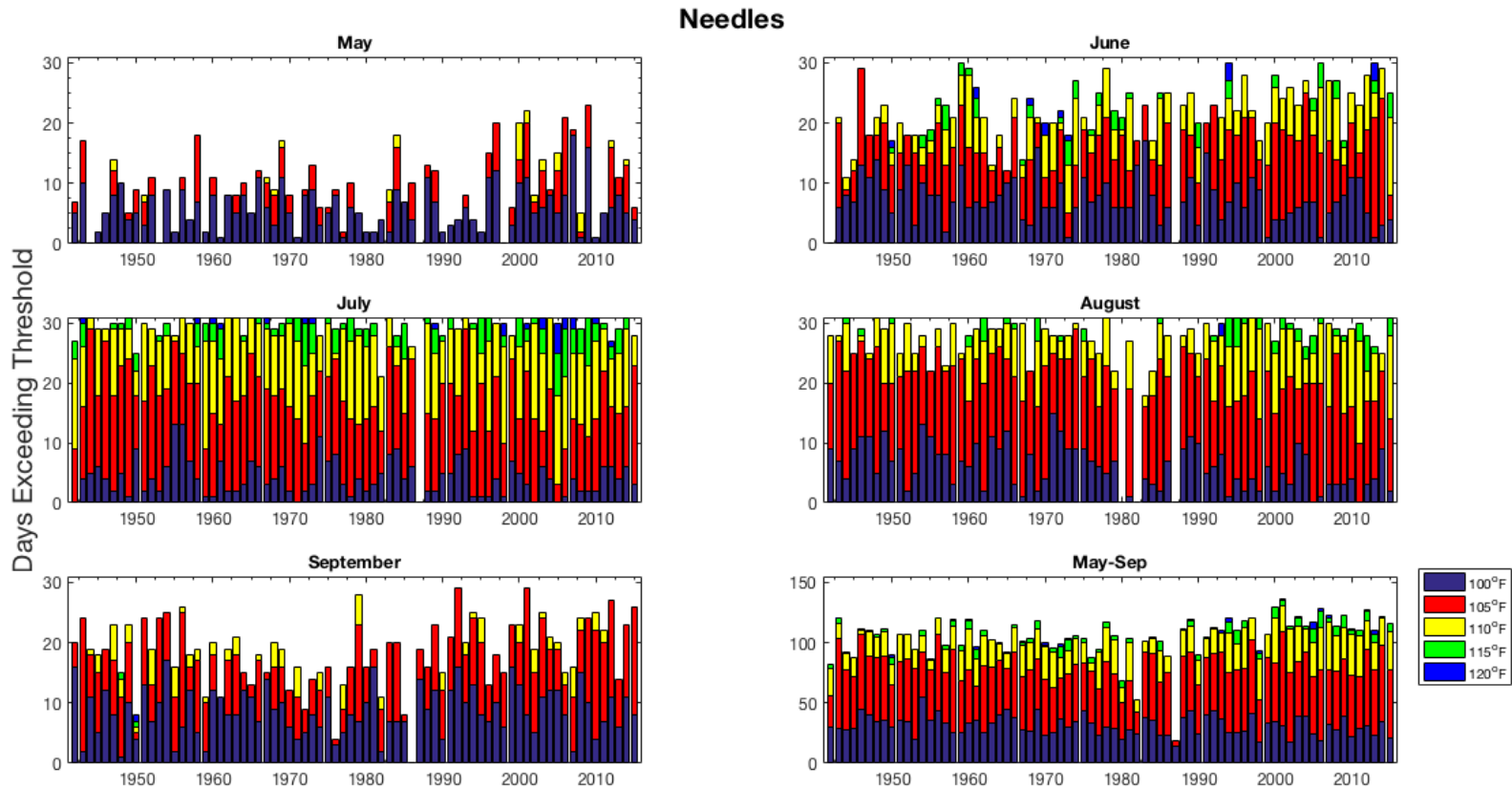
Figure A7-10. The bars illustrate the number of days above a temperature threshold in May, June, July, August and September of a given year. The purple bar indicates the number of days above 100˚F, the red bar is the number of days above 105˚F, the yellow bar is the number of days above 110˚F and the green is the number of days above 115˚F. The last panel depicts the number of days above these thresholds from May through September through time.
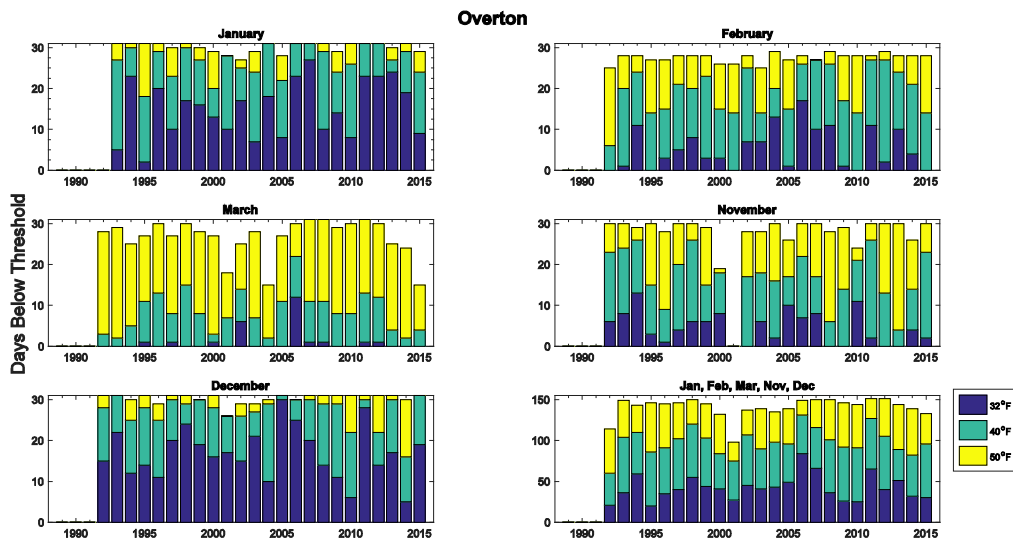
130

Figure A7-11. The bars illustrate the number of days below a temperature threshold in November, December, January, February and March of a given year. The purple bar represents the number of days below 32˚F, the green bar represents number of days below 40˚F, the yellow bar is the number of days below 50˚F. The maximum number of days for January, March and December is 31.

8. Overton
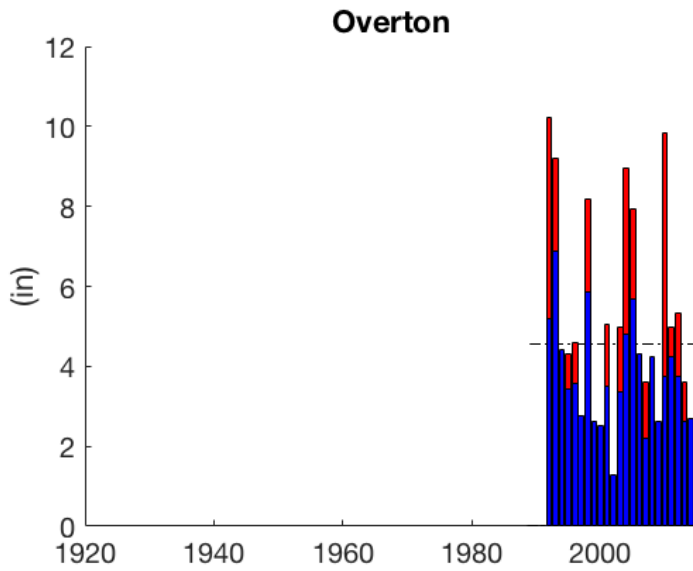
Figure A8-1. The total annual rainfall in inches. The dashed line is the average annual rainfall over the entire period of record. The height of the entire bar represents the total annual precipitation and the red part is the contribution for the 95th percentile events.
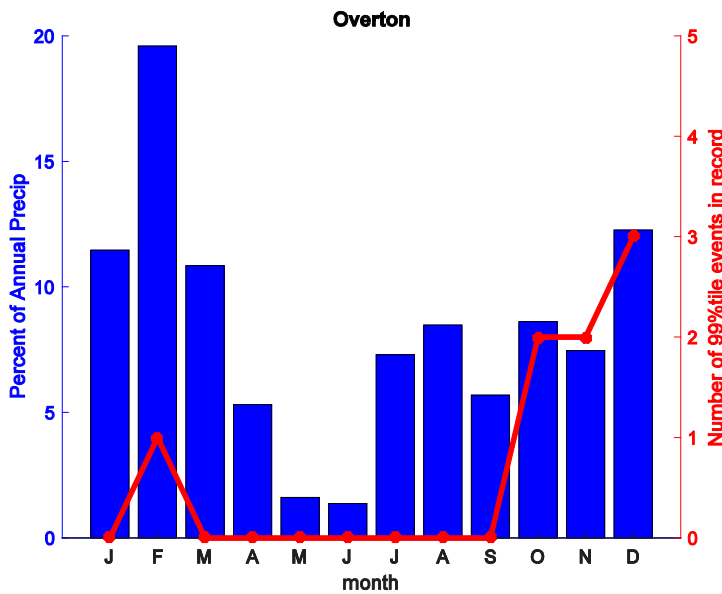
Figure A8-2. The blue bars show the average monthly percent contribution to the total annual rainfall. Thus all 12 bars total 100%. The red line is the number of extreme precipitation events, or 99th percentile events from 1961-1990.
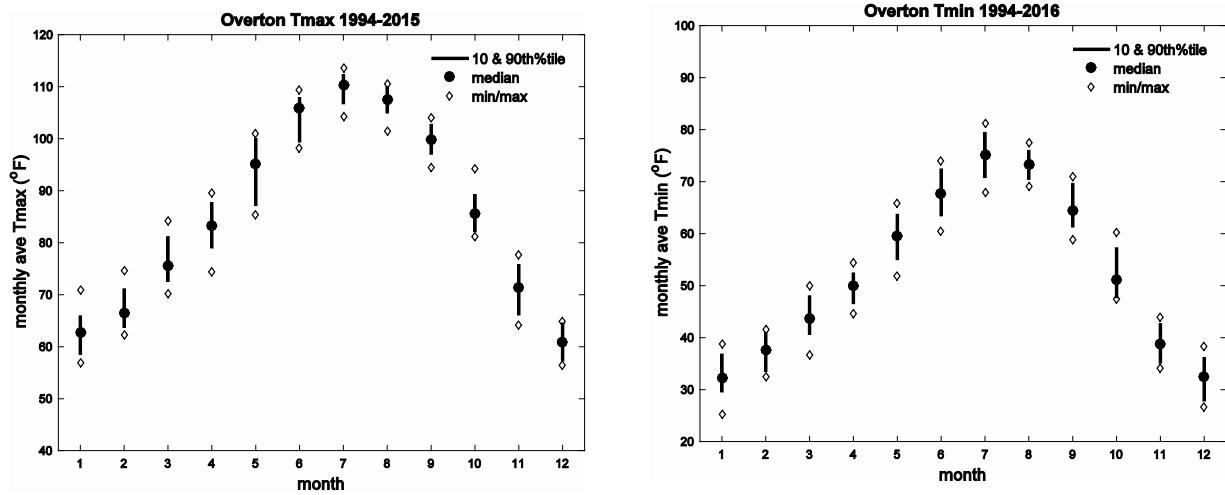
Figure A8-3. For each month (January to December) from 1994-2015, the mean monthly T_{max} (°F) (left) and T_{min} (right) represented by the red circles whereas the line illustrates the range of temperatures in the 10th to 90th percentiles. The diamonds represent the maximum and minimum T_{max} values over the 1994-2015 time period.
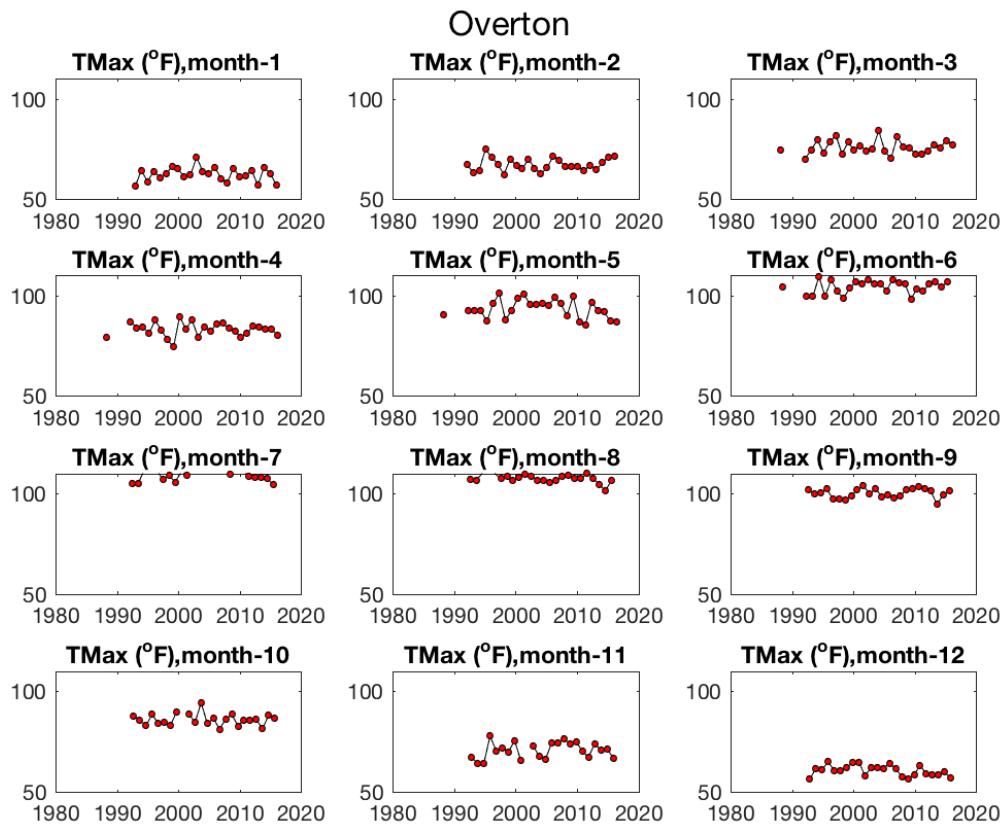
Figure A8-4. Each panel shows the monthly average Tmax (˚F) for each year of record at the Overton station.
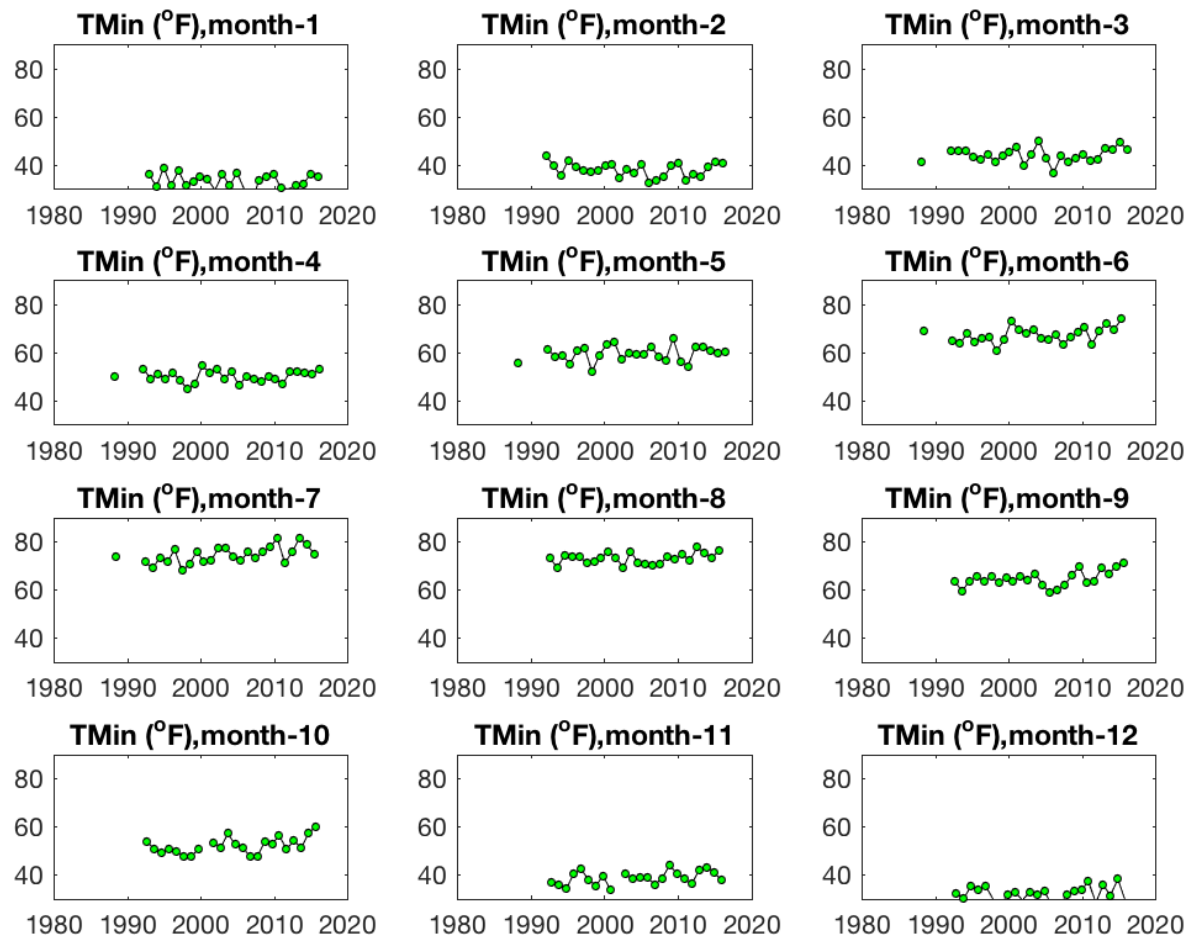
Figure A8-5. Each panel shows the monthly average Tmin (˚F) for each year of record at the Overton station.
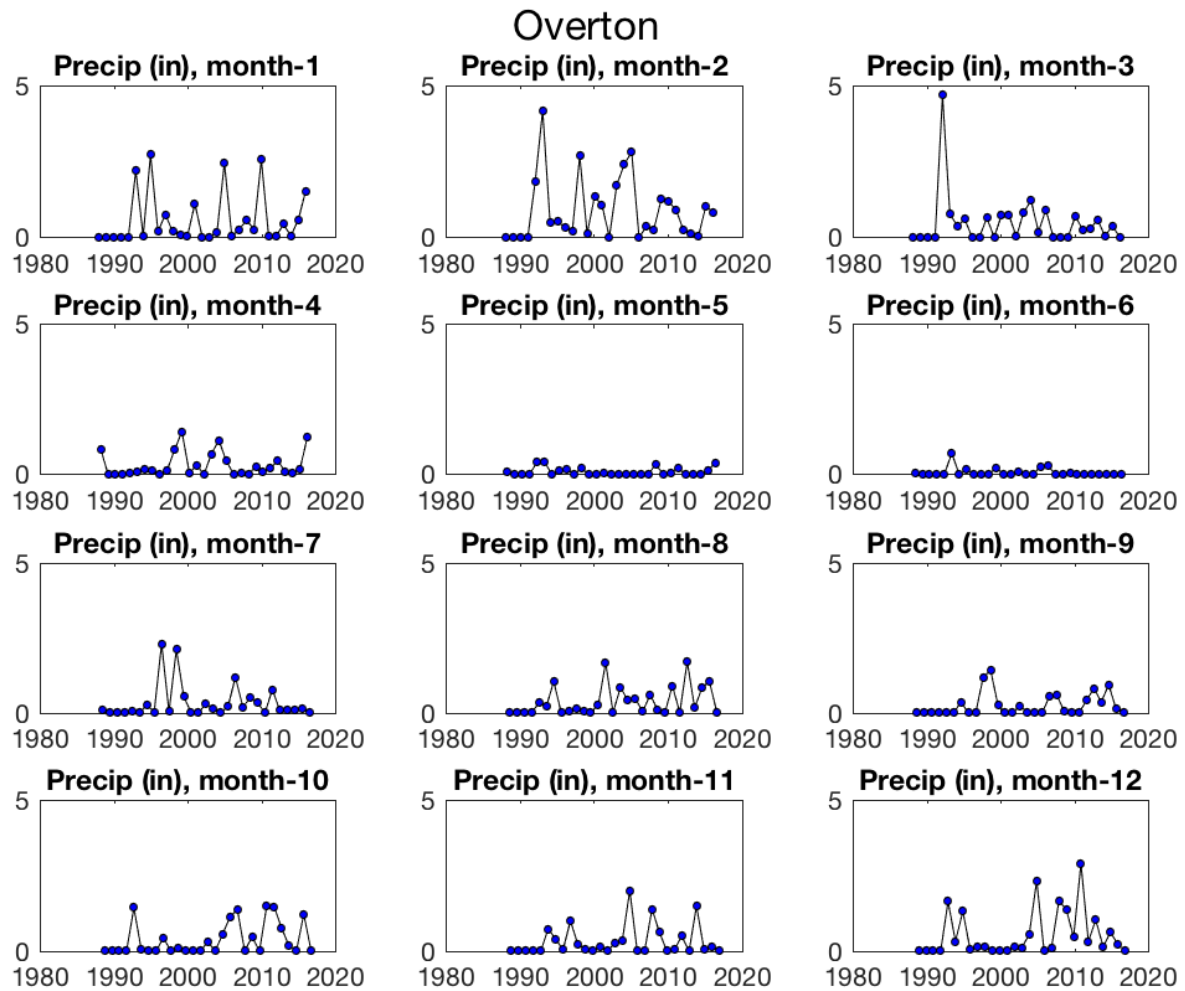
Figure A8-6. Each panel shows the monthly average precipitation (in) for each year of record at the Overton station.
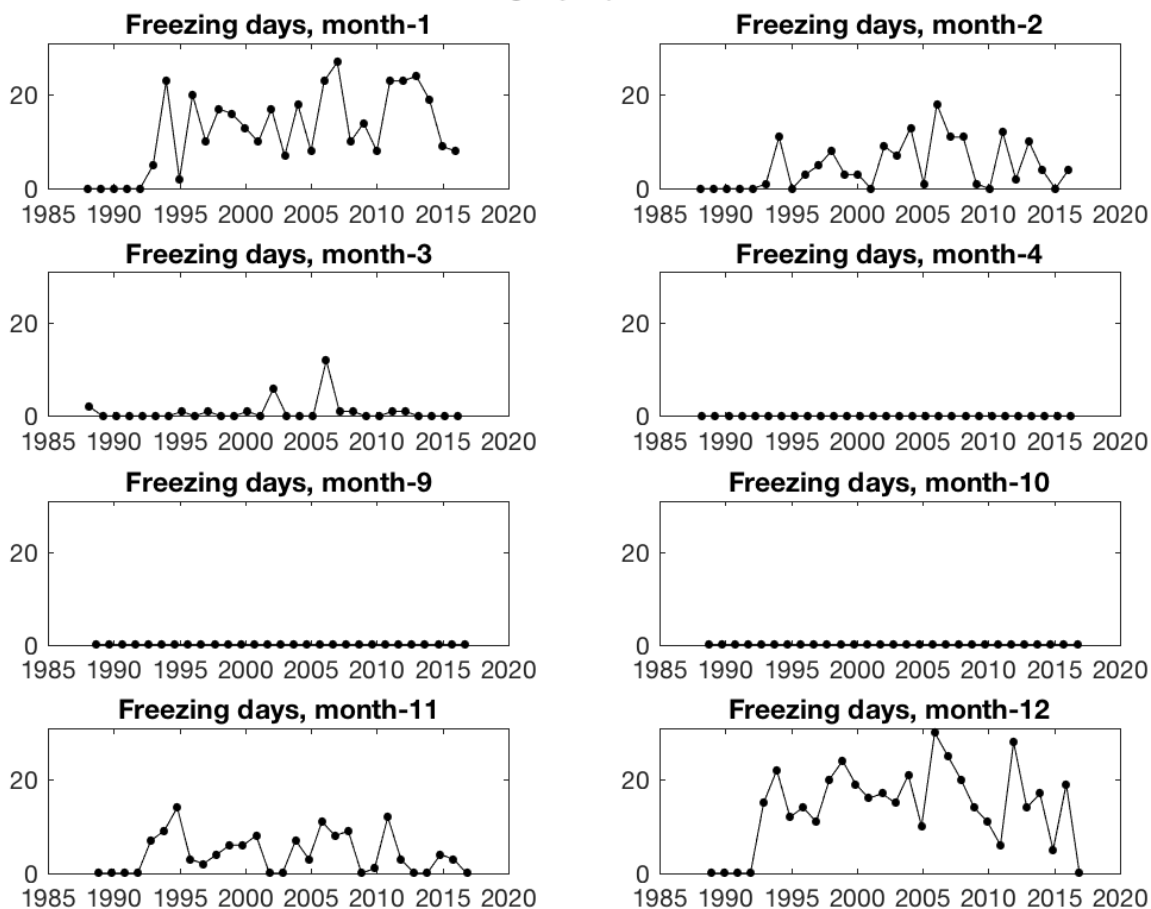
Figure A8-7. Each panel shows the monthly sum of the total number of freezing days for each year of record at the Overton station. The maximum in Jan, March, October, and December is 31 days.
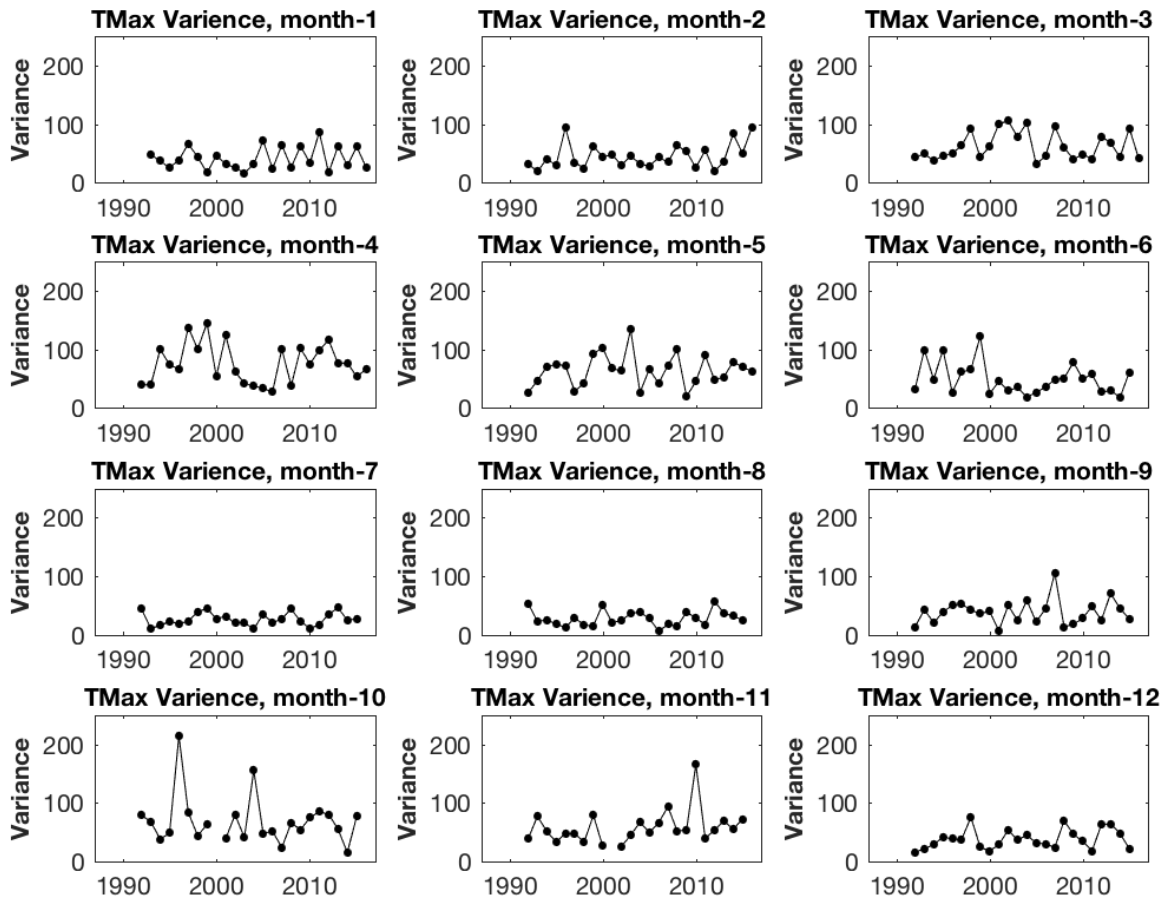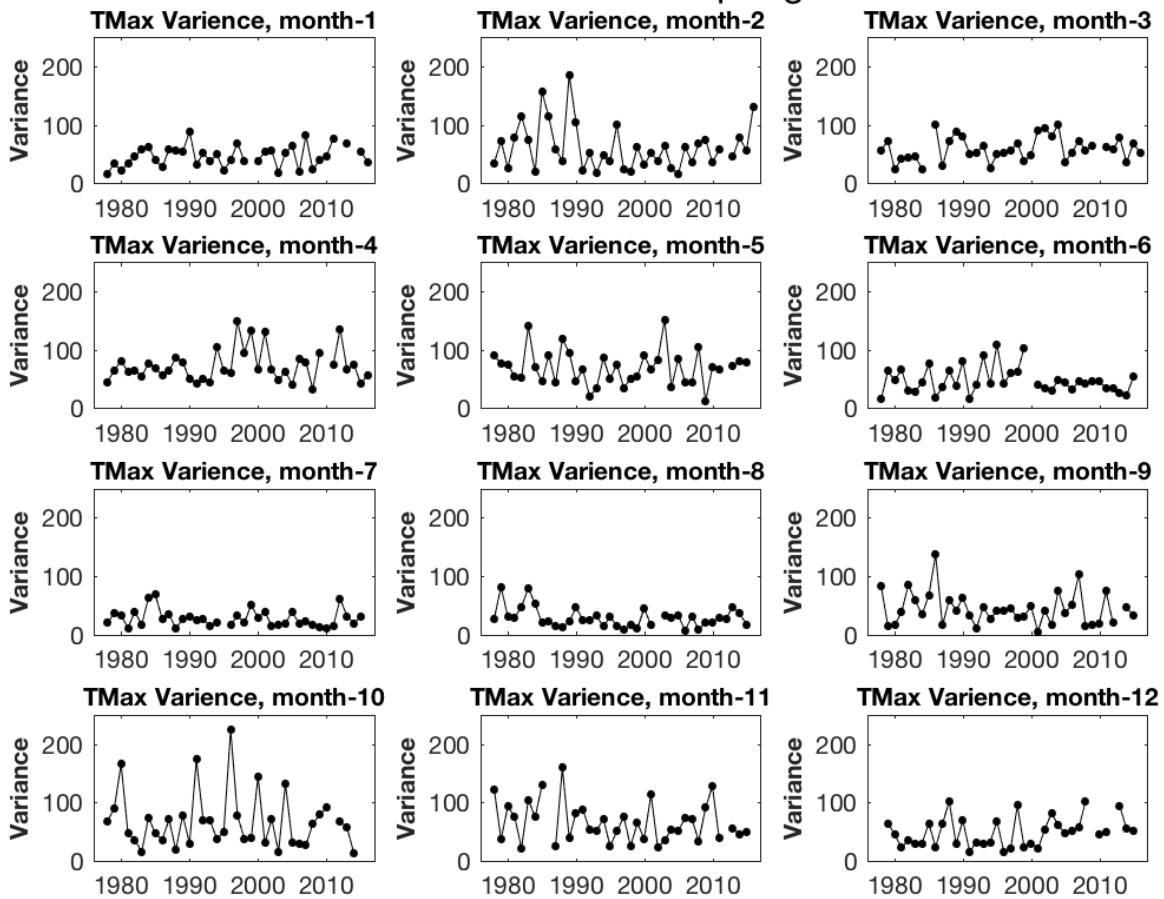
Figure A8-8. Each panel shows the variance (standard deviation squared) in Tmax during a given month at the Overton station.
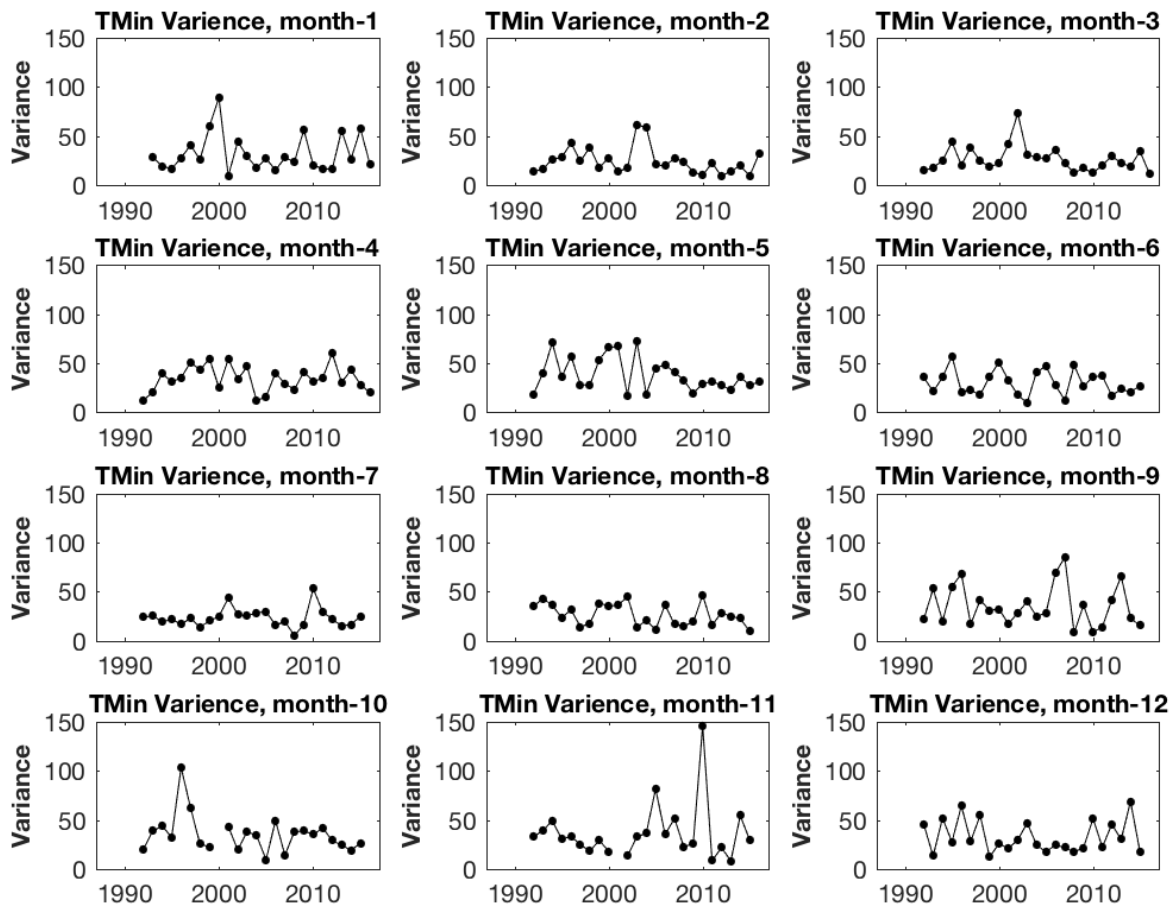
Figure A8-9. Each panel shows the variance (standard deviation squared) in Tmin during a given month at the Overton station.
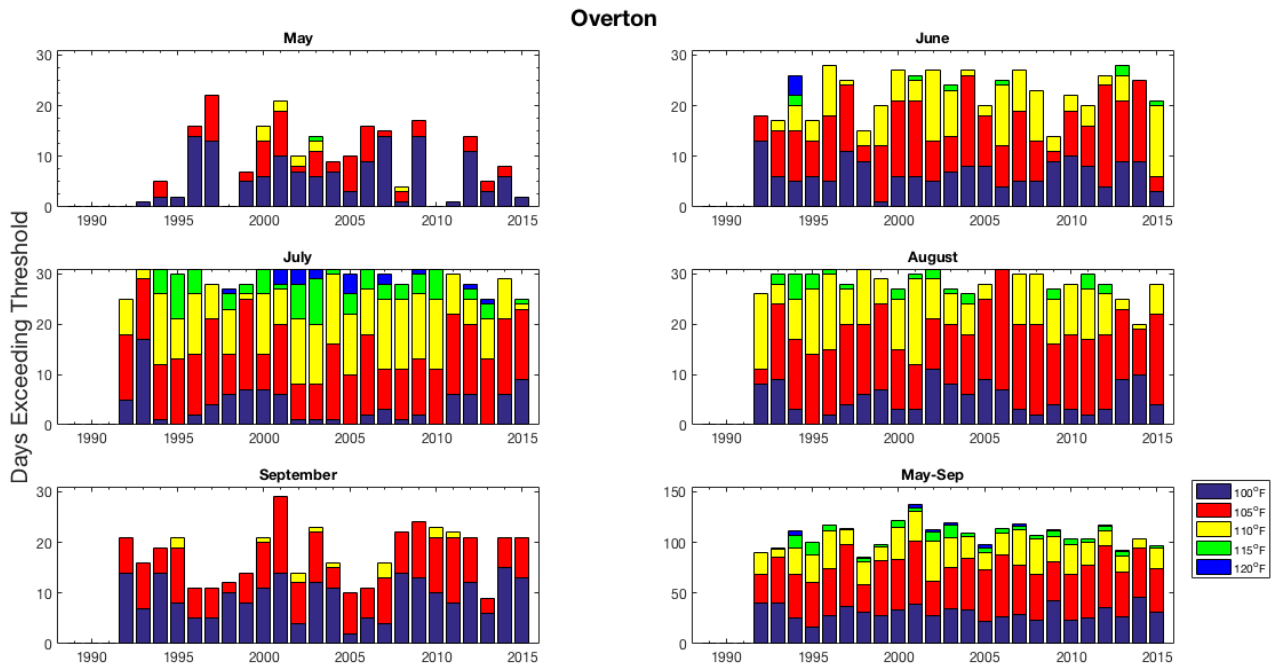
Figure A8-10. The bars illustrate the number of days above a temperature threshold in May, June, July, August and September of a given year. The purple bar indicates the number of days above 100˚F, the red bar is the number of days above 105˚F, the yellow bar is the number of days above 110˚F and the green is the number of days above 115˚F. The last panel depicts the number of days above these thresholds from May through September through time.
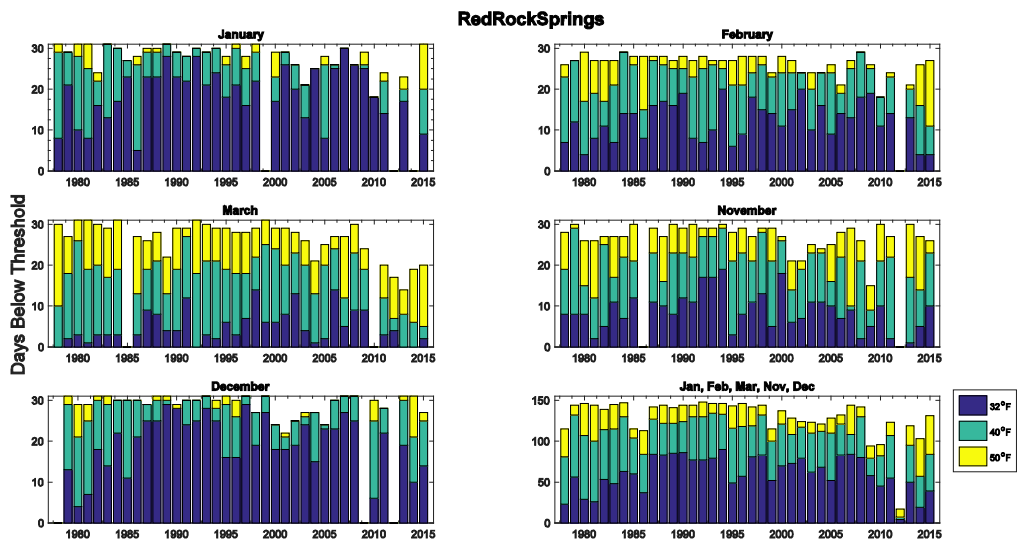

Figure A8-11. The bars illustrate the number of days below a temperature threshold in November, December, January, February and March of a given year. The purple bar represents the number of days below 32˚F, the green bar represents number of days below 40˚F, the yellow bar is the number of days below 50˚F. The maximum number of days for January, March and December is 31.
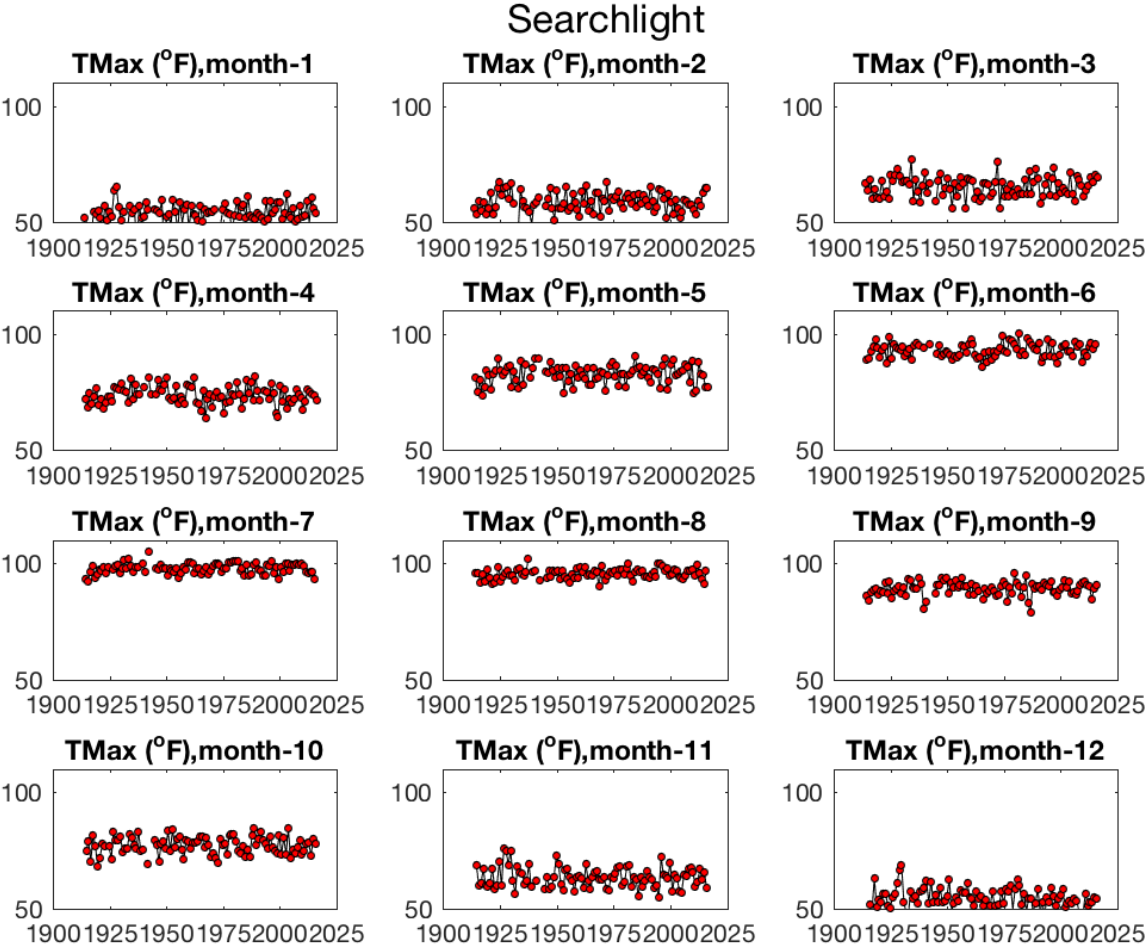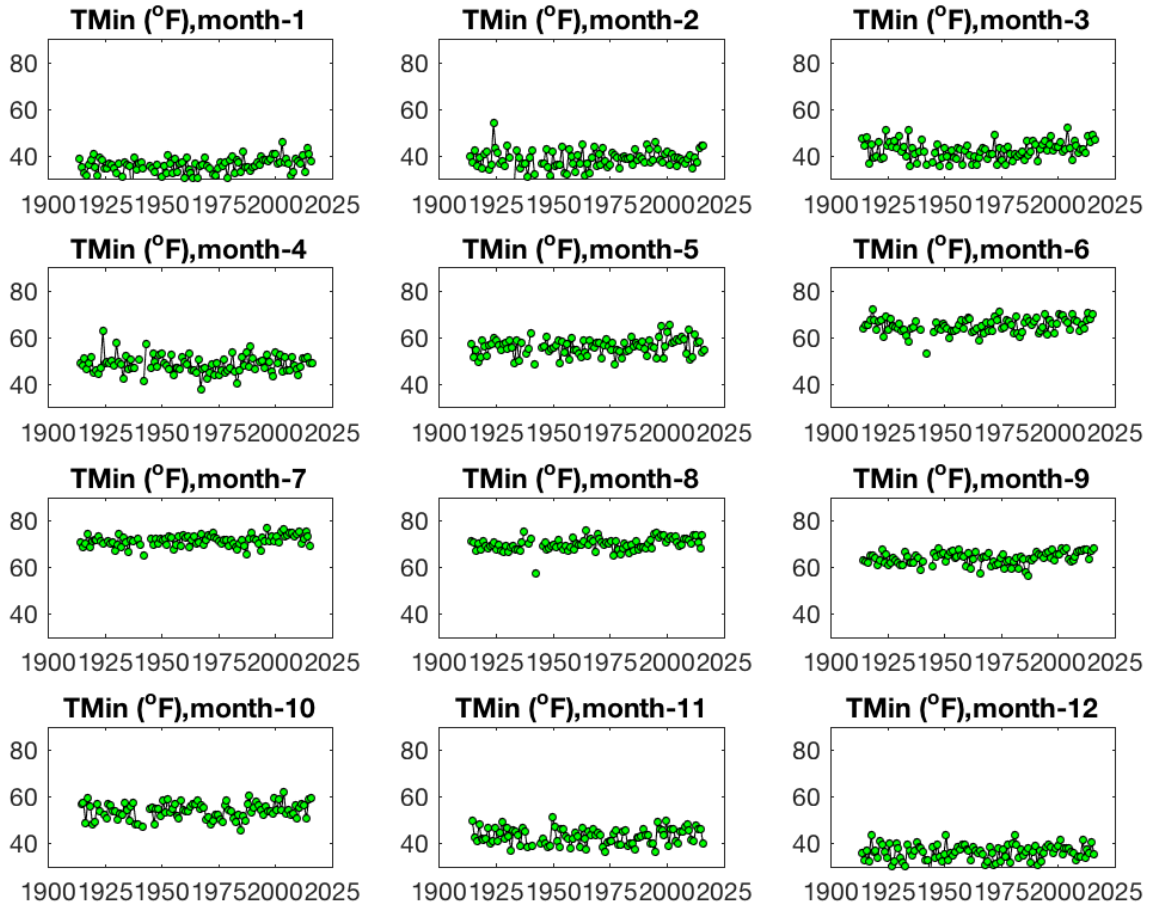
9. Red Rock Springs
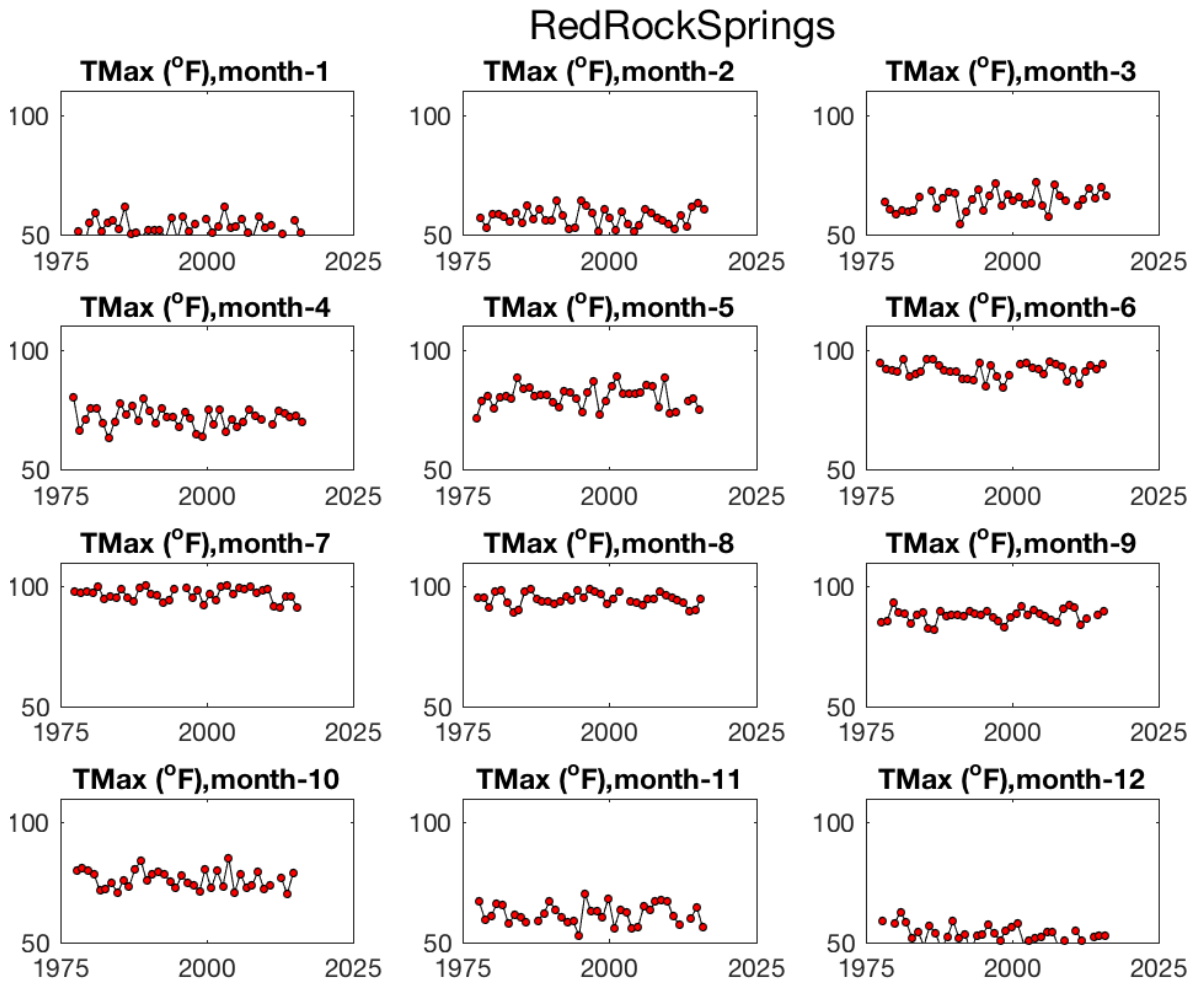
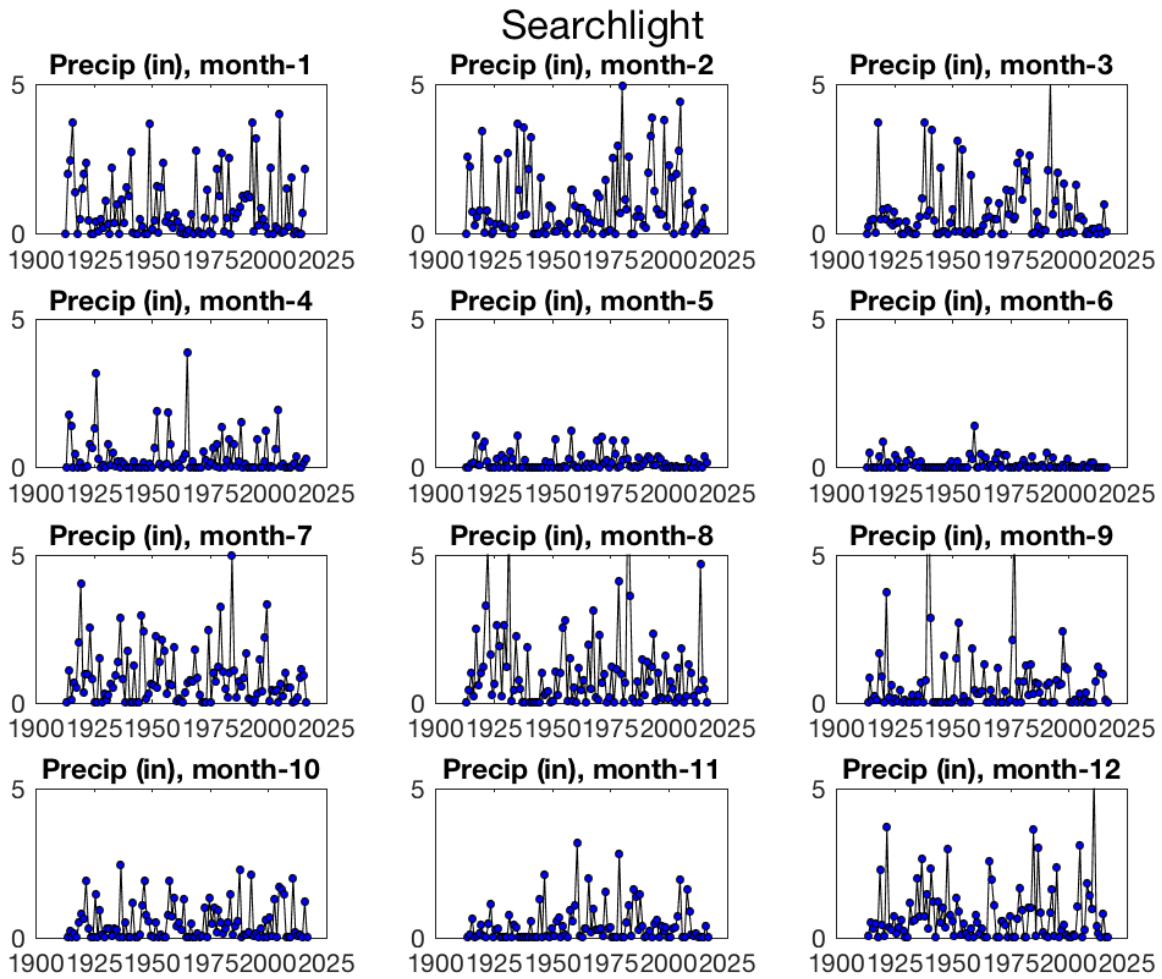Figure A9-1. Each panel shows the monthly average Tmax (˚F) for each year of record at the Red Rock station.
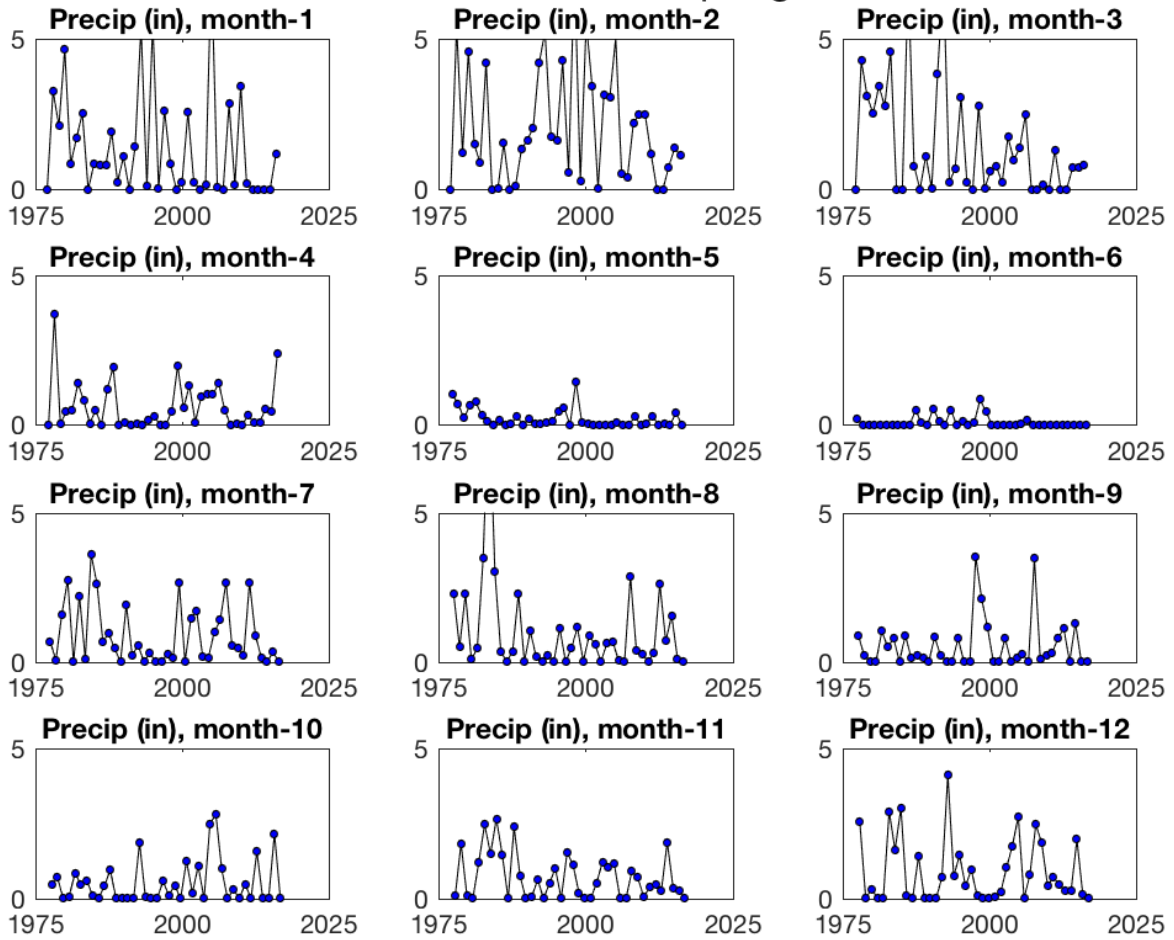
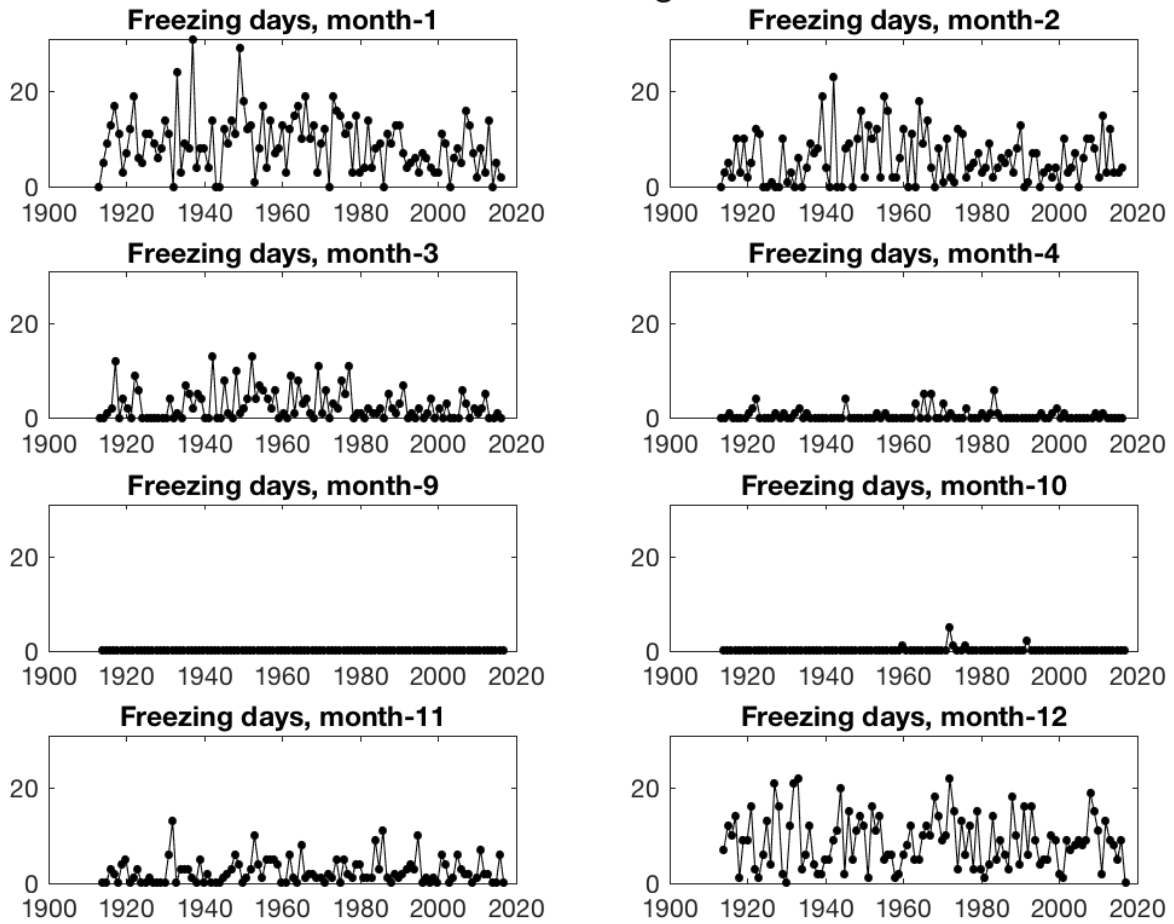Figure A9-2. Each panel shows the monthly average precipitation (in) for each year of record at the Red Rock station.
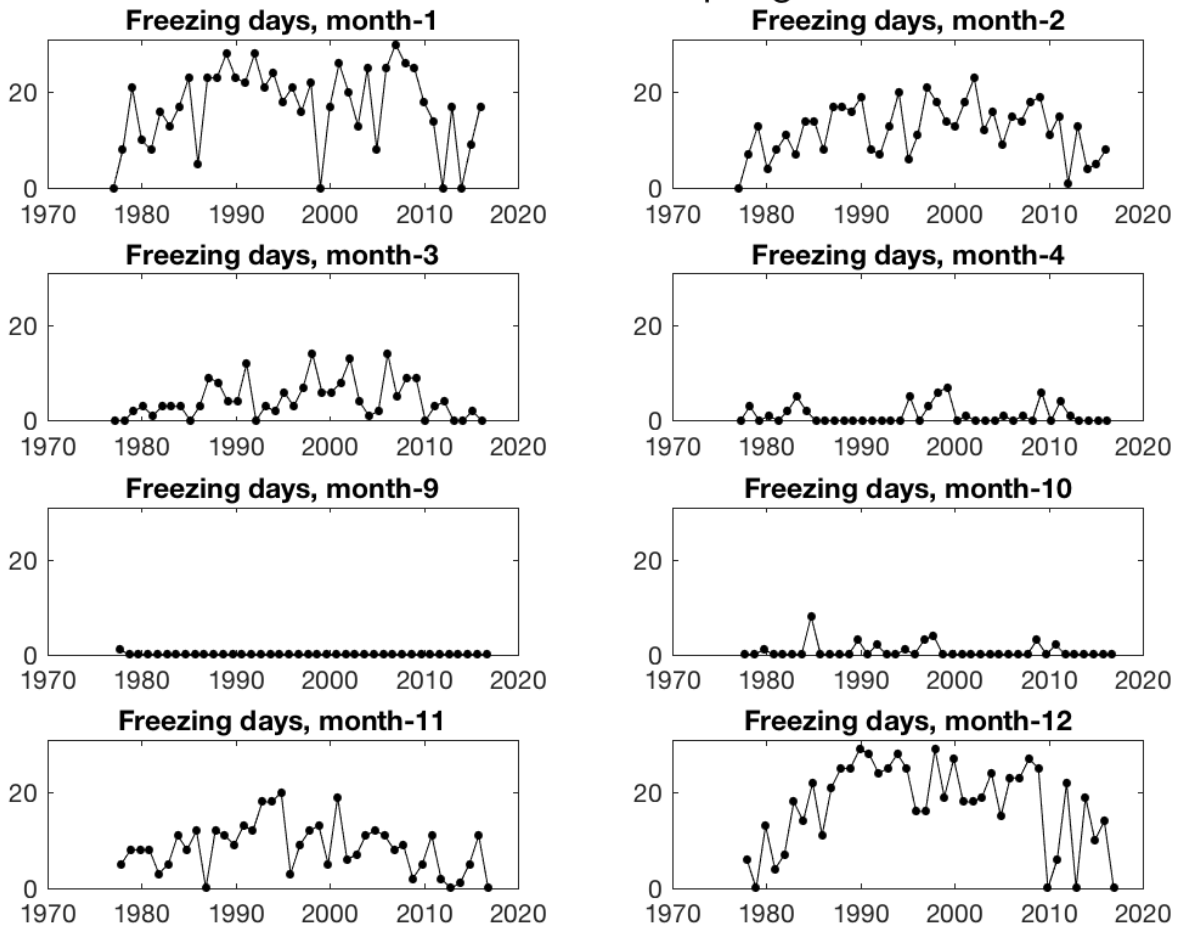
Figure A9-3. Each panel shows the monthly sum of the total number of freezing days for each year of record at the Red Rock station. The maximum in Jan, March, October, and December is 31 days.
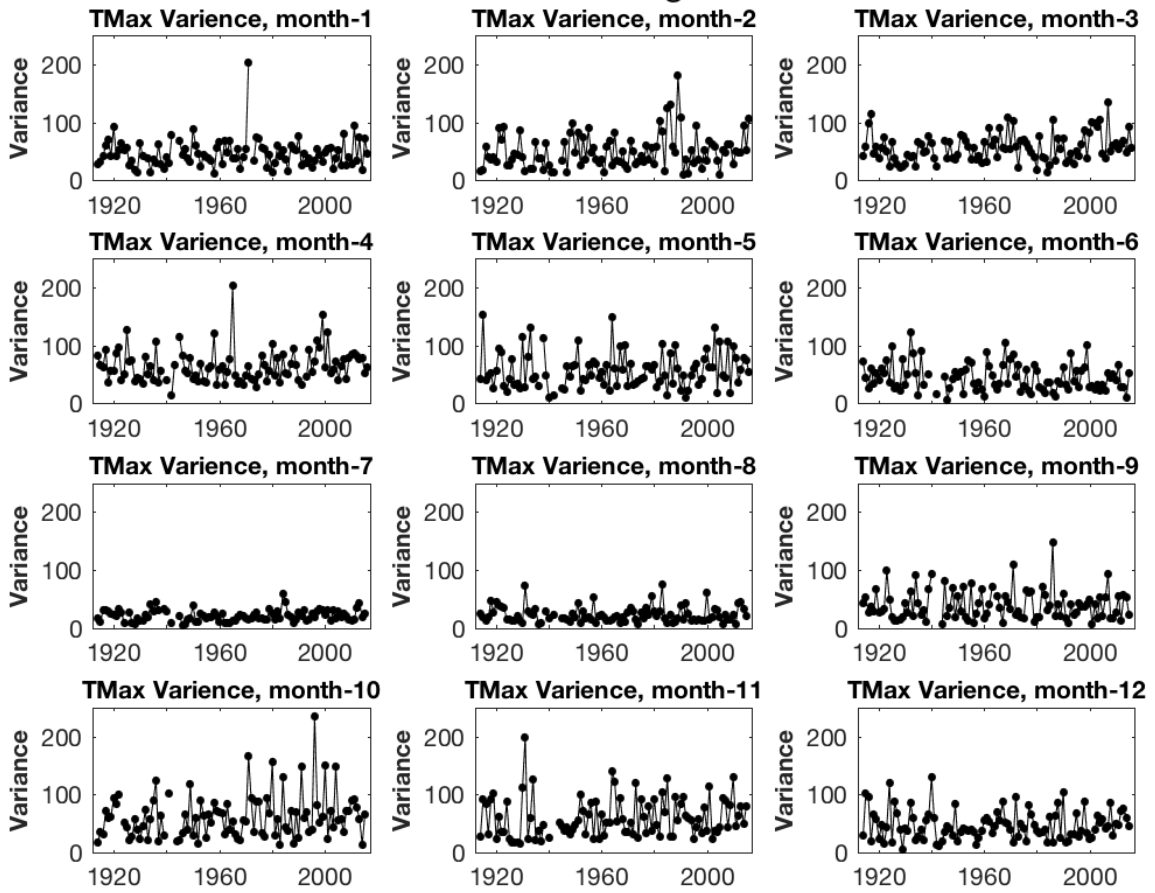
Figure A9-4. Each panel shows the variance (standard deviation squared) in Tmax during a given month at the Red Rock station.
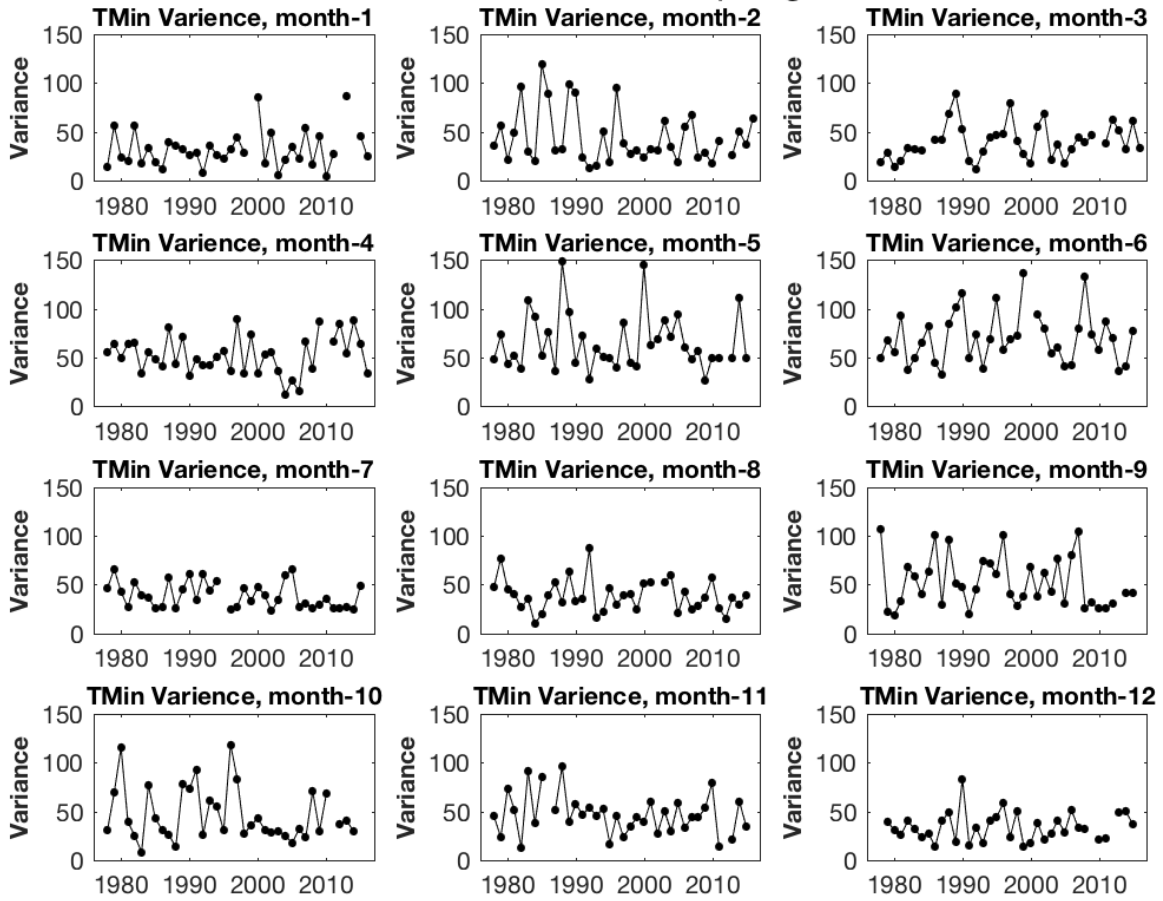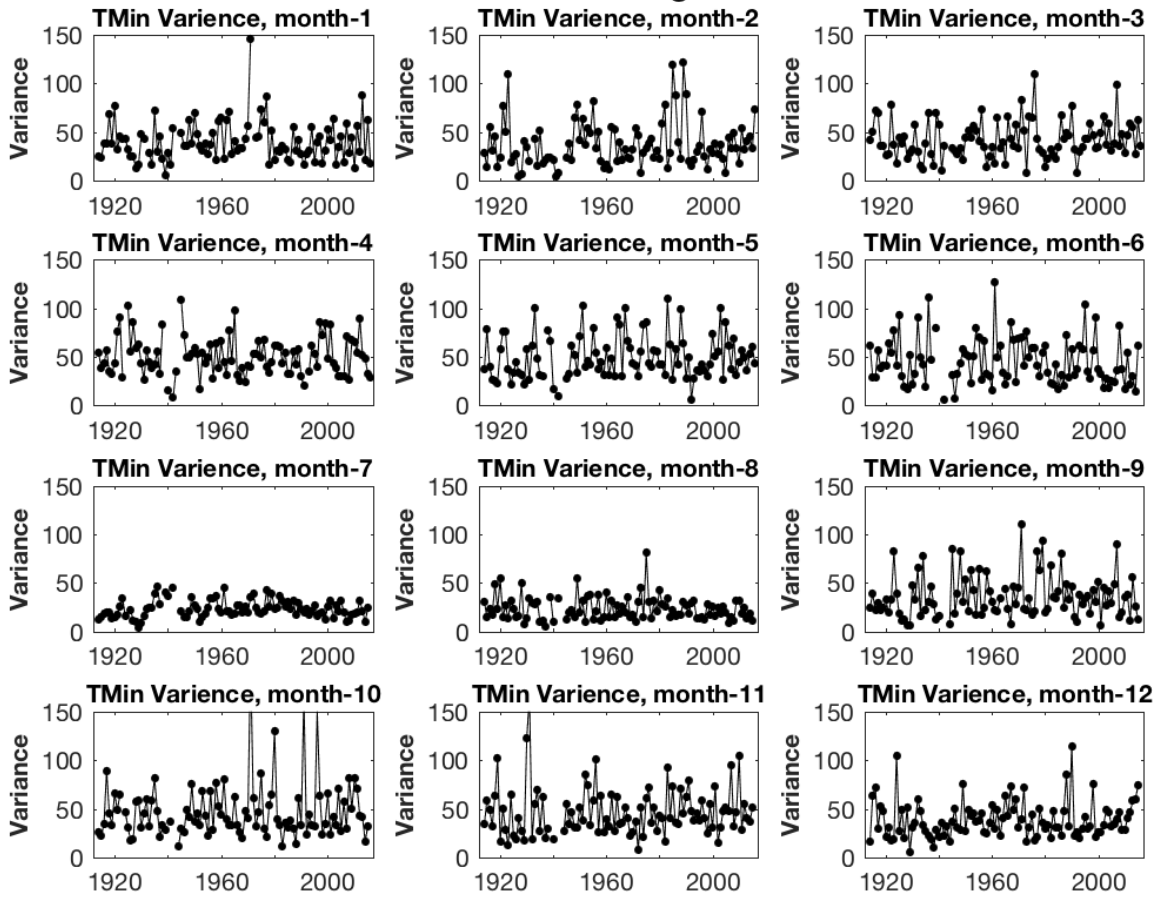
Figure A9-5. Each panel shows the variance (standard deviation squared) in Tmin during a given month at the Red Rock station.
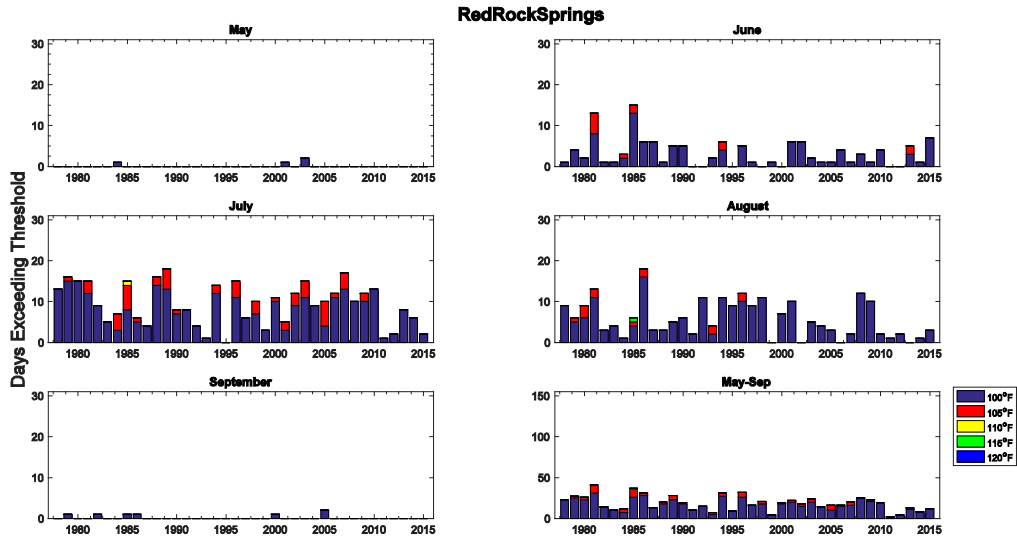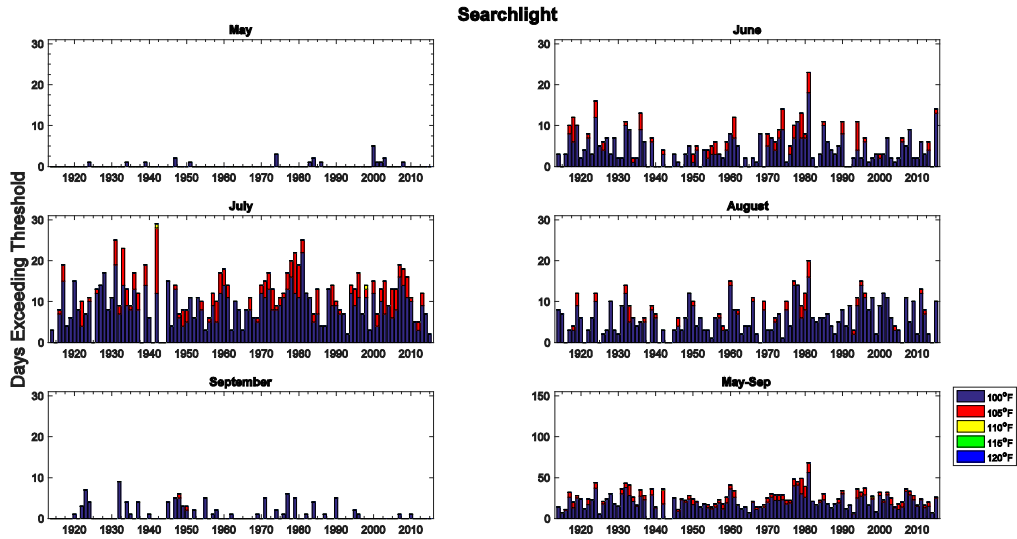
Figure A9-6. The bars illustrate the number of days above a temperature threshold in May, June, July, August and September of a given year. The purple bar indicates the number of days above 100°F, the red bar is the number of days above 105°F, the yellow bar is the number of days above 110°F and the green is the number of days above 115°F. The last panel depicts the number of days above these thresholds from May through September through time.

Figure A9-7. The bars illustrate the number of days below a temperature threshold in November, December, January, February and March of a given year. The purple bar represents the number of days below 32°F, the green bar represents number of days below 40°F, the yellow bar is the number of days below 50°F. The maximum number of days for January, March and December is 31

145

10. Searchlight

Figure A10-1. Each panel shows the monthly average Tmax (˚F) for each year of record at the Searchlight station.

Figure A10-2. Each panel shows the monthly average Tmin (˚F) for each year of record at the Searchlight station.

Figure A10-3. Each panel shows the monthly average precipitation (in) for each year of record at the Searchlight station.

Figure A10-4. Each panel shows the monthly sum of the total number of freezing days for each year of record at the Searchlight station. The maximum in Jan, March, October, and December is 31 days.

Figure A10-5. Each panel shows the variance (standard deviation squared) in Tmax during a given month at the Searchlight station.

Figure A10-6. Each panel shows the variance (standard deviation squared) in Tmin during a given month at the Searchlight station.

Figure A10-7. The bars illustrate the number of days above a temperature threshold in May, June, July, August and September of a given year. The purple bar indicates the number of days above 100°F, the red bar is the number of days above 105°F, the yellow bar is the number of days above 110°F and the green is the number of days above 115°F. The last panel depicts the number of days above these thresholds from May through September through time.
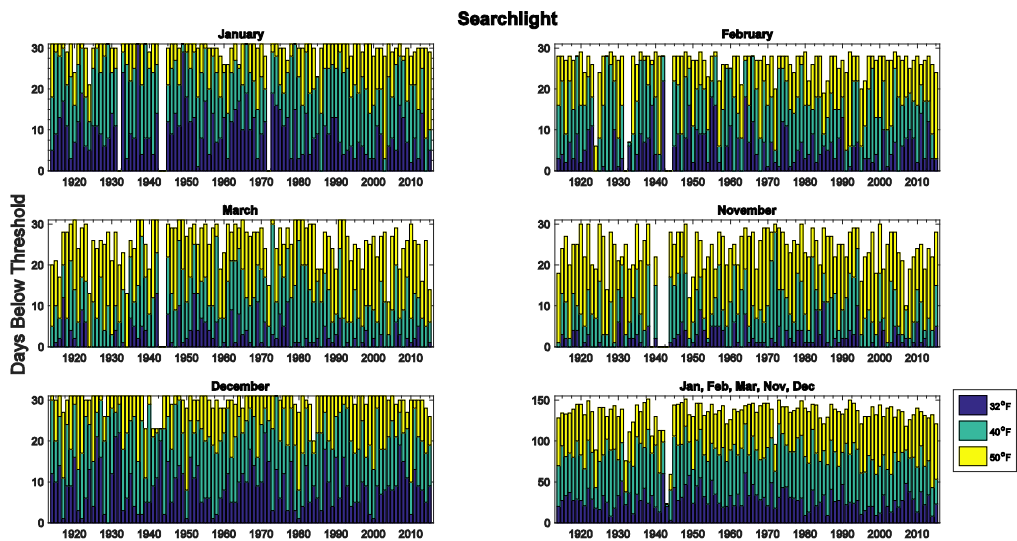
Figure A10-8. The bars illustrate the number of days below a temperature threshold in November, December, January, February and March of a given year. The purple bar represents the number of days below 32°F, the green bar represents number of days below 40°F, the yellow bar is the number of days below 50°F. The maximum number of days for January, March and December is 31.

11. Valley of Fire
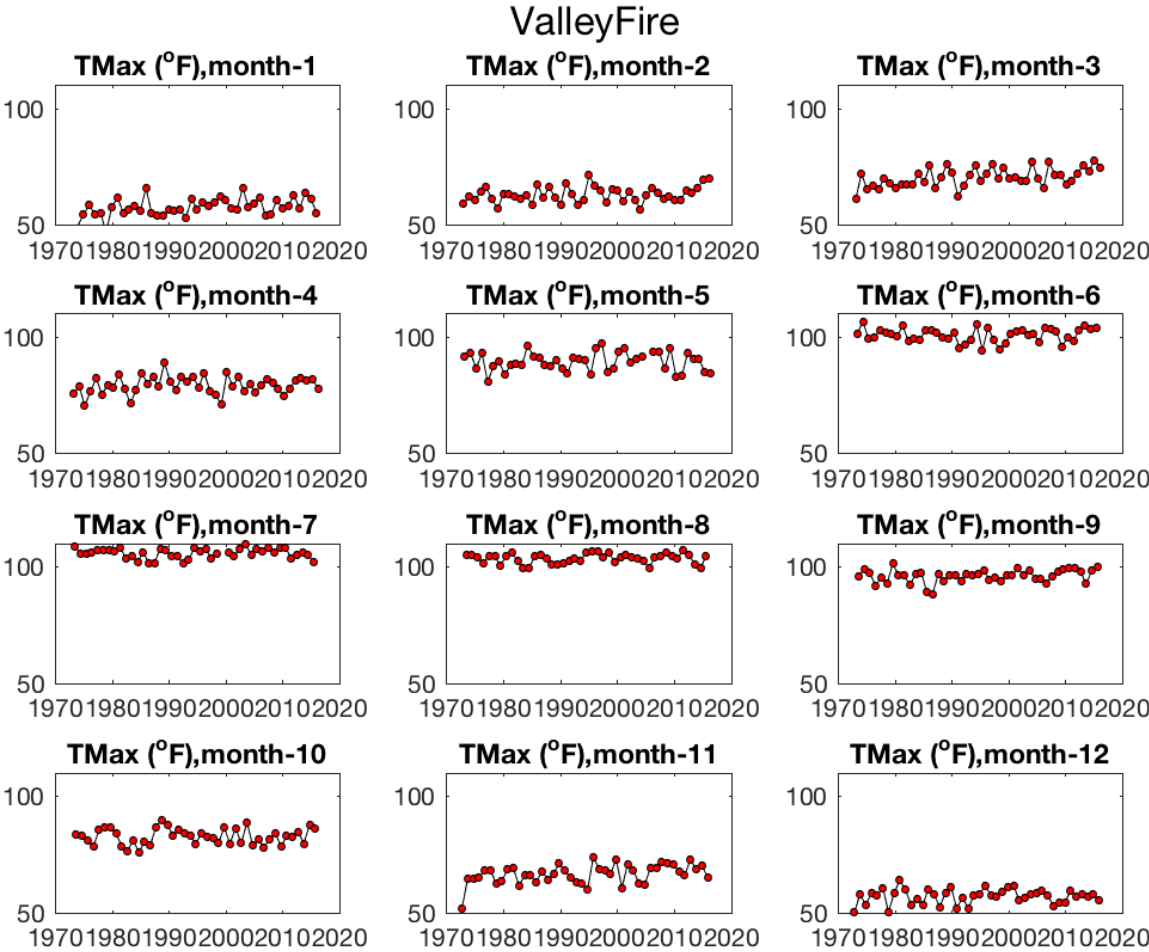
Figure A11-1. Each panel shows the monthly average Tmax (˚F) for each year of record at the Valley of Fire station.
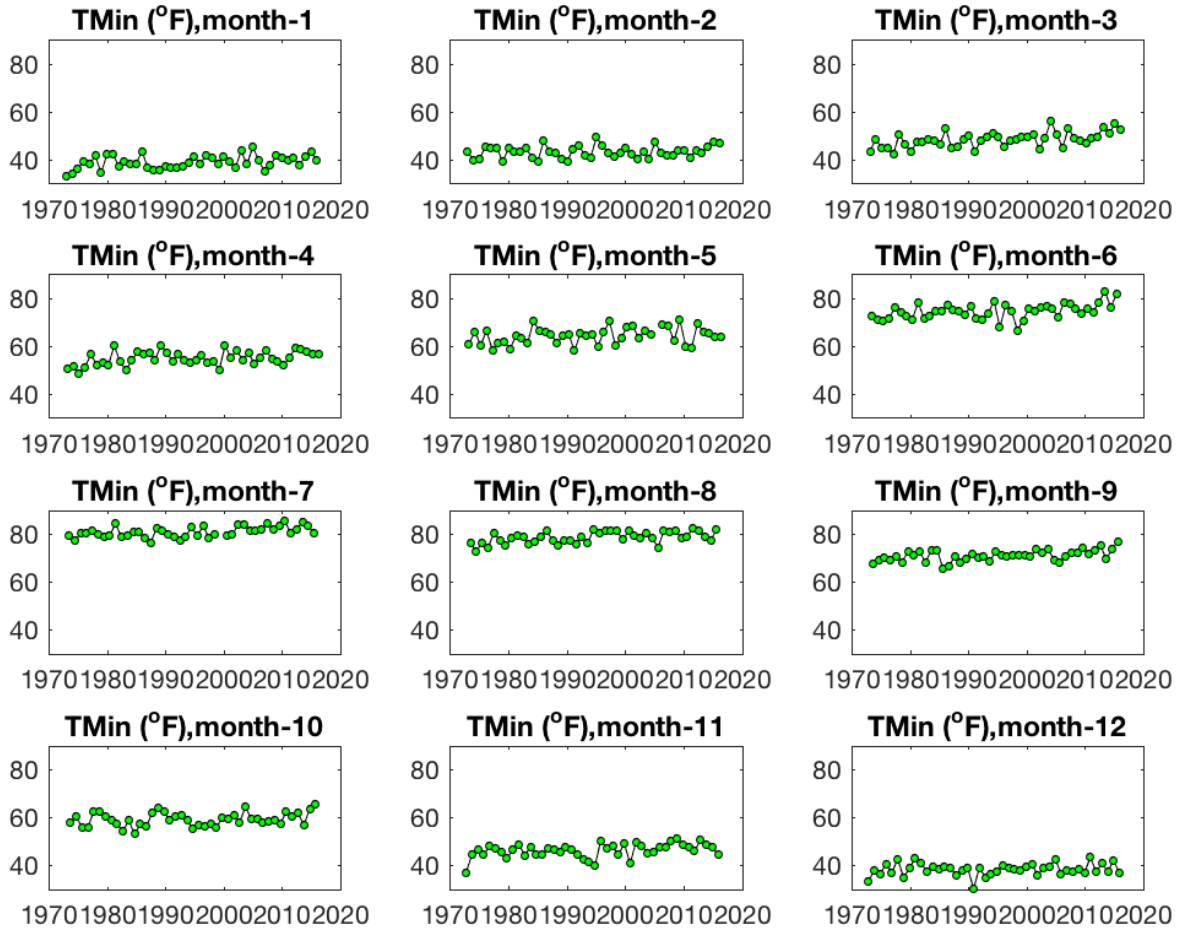
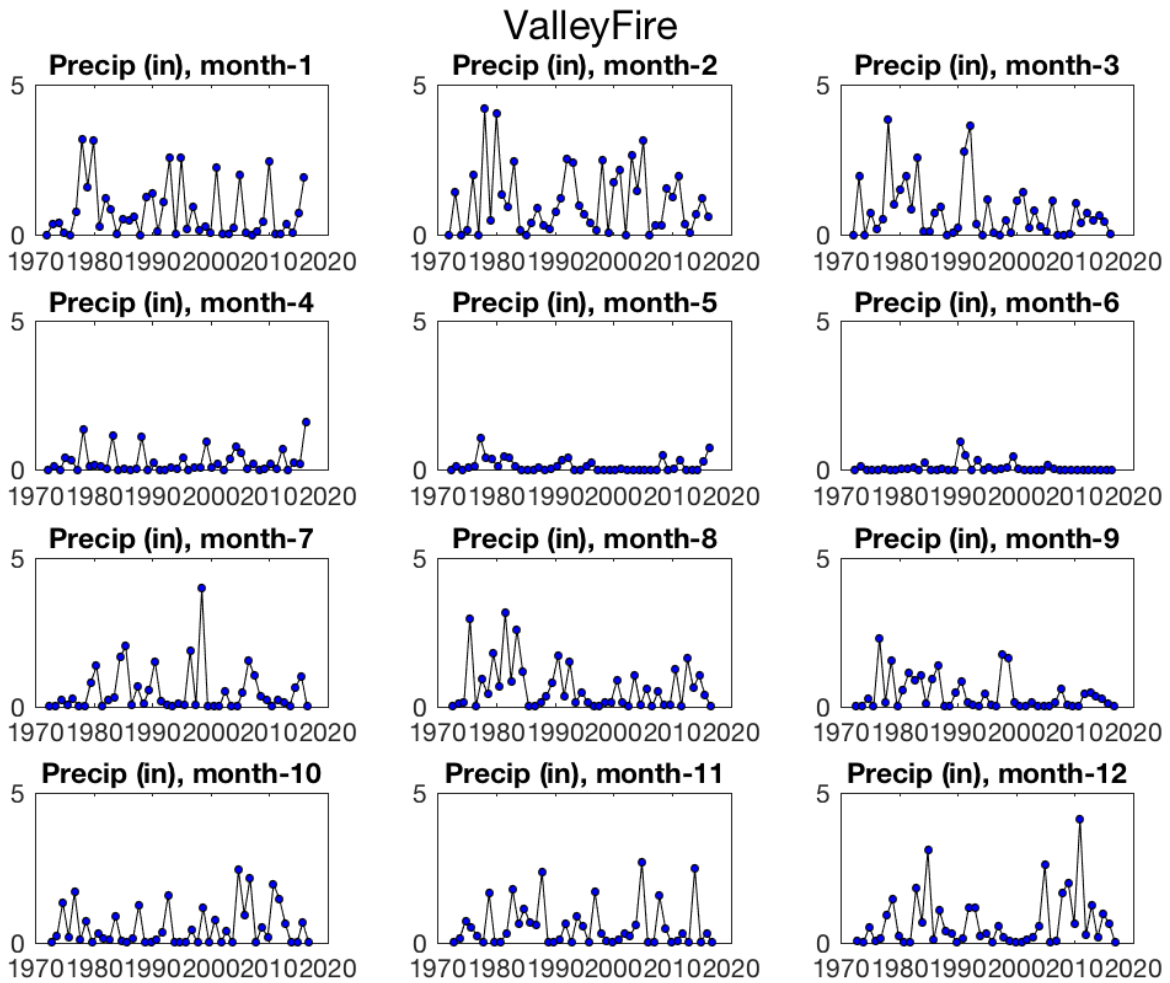Figure A11-2. Each panel shows the monthly average Tmin (˚F) for each year of record at the Valley of Fire station.

Figure A11-3. Each panel shows the monthly average precipitation (in) for each year of record at the Valley of Fire station.

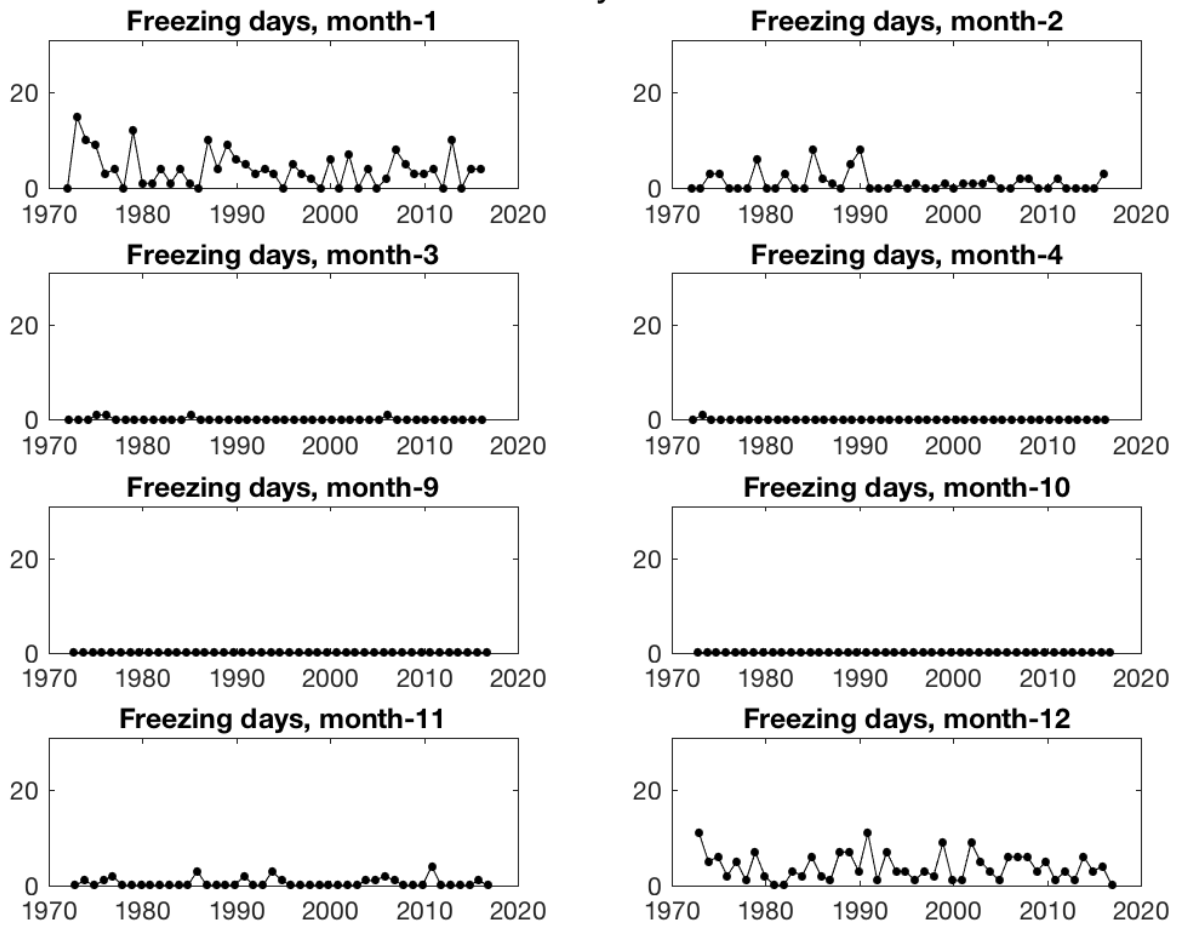Figure A11-4. Each panel shows the monthly sum of the total number of freezing days for each year of record at the Valley of Fire station. The maximum in Jan, March, October, and December is 31 days.
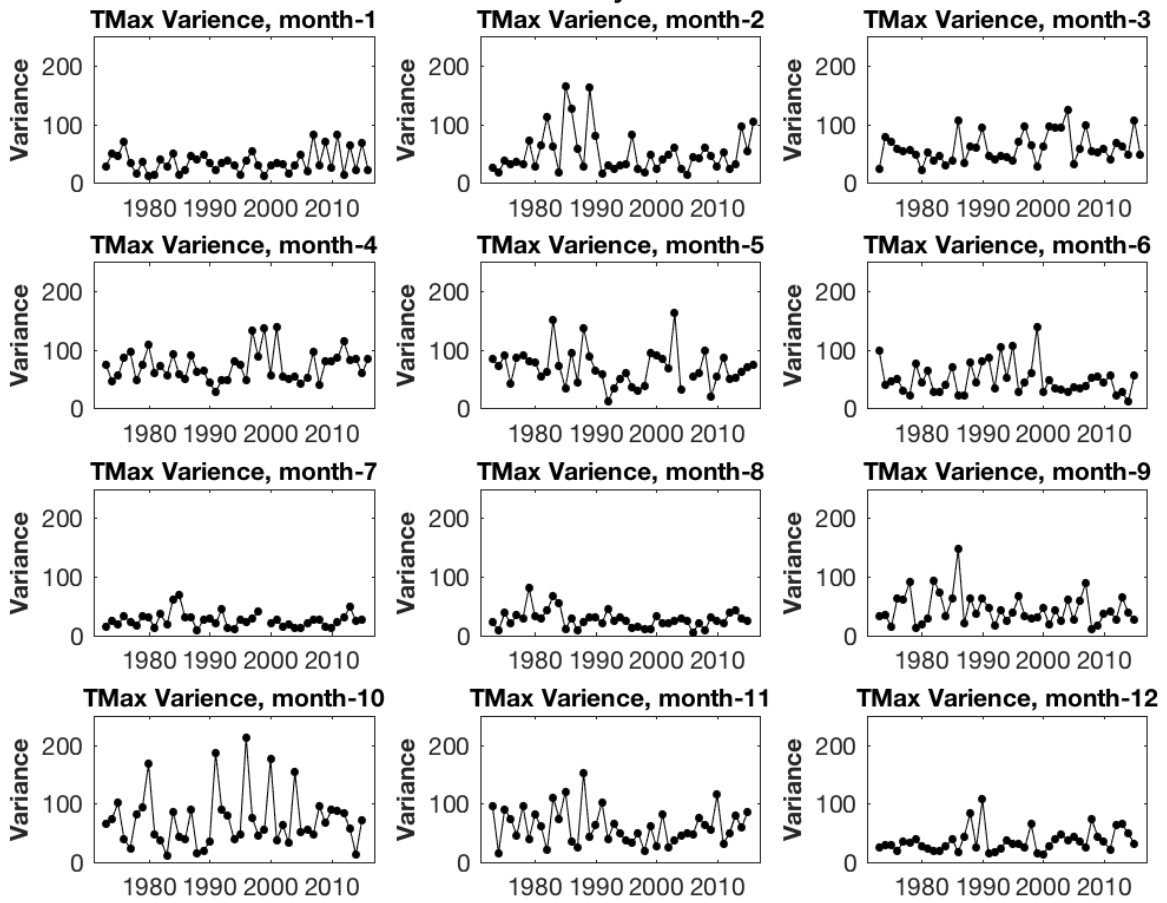
Figure A11-5. Each panel shows the variance (standard deviation squared) in Tmax during a given month at the Valley of Fire station.
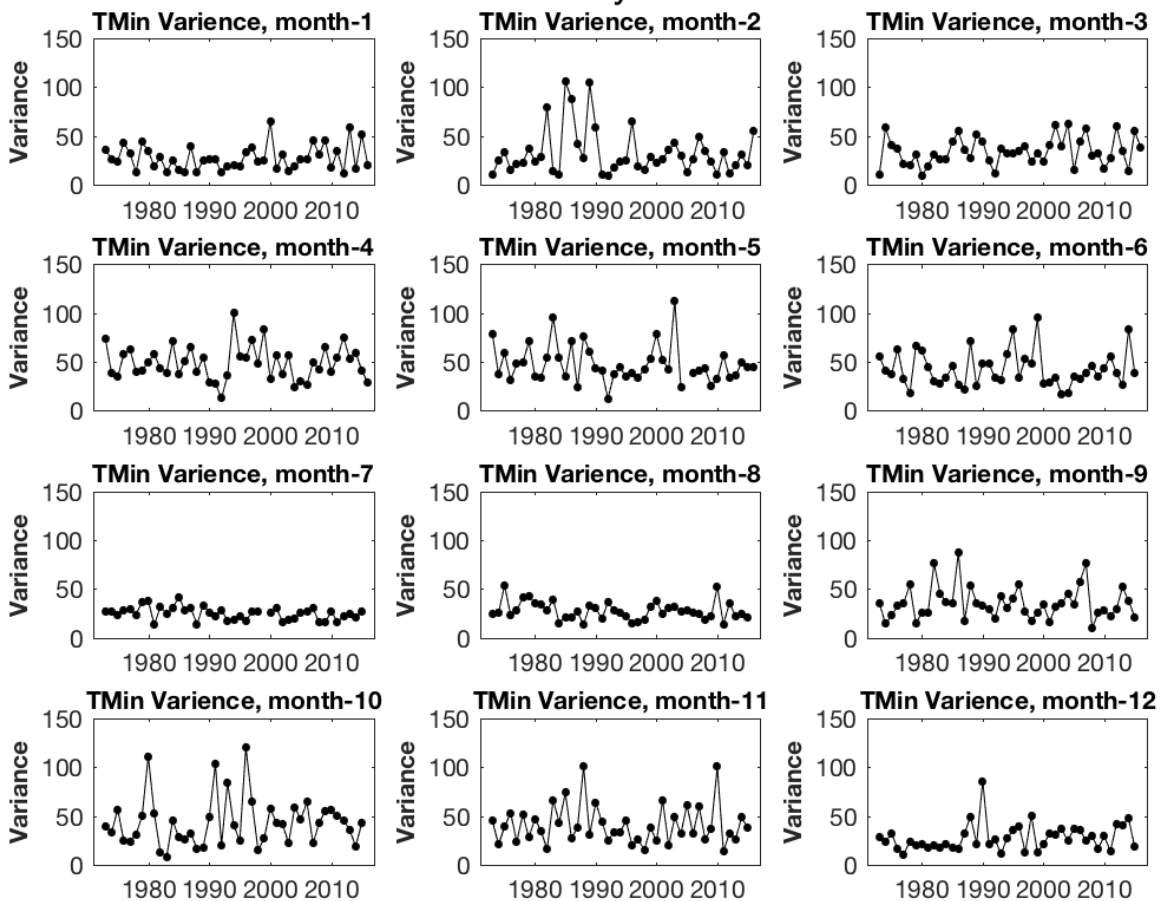
Figure A11-6. Each panel shows the variance (standard deviation squared) in Tmin during a given month at the Valley of Fire station.
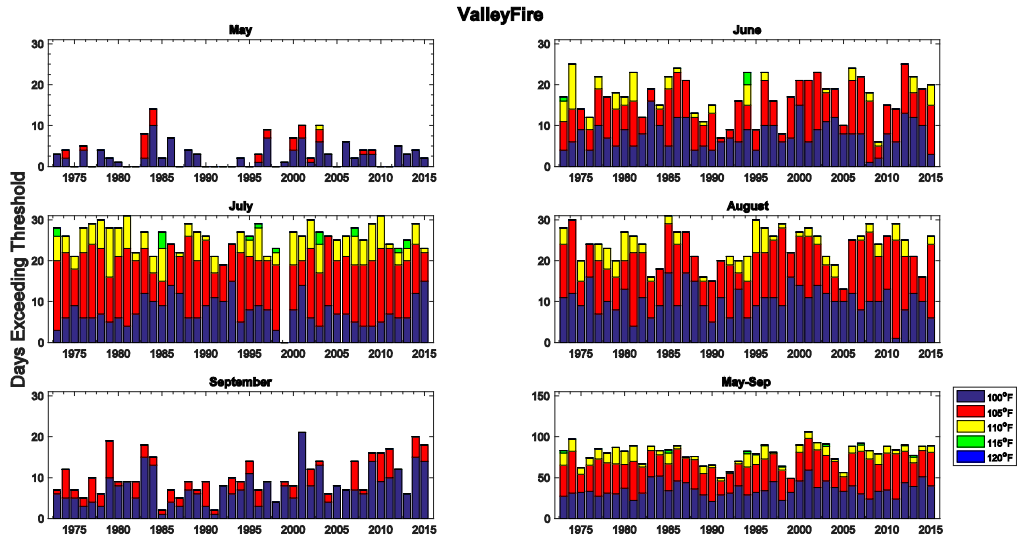
Figure A11-7. The bars illustrate the number of days above a temperature threshold in May, June, July, August and September of a given year. The purple bar indicates the number of days above 100˚F, the red bar is the number of days above 105˚F, the yellow bar is the number of days above 110˚F and the green is the number of days above 115˚F. The last panel depicts the number of days above these thresholds from May through September through time.
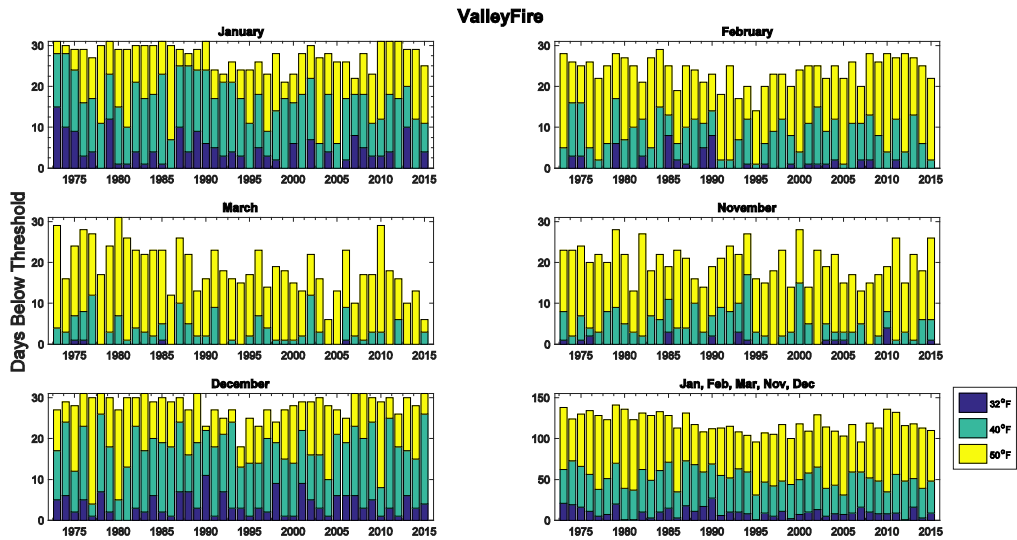

Figure A11-8. The bars illustrate the number of days below a temperature threshold in November, December, January, February and March of a given year. The purple bar represents the number of days below 32˚F, the green bar represents number of days below 40˚F, the yellow bar is the number of days below 50˚F. The maximum number of days for January, March and December is 31.